UNIVERSITAT DE BARCELONA

Synthetic engineering of membrane transport to increase photosynthesis and water use efficiency

Enginyeria sintètica del transport de membrana per tal d'augmentar la fotosíntesi i l'eficiència en l'ús de l'aigua

Carla Minguet Parramona

Synthetic engineering of membrane transport to increase photosynthesis and water use efficiency

Enginyeria sintètica del transport de membrana per tal d'augmentar la fotosíntesi i l'eficiència en l'ús de l'aigua

Memòria presentada per Carla Minguet Parramona per optar al títol de Doctor per la Universitat de Barcelona. Aquest treball s'emmarca dins el programa de doctorat "Biologia Vegetal" corresponent al bienni 2012/2015 del Departament de Biologia Vegetal de la Facultat de Biologia de la Universitat de Barcelona.

Aquest treball ha estat realitzat al Departament de Biologia Vegetal de la Facultat de Biologia de la Universitat de Barcelona sota la direcció del Dr. Salvador Nogués Mestres i al Institute of Molecular, Cell and Systems Biology de la University of Glasgow sota la direcció del Prof. Michael R. Blatt.

Doctorand | Directors de tesis

Carla Minguet Parramona | Dr. Salvador Nogués Mestres | Prof. Michael R. Blatt

BARCELONA, SETEMBRE 2015

Universitat de Barcelona

University of Glasgow

Acknowledgements

I would like to thank my two supervisors Prof. Mike Blatt from the University of Glasgow and Dr. Salvador Nogués Mestres from the University of Barcelona for giving me the opportunity of doing a PhD.

I would like to sincerely thank Prof. Mike Blatt for always being willing to answer my on-going questions, for his guidance, for all his patient teaching and for all the learning I have gained at his side. Furthermore, for giving me the opportunity of travelling for science, for his huge dedication in my thesis and for encouraging me to constantly improve.

M'agradaria agrair al meu supervisor Dr. Salvador Nogués Mestres perquè tot i la distància sempre ha estat ràpid a respondre els meus dubtes, i constantment pendent de tot el procés del doctorat facilitant-m'he cada pas.

I would like to thank all my lab mates, which have become my family during my years in Glasgow. Especially thanks to Dr. Ben Zhang, my PhD mate, from whom I had the pleasure to learn with and to go through this process together. To Dr. Rucha Karnik for her infinite teaching on biochemistry and for never refusing to answer my questions. To Dr. Emily Larson, Dr. Cécile Lefoulon, Wijitra Horaraung and Naomi Donald for their friendship and always cheering me up. To Dr. Sak Waghmare for all his philosophical talks, which have been always very useful. To Adrian Hills for being a great desk mate and expert on resolving all my computer and modelling doubts. To Dr Yizhou Wang for his guidance on modelling. To Dr. Christopher Grefen for his immense guidance on cloning. To Dr. Maria Papanatsiou, Dr. Giorgio Perella, Dr. Amparo Asensi, Mary-Ann Madsen, Prof. Anna Amtmann, Christin Alderhold, Dr. Annegret Honsbein, George Boswell, Craig Carr, Louise Henderson and Lluís Matas for their friendship and for being fabulous lab mates. Many thanks to Amparo Ruiz Prado, not only for her huge help on seed harvesting and plant growth, but also for being a very good friend, gracias. And many thanks to all the people from the Bower Building for their nice friendship and support. I would specially like to thank to Jia Zhao and Min Hou who had join me during the hard process of thesis writing, always being a great company.

Me gustaría agradecer a mis otros compañeros de doctorado Elena, Salva, Claudia y Gladys por resolver mis dudas y facilitarme el trabajo de administración de la Universitat de Barcelona. També vull agrair als meus companys de màster Melanie, Marta i Xavier que també han continuat amb el doctorat i sempre m'han ajudat i guiat en com anaven les coses a Barcelona i animat en la distància.

Als meus companys de la carrera, Berta, Andrea, Aina, Andrea i Jordi, per ser grans amics i donar-me forces per acabar la tesis. A l'Elisenda, per pensar amb mi d'una manera especial, i per ser tan especial per mi. A tots els amics del poble, als que tant m'estimo. I a tots els que d'alguna manera o altra m'han ajudat a fer que això sigui possible.

A la meva família, padrins, tiets, cosins, per creure en mi i recolzar-me sempre. Als meus pares, perquè aquesta tesis mai s'hauria fet sense ells, per estimar-me tant i respectar-me. Però sobretot, per donar-me ales i ensenyar-me a volar, sempre us estaré infinitament agraïda. Al rodamón del meu germà, Arcadi, gràcies per saltar primer.

Joan, per ser-hi sempre i donar-m'ho tot. Gràcies per haver-te creuat en el meu camí.

Table of contents

Abbreviations

A_{sat}	CO_2 assimilation at light saturated
g_s	Stomatal conductance
$V_{c\,max}$	Maximum carboxylation velocity of Rubisco
3-PGA	3-phosphoglycerate
AE1	Erythrocyte anion exchanger 1 (Band 3)
A_{max}	Maximum photosynthetic rates at CO2 saturated
BR	Bacteriorhodopsin
CA	Carbon anhydrase
CCM	Carbon concentrating mechanisms
ChR	Channelrhodopsin
CO_2	Carbon dioxide
G-3-P	Glyceraldehyde phosphate
GFP	Green Fluorescent Protein
HCO_3^-	Bicarbonate
HR	Halorhodopsin
MAGIC	Multiple Approaches to Gain Increased Carbon Dioxide
NpHR	Halorhodopsin from *Natronomonas pharaonis*
OAA	Oxaloacetate
pCO_2	Partial pressure of CO2
PEP	Phosphoenolpyruvate
PEPCK	Phosphoenolpyruvate carboxykinase
RbcL	Large subunit of Rubisco
RFP	Red Fluorescent Protein
Rubisco	Ribulose bisphosphate carboxylase/oxygenase
RuBP	Ribulose bisphosphate
TPT	Triosephosphate Translocator

1. Introduction

1.1 Coping with the increase of world's population

The United Nations estimates a rise from 7 billion people today to 9 billion people on 2050 and above 10 billion people on 2100 (UN 2013). Most of this population growth it is expected to be in developing countries, where poverty and hunger are already a big concern.

The total number of people in the world suffering from hunger has decreased during the last few decades (Figure 1.1). However the number of people that are still suffering from hunger remains elevated. It was estimated that in 2014 there were 805 million people suffering of undernourishment (FAO 2014). The World Food Programme organisation from United Nations has identified some of the reasons of hunger; the most relevant are poverty, the lack of investment in agriculture, climate and weather, war and displacement, unstable markets and food wastage. Aggravating these problems are food and agriculture policies, consumption patterns, the trade system, biofuels and speculation, among others (Paul and Wahlberg 2008).

	Number of undernourished *(millions)* and prevalence *(%)* of undernourishment									
	1990–92		2000–02		2005–07		2008–10		2012–14*	
	No.	%	No.	%	No.	%	No.	%	No.	%
WORLD	1 014.5	18.7	929.9	14.9	946.2	14.3	840.5	12.1	805.3	11.3
DEVELOPED REGIONS	20.4	<5	21.1	<5	15.4	<5	15.7	<5	14.6	<5
DEVELOPING REGIONS	994.1	23.4	908.7	18.2	930.8	17.3	824.9	14.5	790.7	13.5

Figure 1.1. Number of undernourished people (millions) and prevalence (%) of undernourishment, from the years 1990 to 2014. Differences between developed and developing regions, and total world's calculations. The data of 2014 is estimated (FAO 2014).

In order to feed the growing population and simultaneously cope with the hunger problem it will be necessary to increase food production in addition to making policies that allow developing countries to have access to this food. It is predicted that a 70 percent increase in food production will be needed over the next 30-50 years. This increase in food includes cereal and meat production, which have to increase 0.9 billion and 200 million tonnes respectively (FAO 2009).

1.1.1 Agriculture and hunger

Around 70 percent of the world's poor live in rural areas, and many of them rely on agriculture. A growth in agriculture generates an overall economic growth and leads to poverty reduction (FAO 2014). Government investment in agriculture and policies that stimulate agricultural growth are crucial to reduce poverty. Likewise bad governance has negative effects on agricultural growth (Cleaver 2012). An increase in agriculture production and increasing food supplies therefore reduces poverty two-fold by additionally lowering food prices and generating increased incomes for farmers (Wiggins 2004).

Growing conditions of crops have a substantial impact on final production. Agriculture is affected by a range of environmental conditions including temperature, precipitation and soil moisture, climate variability and extremes, fertilization, weeds, pests and pathogens (UN 2010). Most important, the current extremes and climate change constitute important factors in agriculture.

While difficult to predict, the levels of fresh water are expected to increase by 10-40 percent at high latitudes and decrease by 10-30 percent in dry regions. At the same time flood risk is expected to increase, water supplies such as glaciers and snow cover will decline, and there will be an extension of drought-affected areas (Easterling 2007). Other effects include longer and more frequent periods of drought, and higher temperatures (Kurukulasuriya and Rosenthal 2003) leading to desertification. In brief, the consequences of climate change are several and will have a direct impact on agriculture. Overall, the main consequences are a negative effect on long-term water and other resource availabilities, and worsening soil conditions. Furthermore, there will be an increase on diseases and pest on crops and livestock among other consequences (Rosenzweig, Tubiello et al. 2002).

Apart from climate change, there are other factors involved in the long-term water shortage. Some 70 percent of fresh water consumption is used for agriculture. An increase in population thus will also lead to a higher demand for fresh water. Water will be need to fulfil for society the demands of water-intense lifestyles and diets,

altogether serving to complete the food production chain and energy generation, among other activities in different economic sectors (Sauer, Havlík et al. 2010). Thus becoming a limiting factor to ensure sufficient food production.

Another limiting factor for food production is the land availability. Agriculture expansion has been the main cause of deforestation in the planet, followed by other use of forest for raw material and fuel (FAO 2012). After the last ice age, 10.000 years ago, there were 6 billion hectares (54 percent) of forested land area across the world. Since then the global forest area has decreased dramatically. In 2010 the total forest area was estimated to be 31 percent of the total land area, reaching around 4 billion hectares (FAO 2010). The growth on population and the increase of the food, fibre and fuel demand is accelerating forest clearance.

1.1.2 The effect of biofuels on food production

The use of biofuels as an alternative energy source is set to have a significant impact on food production and prices. In the first wave of biofuel production, much was derived from crops that might otherwise go into the food chain. Thus, the use of crops for biofuel production reduces food and feed availability primarily by supplanting food crops as a cash crop for farmers in many areas, increasing food prices. Furthermore, the amount of land required to grow crops destined for biofuels competes with the land required for food production. In the last 10 years the biofuel production has increased 5-fold, rising to over 100 billion litres/year in 2011 and triggering food riots in many developing countries (FAO 2013).

The problem is exacerbated because global biofuel demand is increasing exponentially (Figure 1.2). The use of first generation biofuels (those produced from crops that can also be used in the human food chain) is a real risk for food security. An increase in the use of second generation biofuels (made with crop residues, grasses and trees grown on marginal land) and third generation biofuels (derived from algae) may help decrease the competition for food. A 3 percent lower calorie availability per person in the developing countries is expected if the rates increase in producing first generation biofuels remains constant (FAO 2009).

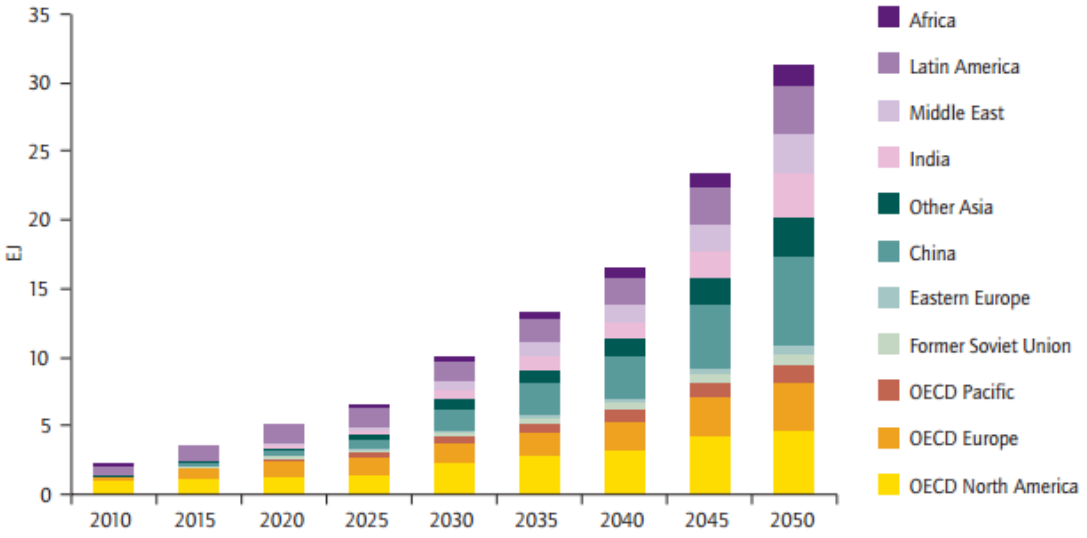

Figure 1.2. Global biofuel demand in exajoules (EJ), by region, from the year 2010 to 2050 (OECD/IEA 2011).

1.1.3 Increase of biomass and agriculture development

One of the grand challenges for this century, therefore, is to enhance crop production. An increase in crop productivity would reduce the negative effect that biofuel production has had on food availability, as well as reducing the high demand on forest land (FAO 2009). Scientific research aimed at increasing plant biomass in crops must be an essential part of the push to increase on agriculture production, and an important part of this effort must be the development of plants with high water use efficiency that can cope with low fresh water availability.

Several scientific groups around the world are working in order to develop solutions for the hunger problem. In 2008, the "4F crops project" was launched in Europe aimed at Food, Feed, Fiber and Fuel. The goal of this program is to analyse and assess all the parameters playing an important role in successful non-food cropping systems in agriculture, alongside the existing food crop systems, to minimise the competition of land. Another project developing solutions for the hunger problem is the international "C4 rice project" from the C_4 Rice Consortium. This project aims to develop C4 photosynthesis in rice by changing rice biochemistry and the structure of rice leaves to a C4-compatible type for a more efficient photosynthesis.

Through the Gates Foundation there are several other projects ongoing directed to promoting agricultural development. For example, the International Crops Research Institute for the Semi-Arid Tropics is currently engaged in a project the purpose of which is to develop high yielding pest and disease resistant legume varieties and to deliver these new varieties to smallholder farmers in Sub-Saharan Africa and South Asia. Another example is the grant awarded to the African Agricultural Technology Foundation for a project aim to develop and distribute improved maize hybrids for Africa that are drought-tolerant, insect-resistant, and higher yielding.

The Green Revolution was able to demonstrate how the improvement on agriculture is a big step forward fighting against hunger. The growth in productivity as a result of the Green Revolution contributed to lower food prices globally. The decrease in prices allowed more people to have access to food, thus increasing the average caloric intake and improving health and life expectancy (Evenson and Gollin 2003). However, new advances in agricultural development are now indispensable to satisfy the needs of a growing world's population. The next step to follow in order to increase crop yield potential is an improve on photosynthesis (Zhu, Long et al. 2010).

1.2 Improving photosynthetic efficiency

Photosynthesis is the force that powers life on Earth. The term photosynthesis was introduced by Charles R. Barnes in 1893 (Barnes 1893). However, the research on the process was begun by Jan Baptist van Helmond in the 17^{th} century (Helmont 1648). Since then, photosynthesis has been accurately studied and all of the process has been well described. In recent years, photosynthesis has regrown as a topic of much interest due to its potential to increase food production. A central part of this effort focuses on critical points that are limiting for the overall process of photosynthesis, with the effort to address ways of improving them in order to increase photosynthesis efficiency.

1.2.1 Process of photosynthesis

The vast majority of plants in the planet, including most of the crops, rely on C_3 photosynthesis. This process consists in the incorporation of a CO_2 molecule into

ribulose bisphosphate (RuBP) in order to create two molecules of 3-phosphoglycerate (3-PGA) (3C molecule) in the Calvin cycle metabolic pathway (Ehleringer and Cerling 2002). Ribulose bisphosphate carboxylase/oxygenase (Rubisco) is the enzyme that catalyses the CO_2 incorporation reaction in this process.

The entrance of CO_2 molecules into the plant tissue takes place through the stomata pore. The CO_2 molecules diffuse through intercellular air spaces to the stroma of the chloroplasts (Evans and Von Caemmerer 1996), where the Rubisco is localised. To enter the chloroplast, the CO_2 has to diffuse through both the inner and the outer chloroplast envelope membranes. These envelopes also mediate the exchange of other metabolites between the cytosol and the chloroplast stroma. The outer envelope of the chloroplasts has a high permeability to small molecules due to the presence of porins. However, some substrate-specific gated pore-forming proteins have been characterised in this envelope during the last decade. The inner envelope it is a more selective membrane acting as a barrier between the stroma and the cytosol (Block, Douce et al. 2007). Once in the stroma, the partial pressure of CO_2 (pCO_2) is lower than the pCO_2 in the atmosphere (C_a) due to the carboxylation activity of Rubisco (Evans, Kaldenhoff et al. 2009).

In the stroma of the chloroplast is where the fixation of the CO_2 takes place via the Calvin cycle. The Calvin cycle comprises a total of 13 reactions catalysed by 11 different enzymes. The first enzyme involved in the cycle is Rubisco, which catalyses the carboxylation of RuBP to obtain two molecules of 3-PGA. The second phase of the cycle is the reduction of the 3-PGA to form glyceraldehyde phosphate (G-3-P) which comprises two reactions and requires ATP and NADPH consumption. G-3-P serves as substrates from which to synthesise sucrose and starch. The final phase of the cycle is the regeneration of the RuBP (Raines 2003). In total there is the consumption of 3 ATP and 2 NADPH molecules for every molecule of CO_2 fixed by Rubisco.

The ATPs and NADPHs required in the Calvin cycle are provided by photophosphorylation in the light-dependent reactions of photosynthesis. This process involves the consumption of water and light energy. It takes place in the thylakoids,

highly organised internal membrane structures forming the grana in the stroma of the chloroplasts, and occurs via proton and electron transport processes (Jensen and Leister 2014). There are three types of photophosphorylation reactions described, cyclic, non-cyclic and pseudo-cyclic, all generated by electron transport chain reactions. The absorption of light by the reaction centers and consequent excitation of the pigments allows the electrons, obtained from the photolysis of water, to move from one acceptor to the adjacent one thus creating strong oxidants. All of these reactions are involved in ATP synthesis; in addition, non-cyclic photophosphorylation also generates oxygen as the final electron acceptor and NADPH. All the three pathways have been observed in isolated chloroplasts and it seems that all of them work *in vivo* (Allen 2003).

The synthesis of ATP and NADPH is generated by chemiosmosis. During the movement of the electrons through the transport chain, H^+ diffuse across the thylakoid membrane from the stroma of the chloroplast into the thylakoid lumen. The concentration of H^+ creates an electrochemical potential gradient, the proton-motive force of chemiosmosis. H^+ are transported back to the chloroplast stroma through ATP synthase. The ATP synthase includes a part embedded in the membrane, CF_0, which forms a proton pore. It interacts with the catalytic component, CF_1, which generates ATP from the phosphorylation of ADP (Mitchell 1966, Feng and McCarty 1990, Allen 2003). The final electron acceptor of the transport chain is ferredoxin, this forms an electron transfer complex with the enzyme ferredoxin $NADP^+$ oxidoreductase, which catalyses the reduction from $NADP^+$ to NADPH (De Pascalis, Jelesarov et al. 1993, Kurisu, Kusunoki et al. 2001). For the reduction from $NADP^+$ to NADPH a proton is required which in turn contributes to the proton gradient across the membrane.

1.2.2 The efficiency of Rubisco

The low efficiency of Rubisco is a main factor limiting photosynthesis. Rubisco has a very slow catalytic rate – typically on the order of 5-6 cycles per second. Its slow catalytic rate, and its fundamental role in nature, explains why Rubisco is the most abundant protein in the world, comprising the 50 percent of leaf nitrogen (Spreitzer

and Salvucci 2002). A further complication is that Rubisco has a low affinity for atmospheric CO_2 and will also incorporate O_2 instead of CO_2 in the fixation reaction through a process called photorespiration (Spreitzer and Salvucci 2002). Photorespiration occurs when Rubisco fixes an O_2 molecule instead of CO_2 and catalyses the oxygenation of RuBP instead of the carboxylation leading to the formation of glycolic acid (Wingler, Lea et al. 2000). Thus, one of the possibilities to increasing the capacity of photosynthesis is through improving Rubisco efficiency.

Modifying the catalytic rate of Rubisco in order to make it more efficient is a big challenge. Rubisco is one of the largest enzymes in nature, with a molecular weight of 560 kDa, and is of a complex nature. The holoenzyme is composed of eight large and eight small subunits (Figure 1.3). The large subunits are 55 kDa each and are encoded in the chloroplast, the small subunits are 15 kDa and are encoded in the nucleus of the cell (Spreitzer and Salvucci 2002). In general, it is considered that there are two main ways of increasing photosynthesis through modifications involving Rubisco. One way, not discussed in this thesis, is to modify the active site of Rubisco in order to improve its catalytic efficiency. The other way is to create a carbon concentrating mechanism (CCM) to increase pCO_2 in the active site of Rubisco, thus reducing photorespiration.

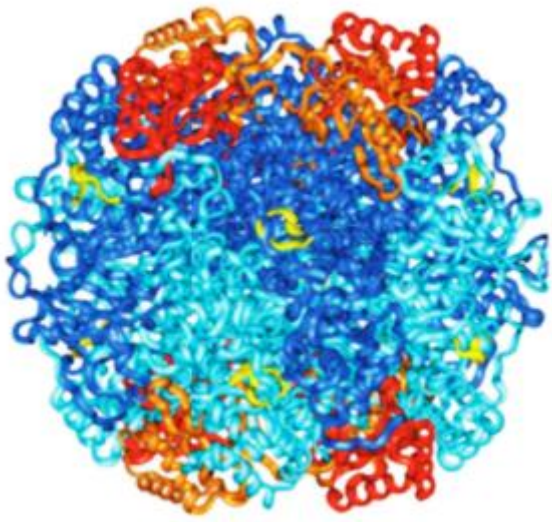

Figure 1.3. Rubisco of spinach. Stereo image of the X-ray crystal structure of the holoenzyme. Composed of eight light (dark and light blue) and eight small (red and orange) subunits. The yellow loops indicate the position of the active sites. Image taken from a previous publication (Spreitzer and Salvucci 2002).

1.2.3 C_4 photosynthesis properties

The main characteristic of plants that carry out so-called C_4 photosynthesis is their ability to concentrate carbon inside the cell where Rubisco is located. This feature provides a rich CO_2 environment to Rubisco, increasing the ratio of carboxylation versus oxygenation reaction.

In high temperatures Rubisco has less specificity for CO_2, and the solubility of CO_2 decreases in comparison with the O_2 one, leading to an increase of photorespiration in C_3 plants (Wingler, Lea et al. 2000). However, because of the CCMs, in high temperatures or low CO_2 concentration conditions C_4 photosynthesis is more efficient than C_3 photosynthesis (Ehleringer and Cerling 2002). Thus, C_4 plants offer clear evidence that CCMs increase the affinity of Rubisco for CO_2, and as a result increase photosynthesis.

C_4 plants originated during the Oligocene, 24-35 million years ago, in an atmosphere with low CO_2 concentrations. Nowadays around 3 percent of all land plants rely on C_4 photosynthesis (Sage 2004). C_4 photosynthesis is based on biochemical and morphological modifications of C_3 photosynthesis, and it almost certainly evolved from the necessity of reducing Rubisco oxygenase activity, thus increasing photosynthetic activity (Ehleringer and Cerling 2002). Some examples of C_4 plants crops are maize, sorghum and sugar cane, however the majority of C_4 species are grasses and sedges, all non-crop plants.

The first acceptor of CO_2 in a C_4 plant is the phosphoenolpyruvate (PEP) carboxylase (PEPC) molecule instead of Rubisco. Here CO_2 is fixed from HCO_3^- and therefore carbon anhydrases (CAs) have an important role in facilitating rapid equilibrium between CO_2 and HCO_3^-. The carboxylation of PEP forms oxaloacetate (OAA), a 4-carbon organic acid molecule, and it takes place in the mesophyll cells. Then, the 4C acid diffuses to a separate compartment where it is decarboxylated to release CO_2 and a pyruvate molecule. The separate compartment takes the form of specialized mesophyll cells, the bundle sheath cells, where Rubisco is localised. Finally, CO_2 released in the bundle sheath cell is fixed by Rubisco and incorporated in the Calvin cycle, much as it happens

in a C_3 plant. The pyruvate molecule is then transported back to the mesophyll cell to regenerate PEP. The high catalytic activity of PEPC allows CO_2 to be effectively concentrated in the bundle sheath cells, PEPC is not sensitive to O_2, and the physical separation from Rubisco ensures that the ratio CO_2/O_2 in the bundle sheath cells is elevated, thereby limiting photorespiration (Ehleringer and Cerling 2002). Overall, C_4 photosynthesis, such as outlined, consumes 5 ATP and 2 NADPH molecules for each CO_2 fixed into a 6 carbon sugar, meaning the consumption of two additional ATP required in C_4 photosynthesis in comparison with the C_3 photosynthesis.

Once converted into OAA in the mesophyll cells, CO_2 has three different ways to diffuse to the bundle sheath cells (Figure 1.4). The difference between the three pathways depends on the different 4C acid decarboxylase enzyme that is used to release CO_2 around Rubisco. OAA can be reduced to malate or transaminated to aspartate to diffuse to the bundle sheath cell. Once in the bundle sheath cell, aspartate can be deaminated to OAA and CO_2 can be release through the action of phosphoenolpyruvate carboxykinase (PEPCK). Aspartate can also be deaminated and reduced to malate, in this case CO_2 will be released by NAD-malic enzyme (NAD-ME). If the CO_2 difuses to the bundle sheath cell as malate, NADP-malic enzyme (NADP-ME) is the one that will decarboxylate it and release CO_2 to Rubisco (Williams, Aubry et al. 2012). The main C_4 crops rely on NADP-ME subtype, considered the most efficient of the three subtypes in relation to the quantum yield (Ehleringer and Pearcy 1983).

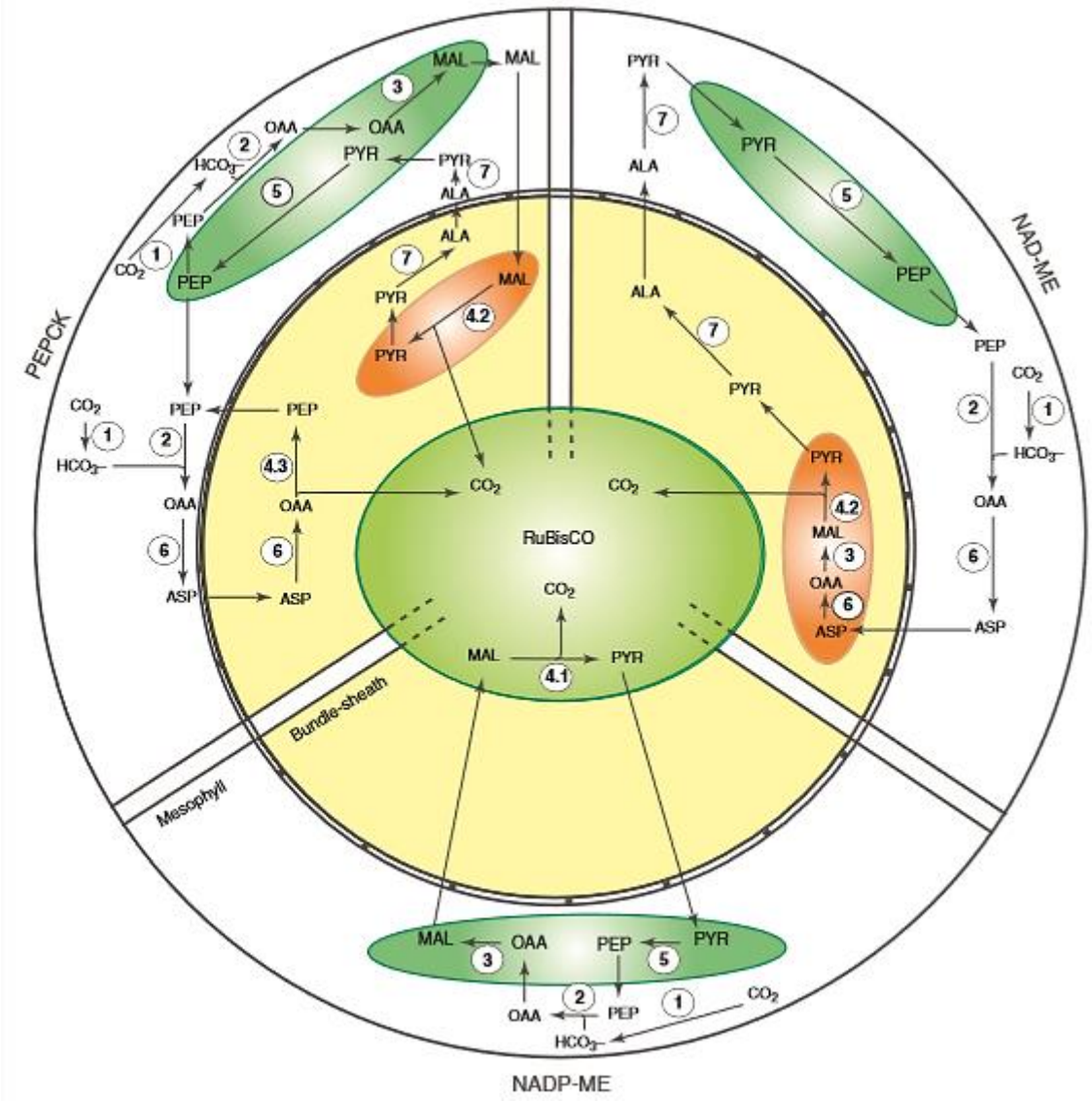

Figure 1.4. Illustration of the three different pathways of the C_4 photosynthesis to diffuse CO_2 from the mesophyll to the bundle sheath cells. CO_2 gets concentrated in the bundle sheath cells around Rubisco. The three pathways (PEPCK, NAD-ME and NADP-ME) are defined by the different enzymes used to decarboxylate the CO_2 and release it around Rubisco. (1) Carbonic anhydrase, (2) phosphoenolpyruvate carboxylase, (3) NAD/PH-malate dehydrogenase, (4.1) NADP-malic enzyme, (4.2) NAD-malic enzyme, (4.3) phosphoenolpyruvate carboxykinase, (5) pyruvate, orthophosphate dikinase, (6) aspartate aminotransferase, (7) alanine aminotransferase. Chloroplasts are coloured in green, mitochondria in orange, mesophyll cells in white and bundle sheath cells in yellow and plasmodesmata in black connecting the two cell types. . Image taken from a previous publication (Williams, Aubry et al. 2012)

The presence of the two different types of mesophyll cells allows a spatial separation anatomy also called Kranz anatomy, present in most C_4 plants. This anatomy is characterised by having two types of photosynthetic cells. The bundle sheath cells

form a ring around the vascular bundles; the mesophyll cells are located next to them, under the leaf epidermis. The bundle sheath cells are large and contain prominent chloroplasts, by comparison with the mesophyll cells (Hatch 1987, Edwards, Franceschi et al. 2001). The presence of suberized lamella in the bundle sheath cell walls helps to prevent the CO_2 diffusion, making the system very effective on concentrating CO_2. This suberized lamella is just present in NADP-ME and PEPCK subtype bundle sheath cells (Hattersley and Browning 1981). The existence of a special leaf anatomy together with the C_4 biochemical pathway result in a very effective CCM that concentrates CO_2 in the bundle sheath cells were Rubisco is localised, and it gives rise to a ratio of CO_2 to O_2 in C_4 photosynthesis that is up to 10 time higher than in C_3 photosynthesis (Furbank and Hatch 1987), thus allowing the plant to increase photosynthesis due to the limited oxygenase activity of Rubisco (CARMO-SILVA, Powers et al. 2008).

There are a few C_4 plants species discovered that instead of presenting Kranz anatomy have spatial separation of the different enzymatic processes within the same cell, called single cell C_4 (SCC_4) plants (Sharpe and Offermann 2014). There are two different structural forms of SSC_4 reported. The first structural form was found in *Borszczowia aralocaspica*. These plants contain a single layer of large chlorenchyma cells with a large central vacuole and a thin layer of cytoplasm between the vacuole and the plasma membrane. The large vacuole separates dimorphic chloroplasts localized at the opposite poles, thus forming a proximal and a distal compartment. They present a compartmentation of the main photosynthetic enzymes in a single photosynthetic cell (Voznesenskaya, Franceschi et al. 2001). The second structural form is found in three different *Binertia* species. It contains two or three layers of chlorenchyma cells with large intercellular spaces in between the cells. Inside the chlorenchyma cells there is a central cytoplasmic compartment filled with mitochondria and granal chloroplasts. The chloroplasts from the peripheral cytoplasm are grana-deficient and lacks mitochondria. The central compartment is interconnected with the peripheral cytoplasm by cytoplasmic channels through the vacuole (Freitag and Stichler 2002, Voznesenskaya, Franceschi et al. 2002).

1.2.4 Engineering Carbon Concentrating Mechanisms (CCM)

C_4 plants are not the only photosynthetic organisms that have naturally occurring CCMs in order to increase the efficiency of Rubisco towards the carboxylation reaction. Another example of CCMs in terrestrial higher plants is crassulacean acid metabolism (CAM). Some 6 percent of all land plants rely on CAM photosynthesis, including plants such as pineapple and agave. The main characteristic of CAM plants is that they separate the enzyme activity temporally. During the night the stomata open to allow CO2 to enter the leaf. During this time, PEPC fixes CO_2 to form malic acid which is then stored as malate, usually in the vacuole. During the day, the stomata remain closed to prevent water loss from the plant. At this time the CO_2 is released by decarboxylation of malate and is captured by Rubisco which incorporates it into the Calvin cycle of photosynthesis (Dodd, Borland et al. 2002). Finally, several algae have also naturally acquired CCMs (Giordano, Beardall et al. 2005), and other aquatic organisms such as cyanobacteria have evolved analogous mechanisms that physically concentrate CO_2 in the neighbourhood of Rubisco.

The possibility of engineering C_3 plants with CCMs thus has motivated research to the challenge of increase photosynthesis by similarly enhancing their effective CO_2 affinity. There are several groups of scientists that have already started looking for ways to express CCMs in C_3 plants. As already mentioned in the first section of this introduction, the C_4 Rice Consortium, funded by the Gates Foundation, is taking over one of the biggest projects to reproduce C4 photosynthesis in a C3 plant, in this case in rice. The project involves an international consortium of researchers who aim to change the biochemistry and the structure of rice leaves in order to install C_4 photosynthesis. The task of such engineering means a hugely complex project due to the difference in anatomy between rice and C_4 plants. The bundle sheath cells in rice are smaller and have less chloroplasts that the ones in C_4 plants. Rice also has more mesophyll cells between vascular bundles making it a big challenge to establish spatial separation of the PEPC and Rubisco enzyme activity. The project is expected to require years for the optimization of the phenotype and field testing before C_4 rice can be commercialised (Von Caemmerer, Quick et al. 2012).

Another strategy to engineer CCMs into C_3 plants would be to reproduce the metabolism of cyanobacteria. Price et al (2011) have discussed two ways of increasing CO_2 around Rubisco based on the metabolism of these organisms. The first way involves transferring bicarbonate transporters from cyanobacteria to the inner envelope of a C_3 plant chloroplast. The second way is to reproduce all the cyanobacterial CCM in C_3 plant chloroplasts. Price, et al. present the results of model analysis that predicts from 5 to 15 percent increase on photosynthesis when bicarbonate transporters from cyanobacteria are transfer to the inner envelope of a C_3 plant chloroplast. They also expect an increase on water use efficiency (WUE) in these conditions, simply because the stomata will not be required to open as much as in normal conditions for the same assimilation rates. Expressing the whole cyanobacterial CCM to a C_3 chloroplasts will be more complex than just transferring the bicarbonate transporters. There is the complexity of transferring a CO_2 uptake system to the thylakoid membranes as well as constructing a microcompartment for the Rubisco, such as carboxysomes, in addition of the bicarbonate transporters. Thus, Price, et al. conclude that expressing the whole CCM from cyanobacteria to the chloroplasts of C_3 will even be photosynthetically more efficient than just transferring the bicarbonate transporters.

Engineering CCMs to a C_3 plant is an efficient way to increase photosynthesis and crop yield. It is important to achieve an increase of photosynthesis without requiring any extra cost of energy for the plants. Fortunately, CCMs are not the only possibility to increase photosynthesis. One other way to increase photosynthesis, as well as WUE, is by improving the speed of stomata movement.

1.3 Role of stomata in photosynthesis

Stomata are small pores found in the epidermis of the areal parts from most of the higher plants. These pores are surrounded by a couple of specialised cells called the guard cells. The main functions of the stomata are to allow the gas exchange between the plant and the environment, mainly CO_2 influx into plant, and to control water vapour loss from the tissue. Stomata have to balance the needs for CO_2 that can enter

the plant to be assimilated during photosynthesis, while preventing the excessive loss of water via transpiration. Stomata typically occupy approximately 5 percent of the leaf surface area. However, because most aerial tissues of plants are coated in a largely impermeable waxy layer, they are the main entrance for CO_2 and account for around to 70 percent of the total water loss from the plant (Willmer and Fricker 1996).

The guard cells function as turgor-operated valves that can open and close depending on endogenous hormonal stimuli and the different environmental conditions. High humidity and low CO_2 induce stomatal opening in order to enhance CO_2 intake. In C_3 and C_4 plants red and blue light induce stomatal opening (Zeiger and Hepler 1977) and dark induces stomatal closure. Stomatal closure is also promoted by high CO_2 concentrations (Assmann 1999), high ozone concentrations (Torsethaugen, Pell et al. 1999) and pathogen elicitors (Lee, Choi et al. 1999). Drought enhances the production of the plant hormone abscisic acid (ABA) that also causes stomatal closing. Other plant hormones such as auxin, cytokinin, ethylene, brassinosteroids, jasmonates, and salicylic acid also have a role in stomatal opening regulation (Acharya and Assmann 2009).

Because stomata play such a key role in gas exchange, their behaviour has very important effects relating to climate change and to biomass yields through photosynthesis. Of global climate change, it is predicted that the future will see an ongoing increase in atmospheric CO_2, increase in temperatures and decrease in fresh water availability (IPCC 2007). As a consequence of the increase in atmospheric CO_2 concentration (C_a), an increase in leaf intercellular concentration of CO_2 (C_i) can be predicted which will favour stomata to close (Mansfield, Hetherington et al. 1990). Indeed, there is good evidence that several plant species are acclimating to the rise in atmospheric CO_2, both by reducing the stomatal density and aperture (Hetherington and Woodward 2003). These characteristics are reproducible in the laboratory. Plants grown in environments with elevated atmospheric CO_2 and under water stress conditions -due to a decrease of fresh water availability- may have a decrease in stomatal conductance, thus enhancing water use efficiency (Medlyn, Barton et al. 2001). In principle this will increase the efficiency of C capture in relation to the

amount of water needed for agriculture, but it also have negative effects, in particular because transpiration is a main factor controlling plant temperature (Mahan and Upchurch 1988). If transpiration is decreased due to a reduction on stomatal conductance, leaf temperature will increase. In addition, a further global increase in temperatures will lead to a plant heat stress with negative effects on crop yield (Radin, Lu et al. 1994, Battisti and Naylor 2009).

Understanding the mechanisms that control stomatal aperture is of a vital importance due to the main role stomata have in photosynthesis and transpiration. Being able to modify the response the guard cells present in the face of different exogenous and endogenous stimulus may help adapting plants to the new changing environments, thus reducing the crop losses in agriculture.

1.3.1 Stomatal opening and closure mechanisms

Stomatal opening and closure is driven by mechanisms that affect turgor pressure and cause the swelling or shrinking of the cells. These changes in volume, in turn, affect the pore's size. The changes in turgor are the result of changes in osmotic salt content followed by osmotic water uptake or release from the guard cells to the adjacent ones. Opening is produced by an influx of K^+, anion and synthesis of organic solutes in the guard cells that cause an increase in the turgor pressure. Stomatal closing is produced by the release of K^+ and anions from the guard cells that drives a reduction on the turgor pressure (Blatt 2000b, Ward, Maser et al. 2009).

A key feature of stomata is the cell wall structure. In guard cells, the cell wall is thicker on the pore side than elsewhere (Figure 1.5). An important consequence is that as turgor increases the cell expands asymmetrically, bowing outwards and allowing the pore to open. Depending on the species guard cells can increase their volume by 40 to 100 percent during the aperture of the stomata (Taiz and Zeiger 2010). Most of the volume gain is localised in the cross section of the guard cells and just a little increase is observed in the elongation. In *Vicia faba*, for example, these changes leads to an increase of 18.56 ± 8.96 percent in volume during the swelling and just a 5.50 ± 3.90 percent gain in elongation of the guard cell tips. Although during the guard cell

elongation step there is no much increase in cell volume, it represents the main force that drives the mechanical deformation for the stomatal opening, by pushing the two guard cells apart (Meckel, Gall et al. 2007).

Figure 1.5. Image of guard cells of *Vicia faba* forming a stoma in the open state. The cell wall in the pore site is thicker than in the rest of the cell and it is appreciated in the image by a much thicker grey line surrounding all the pore. Image taken from a previous publication (Chen and Blatt 2010).

1.3.2 Stomata membrane pumps, transporters and channels

Transport across the guard cell membranes, both tonoplast and plasma membrane, is the motor that drives stomatal opening and closure. All the influx and efflux of osmotic solutes has to access the guard cell through the plasma membrane, because mature guard cells do not have plasmodesmata (Wille and Lucas 1984). This transport requires the function of different pumps, transporters and channels which allow the different ions, mainly K^+ and Cl^-, and organic solutes, such as malate and sucrose, to move across the membranes (Figure 1.6). All of the ion fluxes are subject to their respective electrochemical driving forces.

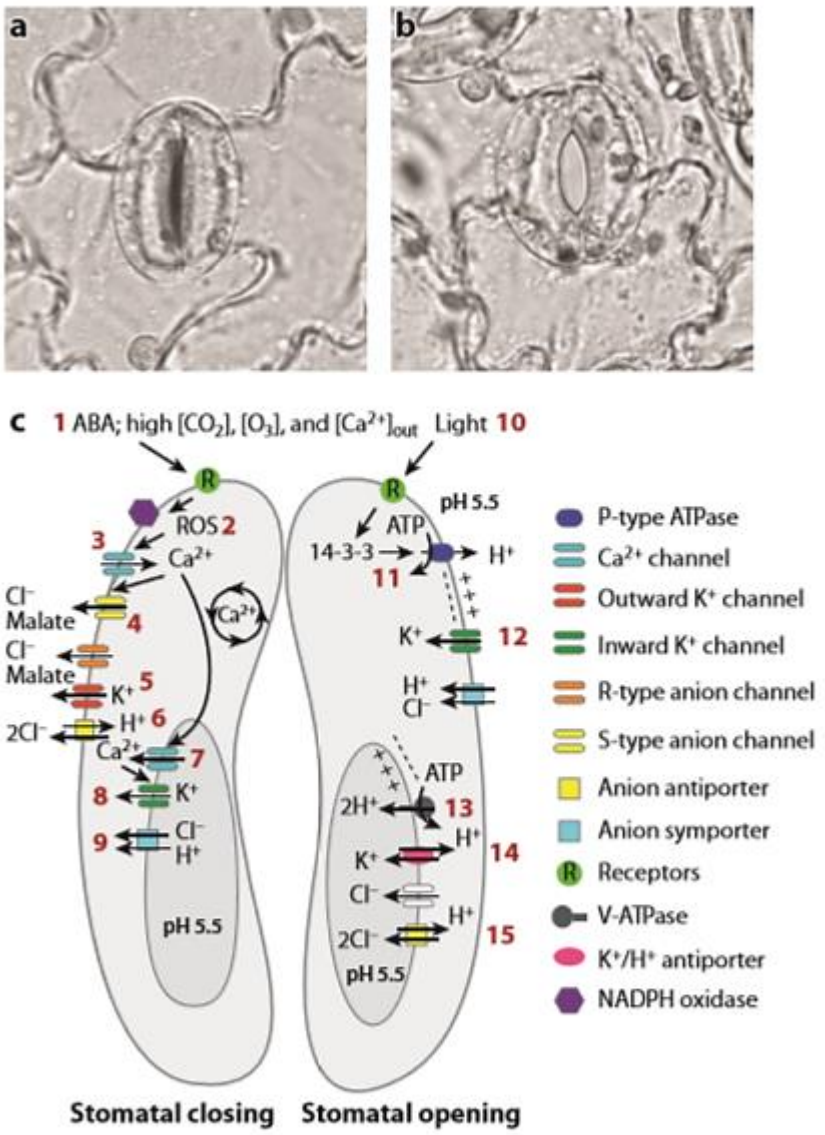

Figure 1.6. Model of stomata fluctuations of osmotic solutes during the opening and the closure. (a) Closed stomata from *Vicia faba*. (b) Open stomata from *Vicia faba*. (c) Scheme of the different channels, transporters and pumps, in the plasma membrane and in the tonoplast of the guard cells, which allow the flux of osmotic solutes during the opening and closure movements of stomata. (1-9) Example of some of the signals that promote stomata closure and the subsequent mechanisms triggered by the different stimuli. (10-15) Capture of light by the receptors and subsequent mechanisms that trigger stomatal opening. Image taken from a previous publication (Ward, Maser et al. 2009).

The vacuole of the guard cell has an essential role during opening and closure of the stomata. It occupies around 80 to 90 percent of the total guard cell volume, so most of the ion fluxes that pass across the plasma membrane also must pass across the tonoplast membrane. Furthermore, vacuoles are a big pool of Ca^{2+} and H^{+} that

contribute to signalling (Blatt 2000b). The guard cell vacuole has the ability of changing volume very rapidly to adapt to the shrinking and swelling required for stomatal movement. For example, the guard cells from *Vicia faba* contain a large vacuole when the stoma is open, but the vacuole divides into several small vacuoles during stomatal closure. The fusion of the little vacuoles during stomatal opening allows a rapid increase of vacuolar volume without having to greatly increase the membrane surface area (Gao, Li et al. 2005).

There is a high activity of transport across the vacuolar and the plasma membrane of the guard cells. Moreover, this transport has to occur in a short period of time. Therefore, the guard cell is able to change the solute contents with a period of 30 minutes in stomata closure and around 2 to 3 hours during stomatal opening (Blatt 2000b). All this activity is made possible thanks to different pumps, transporters and channels, which work in a coordinated manner to trigger stomatal movement.

1.3.2.1 Pumps

There is one family of proton pumps proteins known on the plasma membrane of the plant cells, the H^+-ATPases. This pump protein family is comprised by 11 different members in *Arabidopsis thaliana*, named AHA1 to AHA11 (Axelsen and Palmgren 2001). These pumps are energised by the hydrolysis of ATP and their main role is to pump H^+ outside the cell, causing a pH gradient of 1.5 to 2 units inside alkaline and membrane hyperpolarisation. As a result, these pumps create an electrochemical proton gradient across the plasma membrane necessary for the activation of the ion and metabolite transport, and they provide the energy for the plant nutrient uptake (Serrano 1989, Morsomme and Boutry 2000). The activity of these pumps typically generates membrane potentials with values from around -120 to -160 mV (Palmgren 2001). AHA1 and AHA2 proteins are the most abundant and are present in all plant tissues and organs, thus having a main role on cell ion homeostasis; along with these two pumps, AHA5 is also expressed in the guard cells plasma membrane (Gaxiola, Palmgren et al. 2007).

In the tonoplast there are two different families of proton pumps, the V-ATPase and the V-PPase, both of them transport protons across the membrane to the inside of the vacuole. The V-PPase, unlike the other pumps described, requires a pyrophosphate substrate instead of ATP (Maeshima 2000) and it is induced by K^+. As is the case for the pump in the plasma membrane, their main role is to create a proton gradient that provides the energy for the transport of the different ions and metabolites (Sze, Schumacher et al. 2002). In fact, the energisation of the tonoplast membrane by V-PPase allows K^+ to enter the vacuole against the concentration gradient, thus maintaining cytosolic K^+ homeostasis. In addition of its key role in energisation of the tonoplast, both pumps are key elements for the acidification of the vacuolar lumen (Sze, Li et al. 1999).

Both tonoplast and plasma membranes have one family of calcium pumps, the Ca^{2+}-ATPases. In *Arabidopsis thaliana* this family of calcium pumps is comprised of ten different members named from ACA1 to ACA10. Of these, three - ACA8, ACA9 and ACA10 - are specific to the plasma membrane. The main function of these ATPases is to maintain low levels of Ca^{2+} cytosolic free concentrations in the cell and to participate in the shaping of oscillatory Ca^{2+} signals. Although little is known still about the Ca^{2+}-ATPases in guard cells, it is suggested that the pumps could also be involved in ABA signalling (Schiøtt and Palmgren 2005, Chen and Blatt 2010).

1.3.2.2 H^+-coupled transporters

At both the plasma membrane and tonoplast there are H^+-coupled transporters that utilize the proton electrochemical gradients across the membranes to drive transport of a second solute. These transporters mediate the transport of H^+ accompanied with anions such as Cl^-, malate^{2-}, NO_3^- and PO_4^{2-}; cations such as K^+, Na^+ and Ca^{2+}; or sugars such as hexose and sucrose (Chen and Blatt 2010). These transporters facilitate the transport of these mentioned molecules against their electrochemical gradients. They also contribute to maintaining cytosolic pH and allow the influx of the different solutes during the stomatal opening and the efflux of these molecules during the stomatal closure.

As already mentioned before, the main ions involved in the opening and closure mechanisms of the guard cells are K^+ and Cl^-. Both can be transported by H^+-coupled transporters. In *Vicia faba* for example, the H^+-coupled K^+ symport allows K^+ influx when submillimolar levels of K^+ concentration are present outside the cell, thus moving the cation against its electrochemical gradient (Clint and Blatt 1989, Hills, Chen et al. 2012). The transport of Cl^- also usually happens against its electrochemical gradient, and it is frequently carried by the same transporter that facilitates NO_3^- movement across the membranes (Hills, Chen et al. 2012). The transport of the organic solutes such as sucrose and $malate^{2-}$ is also expected to be H^+-coupled (Ritte, Rosenfeld et al. 1999, Lee, Choi et al. 2008), however little is known about the kinetic details of their transport (Hills, Chen et al. 2012).

1.3.2.3 Channels

There are a variety of K^+, Ca^{2+} and anion channels in the plasma membrane of the guard cells. K^+ channels have a very important role during the stomata opening or closure as they allow the main fluxes for the gain or loss of K^+ in the guard cell (Schroeder 1988). The plasma membrane K^+ channels are divided between inward-rectifying K^+ channels (K_{in}) which allow the influx of potassium, and the outward-rectifying potassium channels (K_{out}) which allow the efflux of the same (Blatt 2008, Dreyer and Blatt 2009, Ward, Maser et al. 2009, Chen and Blatt 2010). Both belong to the Kv-like K^+ channel family that are gated by membrane voltage (Blatt 1991). K_{in} channels are activated by the hyperpolarisation of the plasma membrane during the stomatal opening (Schroeder, Raschke et al. 1987, Schachtman, Schroeder et al. 1992). In the guard cells of *Arabidopsis thaliana* there are five different K_{in} channels, these are called KAT1, KAT2, AKT1, AKT2 and KC1. This last one is an electrically-silent subunit, but because structurally it looks like a K_{in} channel is also classified among this category. The AKT2 channel shows unique gating properties and is often referred to as a voltage-independent channel (Dreyer and Blatt 2009). KAT1 and KAT2 are the most common. Indeed, KAT1 represents the main pathway for K^+ entry into the guard cell and is activated at negative membrane voltages beyond -100 mV. In contrast to the K_{in} channels, K_{out} channels are activated by the depolarisation of the plasma membrane

during the stomatal closure (Ache, Becker et al. 2000). The guard cell outward rectifier K^+ (GORK) channel is the only known K_{out} channel in the guard cell and it constitutes the main route of K^+ efflux during the stomatal closure. K_{out} channels are sensitive to extracellular concentrations of K^+ and their gating is also K^+ dependent (Blatt 1988). This dependence upon external K^+ serves as a failsafe mechanisms for preventing K^+ influx (Blatt and Gradmann 1997).

Other cation channels in the plasma membrane are the Ca^{2+} channels, which genes still remain to be identified. These channels mediate primarily Ca^{2+} influx and are activated by the plasma membrane hyperpolarisation and by ABA (Hamilton, Hills et al. 2000, Pei, Murata et al. 2000). Their activation by ABA in isolated membrane patches suggests that there is a physical association between the ABA site of perception and the localisation of the Ca^{2+} channel (Hamilton, Hills et al. 2000). This ABA activation of Ca^{2+} channels can occur through the production of reactive oxygen species (ROS) as a second messenger (Pei, Murata et al. 2000, Murata, Pei et al. 2001, Kwak, Mori et al. 2003, Wang, Chen et al. 2013). The Ca^{2+} channels characterised to date are also inactivated by elevated cytosolic concentration of Ca^{2+} ($[Ca^{2+}]_i$), thus making these the only self-limited Ca^{2+} channel currently known in plants. The accumulation of Ca^{2+} in the cytosol arises from both the entrance of Ca^{2+} across the plasma membrane as well as from the release of Ca^{2+} from intracellular stores (Blatt 1999b). In this context, the mechanism of self-limitation of the Ca^{2+} channel is a prerequisite for the guard cell to generate oscillatory behaviour in $[Ca^{2+}]_i$ during the closure of the stomata (Minguet-Parramona, Wang et al. 2015).

There are two types of anion channels in the plasma membrane of the guard cells. They are classified based on the structural proteins that give rise to the currents and depending on the activation and deactivation rates, thus they can be rapid (R)-type or slow (S)-type anion channels. The R-type anion channel activation is 1000 times faster than the S-type one. They also differ in sensitivities to membrane voltage. S-type anion channels have a weak-voltage sensitivity, activating at voltages of -120 mV and partially deactivating at voltages around -140 mV; in contrast, the R-type anion channel activates at voltages near -100 mV and it deactivates fully at more negative

voltages (Chen and Blatt 2010). Its role in stomatal movement is very important because, once activated, they allow the efflux of the different anions from the guard cell. More still, they enhance the depolarisation of the plasma membrane to engage the outward-rectifier K^+ channels and thereby contribute to stomatal closure (Roelfsema, Hedrich et al. 2012). Of course, depolarisation of the membrane affects both K^+ channel types: K_{in} channels become inactivated and K_{out} channels become activated, thus it is promoted the efflux of K^+. With the efflux of K^+ and the release of the different anions such as Cl^-, NO_3^- and malate, guard cell loses turgor and the stomata close.

The tonoplast membrane also harbours cation and anion channels that play important roles during stomatal movements. The cation channels can be divided into three different types, fast vacuolar (FV) channel, vacuolar K^+ (VK) channel and slow vacuolar (SV) channel. Genes encoding FV channels still remain to be identified. They are voltage sensitive and are activated by cytosolic alkalinisation. They allow a passive nonselective cation uptake and release at resting $[Ca^{2+}]_{cyt}$, and they become inactivated at elevated $[Ca^{2+}]_{cyt}$ (Allen and Sanders 1996, Ward, Maser et al. 2009, Chen and Blatt 2010). Members of the VK family are called two-pore K^+ channel (TPK). In *Arabidopsis* there are five different genes in this family, the most abundant being TPK1 (Gobert, Isayenkov et al. 2007). These genes allow the efflux of K^+ from the vacuole during the stomatal closure. They are voltage-insensitive, but they are activated by an increase in $[Ca^{2+}]_{cyt}$ (Ward and Schroeder 1994, Chen and Blatt 2010). Members of the SV channel family are also called two-pore cation channels (TPC). Representative of the TPC gene family is the TPC1, it is the most abundant channel protein found in *Arabidopsis*. They allow K^+ flux and Ca^{2+} release from the tonoplast. These channels are voltage regulated and are activated above a $[Ca^{2+}]_{cyt}$ of 500 nM (Pandey, Zhang et al. 2007). It is still unknown whether if TPC1 is functional or not in plants. The difficulty is that it is activated around voltages of +60 mV, but such positive voltages are never thought to occur across the tonoplast. Thus, it is still an enigma as to whether the channels ever open, and if so, which mechanisms allow them to do so. Although it has been demonstrated the association of SV currents with the TPC1 channel, to date only a very weak phenotype has been identified with the *tpc1*

mutation (Peiter, Maathuis et al. 2005), and the link between TPC1 current and its phenotype has not been demonstrated. The anion channels found in the tonoplast are the vacuolar Cl^- (VCL) channels, which allow fluxes of Cl^- and malate^{2-}, indispensable for stomatal opening. They are activated at physiological voltages, when the cytosol is more negative than the vacuole, thus allowing the entrance of Cl^- and malate^{2-} to the vacuole (Pei, Ward et al. 1996, Chen and Blatt 2010).

1.3.3 Transport coordination across the membranes

The processes of stomatal opening and closing are highly coordinated, involving the regulation of multiple transporters at both the plasma membrane and at the tonoplast. A full description is beyond the scope of this chapter, and here I briefly outline the most important of these processes. Stomatal opening is dependent on the activation of the plasma membrane proton (H^+)-ATPases, for example by stimuli such as blue-light (Assmann, Simoncini et al. 1985, Shimazaki, Iino et al. 1986, Kinoshita and Shimazaki 1999) and red-light (Serrano, Zeiger et al. 1988). When H^+-ATPases are activated protons are extruded from the cytoplasm to the outside of the guard cell, which promotes both hyperpolarisation and generation of a pH gradient across the plasma membrane (Blatt and Thiel 1993b). Membrane hyperpolarisation elicits inward currents of K^+, in large part, as a result of the shift of the membrane potential to more negative values at which K^+ channels activate, and in part as a result in the increased driving force for K^+ influx (Thiel, MacRobbie et al. 1992). Membrane hyperpolarisation also energises H^+-coupled anion uptake, mostly of Cl^-, and altogether leads to a K^+ and anion accumulation inside the cell. Because the main ions that move across the membranes are K^+ and Cl^-, the variation in KCl in the guard cells between the open and closed states is very large in comparison with other plant cells. For example, in guard cells of *Vicia faba* the KCl concentration differs from 2 to 4 pmol between the open and closed states, which results in an osmotic variation of 200 to 300 mOsM (Blatt 2000b). Blue and red light also promote the production of sugars that accumulate in the guard cell and participate significantly in the osmotic process that allows the stomata to open (Poffenroth, Green et al. 1992). Furthermore, during the stomatal opening there is a reduction of starch which is converted into malate (Outlaw and

Manchester 1979). As a result, the levels of malate increase inside the guard cell contributing on the accumulation of organic salts to allow the swelling of the guard cells and opening of the stomatal pore.

During the day most of the K^+ and Cl^- ions that enter the cell accumulate within the vacuole together with Mal^{2-}. The accumulation of Mal^{2-} inside the vacuole is related to the acidification of the vacuolar contents. Parallel to Mal^{2-} transport a H^+ influx balances charge via V-ATPases and V-PPases. A lot of the charge balance is achieved by the vacuolar H^+-pumps, however most of the charge balance is assumed by K^+ influx. At the same time, this energisation of the H^+-pumps allows a circulation of H^+ in and out of the vacuole, due to some H^+ re-enter the cytosol by its exchange with other ions such as Cl^-, or Ca^{2+} antiport (Chen, Hills et al. 2012).

During stomatal closure cytosolic Ca^{2+} oscillations occur, H^+-ATPase activity is suppressed and K^+ and anion solutes are released from the guard cell, causing a decrease in turgor pressure (Blatt 2000, Chen, Hills et al. 2012, Minguet-Parramona, Wang et al. 2015). Ca^{2+} oscillations are directly involved in stomatal closure and are thought to be important for accelerating K^+, Cl^- and malate efflux from the guard cell (Chen, Hills et al. 2012, Minguet-Parramona, Wang et al. 2015). Increases in $[Ca^{2+}]_i$ activates Cl^- channels to drive Cl^- efflux. The rise of $[Ca^{2+}]_i$ together with Cl^- release form the guard cell causes a membrane depolarisation. At the same time, depolarisation promotes K^+ and other anion efflux from the guard cell (Thiel, MacRobbie et al. 1992). The rise of $[Ca^{2+}]_i$ also inactivates K_{in} channels (Grabov and Blatt 1999, Chen, Hills et al. 2010b). The vacuole also has a fundamental role in stomatal closure. As the major store of osmotic solute, it contributes to the release of ions and organic solutes to reduce the total osmotic content of the guard cell. This net loss of osmotically active solutes leads to a loss on turgor pressure, which causes the shrinking of the guard cell and the closure of the stomata.

1.3.4 Modelling of the stomata

The development of quantitative systems models arises from the need to put together the huge amount of data accumulated from experimental analysis of guard cells. The

best computational models are able to integrate the behaviour of a complex biological system and to represent complicated chains of events by computer simulation (Fisher and Henzinger 2007). Guard cells are a perfect candidate for systems modelling, both because of the large body of quantitative data available and because their lack of plasmodesmata means they can be treated as a semi-closed system for modelling.

To date it has been possible to experimentally isolate and analyse the main transporters involved on the guard cell movement (noted above) that drive the closure and the opening of the stomata, and to analyse the roles of the sucrose and malate metabolism in these processes (Blatt and Thiel 1993b, Willmer and Fricker 1996, MacRobbie 1997, Thiel and Wolf 1997, Blatt 2000b, Schroeder, Allen et al. 2001b, Pandey, Zhang et al. 2007, Ward, Maser et al. 2009). Experiments on isolated transporters have yielded detailed information permitting descriptions of each flux based on accurate equations constrained by experimental data and basic physical principles. The major transporters analysed include K^+, Cl^-, Ca^{2+} and malate channels, and H^+-ATPases in both tonoplast and plasma membranes. Hills *et al* (2012) reported a computational programme, OnGuard, which pulls together the biophysical, kinetic, and regulatory features of the guard cell transport, signalling and homeostasis (Figure 1.7). This modelling programme is based on the homeostasis, transport and signalling (HoTSig) libraries, which comprise a system of user-editable and expandable descriptors and equations for all of the different transporters at the plasma membrane and the tonoplast.

A

B

C

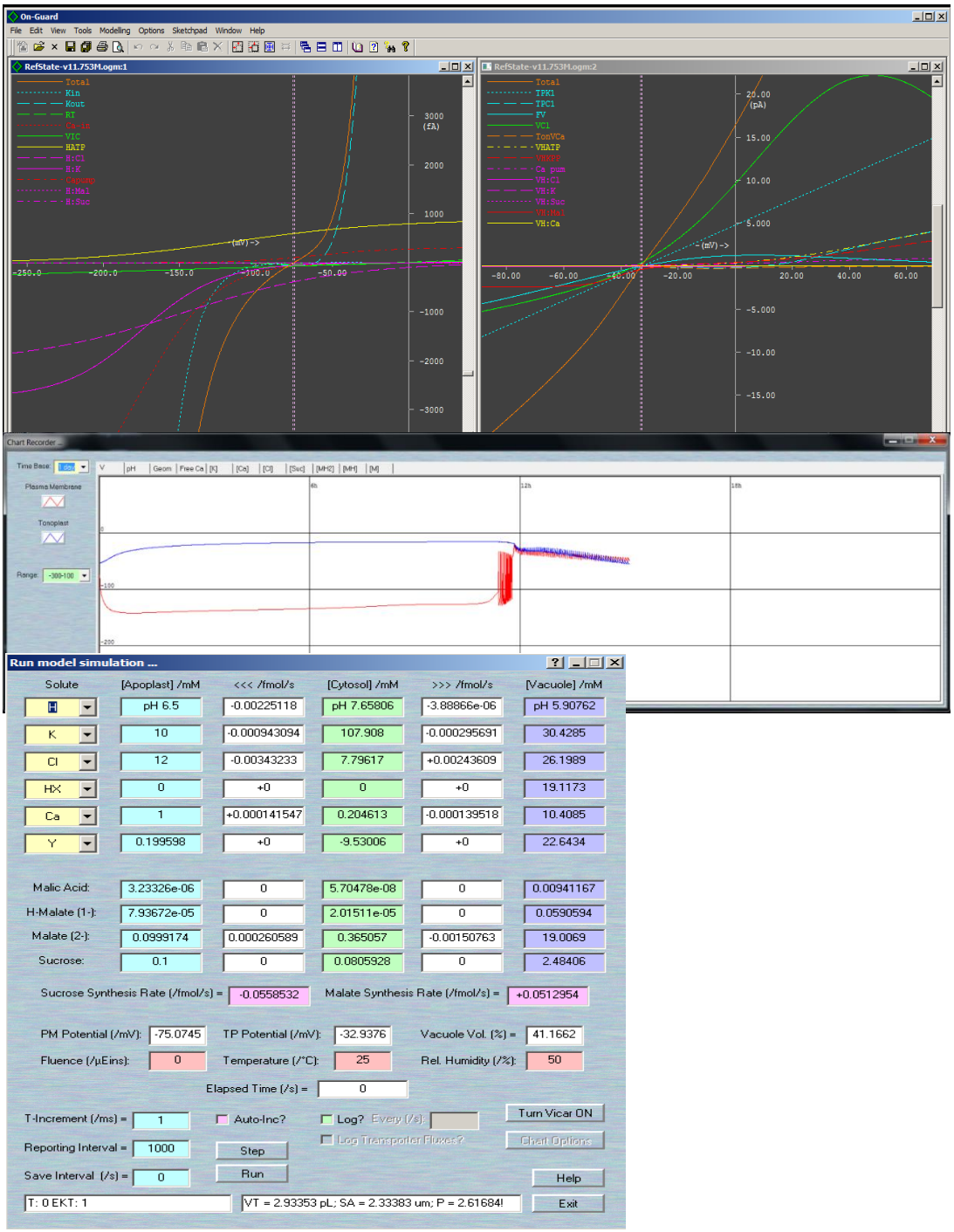

Figure 1.7. OnGuard modelling programme user interface. (A) Current-voltage curves of the different transporters in the plasma membrane (left) and the tonoplast (right) of the guard cell. (B) Chart recorder of the membrane voltage and of each of the ions and organic solutes from the cytosol and vacuole. (C) Detailed output of ionic and organic solute contents from the apoplast, cytosol and vacuole; the fluxes across both membranes; the membrane stomatal voltages; outputs of cell volume, turgor and stomatal aperture; and elapsed time counter. Image taken from a previous publication (Hills, Chen et al. 2012).

The predictive power of the OnGuard model is very accurate and demonstrable (Chen, Hills et al. 2012). For example, Wang et al. (Wang, Papanatsiou et al. 2012) could use the model to explain how the suppression of SLAC1 Cl^- not only slows stomatal closure, but also suppresses current through K_{in} channels in order to slow stomatal opening. Moreover, the model has yielded unexpected and emergent outputs that have been previously supported by experimental data. Some examples are its counterintuitive changes in $[Ca^{2+}]_i$ and cytosolic pH over the diurnal cycle, and an exchange of vacuolar Mal^{2-} with Cl^- subject to the availability of the inorganic anion (Raschke and Schnabl 1978, Thiel, MacRobbie et al. 1992, Blatt and Armstrong 1993, MacRobbie 1995, Willmer and Fricker 1996, Frohnmeyer, Grabov et al. 1998)**.** Thus, it is possible to use the model to simulate a variety of different conditions in the guard cells and to predict how the stomata will respond towards them. In this thesis the OnGuard model has been used as a tool to predict which modifications need to be done in a guard cell in order to have a more efficient stoma.

An efficient stoma is the one that maximises CO_2 uptake for photosynthesis while minimising the amount of water loss through transpiration. In nature, with all the adverse climate conditions, it is a challenge for the plants to have high photosynthesis and an optimum WUE at the same time. Usually a plant with high stomatal conductance tends to have higher photosynthetic assimilation but an enormous water loss. On the other hand, if the stomatal conductance is low, the plant will have better WUE but the rate of photosynthetic assimilation will also be low. This direct dependence of photosynthetic assimilation on conductance, when water availability and other factors are not limiting, has been previously demonstrated (Wong, Cowan et al. 1979). Moreover, it has been shown that the stomatal response towards an environmental stimuli such as light, is much slower than the photosynthetic response towards the same stimuli (Pearcy 1990). Thus, the slow movement of stomatal opening under a light stimuli will limit photosynthesis assimilation by limiting CO_2 uptake. In addition, the slow movement of stomatal closure under a dark stimuli, represents a big decrease in WUE that arises because photosynthesis is reduced, yet there remains an unnecessary loss of water through the stomatal pore,

Thus, one opportunity for improving WUE is through the manipulation of the speed of stomatal response to bring the stomatal conductance in close concordance with the mesophyll CO_2 demand. The idea of manipulating the kinetics of the stomatal response is not new (Lawson, Kramer et al. 2012) and experimental evidence is to hand demonstrating the potential impact on carbon gain and water loss depending on the speed of the stomatal movement, especially to light (Lawson and Blatt 2014). Due to the mechanisms that allow stomatal movements are known, it should be possible to manipulate these mechanics genetically. However, first it is necessary to know what combinations of guard cell manipulations are important to manipulate stomatal kinetics, and therefore achieve improvements on photosynthesis and WUE. Nevertheless, changing the guard cells kinetics still remains a big challenge due to the huge complexity of the guard cells transporters.

Wang *et al* (2014) realised a series of experiments using the OnGuard model to find out which parameters may be modified from the different transporters in order to manipulate the kinetics of the guard cells. They did simulations to check the sensitivity to changes on different parameters, which could be tractable through genetic manipulation of the different transporters. Their results suggest that manipulating the different transporters populations had no effect on the kinetics of the guard cells. In contrast, they show that manipulating the gating of the transporters, mostly of the K^+ channels, may have an effect on the stomatal kinetics. Supporting this data there is a paper from Wang et al (2014b) showing that overexpression of H^+-ATPase in the plasma membrane of the guard cells is not affecting the kinetics but the dynamic range of the stomatal movements. This second, experimental study shows an increase in photosynthesis due to the enhanced opening of the stomata, supporting the data of Wong *et al* (1979) which links a stomatal conductance to a photosynthetic assimilation. In any case, increasing the amount of functional H^+-ATPases proportionally increases the ATP consumption by the plant, having a negative effect on plant efficiency. Instead, changing the gating properties of the channels will not represent an extra energetic cost for the plant.

So far all the attempts on manipulating the population of the guard cells transporters have failed, either because they have no effect on stomatal behaviour or because they are sensitive to the same regulation pathways. Further experiments should focus on manipulating the gating properties of the different membrane transporters instead of manipulating its number. Facing the difficulties to change the kinetic properties of the stomata, it must be evaluated the use of novel synthetic pumps in order to enhance photosynthetic assimilation, as well as WUE, without changing the overall properties of transport.

1.4 Synthetic biology: engineering membrane transport

Synthetic biology comprises the combination of science and engineering to design and build new biological functions and systems. The synthetic biology terminology is quite recent, and was introduced only in 1980 by Barbara Hobom, and again in 2000 by Eric Kool (Benner and Sismour 2005). To date, the majority of work has centred on bacterial systems and more recently has been extended to eukaryotes. The principles are the same, however: to combine the modules of nature into new ways and to build new modules that lead to novel functionalities (Liu and Stewart 2015).

Synthetic biology has yet to be applied in crop improvement in order to satisfy the human needs, but the potential is obvious. Not only could it provide an opportunity to create plants with higher photosynthesis or/and WUE, thus increasing plant biomass, but the techniques might also be used to create plants with a wide range of other characteristics. For example, synthetic approaches could have a great importance in engineering plants to generate specific organic compounds such as carotenoids (Fraser, Enfissi et al. 2009) which are of a great importance in human health. Synthetic biology also has an infinity of applications in other organisms such as bacteria, yeast, algae and cyanobacteria (Wang, Wang et al. 2012b). For example, by using synthetic biology it has been possible to engine *Saccharomyces cerevisiae* yeast capable to produce high levels of artemisinic acid for the production of antimalarial drugs (Ro, Paradise et al. 2006). Similarly, the bacteria *Escherichia coli* has been engineered to

produce high alcohols from glucose, thus enhancing the biofuel production as a renewable carbon source (Atsumi, Hanai et al. 2008).

Synthetic biology is a very powerful field with lot of potential still to be exploited. To date, it has contributed directly to progress in constructing materials, producing energy, and providing food to improve health, among other utilities. However, the pace of synthetic biology remains very slow, possibly because it requires a big investment in time and money, and because our knowledge of biological systems and the complexity of engineering them remain major hurdles (Endy 2005).

1.4.1 Taking advantage of optogenetics

Optogenetics is one branch of synthetic biology and is a new technology. It relates to the expression, in targeted cells, of specific genes codifying for light-sensitive proteins, and the use of light to promote the function of these proteins in order to alter the cell behaviour (Pastrana 2011).

Optogenetics owes its origin to the idea of Francis Crick in 1979 to use light as a tool for activating and deactivating specific brain cells (Deisseroth 2011), and practically it finds roots in the early 1970's when bacteriorhodopsin was first discovered to be a light-activated ion pump (Oesterhelt and Stoeckenius 1971). A few years later halorhodopsin was identified (Matsuno-Yagi and Mukohata 1977), and in 2002 the channelrhodopsin group of proteins was also discovered (Nagel, Ollig et al. 2002), all of them light-activated proteins that combine a light-sensitive domain together with an ion channel or pump (Figure 1.8).

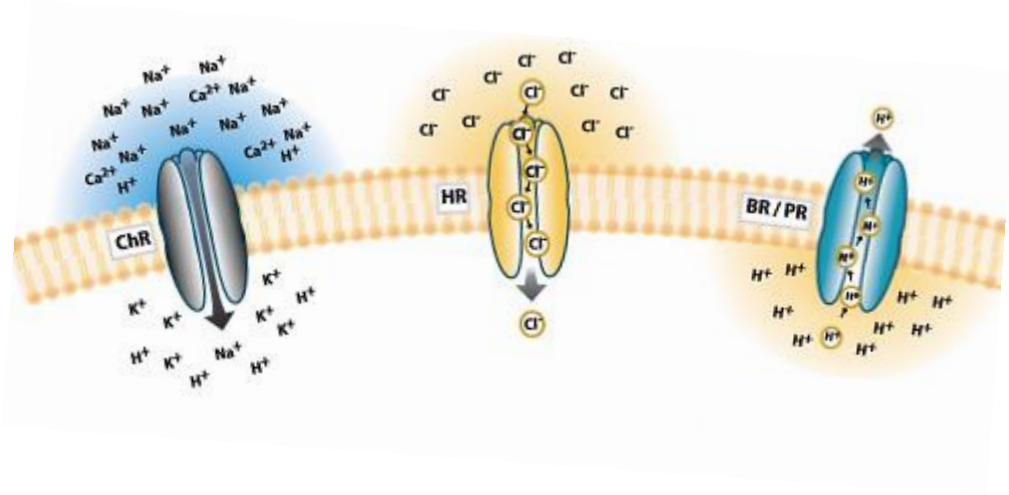

Figure 1.8. Schematic representation of channelrhodopsin, ChR (left) which acts as a light-sensitive ion channel, and halorhodopsin, HR (middle) which acts as a light-sensitive Cl^- pump, both proteins transport ions from the extracellular space to the cell cytosol; and bacteriorhodopsin, BR (right) which acts as a light-sensitive pump that transport the protons form the cytoplasm to the extracellular space. Image taken from a previous publication (Yizhar, Fenno et al. 2011).

By 2010 all of the three proteins were shown to be capable of activating and deactivating neurons in response to light (Deisseroth, Feng et al. 2006, Aravanis, Wang et al. 2007). Much as was originally envisaged by Crick, optogenetics combines new technologies of genetic and optical methods to turn neurons “on and off” in a monitored and control manner. To date, optogenetics has been mostly used to control the membrane voltage of the cells, thus controlling the activity of the different electrically-active ion channels. However, the use of optogenetics can be wider, to the extension of using it to manipulate transport ion fluxes. This idea opens a new range of possibilities in the synthetic biology field. However, the use of optogenetics to manipulate transport is an added challenge, as the inputs required to manipulate ion fluxes is orders of magnitude higher than that required to change membrane voltage.

The three proteins, halorhodopsin, bacteriorhodopsin and channelrhodopsin are seven-transmembrane proteins encoded by opsin genes. All the three proteins are each covalently bind to a retinal molecule (vitamin A-related organic cofactor) and require this adduct to be functional. The retinal molecule is essential for the light absorption and it also plays a major role in the function of the protein. The retinal chromophore isomerises with the absorption of a light photon, driving it to change the

protein conformation and enabling ions to cross from one site to the other site of the membrane (Fenno, Yizhar et al. 2011).

The amino acid sequence of halorhodopsin compared with the one of bacteriorhodopsin reveals a 36 % structure homology of transmembrane domains and 19 % structure homology in the connecting loops (Blanck and Oesterhelt 1987). However, some of the differences amongst the amino acid sequences determinate the differences on ion selectivity between the two proteins. In bacteriorhodopsin the residue Asp^{85} acts as the H^+ acceptor from the Schiff base and initiates the photoreaction cycle. However, in halorhodopsin a Thr replaces Asp85 and, in fact, mutating the Asp for Thr in bacteriorhodopsin gives the protein the ability to transport a Cl^- molecule (Sasaki, Brown et al. 1995).

1.4.2 Halorhodopsin-AE1 coupled transport in the chloroplast

A group of researchers from the United Kingdom and the United States are working together in a synthetic biology project called MAGIC (Multiple Approaches to Gain Increased Carbon Dioxide), started in 2011 out of the NSF/BBSRC Ideas Laboratory in 2010. The aim of the project is to build a CCM mechanism in C_3 plants by the use of optogenetics as a novel strategy to modify ion transport.

The MAGIC project is divided between two main goals, both necessary to increase the amount of CO_2 available for Rubisco. The first goal is to drive an increase of bicarbonate (HCO_3^-) inside the chloroplasts, which will be converted to CO_2 by the enzyme CA. The second goal is to retain the CO_2 where the Rubisco is localised long enough for Rubisco to be able to fix it. Thus, in order to increase the HCO_3^- inside the chloroplasts the researchers proposed a “two-stage pump” in the inner envelope of the chloroplasts placing in series a transport mechanisms to concentrate HCO_3^- in the chloroplasts powered by the halorhodopsin of *Natronomonas pharaonis* (NpHR). This two-stage strategy was expected to maximise the CCM gain driven independently with light energy absorbed by NpHR. NpHR would be used to establish a Cl^- gradient across the chloroplasts inner envelope and this Cl^- gradient would then be used by coupling its flux with a Cl^-/HCO_3^- antiport such as the human anion exchanger AE1 to

concentrate HCO_3^-. Overall, this strategy was expected to raise the concentration of CO_2 at the site of carboxylation of Rubisco. The project also introduced a parallel strategy to redesign NpHR in order to pump HCO_3^- directly and to manipulate the wavelengths of lighted needed so as to avoid light energies necessary for photosynthesis.

The second goal of the MAGIC project is to retain the concentrated CO_2 released from CA by the use of artificial scaffolds for substrate channelling within the chloroplasts. Because CO_2 has a very high rate of diffusion whereas the turnover rate of Rubisco is extremely slow, it is necessary to build mechanisms to retain CO_2 close to the carboxylation site of Rubisco for a long enough time for the Rubisco to capture and fix it.

1.4.2.1 Halorhodopsin of *Natronomonas pharaonis* (NpHR)

The halophilic archaebacteria *Natronomonas pharaonis* was first isolated from soda lakes in Kenya and Egypt, whose pH is around 10.5 and 11. Like other halobacteria*, N. pharaonis* contains halorhodopsin, a seven-helix transmembrane protein found in the cytoplasmic membrane. Halorhodopsin acts as an inward directed light-driven Cl^- pump, with a light absorption wavelength within the visible region, of approximately 588 nm (Schobert and Lanyi 1982).

The NpHR, like other rhodopsins, carries a retinal as a chromophore, which is indispensable for the activity of the protein. Photoisomerisation of the all-trans retinal to 13-cis retinal (Figure 1.9) initiates the transport cycle, allowing the movement of a Cl^- ion molecule across the membrane from the extracellular medium into the cytosol (Figure 1.10). NpHR has a single Cl^- binding site that is closely associated with the retinal moiety (Essen 2002), but the protein is relatively poorly selective among anions and not only transports Cl^- but also has the ability to transport nitrate (Duschl, Lanyi et al. 1990). It has also been shown the ability of NpHR to transport protons in opposite direction when an azide is bound in the chloride binding site of the pump (Váró, Brown et al. 1996). Thus, demonstrating the small photochemical difference between bacteriorhodopsin and halorhodopsin.

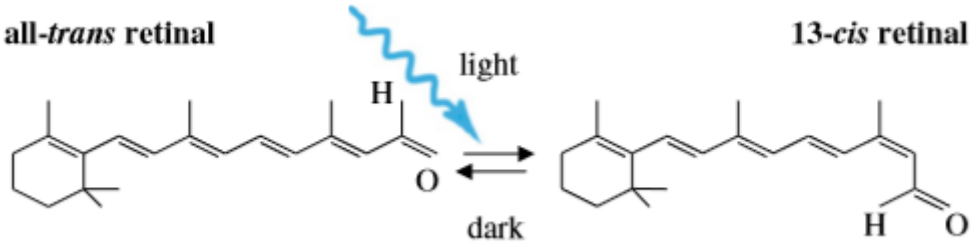

Figure 1.9. Photoisomerisation of all-trans retinal to 13-cis retinal when illuminated by light. Image taken from a previous publication (Wong, Abilez et al. 2012).

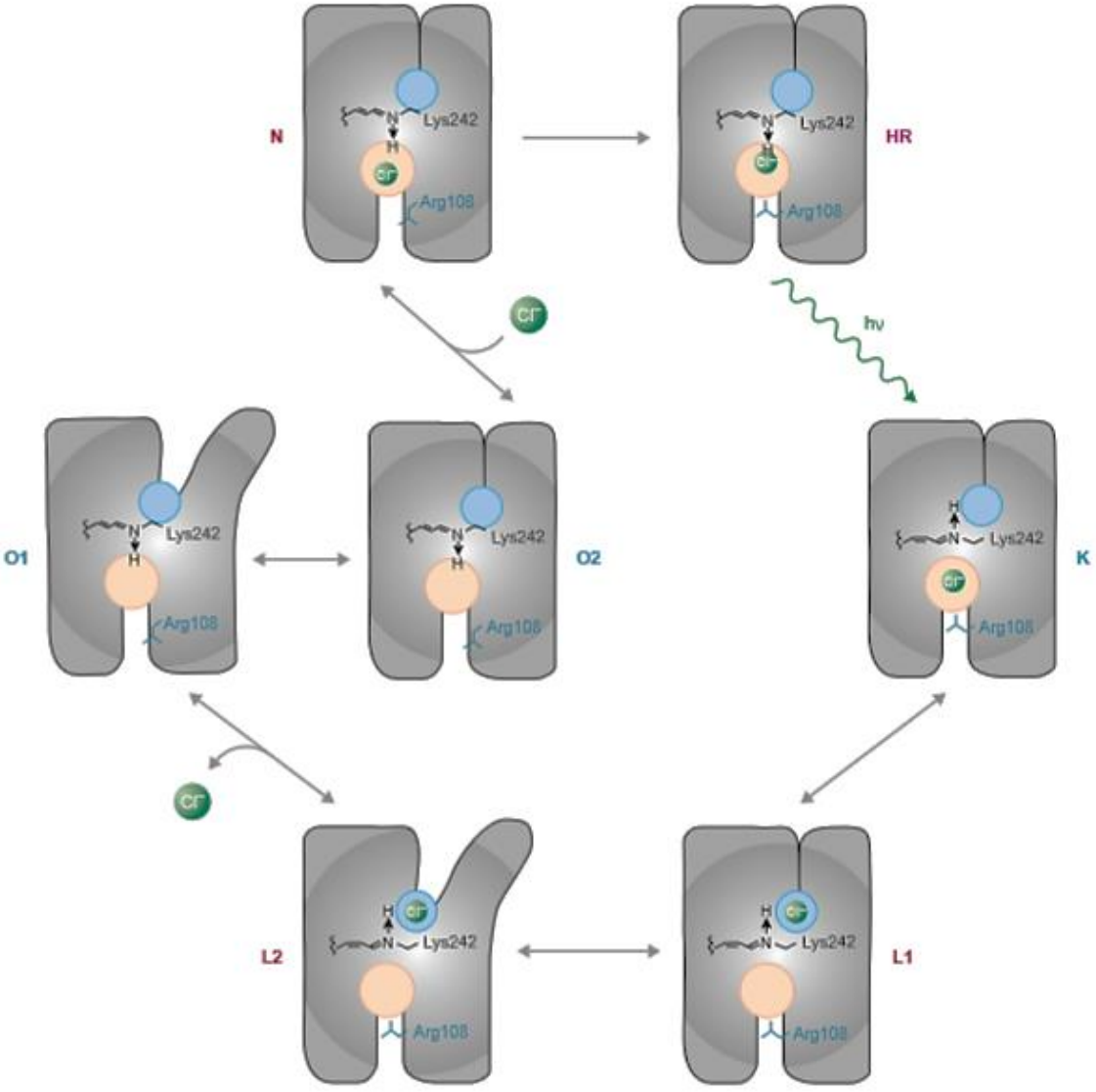

Figure 1.10. Scheme of the different intermediate states from the photocycle of halorhodopsin. The retinal of the protein in the HR state (top left) is photoisomerisated changing from all-trans to 13-cis (K state). The transition to the L states reflects the

movement of the Cl^- molecule from its transport site (orange) to the cytoplasmic release site (blue), and it takes place the opening of the cytosolic pathway. From L to O states there is the release of the Cl^- molecule to the cytoplasm and the retinal molecule reisomerises. During the O states the protein changes its conformation to allow the closure of the cytosolic pathway. From the O to N states the Cl^- molecule is reuptaken into the transport site. Image taken from a previous publication (Essen 2002).

The NpHR transports Cl^- against its electrochemical gradient and will generate a negative membrane voltage inside the cell, which in turn supports ATP synthesis. Electrophysiological experiments in oocytes of *Xenopus laevis* have provided data on the energetic coupling of light with transport. Best estimates, obtained by extrapolating the current-voltage curves of halorhodopsin to the voltage axis, indicate that the pump is at equilibrium when membrane voltage reaches negative values close to -400 mV (Seki, Miyauchi et al. 2007). This figure is consistent with the movement of one Cl^- ion for each photochemical cycle.

When expressing NpHR in mammalian neurons it is not necessary to add an exogenous chemical cofactor as a chromophore, because mammalian cells have sufficient levels of all-trans retinal (Zhang, Wang et al. 2006). However, it may be necessary to add all-trans retinal for the correct function of the protein when expressing NpHR in non-mammalian systems.

1.4.2.2 Human anion exchanger1 (AE1)

The anion exchanger 1 (AE1), also called band 3 protein, is the most abundant integral membrane protein in the erythrocyte membrane of humans and other mammals. It functions as an anion antiporter, catalysing the electroneutral exchange of Cl^- for HCO_3^- across the plasma membrane (Kopito 1985, Lux, John et al. 1989). Due to its abundance and physiological importance it has been very well studied. AE1 comprises two different domains with different functionalities, the N-terminal cytosolic domain is involved in cytoskeletal interactions and the C-terminal membrane domain is responsible of the anion exchange activity. The N-terminal portion is hydrophilic and extends to the cytoplasm where it has multiple binding functions, but is not involved in the anion exchange activity of the protein, thus the removal of this part is not affecting

transport activity (Grinstein, Ship et al. 1978). The C-terminal portion is a hydrophobic transmembrane region and is where the function of the anion exchanger entirely resides (Kopito 1985, Lux, John et al. 1989, Sahr, Taylor et al. 1994).

2. Aim of the thesis

The research explored in this thesis sought to find solutions facing food security. The general objective of this thesis was to develop synthetic biological solutions that might aid in increasing photosynthetic yields and water use efficiency of plants, thereby improving crop yields.

I pursued two different approaches with the common goal of improving plant photosynthesis and WUE. The first approach was part of the MAGIC project, an international consortium funded by the US National Science Foundation (NSF) and the UK Biotechnology and Biological Sciences Research Council (BBSRC). This approach aimed to increase plant photosynthesis by engineering a CCM in the chloroplasts of a C_3 plant in order to reduce the oxygenase activity of Rubisco. The second approach was directed to increase plant water use efficiency by the manipulation of stomatal kinetics, in order to bring stomatal apertures in better temporal concordance with the mesophyll demand for CO_2. The novel characteristic of both approaches was the use of synthetic technologies – sometimes referred to as optogenetics –as a tool to power artificial transport systems in different cell membranes.

Approach 1

My role in the MAGIC project was to elaborate an artificial transport system in the inner envelope of the chloroplasts that could be used to increase the levels of HCO_3^- in the chloroplasts stroma. To this end, the light driven pump halorhodopsin from *Natronomonas pharaonis* (NpHR) was chosen and had to be targeted to the inner envelope of the chloroplasts with the aim to establish a Cl^- gradient across the chloroplast inner envelope. The human anion exchanger AE1 was then to be introduced, also in the inner envelope of the chloroplasts, to allow an exchange of Cl^- per HCO_3^-, thus powering an increase in HCO_3^- in the chloroplasts stroma.

My first goal was to get expression of the bacterial NpHR and the human AE1 proteins in plants and to target them to the chloroplast inner envelope. In addition, a third protein had to be incorporated to the system (bCMO1), in order to provide necessary retinal for the proper activity of NpHR. The second goal was to check for protein

activity and to generate stable Arabidopsis lines. Finally, gas exchange measurements had to be carried out to test the effects of the proteins at the whole plant level.

Approach 2

I followed two different strategies in order to modify stomatal kinetics. The first strategy centered on the manipulation of the gating properties of the guard cell K_{in} channel, KAT1. The second focused on the incorporation of an external pump, NpHR, in the guard cell plasma membrane and tonoplast. To gain insights into the likely behaviours in each case, I made use of the OnGuard platform to simulate *in silico* both strategies and check for the effects on ion transport and stomatal behaviour.

Constructs expressing KAT1 and KAT1 mutants with modified gating properties had to be created, as well as constructs expressing NpHR in the plasma membrane and the tonoplast of the guard cell. All of the proteins had to be expressed under the expression of a specific guard cell promoter. Furthermore, Arabidopsis plants transformed with the different constructs had to be made in order to check for gas exchange measurements and to compare the results obtained with the model predictions.

3. Table of performed experiments

Table 3.1. Summary of the different experiments performed.

Chapters	**Proteins involved**	**Performed experiments**
Engineering CCM in chloroplasts	Primary: NpHR, AE1 Secondary: bCMO1	- Cloning for proteins expression in the inner envelope of the chloroplasts or stroma. - Confocal imaging to corroborate the correct localisation of the proteins - Obtaining stable lines of Arabidopsis transgenic plants - Gas exchange measurements on the transgenic plants
Manipulating stomatal kinetics	Primary: KAT1 $KAT1^{D105E}$ $KAT1^{D102W}$	- Simulate the effects of KAT1 $V_{1/2}$ modifications by OnGuard modelling - Cloning for expression of KAT1 and its mutants in the guard cells - Obtaining stable lines of Arabidopsis transgenic plants - Gas exchange measurements on the transgenic plants
	Primary: NpHR Secondary: AHA2	- Simulate the effects of guard cell NpHR expression by OnGuard modelling - Cloning for NpHR expression in plasma membrane - Confocal imaging to corroborate the correct localisation of the NpHR in the plasma membrane - Obtaining stable lines of Arabidopsis transgenic plants

4. Materials and methods

All the chemicals used in this thesis were purchased form Sigma Aldrich (Poole, UK), VWR International (Poole, UK) or Fisher Scientific (Southampton, UK) unless otherwise stated. All the enzymes used for molecular biology experiments were purchased either from Invitrogen (Life Technologies, Paisley, UK), New England Biolabs (NEB, Hitchin, UK), or Promega (Madison, USA). All the customised primers were purchased from Invitrogen.

4.1 Buffers, Solutions and Reagents

Table 4.1. Table of buffers, solutions and reagents used in molecular biology, chloroplasts isolation and plant biology in this research.

Molecular Biology	
LB Medium	1% tryptone, 0.5% yeast extract, 1% NaCl, pH7.5 (1.5% bacto agar for plates)
Solution-1 (Resuspension Buffer)	50mM Tris-HCl (pH 8), 10mM EDTA, 100 µg ml^{-1} Rnase A, 0.01% lysozyme
Solution-2 (Lysis Buffer)	200mM NaOH, 1%SDS
Solution-3 (Neutralisation Buffer)	3M potassium acetate (pH 5.5 with acetic acid)
TE Buffer (Elution Buffer)	10 mM Tris-HCl, 0.1 mM EDTA, pH 8.5
10x SDS Running Buffer	25mM Tris, 250 mM glycine, 0.1% SDS
50xTAE stock solution	2 M Tris, 5.7 % acetic acid, 50 mM EDTA
TB solution	85 mM $CaCl_2$/15% glycerol
6x Loading Buffer	0.25 % bromophenol blue, 0.25 % xylene cyanol, 15 % ficoll
Sterilisation solution	70 % ethanol, 0.01 % Triton X-100
Lower Buffer (4x)	1.5 M Tris pH 8.8, 6 M HCl, 0.4 % SDS
Upper Buffer (4x)	0.5 M Tris pH 6.8, 6 M HCl, 0.4 % SDS, bromophenol blue

Homogenisation Buffer (HB Buffer)	50 mM Tris-HCl pH 7.4, 500 mM Sucrose, 10 % Glycerol, 20 mM EDTA, 20 mM EGTA, 50 mM NaF, 10 mM Ascorbic acid, 5mM DTT
Electrophoresis Running Buffer (10x)	121.4 g Tris pH 8.3, 567 g Glycine, 40 g SDS water up to 4 L
Bijerrums Buffer	6.1 g/l Tris, 2.4 g/l Glycine, 20 % Methanol
TBS Solution	8 g/l NaCl, 3 g/l Tris pH 7.4 with HCl
DYE buffer with DTT (4x)	8 % SDS, 10x DTT 1 M, 30 % Glycerol, 1 M Tris pH 6.8
Ponceau S Solution	2 g/l Ponceau S, 5 % acetic acid
Blocking solution	5 % milk powder (Marvel, Iceland, UK) in TBS solution
Antibody solution	Antibody in TBS Solution, 2 % blocking agent
Chloroplast isolation	
1x Chloroplast Isolation Buffer (CIB) without BSA	0.33 M Sorbitol, 1 M Tris-HCl pH 7.8, 1 M $MgCl_2$, 200 mM EDTA-NaOH pH 7.8
1x Chloroplast Isolation Buffer (CIB) wiht BSA	0.33 M Sorbitol, 1 M Tris-HCl pH 7.8, 1 M $MgCl_2$, 200 mM EDTA-NaOH pH 7.8, 0.1 % BSA
Plant biology	
Infiltration Medium	10mM $MgCl_2$, 100 µM Acetosyringone
BASTA plates	MS medium 2.2 g/l, 1 % Agar 10 g/l, 1:1000 BASTA

Table 4.2. Table of antibiotics used in this research

Antibiotic	Final working concentration (mg/l)
Ampicillin	100
Gentamycin	20
Kanamycin	25
Rifampicin	50
Spectinomycin	100
Streptomycin	10

4.2 Bacterial growth and transformation

4.2.1 Preparation of *E. coli* TOP 10 and ccdB resistant chemical competent cells

A frozen 100 µl aliquot of chemical competent TOP10 cells or ccdB resistant cells was inoculated into 5 ml LB medium containing Streptomycin and grown in a shaking incubator at 180 rpm, 37°C overnight. The 5 ml overnight culture was inoculated into 500 ml LB medium containing Streptomycin and grown in a shaking incubator at 180 rpm, 37°C for approximately 3 hours until the OD_{600} reached 0.3-0.4. The bacterial culture was centrifuged for 5 min at 4000 rpm, 4°C, the supernatant was discarded. The cell pellet was carefully resuspended in 20 ml sterile 100 mM $MgCl_2$ and the centrifugation step was repeated. The supernatant was discarded, the bacterial pellet was resuspended in 50 ml sterile 100 mM $CaCl_2$ and the centrifugation was repeated. Finally, the bacteria pellet was resuspended in 10 ml of sterile TB solution. The final bacterial culture was kept in 100 µl aliquots, frozen into liquid nitrogen and stored in -80°C.

4.2.2 Transformation of chemical competent E.coli by heat shock

A 100 µl chemical competent *E.*coli cells aliquot was taken out from the -80°C freezer and thawed on ice for 5 min. 5 µl of a 150 ng/µl DNA plasmid were added into the cells aliquot and incubated on ice for 10 min. The cells were transformed via the heat shock procedure by incubation of 45 sec in a 42°C water bath. 400 µl of LB Medium were added into the aliquot to allow cells growth and it was incubated for 1 hour in the shaker incubator at 180 rpm, 37°C. After incubation the cells were spin down at maximum speed for 15 sec. 400 µl of supernatant were discarded and the pellet was resuspended with the remaining 100 µl of supernatant. The cells were plated on a LB agar plate containing the corresponding antibiotic. The plate was incubated at 37°C overnight.

4.2.3 Preparation of *Agrobacterium tumefaciens* chemical competent cells

A frozen 200 µl aliquot of chemical competent *A. tumefaciens* cells, agro-strain GV3101-pMP90-RK, was inoculated into 20 ml of LB medium containing the antibiotics Rifampicin, Gentamycin and Kanamycin. The culture was incubated in the shaker at 180 rpm, 28°C overnight. The overnight 20 ml culture was inoculated into 500 ml of LB medium containing those three antibiotics mentioned previously and incubated for 4-6 hours at 180 rpm, 28°C until the OD_{600} was 0.5-0.7. The cells were centrifuged for 10 min at 4000 rpm, 4°C. The supernatant was discarded, the pellet was resuspended in 100 ml 0.15 M $NaCl_2$ and the centrifugation was repeated. Bacterial pellet was resuspended in 10 ml 20 mM ice-cold $CaCl_2$. The final competent cells were kept in 200 µl aliquots, frozen into liquid nitrogen and stored at -80°C.

4.2.4 Transformation of *A. tumefaciens* by heat shock

A 200 µl *A. tumefaciens* cells aliquot frozen at -80°C was thawed at room temperature for 5 minutes. 2-5 µl of a 150 ng/µl DNA plasmid were added into the aliquot and it was incubated on ice for 5 min. It was merged into liquid nitrogen for 5 min and incubated in the 37°C water bath for another 5 min as a heat shock to transform the DNA into the *Agrobacterium* cells. 800 µl of LB medium were added to allow cells growth and it was incubated for 2 hours in the shaker at 180 rpm, 28°C. The cell culture was centrifuged at full speed for 30 sec, 850 µl of supernatant were discarded and the pellet was resuspended in the remaining 150 µl of supernatant. The cell culture was plated on an LB agar plate containing Rifampicin, Spectinomycin and Gentamycin. The plate was covered with parafilm and incubated for 2 days in the incubator at 28°C.

To keep transformed *Agrobacteriu*m glycerol stocks, few colonies were picked from the *Agrobacterium* plate after the 2 days incubation, and were inoculated in 4 ml of LB medium containing the selected antibiotics. The cell cultures were grown overnight in the shaker at 180 rpm, 28°C. 930 µl of each cell culture was mixed with 70 µl of 100 % glycerol and kept at -80°C. The rest of the cell culture was used for DNA verification,

just the cultures containing the correct plasmid were kept and the others were discarded.

4.3 Molecular Biology

4.3.1 Primers design, ordering and preparation

For the primers design the annealing temperature was calculated using the NetPrimer Analysis Software (http://www.premierbiosoft.com/netprimer/), whcich uses the nearest neighbour thermodynamic theory and gives an accurate primer melting temperature. Editseq from DNASTAR was used for the primer design and Vector NTI was used to check for the correct gene sequence. The primers were purchased from Invitrogen. Once the primers were received the DNA was diluted with double distilled water to make 100 µM stock aliquots. 100 µl of 10 µM working aliquots were prepared and kept at -20°C. The different primers used for this research are listed in the annex.

4.3.2 PCR reaction

All the PCRs were performed with the KOD Hot Stat DNA Polymerase (Novagen, USA). The dNTP mixture (2 mM of each NTP), 10x Reaction Buffer and MgSO2 solution (25 mM) were provided from the manufacturer together with the KOD Hot Start DNA Polymerase. The set-up of PCR reaction is showed in the Table 4.3. PCR reactions were prepared in 0.2 ml standard thin-walled PCR tubes. The PCR reaction mix was prepared and kept on ice until the lid of the Thermal Cycler (96 Universal Gradient, peqSTAR, peqlab, UK) was preheater to 100°C. The program was paused until insertion of the tube containing the PCR reaction mix. The typical cycling conditions used depended on the type of PCR used, one-step PCR (Table 4.4) for the direct amplification of an entry clone from a DNA template, or two-step PCR (Table 4.5) which allowed to link together two different DNA template fragments to create the entry clone desired.

Table 4.3. Set-up for one-step and two-step PCR reaction

Component	**µl added/reaction**
Distilled water	To 50
10x Reaction Buffer	5
$MgSO_4$	3
dNTP	5
DMSO	2.5
KoD	1
Sense primer	1.5
Antisense primer	1.5
Template	1
Template 2 (for 2 step PCR)	1

Table 4.4. Settings of one-step PCR reaction

Frequency	Step	Temperature (°C)	Time (sec)
1x	Initial denaturation	95	120
35x	Denaturation	95	20
	Primer annealing	58	10
	Primer extension	70	20
1x	Final extension	70	120
1x	Final temperature	4	∞

Table 4.5. Settings of two-step PCR reaction

1st PCR

Frequency	**Step**	**Temperature (°C)**	**Time (sec)**
1x	Initial denaturation	95	120
35x	Denaturation	95	20
	Primer annealing	58	10
	Primer extension	70	20
1x	Final extension	70	120
1x	Final temperature	4	∞

2nd PCR

Frequency	Step	Temperature (°C)	Time (sec)
1x	Initial denaturation	95	120
35x	Denaturation	95	20
	Primer annealing	56	10
	Primer extension	70	90
1x	Final extension	70	120
1x	Final temperature	4	∞

4.3.3 PCR purification

Purification of PCR products was done with the PureLink® Quick PCR Purification Combo Kit protocol from Invitrogen. All the buffers, spin columns and wash tubes were provided from the manufacturers. To start, 4 volumes of Binding Buffer were added to 1 volume of PCR reaction. The mixture was added into a spin column inside a wash tube, and centrifuged at room temperature and 10000 g for 20 seconds. The flow through was discarded and the spin column was replaced into the wash tube. 700 µl of Wash Buffer were added into the spin column and it was centrifuged again at 10000 g for 20 seconds. The flow through was discarded and the spin column was replaced into the wash tube. The spin column was centrifuged again at maximum speed for 3

minutes to remove any residual Wash Buffer, and the wash tube was discarded. The column was replaced into a 1.5 ml eppendorf tube and 50 µl of Elution Buffer were added into the center of the column. The column was incubated for 1-5 min at room temperature and centrifuged at maximum speed for 1 min, this step was repeated one more time. After the second centrifugation the 1.5 ml eppendorf tube contained the purified PCR product.

4.3.4 Plasmid Extraction and purification, and PEG purification

Four ml of selective LB Medium were inoculated with individual *E. coli* colonies, picked from selective LB plates, and grown overnight in the shaking incubator at 180 rpm, 37°C. The bacterial culture was sedimented by centrifugation at 15 K rpm for 30 sec and supernatant was discarded. The bacteria pellet was resuspended in 400 µl 4°C ice-cold Solution-1 and incubated at room temperature for 10 min. To extract plasmids through alkaline lysis, 400 µl of Solution-2 were added and mixed with the bacterial resuspension by inverting the tubes several times. After incubation at room temperature for 5 min, cellular debris and denatured chromosomal DNA was precipitated by addition of 400 µl ice-cold Solution-3 and centrifuged at 15 K rpm and 4°C for 10 min. 1 ml of the supernatant was transferred to a fresh tube, mixed with 1 ml Chloroform:Isoamylalcohol (24:1) and centrifuged at 15 K rpm, 4°C for 1 min. Centrifugation yielded an upper aqueous phase containing plasmid DNA and a lower organic phase. Nine hundred µl of the upper phase were transferred to a fresh tube and 900 µl ice-cold isopropanol were added in order to precipitate the DNA. DNA was pelleted by centrifugation at 15 K rpm, 4°C for 20 min and the supernatant was discarded. The pellet was washed in 70 % Ethanol and centrifuged as before. The pellet was air-dried for 10–20 min. If plasmid DNA was used for restriction analysis, the pellet was resuspended in TE Buffer and incubated at 70°C for 10 min. For PEG purification the DNA pellet was resuspended in 64 µl Tris-HCl (pH 8), 16 µl NaCl and 80 µl 14% PEG8000, and incubated at 4°C for 10–20 min. The DNA was centrifuged at 15 K rpm and at 4°C for 20 min, the supernatant was carefully discarded using pipette and the pellet was washed wit 70 % ethanol as before. The air-dried pellet was resuspended in 50–100 µl TE Buffer. Plasmid preparations were stored at -20°C.

4.3.5 Restriction enzyme digest

PCR products and DNA plasmids were digested with restriction enzymes obtained from NEB (New England BioLabs). The analysis was performed with appropriate buffers according to manufacturer's instructions. All digests were carried out in a total volume of 20 µl, the standard set-up for a restriction digest is shown in Table 4.6. Double digestions were performed with two enzymes that were able to work efficiently in the reaction buffer according to the Double Digest Finder of NEB (https://www.neb.com/tools-and-resources/interactive-tools/double-digest-finder). Restriction digest reactions were incubated at 37°C for 1 hour and analysed by agarose gel electrophoresis.

Table 4.6. Set-up of a standard restriction digest reaction.

Reagent	**Quantity (µl)**
Double distilled H_2O	16.5
10x buffer	2
DNA	1
Enzyme 1	0.25
Enzyme 2	0.25

4.3.6 Agarose gel electrophoresis

The products of PCR and restriction enzyme digests were resolved by agarose gel electrophoresis. The DNA sample was mixed with 6x Loading Buffer. For fragments between 400 and 3000 bp a 1.5 % agarose gel was used. For the preparation of the agarose gel, 1.5 % agarose powder was mixed with 1xTAE solution and 50 µl/l ethidium bromide solution. The agarose gel was run into a tank filled with 1xTAE solution and run at 100 to 140 V for approximately 45 min. The DNA bands were visualised under UV light on a GelDoc 2000 scanner (Bio-Rad).

4.3.7 Gel extraction and purification

To extract DNA from the agarose gel, the band of interest was cut from the gel under UV light. The DNA extraction and purification of the gel was done according to the PureLink® Quick Gel Extraction and PCR Purification Combo Kit protocol from Invitrogen (Life Technologies, Paisley, UK). All the buffers, spin columns and wash tubes were provided by the manufacturer. The gel was weighted and 3 volumes of Gel Solubilisation Buffer were added for every 1 volume of gel. In cases in which agarose gels with a higher concentration of agarose than 2 % (w/v), 6 volumes of Gel Solubilisation Buffer were added for every 1 volume of gel. The mixture was incubated at 50°C in a heat block for at least 10 min until the gel was completely dissolved. After the gel was dissolved, it was incubated in the same conditions for 5 additional minutes. The dissolved gel mixture was pipetted into the center of a spin column inserted in a wash tube. The column was centrifuged at 10 K rpm for 20 sec. The flow through was discarded and the column was replaced into the wash tube. 700 µl of Wash Buffer were added to the spin column and centrifuged again at 10 K rpm for 20 sec. The flow through was discarded and the spin column was reintroduced into the wash tube. The spin column was centrifuged for 3 min at maximum speed to remove any residual Wash Buffer. The wash tube was discarded and the spin column was placed into a 1.5 ml Eppendorf tube. 50 µl of Elution Buffer were added to the center of the spin column and the mixture was incubated at room temperature for 1-5 min. The spin column was centrifuged at 10 K rpm for 1 min. The purified DNA was remaining in the 1.5 ml Eppendorf tube and the spin column was discarded.

4.3.8 DNA quantification and sequencing

DNA concentration was determined by spectrophotometry (BioPhotometer plus 6132, Eppendorf, Germany). The absorbance was measured in optical density units of a suitable dilution in distilled water at 260 nm. A 50 µl UVette 220-1600 nm single sealed cuvette (Eppendorf, Germany) was used. The absorbance value was corrected against a distilled water blank and multiplied with the dilution factor 50 to obtain DNA concentration in ng/µl. The DNA plasmids were send to GATC for sequencing (GATC

Biotech, Germany) for the correct verification of the construct. The sequencing data received from GATC was analysed with the SeqMan (part of the DNASTAR software).

4.3.9 DNA ligation reactions

Ligation reactions of DNA with sticky and blunt ends were carried out with T4 DNA ligase (NEB, Hitchin, UK). Reactions were set up as instructed by the manufacturer. The 10x Ligase buffer was stored in small aliquots to avoid degradation of its ATP content. It was commonly used an insert:vector ratio of 6:1, adaptable to the circumstances. Incubations were at room temperature for 3-4 hours, or overnight at 4°C. The ligation reaction product was used for bacterial transformation.

4.3.10 Gateway cloning

Gateway™ technology (Life Technologies, Paisley, UK) was used to clone some of the DNA sequences. This technology is based on the bacteriophage lambda site-specific recombination system, which facilitates the integration of lambda into the *E. coli* chromosome and the switch between the lytic and lysogenic pathways. Lambda-based recombination involves the DNA recombination sequences (*att* sites) and the proteins that mediate the recombination reaction (*i.e.* Clonase™ II enzyme mix). These specific sequences called *att* (attachment) sites are used to generate clones and to subclone into expression vectors. In lambda integration, recombination occurs between *att*B and *att*P sites to give rise to *att*L and *att*R sites.

The efficiency of the system lies in the use of a *Gateway™ cassette* that contains the toxic *ccd*B gene and a Chloramphenicol resistance gene in the gateway entry and destination vectors. Recombination removes this cassette from the vectors by cutting and replacing it with the gene of interest. Un-recombined vector, that still contains the *ccd*B gene, prevents growth in standard *E. coli* cells (Top10™, XL1blue™, DH5α™), providing a selection mechanism for transformed cells. To amplify the Gateway-cassette containing vectors are needed special *ccd*B-resistant *E.coli* cells and counterselected using chloramphenicol (*ccd*B-survival cells™).

4.3.10.1 BP reaction

For Entry clone generation, the BP-reaction, there is a recombination between the bacterial (B) attachment sites, called *att*B and the phagal (P) attachment sites, called *att*P creating an *att*L site (Figure 4.1). This reaction is catalysed by BP Clonase™ II enzyme mix.

Figure 4.1. Representation of a BP clonation. The *att*B parts from the PCR product attach to the *att*P sites from the donor vector to create an Entri clone with *att*L attachment sites.

Depending on the type of Entry clone desired it was selected the corresponding Donor vector from the Gateway technology. All the Donor vectors and Entry clones used are specified in the results chapters.

4.3.10.2 LR reaction

For Expression clone generation, the LR-reaction, there is a recombination between an *att*L substrate (Entry clone) with an *att*R substrate (Destination vector) to create an *att*B-containing expression clone (Figure 4.2). This reaction is catalysed by LR Clonase™ II enzyme mix. All the Destination vectors and Entry clones used for each Expression clone are specified in the results chapters.

Figure 4.2. Representation of a LR-reaction. Recombination between entry clone *att*L substrate and destination vector *att*R substrate to create and *att*B-containing expression clone.

4.4 Plant material and methods

4.4.1 Growth conditions of Nicotiana tabacum

Nicotiana tabacum plants were used in this study to get plant transient transformation with the desired proteins. Tobacco plants were grown in a growth room with long day conditions in a cycle of 16 hours light and 8 hours of darkness, light was supplied at 300 µmol m^{-2} s^{-1} starting at 8 am, temperature was 22°C and humidity was 60-70 %. Tobacco plants were 5-6 weeks old at the time of infiltration.

4.4.2 Transient Transformation of Nicotiana tabacum

Nicotiana tabacum plants were transformed with the *Agrobacterium*-mediated infiltration method. Firstly, a treatment on *Agrobacterium* cells was done before the transformation. 2 ml from an overnight culture of *Agrobacterium* transformed cells was spun down in the centrifuge at 8 K rpm for 3 min. Supernatant was discarded and 2 ml of Infiltration Medium was added to the pellet. The pellet was gently mixed with the Infiltration Medium solution and centrifuged again at same conditions; this step was repeated one more time. The supernatant was discarded and 1 ml of Infiltration Medium was added and gently mixed with the pellet. OD_{600} was established between 0.4 and 0.8 using the Infiltration Medium and the cells were incubated on ice for 3-4 hours before the infiltration.

Plants between 4-6 weeks old were chosen for the transformation. From 4 to 6 hours before the infiltration the plants were well watered. To infiltrate tobacco plants 1 ml syringes were used. The epidermis on the underside of 2^{nd} to 4^{th} youngest leaf was

grazed (1-2 mm) by a sharp tool. The Infiltration Medium solution containing the *Agrobacterium* suspension was injected into the abaxial epidermis of leaf by pressing the opening of the 1 ml syringe firmly to the wound. Plants were watered and returned back to the growth room. Expression was analysed 72 hours after infiltration.

4.4.3 Growth conditions of Arabidopsis thaliana

Arabidopsis thaliana plants were used in this study to generate stable transgenic lines by floral dipping. Arabidopsis seeds were sown onto the nutrient-rich Levington F2+S 3 compost (Coulders, Glasgow, UK), which was treated with Intercept 70 WG (Scotts, Ipswich, UK), a systemic insecticide. Plants were grown in a growth room on long day conditions with a cycle of 16 hours light and 8 hours of darkness, light provided at 300 µmol m^{-2} s^{-1} starting at 8 am, temperature was 22°C and humidity was 60-70 %. When the plants were 2-3 weeks old they were transplanted in 15 cm of diameter pots. The pots were filled with soil and covered with a mesh to avoid soil loses when proceeding with the floral dipping. In each pot around 10 plants were transplanted with the same separation distance from one to the other. Once the first stems from each plant were around 20 cm told they were cropped in order to increase and synchronise inflorescence. After 5 weeks of growth the inflorescence was ready for the floral dipping procedure.

4.4.4 Floral dipping transformation of Arabidopsis thaliana

Glycerol stocks of transformed *A. tumefaciens* cells were inoculated into 5 ml of LB medium with the corresponding antibiotics and it was grown in the incubator shaker at 180 rpm, 28°C overnight. The bacterial culture was inoculated into 300 ml of LB medium containing the corresponding antibiotics and incubated in the shaker at 180 rpm, 28°C for 4-5 hours until an OD_{600} around 0.8 was achieved. The bacteria were centrifuged at full speed for 10 minutes. The supernatant was discarded and the pellet was resuspended with 5 % sucrose to reach an OD_{600} between 0.4 and 0.6. A solution of 0.02 % Silwet L-77 (GE, Silicones, Friendly, USA) was added to the cell culture and the mix was poured into a final container used for the floral dipping procedure (Clough and Bent 1998). Each plant was dipped into the bacterial suspension for 1 min,

ensuring complete immersion of flower buds. Transformed plants were covered with a plastic bag overnight to increase the relative humidity around the recently transformed flowers. The procedure was repeated after 7 days of transformation for a maximum transformation efficiency. Once the stems had produced enough seeds they were tied together and left to dry. When the plants were dry it was possible to harvest the seeds, which were kept in a place with low humidity and darkness.

4.4.5 Arabidopsis thaliana seeds sterilization

Arabidopsis seeds were sterilised with 70 % ethanol and 0.01 % Triton X-100. All the procedure was done in sterile conditions under the hood. Around 200 seed were poured into a 1.5 ml Eppendorf tube. 1 ml of the sterilisation solution was mixed with the seeds for 10 minutes by gentle inverting. This sterilisation solution was removed carefully by pipetting, 1 ml of 100 % ethanol was added to the seeds and mixed by gently inverting for 10 min. The ethanol was discarded by pipetting carefully and the seeds were left 1 hour under the hood for air dry. After 1 hour sterile double distilled water was added to the seeds and kept in the fridge at dark and 4°C ready to be used.

4.4.6 Selection of transformed Arabidopsis thaliana plants

All the expression vectors used in the generation of stable transgenic Arabidopsis lines carried a BASTA resistance gene. The first generation of transformed seeds (T1) was sown densely onto soil in a 40x20 cm tray and kept in the dark at 4°C for 48 h to synchronise germination. Trays were moved into the growth chamber under long day conditions as mentioned before. After a period of 2 weeks the plants had their first pair of leaves and were ready for BASTA selection. The selection was done by spraying the plants with BASTA herbicide (1:1000 in H_2O, Bayer, Cropscience, Mannheim, Germany) approximately 4-6 times and the procedure was repeated every 3 days. The resistant plants were transferred to individual pots for growth and seed harvesting. Seeds for T2 and T3 generation were selected in the same manner. T4 generation seeds were selected under BASTA agar plates selection.

4.4.7 BASTA agar plates selection

Arabidopsis T4 generation seeds were selected in BASTA plates for a better recount of the plants that germinate, in order to verify the homozygote lines. All of this procedure was done under the hood in sterile material and sterile conditions. In each plate 100 seeds were sown distributed carefully separated the same distance one of the other. The seeds were sowed by carefully pipetting with a cut tip, to allow enough space for just one seed to be deposited in the plate each time. Once all the seeds were sown, the plates were sealed with tape and kept in a growth chamber with constant light (100 µmol m^{-2} s^{-1}) at 20ºC. After 3-4 weeks the plants grown in each plate were counted. Plants from non-homozygous lines were individually transplanted to soil and grown for seed harvesting. The same BASTA plate selection procedure was carried out on these plants.

4.4.8 Chloroplast isolation

Chloroplasts isolation was carried out on tobacco transiently-transformed leaves as well as stable *A. thaliana* plants. In both cases the protocol was the same. Approximately 30 g of leaf tissue were washed and cut in small pieces; the midrib veins were removed from tobacco leaves. The cut plant tissue was mixed in a blender together with 1xCIB Buffer with BSA and blended with 2-3 strokes. The blended mixture was filter through a 300 µm net and centrifuged at 200 rpm for 3 minutes. The white pellet obtained was discarded and the supernatant was centrifuged again at 4 K rpm for 7 min. The supernatant was discarded and the pellet was gently broken by tapping with a finger. The pellet was resuspended in 2 ml of 1x CIB Buffer with BSA and mixed gently by pipetting up and down. 6 ml of the chloroplast suspension were added very gently in the top of a 10 ml 40 % Percoll in 1x CIB Buffer with BSA layer. The suspension was centrifuged at 1.7 K rpm for 6 minutes. The intact chloroplasts appeared as a green pellet in the bottom of the tube, the broken chloroplast forming an upper layer in solution above. This upper layer of broken chloroplast was carefully removed by pipetting, leaving only the pellet containing the intact chloroplast. The pellet with the intact chloroplasts was resuspended in 1 ml of 1x CIB Buffer without BSA.

4.5 Western Blot analysis

4.5.1 Protein extraction from plant samples

All the plant tissues to be used for Western blot analysis were previously kept in the freezer at -80°C. For sample preparation, the plant tissue was taken out from the freezer, kept in dry ice and smashed. 200 µl of HB Buffer plus protease inhibitor (Roche Complete mini-EDTA free) was added to the smashed plant sample and it was suspended by vortexing. The mixture was kept on ice for 1 hour and vortexed again. The mixture was spun down at 3 K rpm for 0.5 min. The supernatant containing the sample was removed and transferred to a fresh 2 ml Eppendorf tube, the pellet was discarded. Two-hundred-fifty µl of DYE Buffer with DTT was added to the supernatant and the mix was sonicated. The final mixture was boiled at 70°C for 40 min and spin down at full speed for 2 min. The mixture was ready to be run into the SDS-PAGE gel or it could be stored at -20°C.

4.5.2 SDS-PAGE

SDS-PAGE (Sodium Dodecyl Sulphate Polyacrylamide Gel Electrophoresis) was used to separate proteins on acrylamide gels. It was used a mini gel format (Protean III, Bio-Rad) according to the Laemmli procedure (Laemmli 1970). For this purpose, a 3.9 % stacking gel with either 8 % or 10 % separating gel was used Table 4.7.

Table 4.7.

SDS-polyacrylamide stacking gel 3.9%

10ml for 4 gels

Acrylamide (30 %)	1.3 ml
Upper Buffer (4x)	2.5 ml
H2O	6.1 ml
Ammonium persulfate APS	0.1 ml
TEMED	0.01 ml

SDS-polyacrylamide separating gel 8%

15ml for 4 gels

Acrylamide (30 %)	4 ml
Lower Buffer (4x)	3.75 ml
H2O	7.25 ml
Ammonium persulfate APS	0.05 ml
TEMED	0.01 ml

SDS-polyacrylamide separating gel 10%

15ml for 4 gels

Acrylamide (30 %)	5 ml
Lower Buffer (4x)	3.75 ml
H2O	6.25 ml
Ammonium persulfate APS	0.05 ml
TEMED	0.01 ml

The glass plates which maintain the gel for solidification were assembled in the cuvette and any leaking was discarded by introducing 70 % ethanol. Once the leakage was discarded the 70 % ethanol was removed and 3.3 ml of separating gel was poured. Two hundred µl of isopropanol were added to assure the complete horizontal level of the top of the gel. After 45 minutes the gel was polymerised and the isopropanol was removed. On top of the separating gel, 2 ml of stacking gel was poured until it reached the top of the glass plate, where a comb with 10-15 wells was inserted. After another polymerisation time of about 20 minutes the combs where removed, and the plates with the gel were introduced into a tank with 1x Running Buffer. Before adding the plant samples into the gel, all samples were boiled at 70°C for 40 min and spun down at full speed for 2 min. Twenty µl from each sample supernatant was loaded in a well of the gel, and 3 µl of PageRuler Plus Prestained Protein Ladder (Thermo fisher scientific, USA) was loaded in one lane as a protein marker. The gel was run at 120 V until the proteins were concentrated at the end of the stacking gel; subsequently the voltage was changed to 150 V.

4.5.3 Western blot

After running the gels, they were washed and equilibrated on Bijerrums Buffer. A semi-dry blotting system (Perfect Blue Semi-Dry Electro Blotter, paqlab, Germany) was used for the transfer of proteins from the gel to the membrane. Thin and thick blotting paper (Blotting Pad 707, VWR, USA) and transfer membrane (BioTrace NT Nitrocellulose Transfer Membranes, Pall Life Sciences, USA) were cut to match the size of the gel and saturated in cold Bijerrums Buffer. The gels were organised with the transfer membranes and blotting paper in a sandwich style. The sandwich was assembled by putting first a layer of thick blotting paper followed by a layer of thin blotting paper, then the transfer membrane was added, and on the top of the membrane the gel was placed. On the top of the gel another thin paper was placed followed by a thick paper. Once the sandwich was assembled, it was placed into the blotting system and the air between the layers was removed by little pressure performance. A little amount of Bijerrum Buffer was added in the top of the gel to keep it wet during all the transfer. The lid of the blotting system was assembled with the screwing knobs. And the gel was connected to a voltage of 10 V for 1 hour.

After the transfer, the membrane was incubated at room temperature for at least 1 hour in Blocking Solution, with slow movement on a horizontal shaker. The membrane was transferred into primary antibody solution and incubated overnight at 4°C on a horizontal shaker with slow movement. The membrane was washed three times with TBS Solution at room temperature with fast movement horizontal shaker, 10 min per wash, and it was incubated with the secondary antibody solution for 3-6 h at room temperature. The secondary antibody was either an anti-rabbit HRP (1:20000; Goat Anti-Rabbit IgG-Horseradish Peroxidase, G21234, GE Healthcare, USA) or an anti-rat HRP (1:20000; Rabbit Anti-Rat IgG H&L (HRP), ab6734, Abcam, UK). After incubation with the second antibody, the membrane was washed three times with TBS Solution as described before.

Detection of the proteins was by chemiluminescent signal from substrate for the HRP enzyme (SuperSignal West Femto Chemiluminescent Substrate, Thermo Fisher

Scientific, USA). The chemiluminescent signal was caught on an imaging platform (Fusion spectra, Vilber Lourmat, France) according to the manufacturer's instructions.

4.6 Confocal imaging

Tobacco plants three days after transformation or Arabidopsis transgenic plants were used for confocal microscope analyses (Fricker, Runions et al. 2006). The part of the plant to be analysed was cut (1x1 cm) and infiltrated with tap water for air removal between the cells. The plant sample was placed on a glass slide and covered with a coverslip, and a drop of water was injected between the plant tissue and the coverslip to remove any possible air bubbles. All imaging was carried out using a Zeiss LSM510-META confocal microscope (Zeiss, Jena, Germany). Fluorescence from Green Fluorescent Protein (GFP)-tagged molecules was excited with an Argon Laser at 488 nm and 15% intensity using a 488 nm dichroic mirror. The emitted light above 488 nm was directed by a 545 nm dichroic mirror into two detection channels. GFP emission was collected with a 505–530 nm emission interference filter in one channel and chlorophyll fluorescence was detected after passage through a longpass 560 nm emission filter in another channel. Fluorescence from Red Fluorescent Protein (RFP)-tagged molecules was excited with a HeNe Laser at 543 nm and 50% intensity. The emitted light above 530 was directed by a 560 nm dichroic mirror into two detection channels. RFP emission was collected with a bandpass 560–615 nm emission filter in one channel and chlorophyll fluorescence was detected using 635 VIS dichroic mirror between 643 and 707 nm with the META head.

4.7 Modelling

For the modelling work, the OnGuard software (www.psrg.org.uk) was used. The models were driven through a diurnal cycle of 12 hours of light and of 12 hours of dark (Chen, Hills et al. 2012, Wang, Papanatsiou et al. 2012, Wang, Hills et al. 2014). The NpHR parameters were incorporated in the model for the plasma membrane and tonoplast pump expression. The pump was set up to be light-activated with a $L_{1/2}$ of 5000 μEinsteins m^{-2} s^{-1} while the other parameters from the model were not modified. The model was run to test different numbers of pumps expressed in the tonoplast and

the plasma membrane, starting with 200000 pumps expressed in one or the other membrane up to a maximum of 5 million pumps. For the KAT1 experiments, only the $V_{1/2}$ properties of the K_{in} channels were modified from values of -180 mV (the wild-type characteristics) to values of -120 mV, -160 mV, -200 mV and -240 mV. The model was run in the four different conditions for 5 days, and the data of the days 2 and 5 was analysed.

4.8 Gas exchange measurements

The analysis of gas exchange measurements was carried out with LI-6400XT open system (LI-COR Bioscience GmbH, Bad Homburg, Germany) supplied with a leaf chamber fluorometer (LI6400-40). The LI-COR system is based on infrared gas analysis (IRGA) principle. The basic principle of gas exchange measurements lies in determining how much H_2O and CO_2 is used or produced by plant tissue. In the LI-COR system the air is pumped through a reference chamber at a set flow rate (mol air s^{-1}) and it determines the H_2O and CO_2 mole fractions (mol H_2O mol air-1 or mol CO2mol air -1) of the air by infrared gas analysis by IRGA. Once again, the same air is passed through the sample chamber at the same flow rate and the H_2O and CO_2 mole fractions are determined, after the air contact with the plant leaf. CO_2 and H_2O absorb the infrared radiation at specific wavelengths. The absorbance at the molecule-specific wavelengths is detected inside both IRGAs and transformed into voltage signals, which are then compared between the sample and reference IRGA. Out of the different mole fraction differential between the reference and the sample chambers, the LI-COR calculates the photosynthetic assimilation rate (A) and the transpiration rate (E). In order to ensure that sample and reference IRGA read the same air mole fractions, both chambers have to be checked against each other in a process called matching. The matching allows to adjust the sample chamber read out with the one from the reference chamber.

4.8.1 Plant preparation for LI-COR analysis

Arabidopsis transgenic plants from T1 to T4 generation were used for LI-COR experiments. The seeds of the selected lines for LI-COR analysis were sowed into 15 cm

of diameter pots and kept at 4°C in the dark for 48 hours to synchronise germination. The pots were moved to a short day growth rooms with 60 % humidity, 22°C, and 150 µmol m^{-2} s^{-1} of light from 9 am to 6 pm. The plants were selected in BASTA treatment described before. The resistant plants were transplanted into individual pots of 5 cm of diameter covered with a mesh to prevent soil pouring when manipulating the plant. Once the LI-COR experiments were finalised, two leaves from each plant were cut and kept at -80°C for further western blot analysis.

4.8.2 A/Ci curves

A/Ci curves were analysed from leaves of Arabidopsis transgenic lines. The leaves were big enough to cover the hole of the LI-COR chamber area. The curves were measured from 0 to 1500 µmol mol^{-1} of CO_2, at a saturating light of PQuantum 500 µmol m^{-2} s^{-1} (10 % Blue). The leaf temperature was settle at 22°C, and the humidity was kept at values around 60 % with a set flow rate of 200 µms. CO_2 assimilation at light saturated (Asat) and the maximum photosynthetic rates at CO_2 saturated (Amax) and were estimated using equations developed by Von Caemmerer and Farquhar (1981). Estimations of the maximum carboxylation velocity of Rubisco (Vc,max) were made by fitting a maximum likelihood regression below and above the inflexion of the A/Ci response using the method by McMurtrie and Wang (1993, Nogués and Baker 2000). Stomatal conductance (Gs) was calculated from the conductance values of the leaves at 390 ppm of reference CO_2.

4.9 Statistics

Data analysis was carried out using SigmaPlot 12 (Systat Software Inc.) Statistically significant differences were analysed and reported as means ± SE as appropriate, with significance determined by One-way ANOVA. Differences were considered significant at a probability level of $P < 0,05$.

5. Results

5.1. Engineering a CCM in the chloroplast

In this chapter I present the results of the part of my research involved in the first goal of the MAGIC project, with the aim to drive an increase of HCO_3^- inside the chloroplasts. As previously mentioned, the overall aim of the project is to maximise CCMs gain using a two-stage strategy driven independently with light energy absorbed by NpHR. The proposed use of NpHR is to establish an inward Cl^- gradient across the chloroplasts inner envelope, which will provide the driving force for the antiport of Cl^- per HCO_3^- by AE1.

A possible obstacle to consider when looking for functionality of NpHR in plants is the lack of retinal in these organisms, an indispensable molecule for the activity of the protein. It is not known if NpHR requires the external addition of retinal in plants, or whether it is able to use another molecule produced by the plant and similar enough to provide for its activity. Therefore, a third protein was added as an expression target to the project, beta-carotene 15,15'-monooxygenase (bCMO1), in order to provide the retinal. bCMO1 is an animal enzyme capable of converting beta-carotene and O_2 into two all-trans retinal molecules.

The aim of the work presented in this chapter was to target the two transmembrane proteins, NpHR and AE1, to the inner envelope of the chloroplast, and the soluble protein, bCMO1, to the stroma. Thereafter the work was directed to assessing the localisation of the proteins, to checking for activity and their effects on photosynthesis assimilation and stomatal conductance.

5.1.1. Cloning and Confocal Imaging

5.1.1.1. Expression of the proteins in the plant cell

None of the three proteins used in this project is naturally found in plants. The NpHR used in this research was from the bacteria *Natronomonas pharaonis*, the AE1 was human and the bCMO1 was from mouse. First, it was necessary to check if the genes coding for each protein were able to express in the plant cell. I started by cloning the

NpHR and AE1 genes under the expression of to constitutive promoters, the Arabidopsis UBQ-10 promoter and the strong promoter 35S. In order to aid analysis in vivo, I cloned the NpHR and the AE1 proteins with the mentioned promoters and either GFP or RFP as C-terminal fusions to provide fluorescent markers (Table 5.1.1) for protein localisation in the confocal microscope. The destination vectors used for the expression of the proteins are shown in the Table below, together with the entry clones and the final expression constructs.

Table 5.1.1 List of the expression constructs containing NpHR and AE1.

Expression construct	Entry clone (All in pDONR207)	Destination vector	Promoter	SM
pUBQ::NpHR-GFP	NpHR-wo	pUBC-GFP-Dest	UBQ10	S.10.7
pUBQ::NpHR-RFP	NpHR-wo	pUBC-RFP-Dest	UBQ10	S.10.7
pUBQ::AE1-GFP	AE1-wo	pUBC-GFP-Dest	UBQ10	S.10.7
pUBQ::AE1-RFP	AE1-wo	pUBC-GFP-Dest	UBQ10	S.10.7
35S::NpHR-GFP	NpHR-wo	pH7FWG2	35S	S.10.8
35S::NpHR-RFP	NpHR-wo	pB7RWG2	35S	S.10.8
35S::AE1-GFP	AE1-wo	pH7FWG2	35S	S.10.8
35S::AE1-RFP	AE1-wo	pB7RWG2	35S	S.10.8

Entry clones and destination vectors used for their production, with the respective promoter and fluorescent tag. The pUBC-GFP/RFP-Dest (Grefen, Donald et al. 2010) are Gateway-compatible vectors with C-terminal fluorescent tags incorporating the UBQ-10 promoter of Arabidopsis. pH7FWG2 and pB7RWG2 (Karimi, Depicker et al. 2007) are Gateway-compatible vectors with C-terminal fluorescent tags incorporating the 35S promoter, which gives a much stronger expression than the UBQ-10. pDONR207 is an entry vector from Gateway technology (Life Technologies) containing the *att*B1 and *att*B2 recombination sites. SM: supplemental material.

With all of the mentioned expression constructs I was able to transiently transform tobacco by *Agrobacterium tumefaciens*-mediated gene transfer using the leaf infiltration method. Three days after transformation I obtained confocal images showing the expression of the proteins. Both, AE1 and NpHR, proteins were well expressed in tobacco. However, the fluorescence signal for the constructs preceded by

the UBQ-10 promoter was very low in comparison with the ones preceded by the 35S promoter. The fluorescence signal indicated tonoplast localisation of NpHR (Figure 5.1.1) characterised for fluorescence signal in the tonoplast invaginations, it is also possible to observe how the signal doesn't reach the cell wall completely, thus discarding plasma membrane localisation. In contrast, AE1 fluorescence indicated ER expression (Figure 5.1.2), characterised for fluorescence signal around the whole nucleus and by the visualisation of the ER network. The confocal images indicating the localisation of the proteins are shown below.

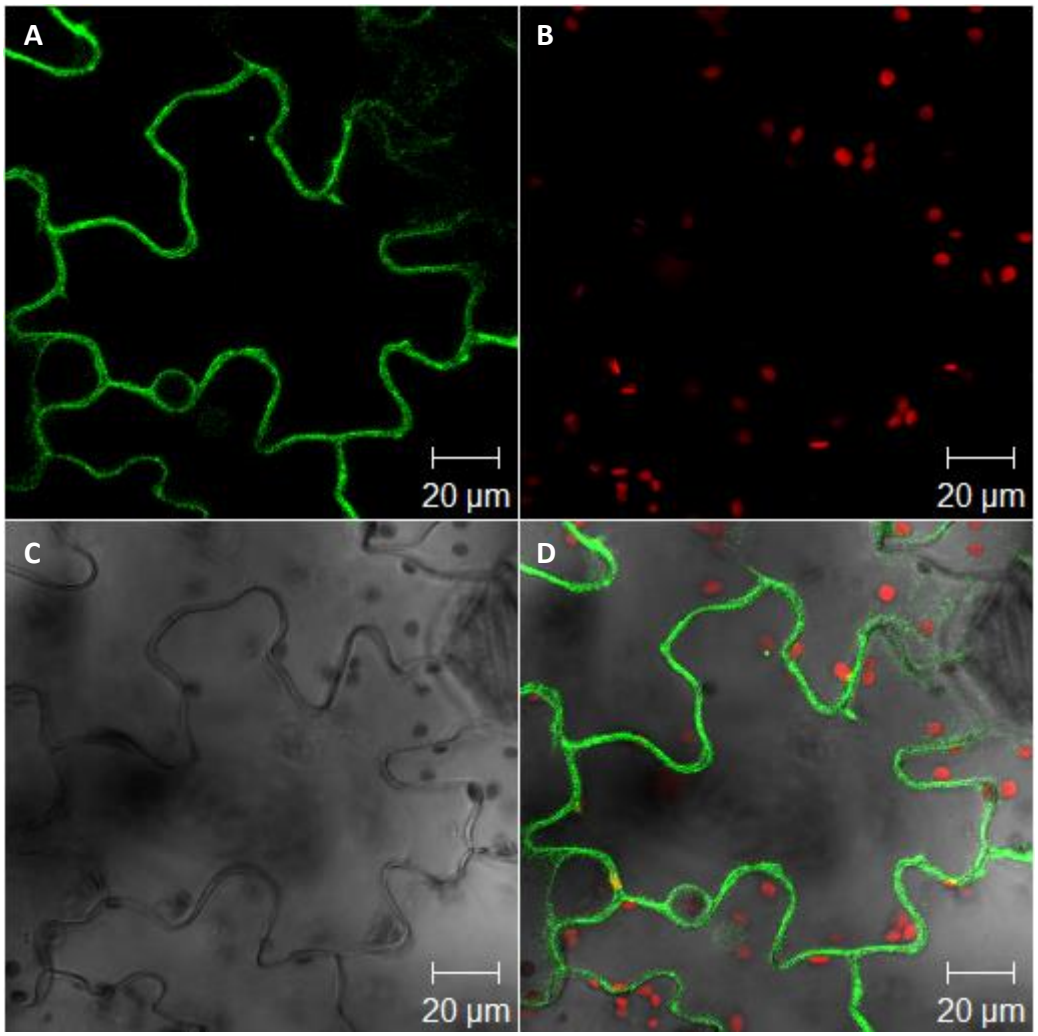

Figure 5.1.1. Expression of the construct 35S::NpHR-GFP in transient transformed tobacco leaves after 3 days of transformation. The GFP fluorescence indicates tonoplast localisation of NpHR in the epidermal cells (green A, D). The chlorophyll auto fluorescence is shown in red (B, D) indicating the localisation of the chloroplasts. C is the bright field image, and D shows a merged image. The images are from 13 slice-Z-

stack through the epidermal cell with a 2.75 µm interval between slices. In all the images the scale bar is 20 µm.

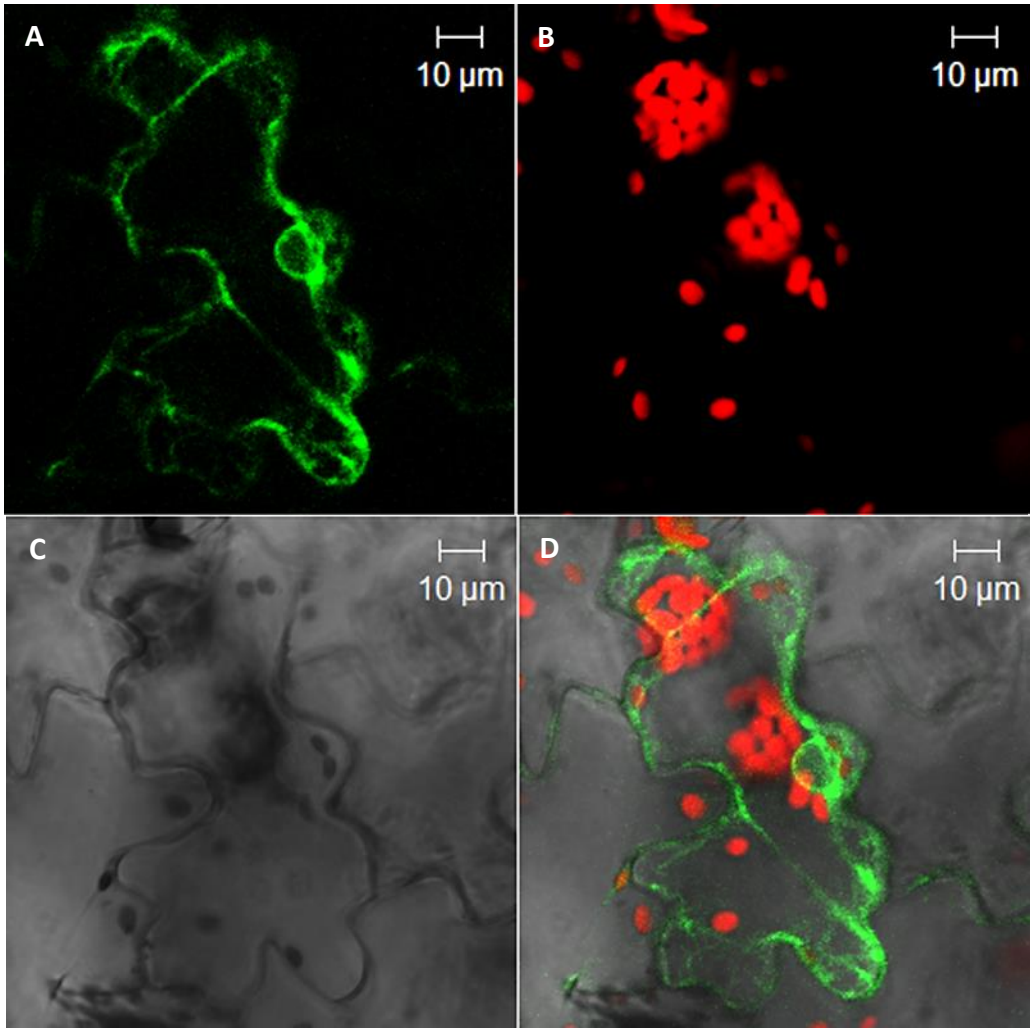

Figure 5.1.2. Expression of the construct 35S::AE1-GFP in transient transformed tobacco leaves after 3 days of transformation. The GFP fluorescence indicates ER localisation of AE1 in the epidermal cells (green A, D). The chlorophyll auto fluorescence is shown in red (B, D) indicating the localisation of the chloroplasts. C is the bright field image, and D shows a merged image. The images are from 8 slice-Z-stack through the epidermal cell with a 2.25 µm interval between slices. In all the images the scale bar is 10 µm.

Once it was confirmed the expression of both NpHR and AE1 proteins in plant, I cloned the different protein genes with a chloroplasts target sequence in order to drive the different proteins to the chloroplasts. I used the triosephosphate translocator (TPT) leader sequence, a signal sequence that targets transmembrane proteins to the inner

envelope of chloroplasts, to target NpHR and AE1 to the chloroplast membrane. The different constructs I made are listed in the table below (Table 5.1.2).

Table 5.1.2. List of the expression constructs containing NpHR and AE protein with the TPT leader sequence.

Expression construct	Entry clone (All in pDONR207)	Destination vector	Promoter	SM
pUBQ-TPT-NpHR-GFP	TPT-NpHR-wo	pUBC-GFP-Dest	UBQ10	S.10.9
pUBQ-TPT-NpHR-RFP	TPT-NpHR-wo	pUBC-RFP-Dest	UBQ10	S.10.9
pUBQ-TPT-AE1-GFP	TPT-AE1-wo	pUBC-GFP-Dest	UBQ10	S.10.9
pUBQ-TPT-AE1-RFP	TPT-AE1-wo	pUBC-RFP-Dest	UBQ10	S.10.9
35S::TPT-NpHR-GFP	TPT-NpHR-wo	pH7FWG2	35S	S.10.10
35S::TPT-NpHR-RFP	TPT-NpHR-wo	pB7RWG2	35S	S.10.10
35S::TPT-AE1-GFP	TPT-AE1-wo	pH7FWG2	35S	S.10.10
35S::TPT-AE1-RFP	TPT-AE1-wo	pB7RWG2	35S	S.10.10

Entry clones and destination vectors used for their production, with the respective promoter and fluorescent tag. The pUBC-GFP/RFP-Dest (Grefen, Donald et al. 2010) are Gateway-compatible vectors with C-terminal fluorescent tags incorporating the UBQ-10 promoter of Arabidopsis. pH7FWG2 and pB7RWG2 (Karimi, Depicker et al. 2007) are Gateway-compatible vectors with C-terminal fluorescent tags incorporating the 35S promoter, which gives a much stronger expression than the UBQ-10. pDONR207 is an entry vector from Gateway technology (Life Technologies) containing the *att*B1 and *att*B2 recombination sites. SM: supplemental material.

I used the new constructs I made containing the TPT leader sequence to transiently transform tobacco. Again I followed the infiltration method to transform tobacco leaves. Confocal images were taken three days after the transformation, when the expression in tobacco is normally strong. Expression of both proteins was localised in the inner envelope of chloroplasts from epidermal and mesophyll cells under the 35S promoter (Figures 5.1.3-5.1.6). No protein signal was detected when the proteins were express under the UBQ-10 promoter. Worth to mention that some of the transformed chloroplasts presented an atypical morphology (Figure 5.1.3), characterised by a more

swollen shape and not equal distribution of the grana. This atypical morphology is analysed below, in the protein activity section.

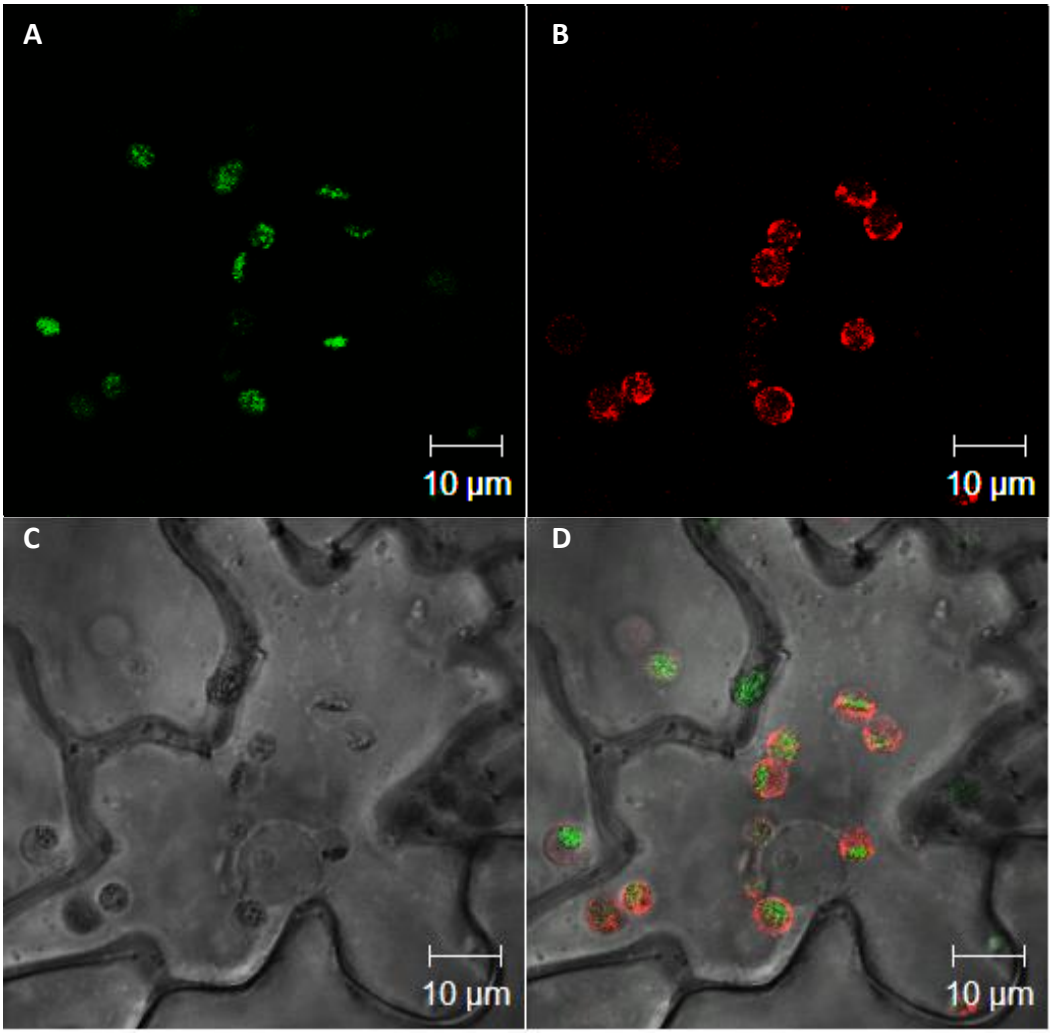

Figure 5.1.3. Expression of the construct 35S::TPT-NpHR-RFP in transient transformed tobacco leaves after 3 days of transformation. The RFP fluorescence indicates localisation of NpHR in the chloroplasts envelope of epidermal cells (red B, D). The chlorophyll autofluorescence is shown in green (A, D) indicating the localisation of the chloroplasts. C is the bright field image, and D shows a merged image. The images are from 15 slice-Z-stack through the epidermal cell with a 0.7 µm interval between slices. In all the images the scale bar is 10 µm.

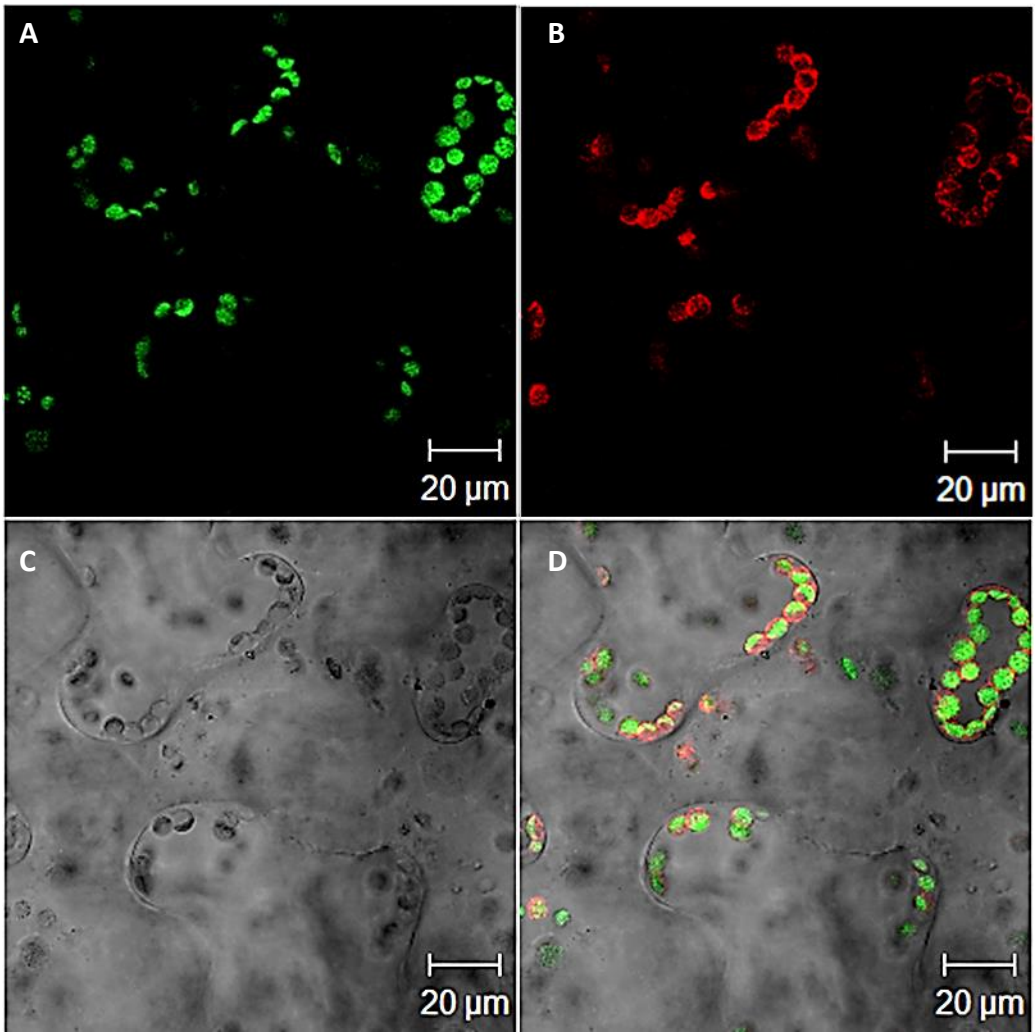

Figure 5.1.4. Expression of the construct 35S::TPT-NpHR-RFP in transient transformed tobacco leaves after 3 days of transformation. The RFP fluorescence indicates localisation of NpHR in the chloroplasts envelope of mesophyll cells (red B, D). The chlorophyll autofluorescence is shown in green (A, D) indicating the localisation of the chloroplasts. C is the bright field image, and D shows a merged image. The images are from a single scan of mesophyll cells. In all the images the scale bar is 20 µm.

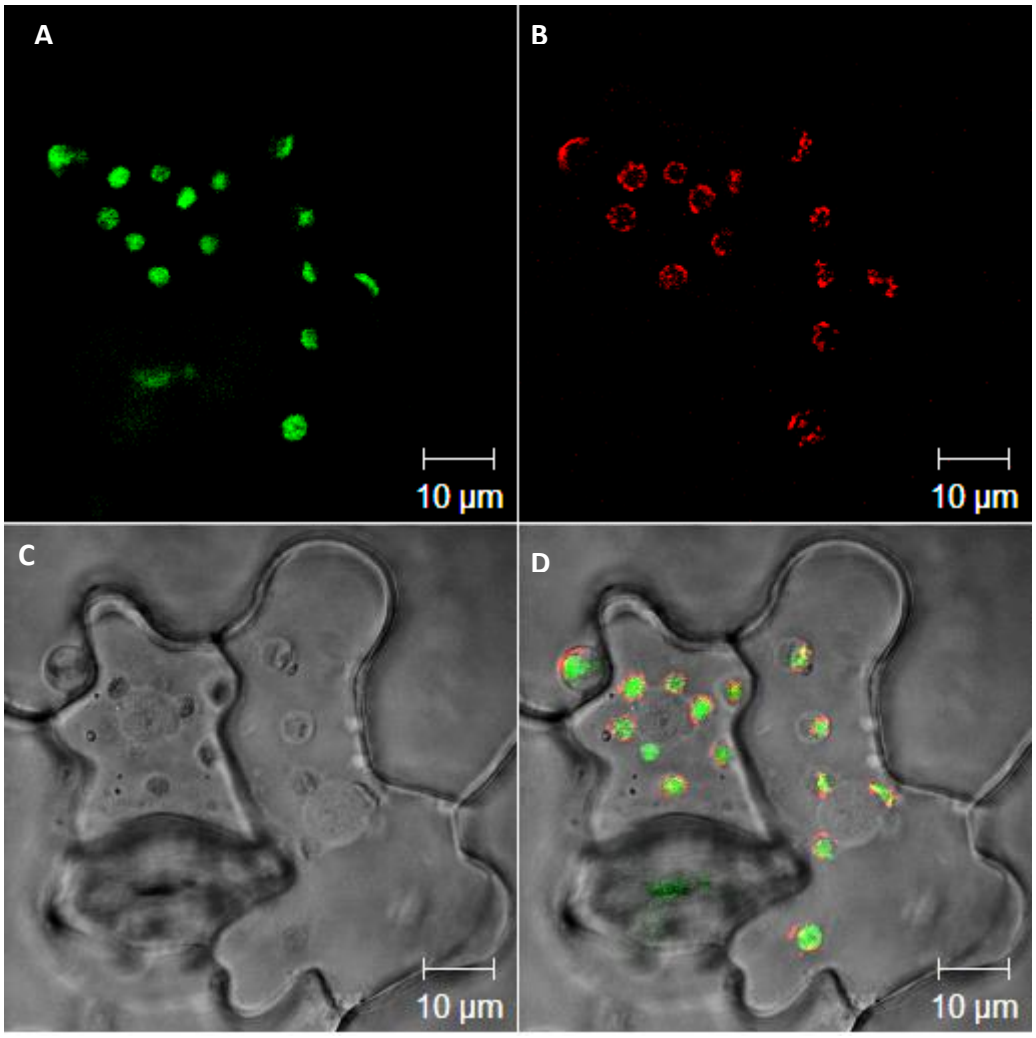

Figure 5.1.5. Expression of the construct 35S::TPT-AE1-RFP in transient transformed tobacco leaves after 3 days of transformation. The RFP fluorescence indicates localisation of AE1 in the chloroplasts envelope of epidermal cells (red B, D). The chlorophyll autofluorescence is shown in green (A, D) indicating the localisation of the chloroplasts. C is the bright field image, and D shows a merged image. The images are from a single scan of epidermal cells. In all the images the scale bar is 10 µm.

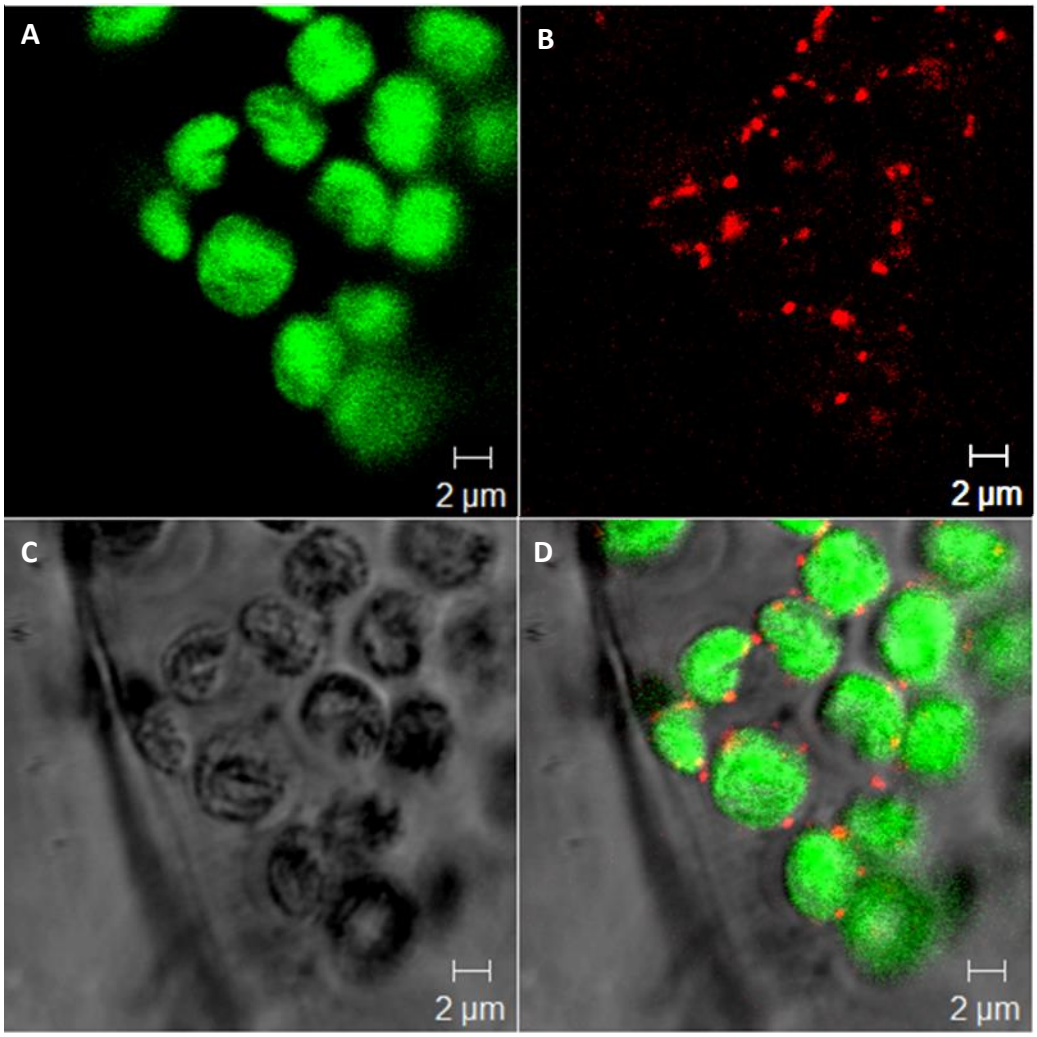

Figure 5.1.6. Expression of the construct 35S::TPT-AE1-RFP in transient transformed tobacco leaves after 3 days of transformation. The RFP fluorescence indicates localisation of AE1 in the chloroplasts envelope of mesophyll cells (red B, D). The chlorophyll autofluorescence is shown in green (A, D) indicating the localisation of the chloroplasts. C is the bright field image, and D shows a merged image. The images are from a single scan of mesophyll cells. In all the images the scale bar is 2 µm.

The confocal images showed that both of the proteins were expressed and localised in the periphery of chloroplasts from epidermal as well as mesophyll cells. In some images it could be seen AE1 protein expression presenting punctuations (Figure 5.1.6) instead of being uniformly distributed amongst the membrane. In order to verify the localisation of the proteins in the envelope of the chloroplasts I carried out line scans from images of transformed chloroplasts using the Zeiss LSM confocal software. The line scan gives information about the intensity of the fluorescence captured by the different channels positionally along a line drawn in an image. Figure 5.1.7 shows an example of line scan realised on a chloroplasts expressing the AE1 protein tag to a RFP

fluorescent marker. In the figure, the line scan shows RFP fluorescence localised in the edges of the chloroplasts, whereas in the inside of the chloroplasts there is chlorophyll fluorescence but not AE1. The fact that the intensity of the protein and chlorophyll fluorescence does not coincide indicates that the protein is localised in the envelope of the chloroplasts.

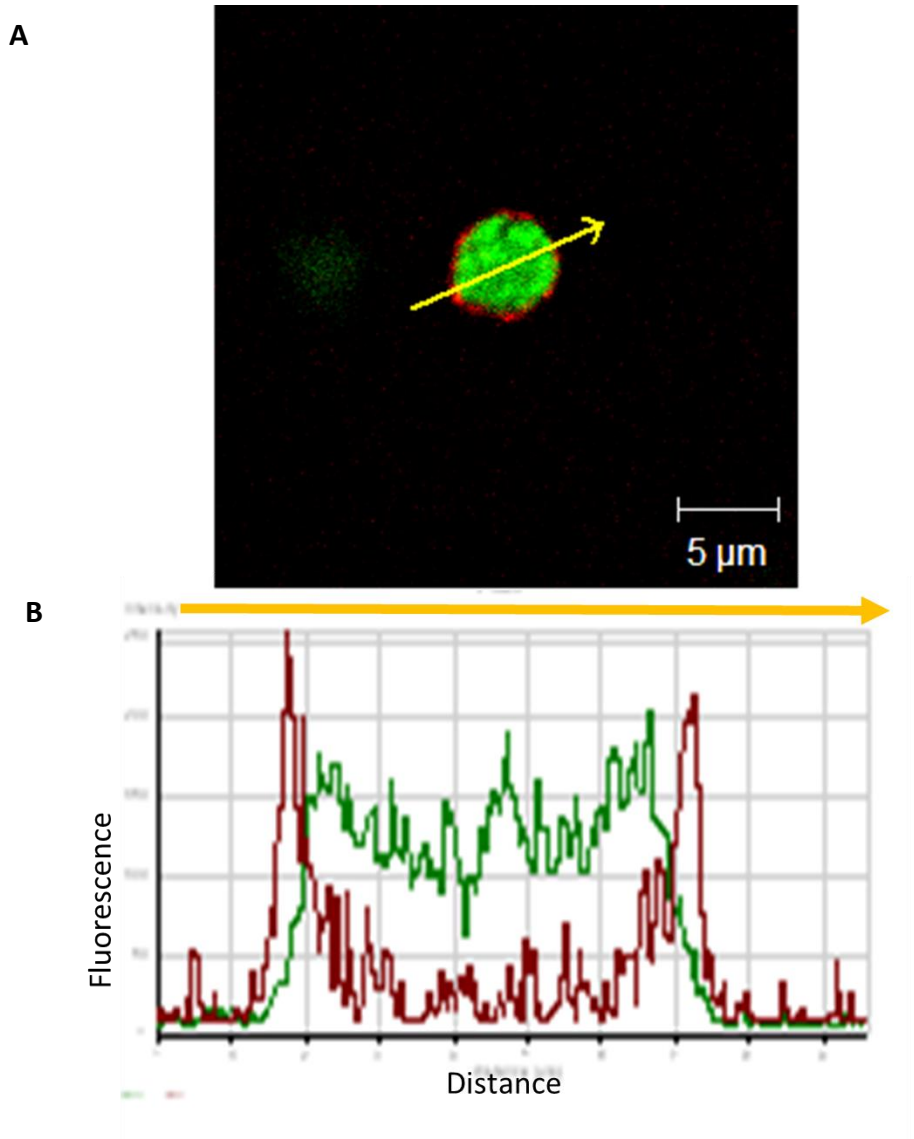

Figure 5.1.7. Line scan of a chloroplast transformed with the AE1 protein. (A) Merged confocal image showing expression of the construct 35S::TPT-AE1-RFP (red) in a chloroplasts of a transient transformed tobacco leaf, after 3 days of transformation. The yellow arrow drawn indicates the part of the image from where the intensity of fluorescence is calculated. The amount of intensity in relation to the distance is shown in B. The localisation of the RFP fluorescence indicates that AE1 is express in the

chloroplasts periphery (red A, B). The chlorophyll autofluorescence is shown in green (A, B). The scale bar of the image is 5 µm.

Once expression and localisation were confirmed for NpHR and AE1 proteins in the chloroplasts envelope, work began with bCMO1. I chose not to use the UBQ-10 promoter, given the poor signal observed when it was used with NpHR and AE1. Thus, bCMO1 was expressed under the 35S promoter. First, I cloned bCMO1 without any target sequence to test if it was possible to express it in plants, and if so, where it was localised. Thereafter, I cloned bCMO1 fused with the leader sequence of the large subunit of Rubisco (RbcL), which drives proteins to the stroma of the chloroplasts. The table of the different constructs expressing bCMO1 is shown below (Table 5.1.3).

Table 5.1.3. List of the expression constructs expressing bCMO1 with and without RbcL target sequence.

Expression construct	Entry clone (All in pDONR207)	Destination vector	Promoter	SM
35S::bCMO1-RFP	bCMO1-wo	pB7RWG2	35S	S.10.11
35S::RbcL-bCMO1-6His-RFP	RbcL-bCMO1-wo	pB7RWG2	35S	S.10.11

Entry clones and destination vectors used for their production, with the respective promoter and fluorescent tag. pB7RWG2 (Karimi, Depicker et al. 2007) is a Gateway-compatible vector containing 35S promoter and C-terminal RFP fluorescent tag. pDONR207 is an entry vector from Gateway technology (Life Technologies) containing the *att*B1 and *att*B2 recombination sites. SM: supplemental material.

I transiently transformed tobacco leaves with the constructs containing bCMO1 by the *Agrobacterium*-mediated infiltration method. Three days after infiltration I was checked for protein expression under the confocal microscope. When the RbcL target sequence was absent, bCMO1 expression was localised in the cytoplasm (Figure 5.1.8) of epidermal cells. Cytoplasm localisation is characterised by the signal localisation in cytosolic strands and also inside the nucleus. When the RbcL sequence was included, bCMO1 was localised in the stroma of the chloroplast (Figure 5.1.9). To confirm the stroma localisation of the bCMO1 I made line scans of chloroplast expressing the protein (Figure 5.1.10). The line scans show that the expression of the protein co-

localises with the chlorophyll fluorescence, indicating its location in the inside of the chloroplasts.

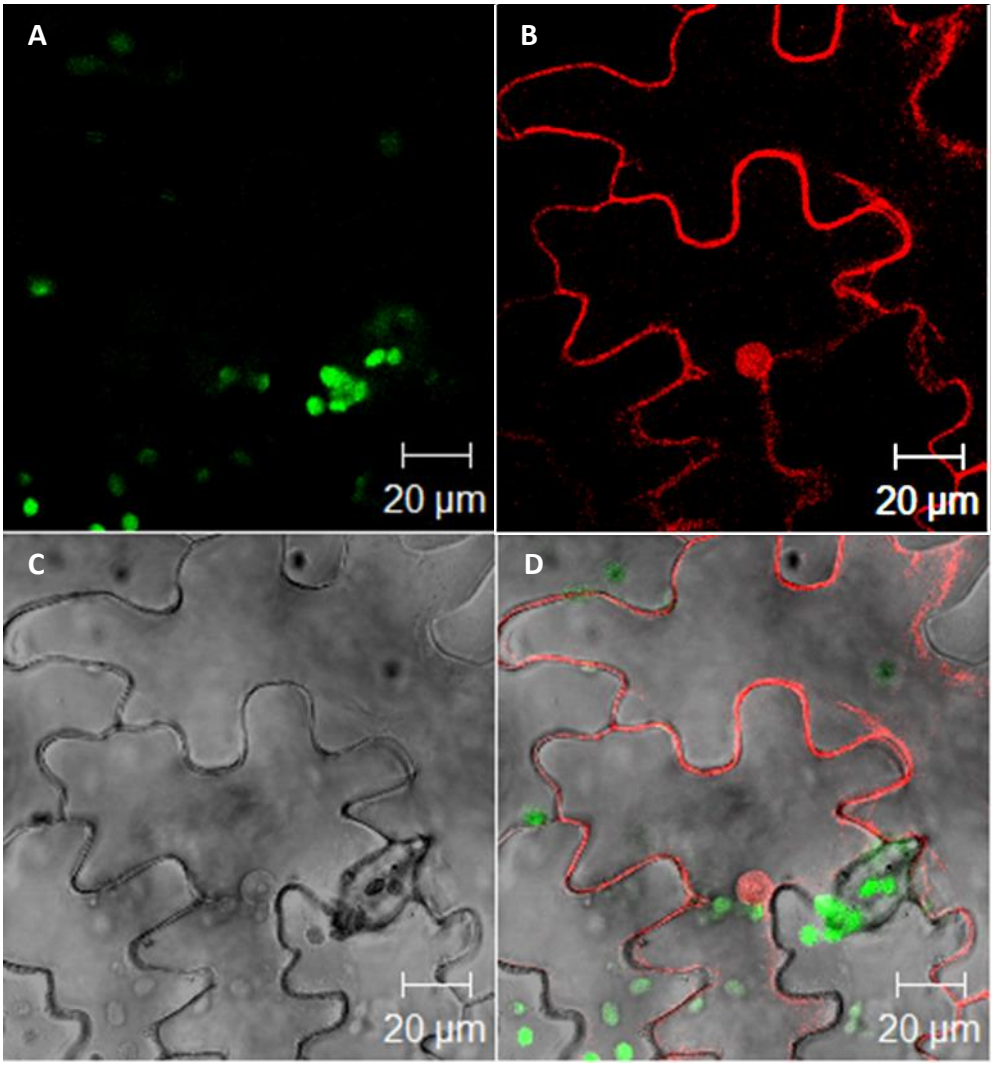

Figure 5.1.8. Expression of the construct 35S::bCMO1-RFP in transient transformed tobacco leaves after 3 days of transformation. The RFP fluorescence indicates cytoplasm localisation of bCMO1 in the epidermal cells (red B, D). The chlorophyll autofluorescence is shown in green (A, D) indicating the localisation of the chloroplasts. C is the bright field image, and D shows a merged image. The images are from 33-slice Z-stack through the epidermal cell with a 0.75 µm interval between slices. In all the images the scale bar is 20 µm.

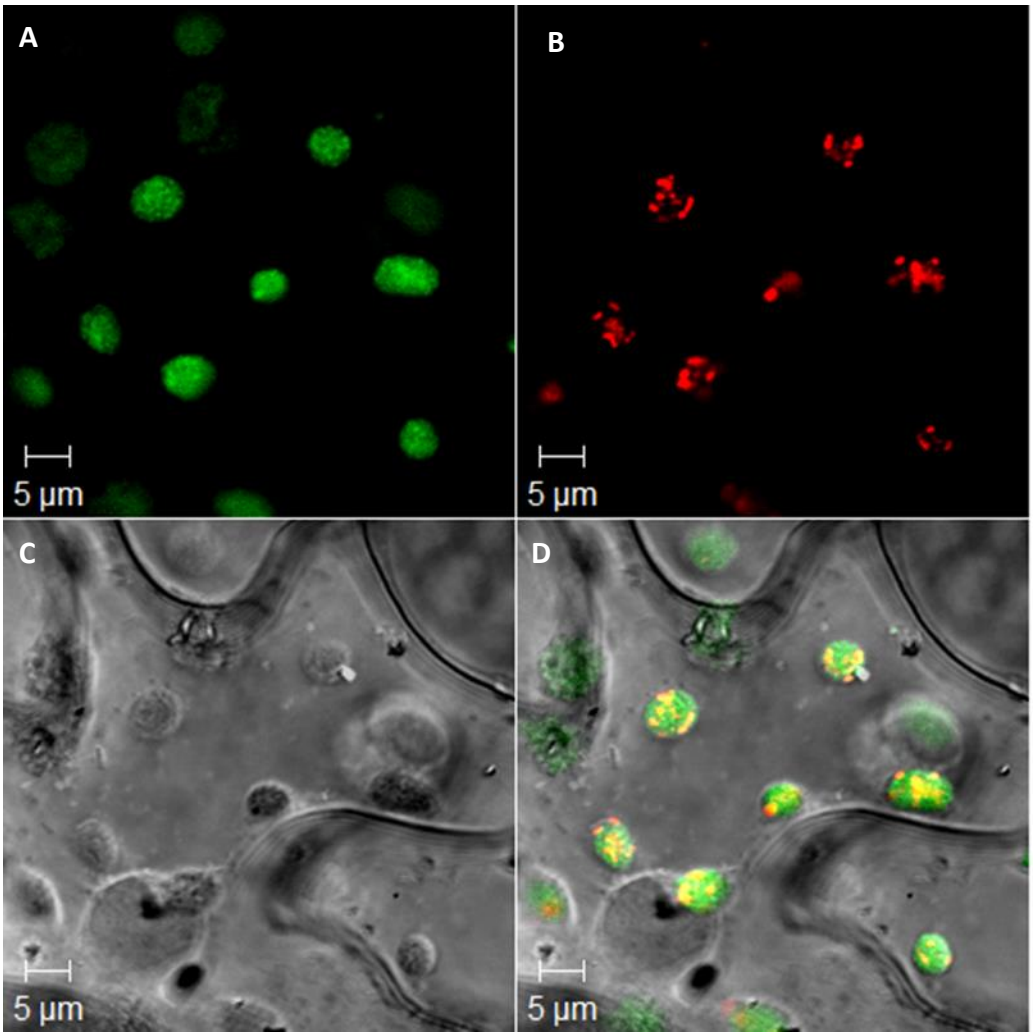

Figure 5.1.9. Expression of the construct 35S::RbcL-bCMO1-RFP in transient transformed tobacco leaves after 3 days of transformation. The RFP fluorescence indicates localisation of bCMO1 in the chloroplasts stroma of epidermal cells (red B, D), which presents punctuations. The chlorophyll auto fluorescence is shown in green (A, D). C is the bright field image, and D shows a merged image. The images are from a single scan of epidermal cells. In all the images the scale bar is 5 µm.

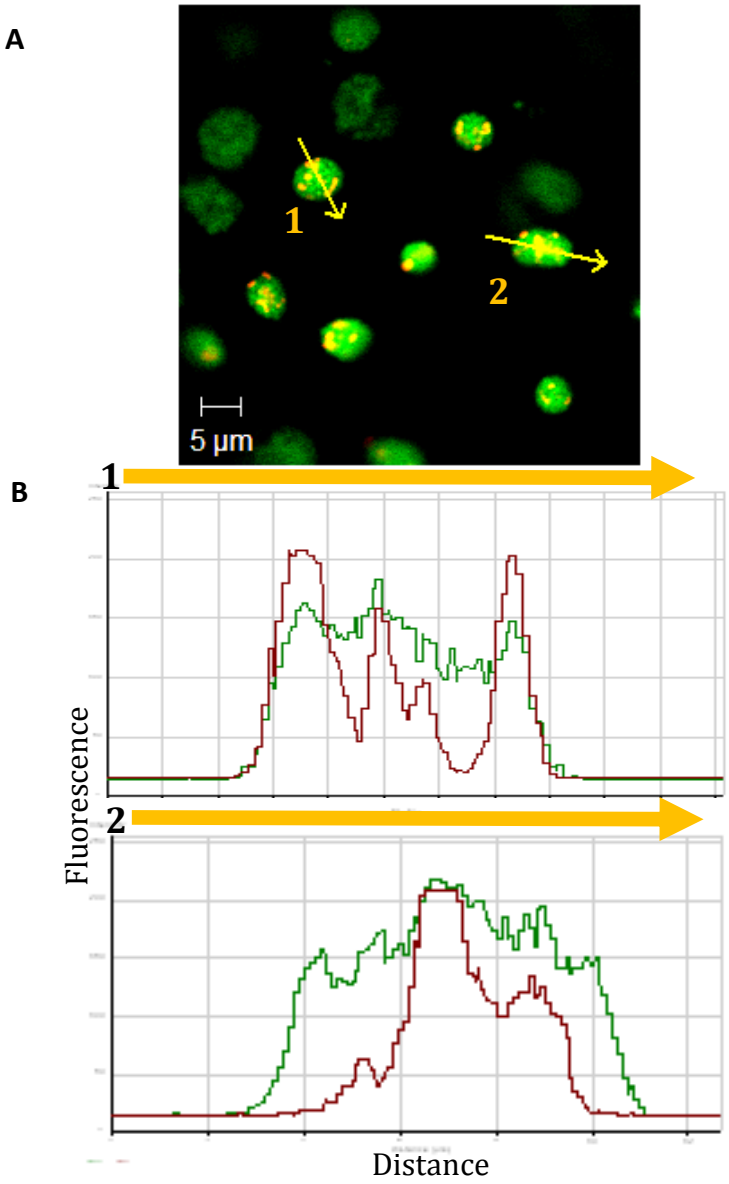

Figure 5.1.10. Line scans of a chloroplast transformed with the bCMO1 protein. (A) Merged confocal image showing expression of the construct 35S::RbcL-bCMO1-RFP (yellow) in a chloroplasts of a transient transformed tobacco leaf, after 3 days of transformation. The chlorophyll autofluorescence is shown in green (A, B). The yellow arrows drawn in A (1, 2) indicate the part of the image from where the intensity of fluorescence was calculated. The amount of fluorescence intensity in relation to the position along the arrow is shown in B (1, 2). The co-localisation between the RFP fluorescence and the chlorophyll is shown in yellow (A) indicating bCMO1 expression in the inside of the chloroplasts, against presenting punctuations. The scale bar of the confocal image is 5 µm.

In conclusion, NpHR, AE1 and bCMO1 could be expressed in plant cells, specifically in tobacco leaves under transient transformations by *A. tumefaciens*. Both

transmembrane proteins, NpHR and AE1 could be targeted to the inner envelope of chloroplasts by a TPT leader sequence. bCMO1 could be targeted to the stroma of the chloroplasts by RbcL leader sequence.

5.1.1.2 Co-localisation of the proteins

All the three proteins could be expressed in tobacco chloroplasts separately. However, the intention of the project was to express NpHR and AE1 together in the same chloroplasts. Furthermore, expression of the three proteins together bCMO1, NpHR and AE1, was necessary in case NpHR required an external source of retinal.

Before working with bCMO1 I wanted to make sure that NpHR and AE1 could be expressed in the plant at the same time. I transiently transformed tobacco combining the expression constructs expressing for NpHR and AE1 mentioned in the previous section. To transform the same tobacco leaf with the two different proteins, I combined *Agrobacterium* containing a construct expressing for NpHR with *Agrobacterium* containing a construct expressing for AE1.

For the co-localisation of the proteins I selected just the constructs with the 35S promoter for a strong expression, and the TPT leader sequence for chloroplast localisation. For each combination, I selected expression constructs having different tags on the NpHR and AE1 proteins in order to distinguish between the two proteins under the confocal microscope. Thus, I tagged AE1 with GFP and NpHR with RFP, and vice versa. The combinations of constructs are shown in the Table 5.1.4.

Table 5.1.4. Combination of AE1 and NpHR constructs for co-localisation expression.

Combination	Expression construct	Combined with
1	35S::TPT-AE1-GFP	35S::TPT-NpHR-RFP
2	35S::TPT-AE1-RFP	35S::TPT-NpHR-GFP

In both cases it was possible to find co-localisation of both proteins (Figure 5.1.11 and 5.1.13) as demonstrated with a line scan (Figure 5.1.12). However, it was observed that after the infiltration with the combinations not all the tobacco cells were transform with both constructs. In some cases, one cell expressed only one protein whereas the neighbour cell expressed the other protein (Figure 5.1.14, 5.1.15). This pattern of transformation was expected, because each transformation event is essentially independent. Thus, the probabilities were therefore significant that some cells might be transformed by only a single *Agrobacterium* and, hence, carry only one of the proteins.

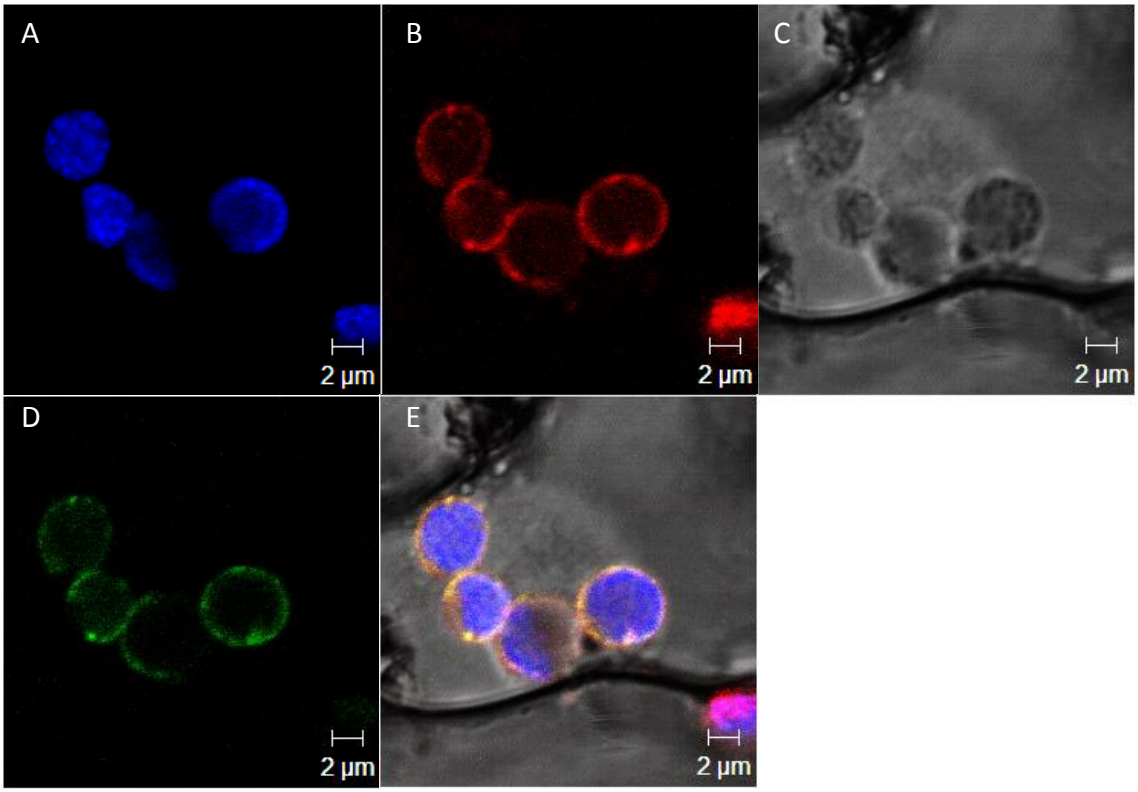

Figure 5.1.11. Expression of the construct 35S::TPT-AE1-GFP co-expressed with the construct 35S::TPT-NpHR-RFP (combination 1) in transient transformed tobacco leaves, after 3 days of transformation. NpHR (red, B) and AE1 (green, D) expression is localised in the inner envelope of chloroplasts. The chlorophyll autofluorescence is shown in blue (A, E) indicating the localisation of the chloroplast. C is the bright field image, and E shows a merged image where it is possible to see the co-localisation of both proteins (yellow). The images are from 12-slice Z-stack through epidermal cells with a 0.75 µm interval between slices. In all the images the scale bar is 2 µm.

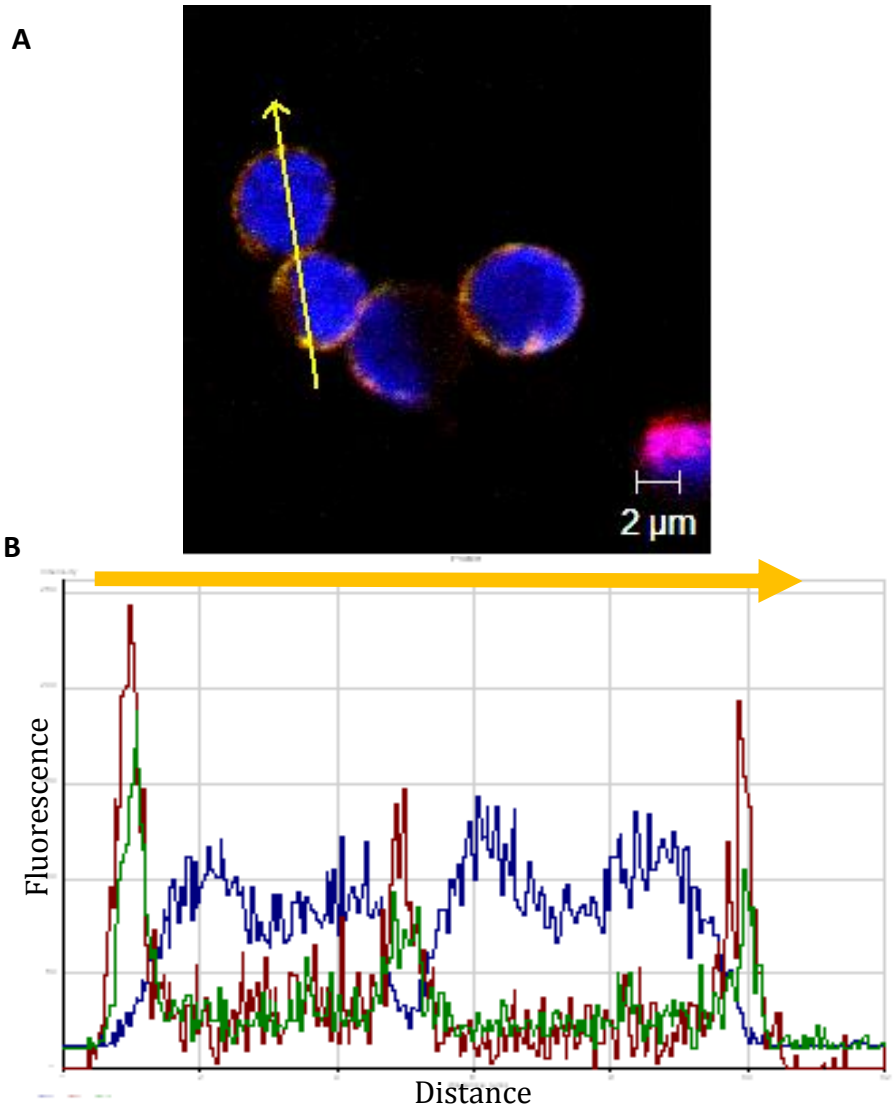

Figure 5.1.12. Line scan of chloroplasts transformed with the combination 1 (Table 4) which combines NpHR-RFP with AE1-GFP proteins. (A) Merged confocal image showing expression of AE1 and NpHR (yellow) in a chloroplasts of a transient transformed tobacco leaf, after 3 days of transformation. The co-localisation between the RFP and GFP fluorescence is shown in yellow (A) in the periphery of the chloroplasts. The chlorophyll autofluorescence is shown in blue (A, B) indicating the localisation of the chloroplasts. The yellow arrow drawn in A indicates the part of the image from where the intensity of fluorescence is calculated. The amount of fluorescence intensity in relation to the distance traced by the arrow is shown in B. In B the intensity of the AE1-GFP fluorescence is shown in green and the intensity of NpHR-RFP fluorescence is shown in reed and both intensities are not co-localised with the chlorophyll intensity (blue) indicating proteins localisation in the envelope of the chloroplasts. The graph (B) The scale bar of the confocal image is 2 µm.

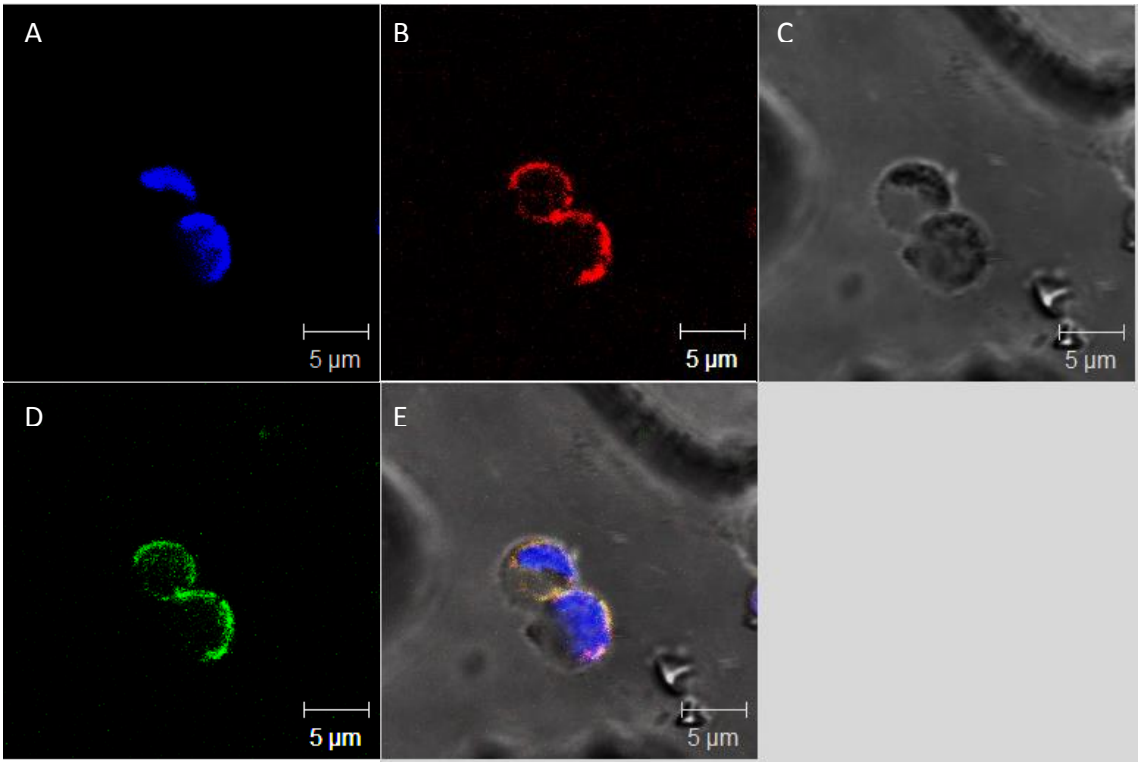

Figure 5.1.13. Expression of the construct 35S::TPT-AE1-RFP co-expressed with the construct 35S::TPT-NpHR-GFP (combination 2) in transient transformed tobacco leaves, after 3 days of transformation. AE1 (red, B) and NpHR (green, D) expression is localised in the inner envelope of chloroplasts. The chlorophyll autofluorescence is shown in blue (A, E) indicating the localisation of the chloroplast. C is the bright field image, and E shows a merged image where it is possible to see the co-localisation of both proteins (yellow). The images are from a single scan of epidermal cells. In all the images the scale bar is 5 µm.

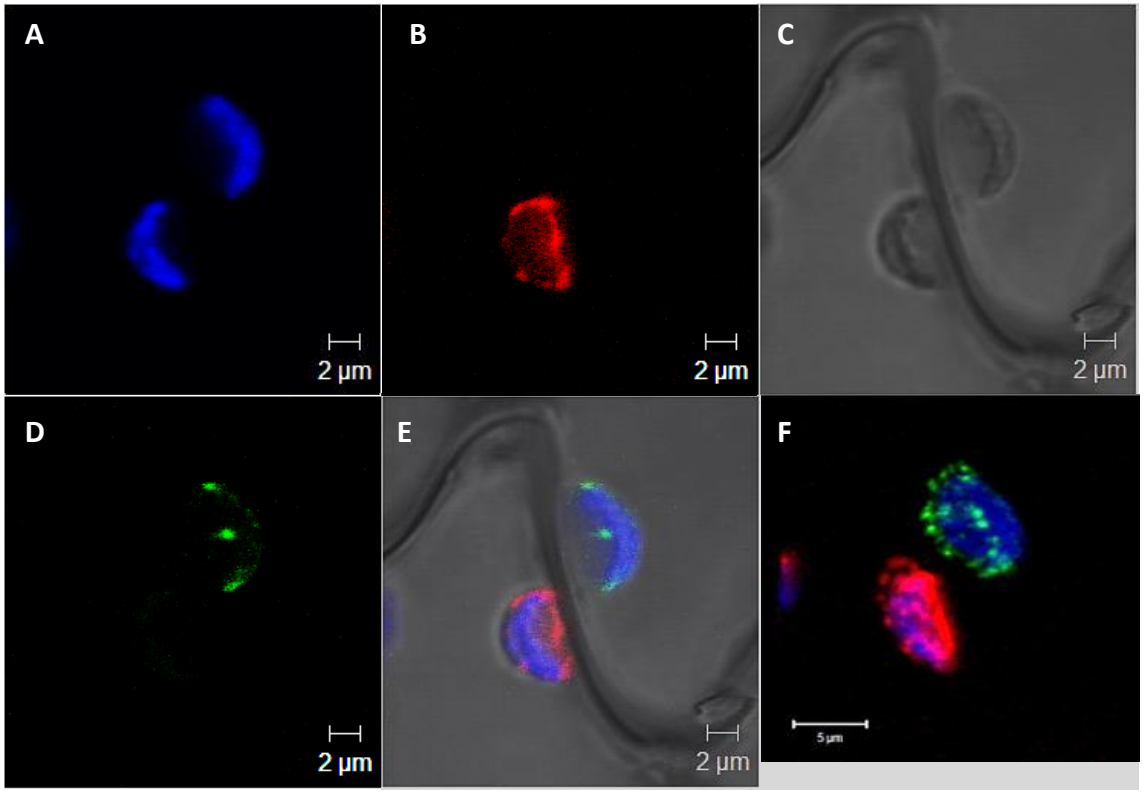

Figure 5.1.14. Expression of the construct 35S::TPT-AE1-GFP co-expressed with the construct 35S::TPT-NpHR-RFP (combination 1) in transient transformed tobacco leaves, after 3 days of transformation. NpHR (red, B) and AE1 (green, D) expression is localised in the inner envelope of chloroplasts. The chlorophyll autofluorescence is shown in blue (A, E). C is the bright field image, and E shows a merged image. There is no co-localisation of the proteins due to each cell from the image is transformed with a different construct. From A to E the images are from 13-slice Z-stack through the chloroplasts with a 0.75 µm interval between slices. The image F is a 3D reconstruction from the Z-stack mentioned. The scale bar from the image A to E is 2 µm and 5µm for the image F.

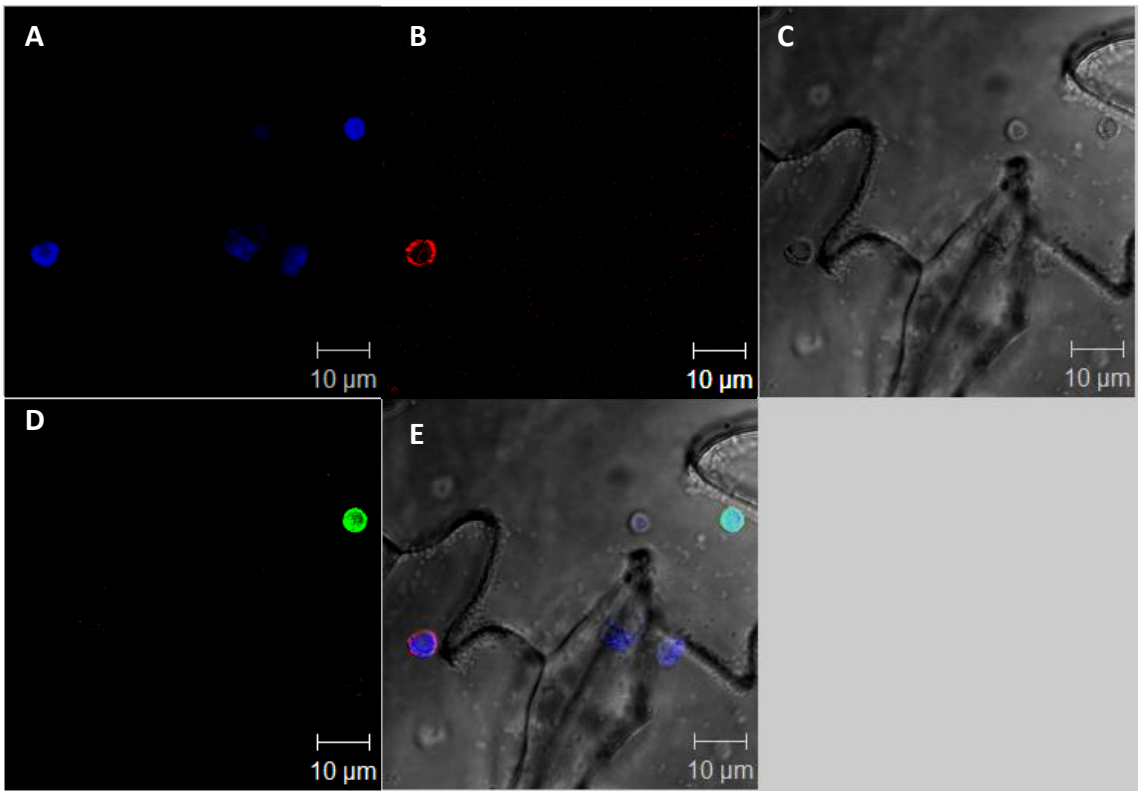

Figure 5.1.15. Expression of the construct 35S::TPT-AE1-RFP co-expressed with the construct 35S::TPT-NpHR-GFP (combination 2) in transient transformed tobacco leaves, after 3 days of transformation. AE1 (red, B) and NpHR (green, D) expression is localised in the inner envelope of chloroplasts. The chlorophyll autofluorescence is shown in blue (A, E) indicating the localisation of the chloroplast. C is the bright field image, and E shows a merged image. There is no co-localisation of the proteins due to each cell from the image is transformed with a different construct. The images are from a single scan of epidermal cells. In all the images the scale bar is 10 µm.

To avoid the problem of cells carrying only one or the other construct, it was necessary to express both constructs together in the same vector. For this purpose, I used a vector which incorporated two cassettes on a single vector backbone, each with its own promoter and terminator, thus allowing the expression of two different proteins with different tags with every transformation event. Thus, every cell transformed could be certain to carry both expression constructs. The vector I used was pFRETgc-2in1-CC (Hecker, Wallmeroth et al. 2015), which is a Gateway compatible vector. It contained a 35S promoter for each cassette, a C-terminal mCherry tag with the first cassette, and C-terminal GFP tag with the second cassette. To simplify construct insertion, the first cassette contained *att*B1 and *att*B4 recombination sites, and the second cassette

contained *att*B2 and *att*B3 recombination sites. Thus, to create the entry clones I used the Gateway entry vectors pDONR221-P1P4 and pDONR221-P3P2 which match with the recombination sites of this 2in1 vector as described. The different 2in1 constructs I made are shown in the table below (Table 5.1.5).

Table 5.1.5. List of the expression constructs obtained combining AE1 with NpHR and bCMO1 with NpHR.

Expression construct	Entry clone	SM
Cassette 1: 35S::TPT-AE1-mCherry Cassette 2: 35S::TPT-NpHR-GFP	TPT-AE1-wo (in pDONR221-P1P4) TPT-NpHR-wo (in pDONR221-P3P2)	S.10.12
Cassette 1: 35S::RbcL-bCMO1-mCherry Cassette 2: 35S::TPT-NpHR-GFP	RbcL-bCMO1-wo (in pDONR221-P1P4) TPT-NpHR-wo (in pDONR221-P3P2)	S.10.12

In both cases the Destination vector is pFRETgc-2in1-CC. Both proteins from the same expression construct have different fluorescent tag to allow the differentiation between the proteins under confocal imaging. The protein inserted in the first cassette is tag to mCherry, whereas the protein inserted in the second cassette is tag to a GFP. All of the proteins are cloned under the expression of the 35S promoter, which is already incorporated in the 2in1 vector used. wo: without stop codon. SM: supplemental material.

As shown in Table 5.1.5, I used the 2in1 vector not only to combine NpHR with AE1 but also to combine NpHR with bCMO1. I transiently transformed tobacco leaves with Agrobacterium containing one or the other 2in1 constructs. Localisation of the proteins was check under confocal three days after transformation. Both proteins were well expressed in the chloroplasts of tobacco epidermal cells and the confocal images show co-localisation of the proteins (Figures 5.1.16 and 5.1.18). A line scan shown in Figure 5.1.17 indicates NpHR localisation in the periphery of the chloroplasts whereas bCMO1 is localised in the inside.

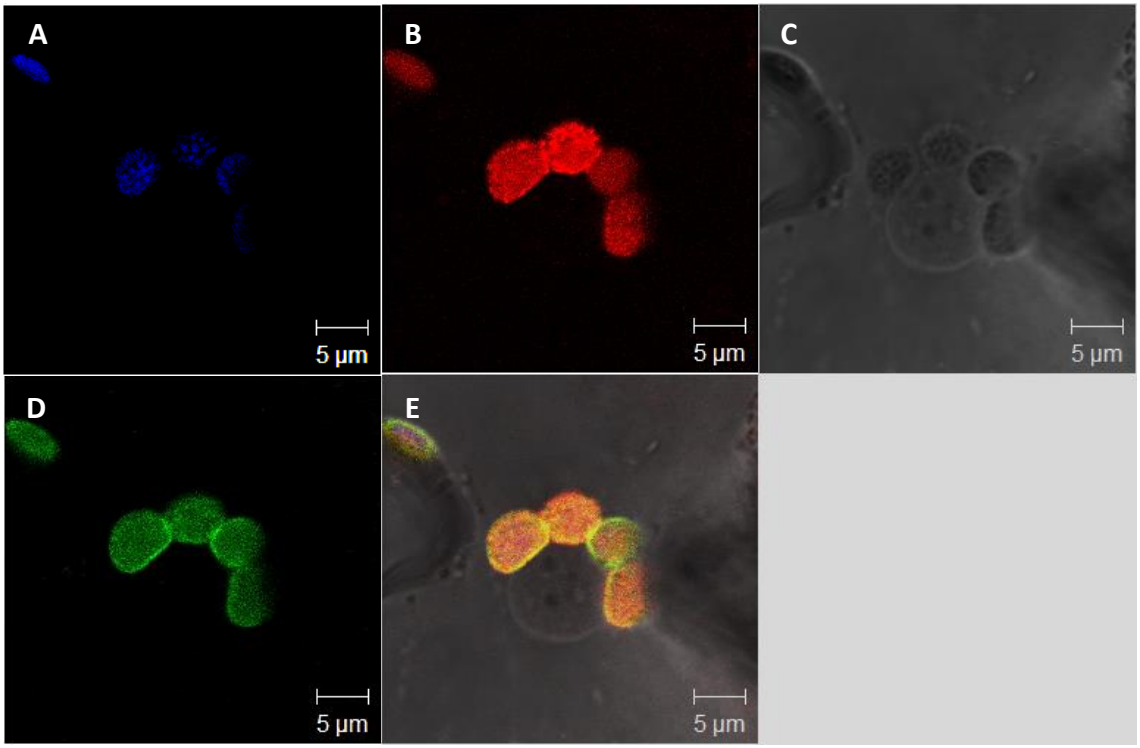

Figure 5.1.16. Expression of a 2in1 vector containing TPT-bCMO1-mCherry in the first cassette tag to a mCherry and TPT-NpHR-GFP in the second cassette tag to a GFP. bCMO1 (red, B, E) expression is localised in the stroma of the chloroplasts. NpHR (green, D,E) expression is localised in the inner envelope of the chloroplasts. The chlorophyll auto fluorescence is shown in blue (A, E) indicating the localisation of the chloroplasts. C is the bright field image, and E shows a merged. The images are from 9-slice Z-stack through epidermal cells with a 0.75 µm interval between slices. In all the images the scale bar is 5 µm.

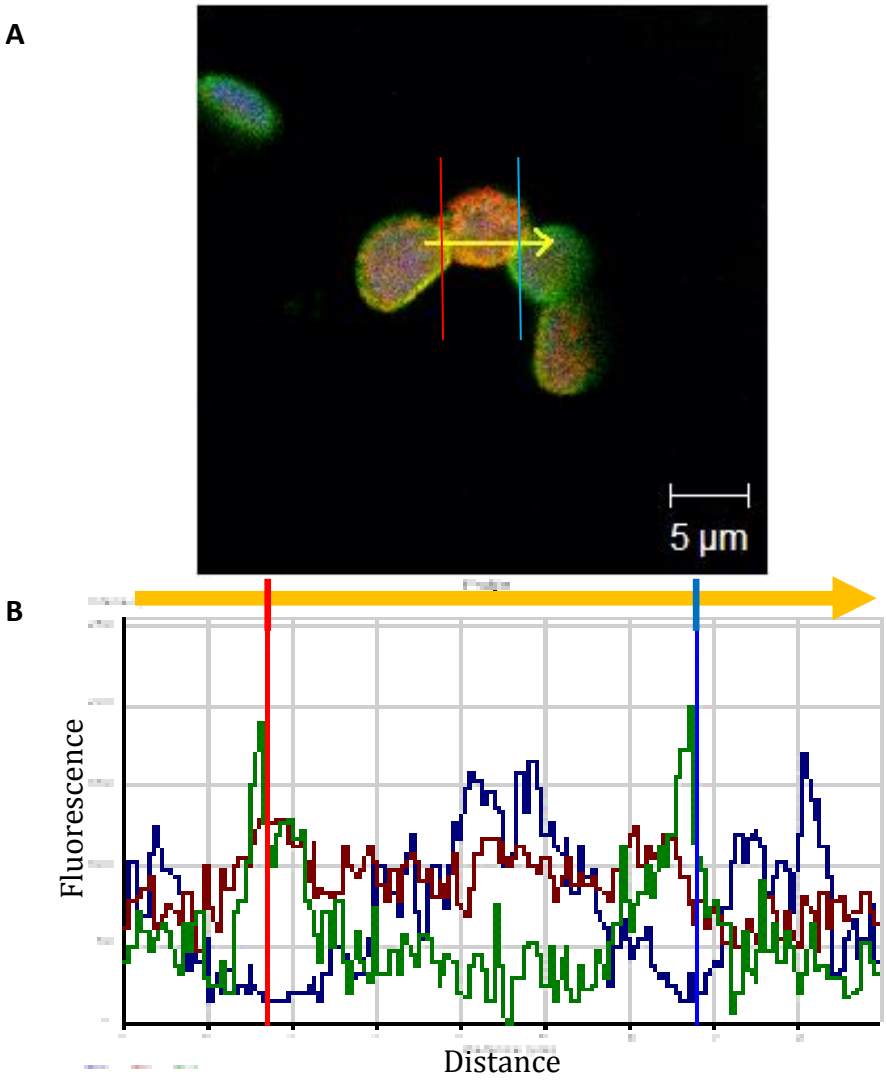

Figure 5.1.17. Line scan of chloroplasts transformed with the 2in1 vector containing TPT-NpHR-GFP and RbcL-bCMO1-mCHerry proteins. (A) Merged confocal image showing expression of NpHR (green) and bCMO1 (red) in a chloroplasts of a transient transformed tobacco leaf, after 3 days of transformation. The chlorophyll autofluorescence is shown in blue (A, B). The yellow arrow drawn in A indicates the part of the image from where the intensity of fluorescence is calculated. The red and blue vertical lines (A, B) indicate the point where the arrow is drawn over the chloroplasts membrane. The amount of fluorescence intensity in relation to the distance traced by the arrow is shown in B. In B the intensity of the NpHR-GFP fluorescence is shown in green and the intensity of bCMO1-mCherry fluorescence is shown in reed. bCMO1 is co-localised with chlorophyll autofluorescence inside the chloroplasts, whereas NpHR is just localised in the edges of the chloroplasts. The scale bar of the confocal image is 5 µm.

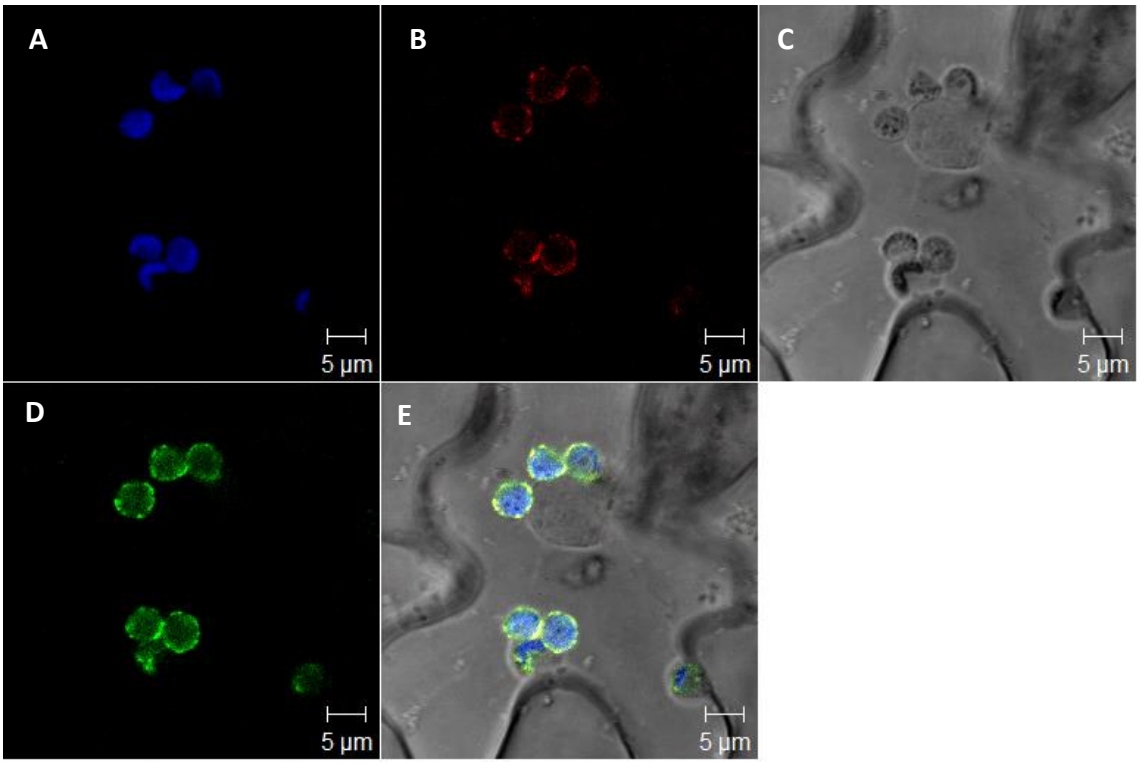

Figure 5.1.18. Expression of a 2in1 vector containing TPT-AE1-mCherry in the first cassette tag to a mCherry and TPT-NpHR-GFP in the second cassette tag to a GFP. AE1 (red, B, E) and NpHR (green, D, E) expression are localised in the inner envelope of the chloroplasts. The chlorophyll autofluorescence is shown in blue (A, E) indicating the localisation of the chloroplasts. C is the bright field image, and E shows a merged image where it is possible to see the co-localisation of both proteins (yellow). The images are from 17- slice Z-stack through epidermal cells with 0.75 µm interval between slices. In all the images the scale bar is 5 µm.

Following successful transformations with the 2in1 vector to express both proteins in every transformed cell, I sought to express all three proteins together. To go this one step further it was necessary to express the three proteins together, NpHR, AE1 and bCMO1, from a single vector in order to express the three proteins together in every transformed cell. Therefore, I created an expression construct containing the three genes together, which I called 3in1. To do it I inserted a 35S::RbcL-bCMO1-6His by classical cloning in a restriction site area between the two different cassettes of the 2in1 vector. The final expression construct obtained is shown in Figure 5.1.19. The 3in1 expression construct contains TPT-AE1-mCherry, RbcL-bCMO1-6His and TPT-NpHR-GFP, all under independent expression control of 35S promoters. Additionally, I tagged bCMO1 to a 6 histidine tag, as this construct is not identifiable by fluorescence under

confocal microscopy. Instead, I demonstrated bCMO1 expression by Western blot analysis with an anti-histidine antibody.

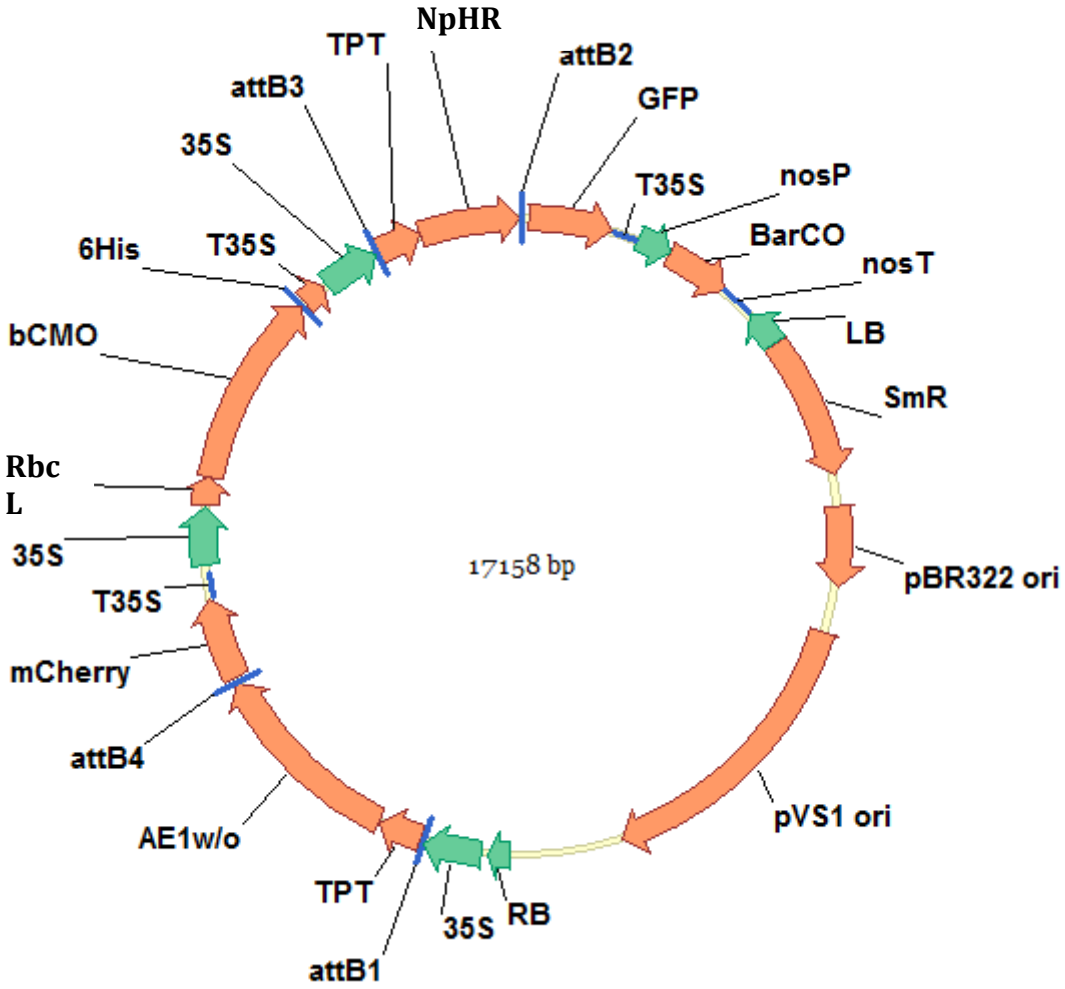

Figure 5.1.19. 3in1 expression construct. The construct contains 35S::TPT-AE1-mCherry, 35S::RbcL-bCMO1-6His and 35S::TPT-NpHR-GFP. pBR322ori/pVS1ori: replication origins. RB/LF: right/left border. SmR: spectinomycin resistance. BarCO: BASTA resistance. nosP/nosT: nos promoter/nos terminator. T35S: 35S terminator. 35S: 35S strong promoter. mCherry/ GFP: red/green fluorescent marker. 6His: 6 histidine tag. TPT: triosephosphate translocator target sequence. RbcL: Rubisco large subunit target sequence. AE1: anion exchanger1. NpHR: *Natronomonas pharaonis* halorhodopsin. bCMO1: beta-carotene 15,15'-monooxygenase. *att*B1/ *att*B2/ *att*B3/ *att*B4: recombination sites. The whole construct is 17158 bp. See Sup. Fig. 10.13.

I used the 3in1 expression construct to transiently transform tobacco with the *Agrobacterium*-mediated infiltration method. After three days of transformation, I checked for protein expression in the confocal microscope. Both protein tags marking

AE1 and NpHR were clearly expressed in the tobacco chloroplast envelope (Figure 5.1.20 A-E). I kept transformed plant tissue for a Western blot analysis, which allowed me to verify expression of the bCMO1 protein (Figure 5.1.20 D). The Western blot demonstrates the expression of bCMO1 in tobacco. (Figure 5.1.20 F).

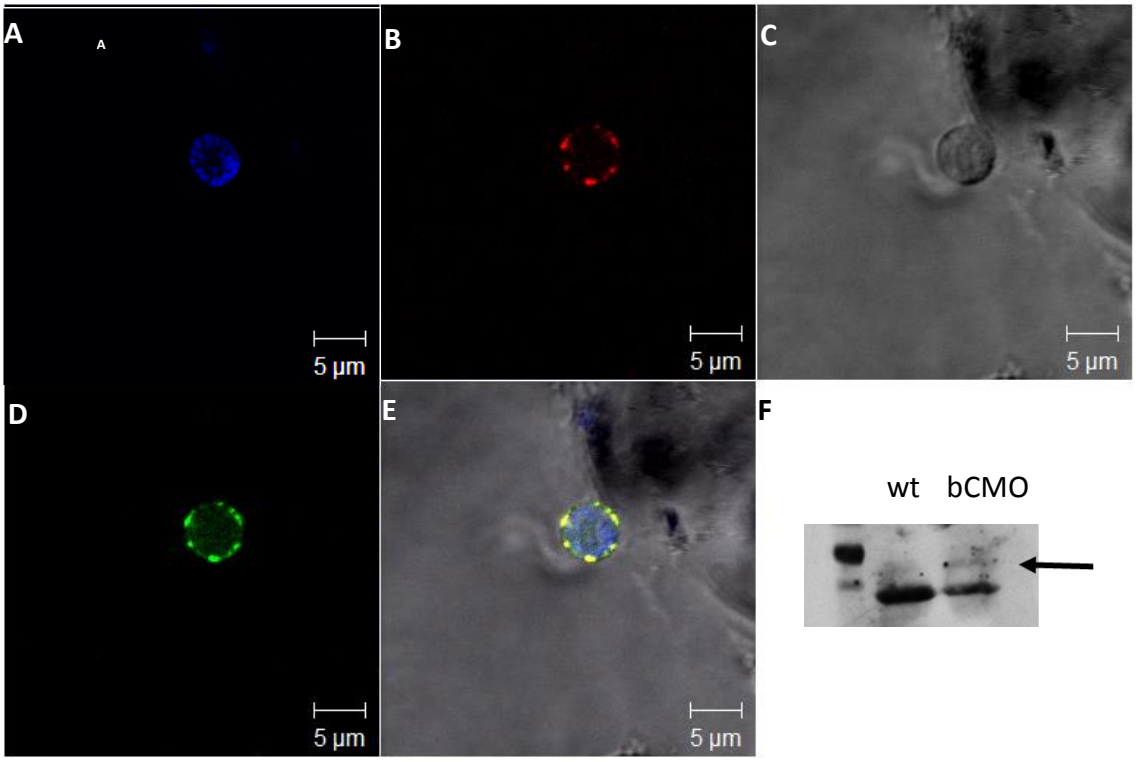

Figure 5.1.20. A-E Expression of the 3in1 expression construct. The construct contains 35S::TPT-AE1-mCherry, 35S::RbcL-bCMO1-6His and 35S::TPT-NpHR-GFP. AE1 (red, B) and NpHR (green, D) expression is localised in the inner envelope of the chloroplasts. The chlorophyll autofluorescence is shown in blue (A, E). C is the bright field image, and E shows a merged image where it is possible to see the co-localisation of both proteins (yellow). F shows the western blot analysis carried out with commercial anti histidine antibody, the arrow indicates the bCMO1 protein at 74 KDa, not expressed in the wild-type (wt) sample. The low thick band below is Rubisco expression. The images are from 19-slice Z-stack through epidermal cells with 0.75 µm interval between slices. In all the images the scale bar is 5 µm.

Figure 5.1.21 and 5.1.22 show control images from confocal microscope run with GFP and RFP settings with untransformed chloroplasts. In both figures just the chlorophyll autofluorescence is appreciable, no other fluorescence signal was detected using the standard settings of these studies. In conclusion, it was possible to express the three

proteins (AE1, NpHR and bCMO1) in tobacco chloroplasts from transiently transformed tobacco leaves. The three proteins were able to co-express together in the desired targeted place.

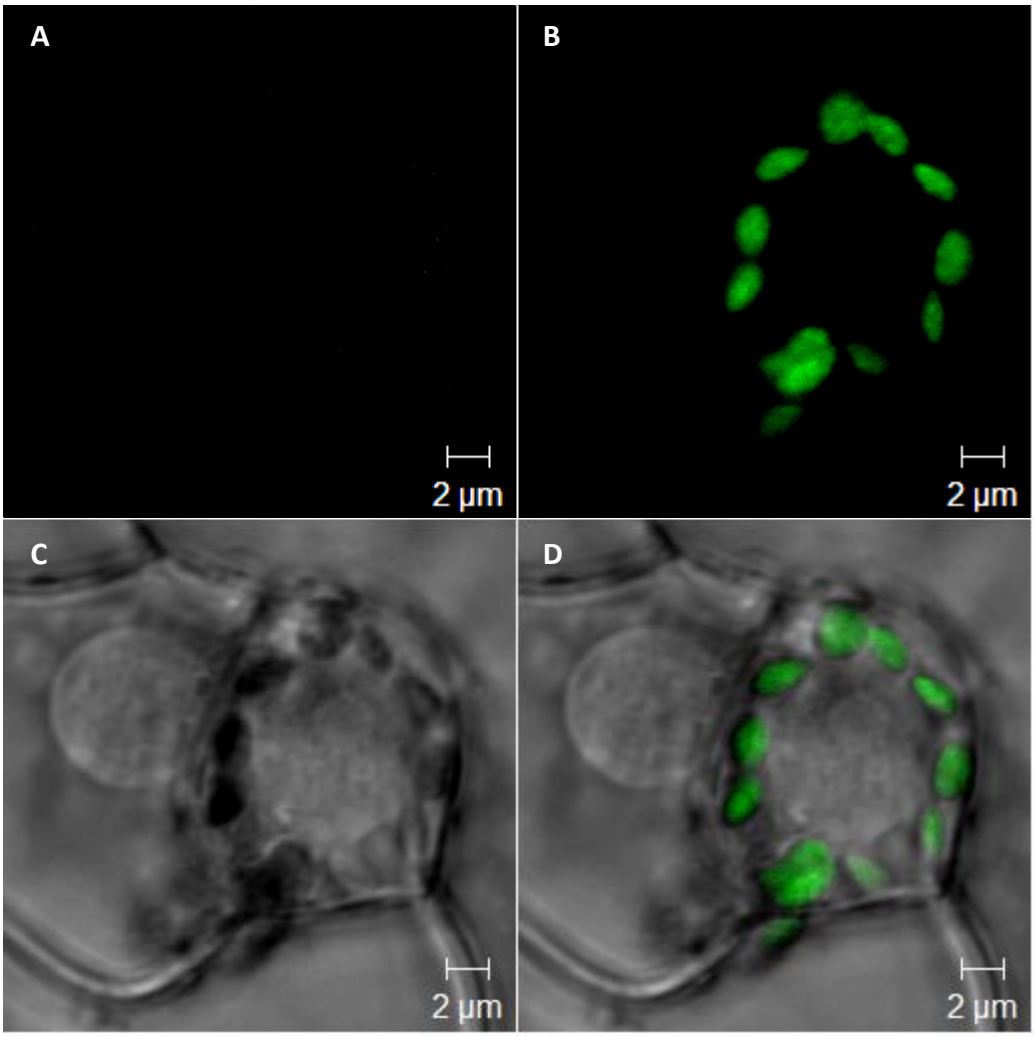

Figure 5.1.21. Confocal microscopy image from an untransformed tobacco leaf using GFP confocal settings. Chlorophyll fluorescence (green, B, D) indicates the localisation of the chloroplasts. A shows the GFP channel from the confocal, where not fluorescence is detectable. C is the bright field image, and D is the merged image. The images are from 12-slice Z-stack through epidermal cells with 0.6 µm interval between slices. In all the images the scale bar is 2 µm.

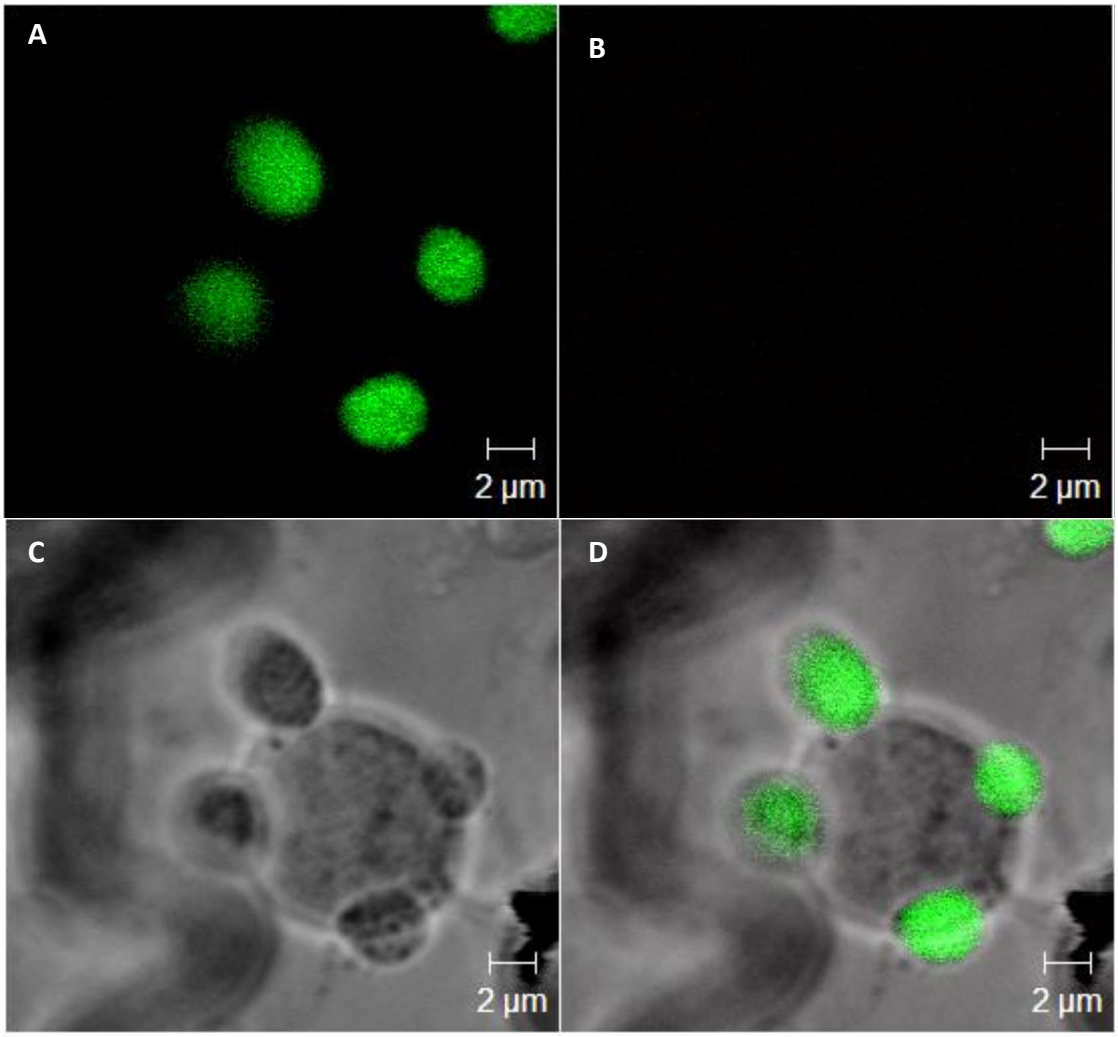

Figure 5.1.22. Confocal microscopy image from an untransformed tobacco leaf using RFP confocal settings. Chlorophyll fluorescence (green, B, D). A shows the RFP channel from the confocal, where no fluorescence is detectable. C is the bright field image, and D is the merged image. The images are from 12-slice Z-stack through epidermal cells with 0.8 µm interval between slices. In all the images the scale bar is 2 µm.

5.1.2. Functional activity of the expressed proteins

From the confocal images it was observed that some of the transformed chloroplasts presented an atypical morphology, already mentioned at the beginning of this results chapter. This atypical morphology was characterised by a more swollen shape of the organelle compared to the ones from untransformed cells. Another characteristic of some transformed chloroplasts was the shift of the chlorophyll to one side of the chloroplasts instead of being well distributed as it is in the non-transformed ones. The atypical morphology was observed in the chloroplasts expressing the NpHR or AE1 membrane proteins. This atypical morphology could be the result of the protein activity, by causing ion fluxes across the chloroplasts membrane and affecting the osmolarity of the chloroplasts. However, it could also be possible that the presence of the proteins itself was already modifying the chloroplasts morphology, and not being related with the protein activity.

Figure 5.1.3 is an example of chloroplasts presenting an atypical morphology when expressing NpHR. In the Figure 5.1.23 I show another example of chloroplasts presenting a severe and atypical morphology, in this case when expressing AE1. Figure 5.1.24 shows chloroplasts expressing both, NpHR and AE1, proteins and again the atypical chloroplast morphology can be observed. Compare this phenology with Figure 5.1.25, which provides an example of untransformed chloroplasts. The differences in morphology between the control and the transformed chloroplasts were very easily detected. To discard the possibility that the atypical morphology was caused by the *Agrobacterium*, I infiltrated tobacco leaves with *Agrobacterium* carrying the empty T-DNA plasmid. Under confocal microscopy 3 days after infiltration and following the same protocol as before, but chloroplast morphology was not affected (Figure 5.1.26), indicating the effect on chloroplasts morphology was not the consequence of *Agrobacterium* exposure itself.

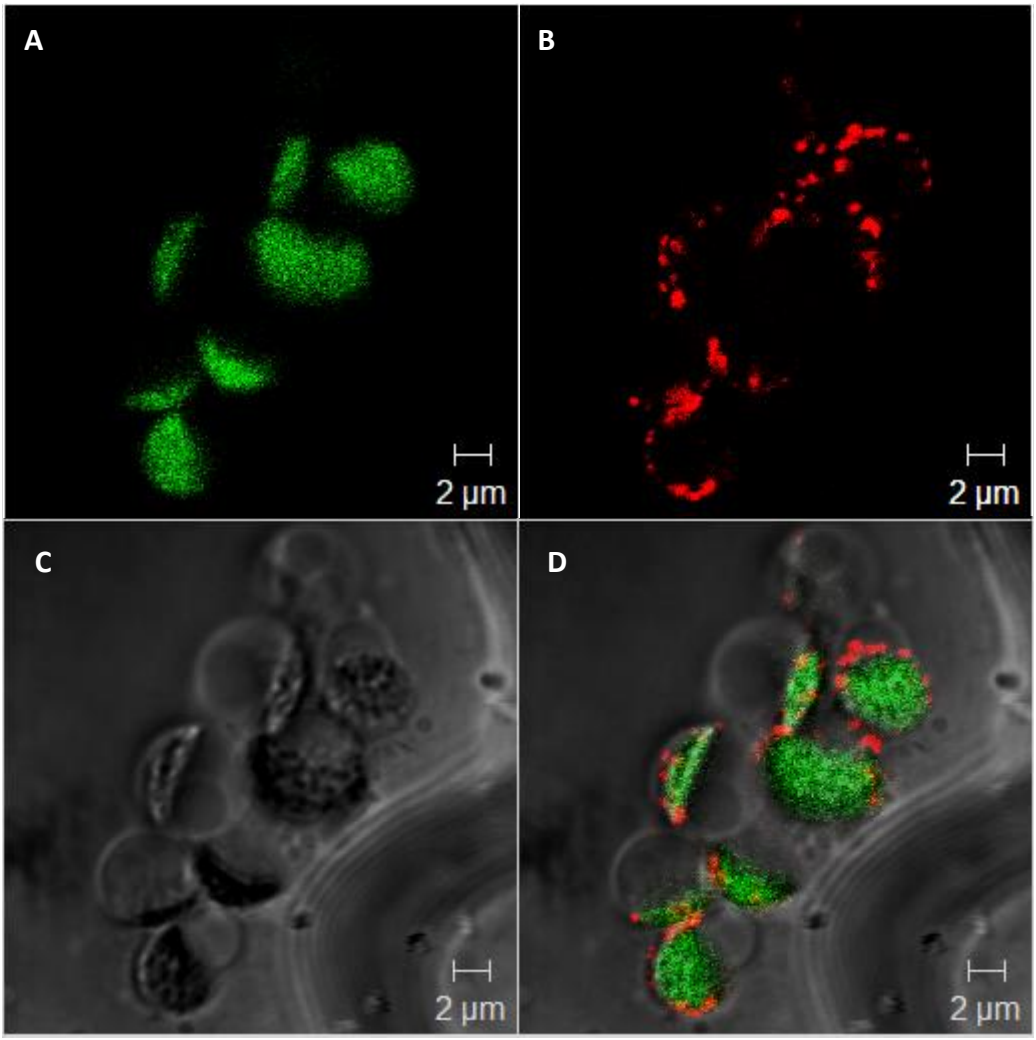

Figure 5.1.23. Atypical morphology chloroplasts expressing AE1 protein. Confocal image of the construct 35S::TPT-AE1-RFP in transient transformed tobacco leaves after 3 days of transformation. The RFP fluorescence indicates localisation of AE1 in chloroplasts of epidermal cells (red B, D). The chlorophyll autofluorescence is shown in green (A, D). C is the bright field image, and D shows a merged image. The images are from a single scan of epidermal cells. In all the images the scale bar is 2 µm.

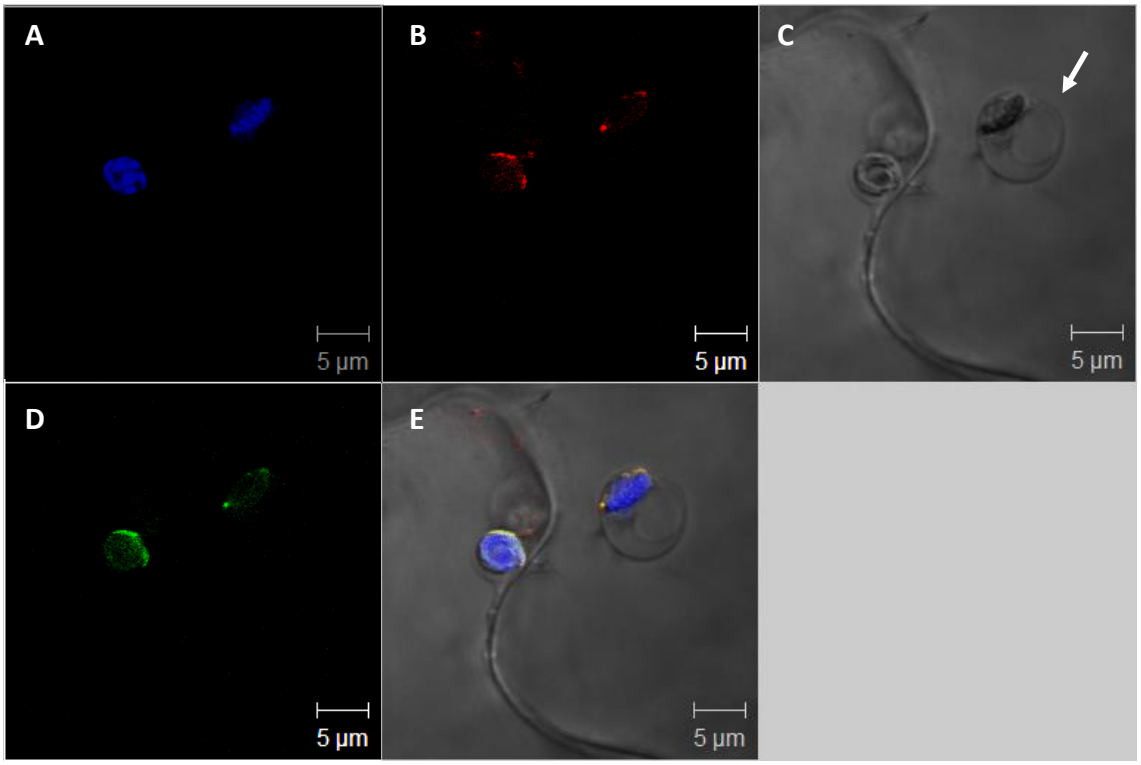

Figure 5.1.24. Atypical morphology chloroplasts expressing AE1 and NpHR protein. Expression of a 2in1 vector containing TPT-AE1 in the first cassette tag to a mCherry and TPT-NpHR in the second cassette tag to a GFP. AE1 (red, B) and NpHR (green, D) expression in chloroplasts of epidermal cells. The chlorophyll autofluorescence is shown in blue (A, E). C is the bright field image, and E shows a merged image where it is possible to see the co-localisation of both proteins (yellow). An arrow is indicating a swollen chloroplasts in image C. The images are from 20-slice Z-stack through epidermal cells with 0.6 µm interval between slices. In all the images the scale bar is 5 µm.

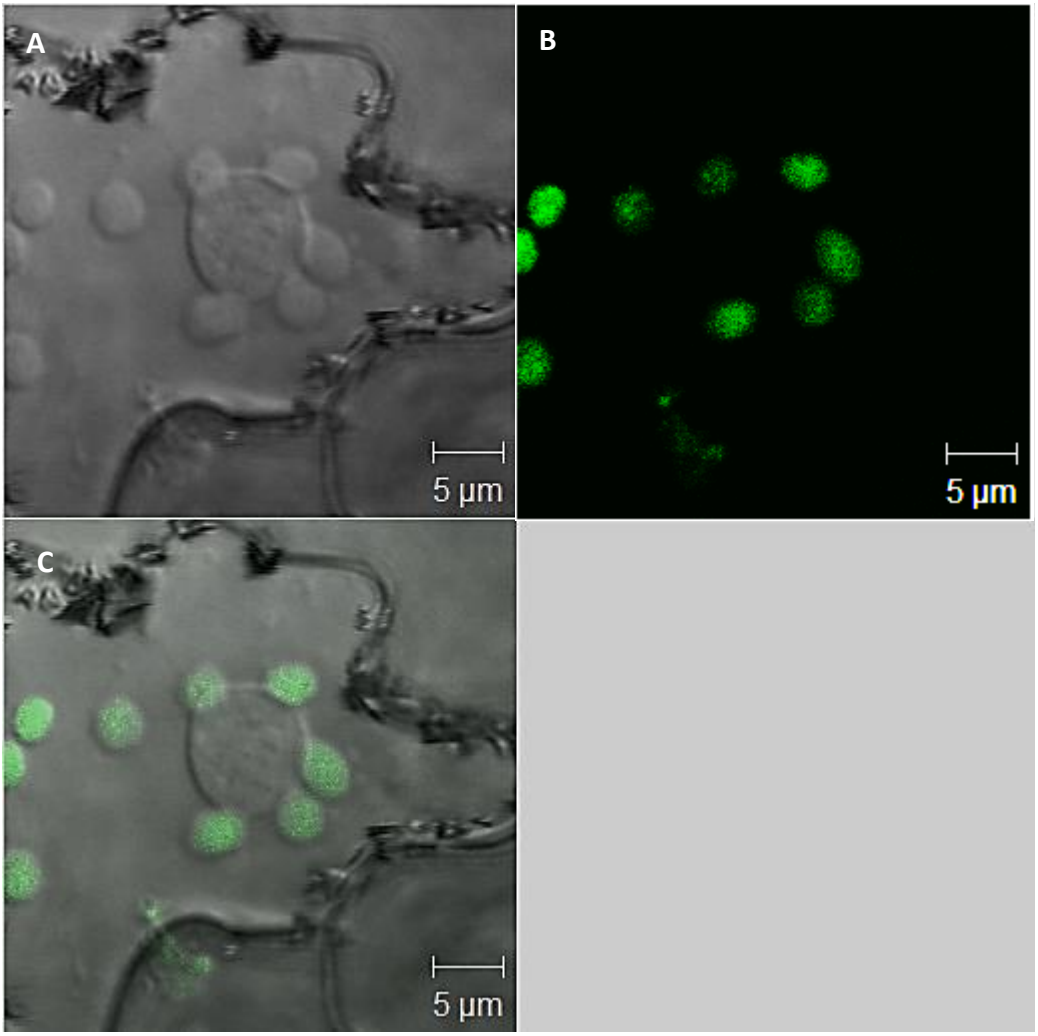

Figure 5.1.25. Confocal microscope image from an untransformed tobacco leaf chloroplasts. Chlorophyll fluorescence (green, B, C). A shows the bright field image and C is merged image. The images are from a single scan of epidermal cells. In all the images the scale bar is 5 µm.

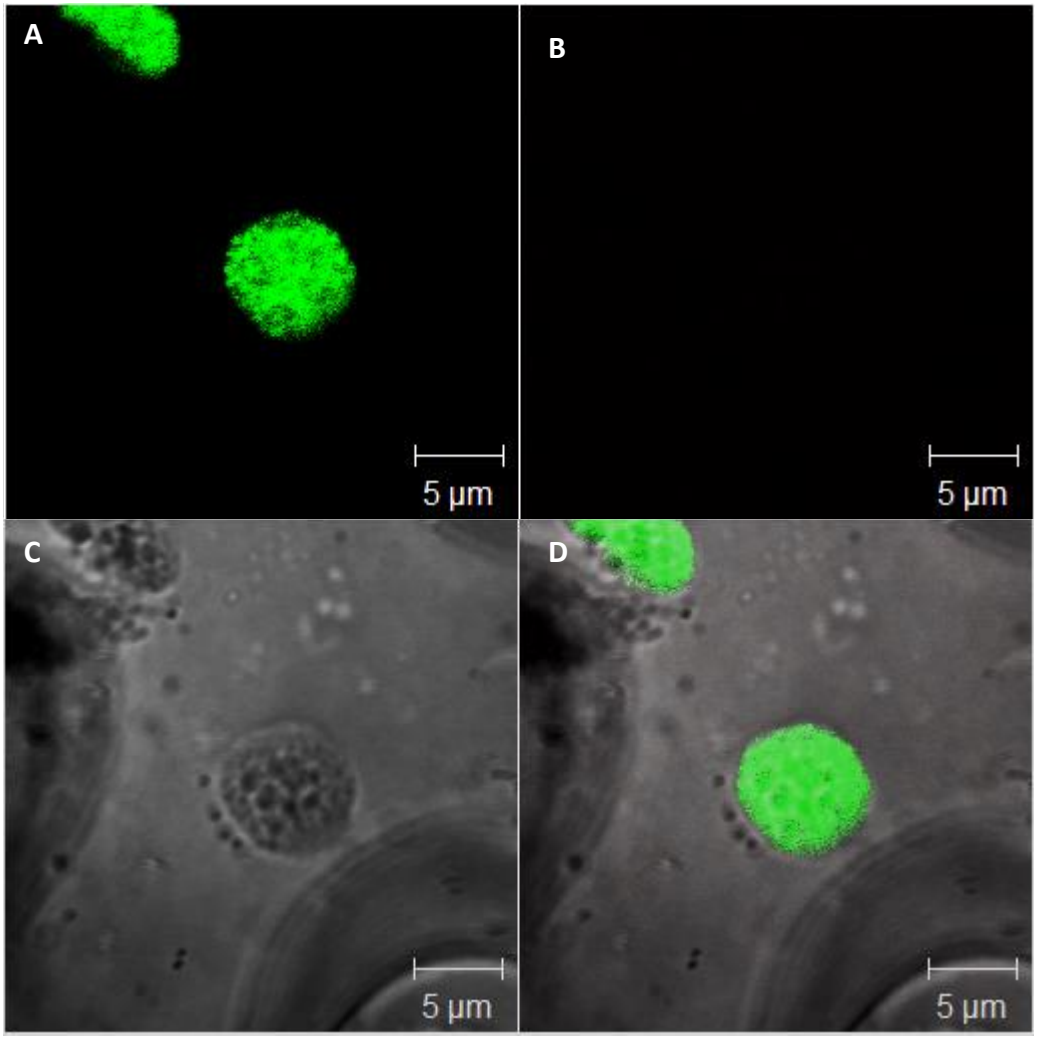

Figure 5.1.26. Epidermal cells chloroplasts confocal microscope image from a tobacco leaf transiently transformed with untransformed Agrobacterium. Chlorophyll fluorescence (green, A, D). C is the bright field image and D is a merged image. The images are from 14-slice Z-stack through chloroplasts with 0.75 µm interval between slices. In all the images the scale bar is 5 µm.

Observed the atypical morphology it was established a method to classify the chloroplasts in different levels depending on how severe was the affection. It was established level 0 for the non-affected chloroplasts; level 1 for the chloroplasts presenting a moderate level of atypical morphology; and level 2 for the chloroplasts presenting a strong affection (Figure 5.1.27).

Following these criteria it was possible to calculate the chloroplasts atypical morphology degree average between the chloroplasts expressing the different proteins (Figure 5.1.27D). As a control there were analysed chloroplasts transformed

with non-transformed *Agrobacterium*, again to discard the effects of *Agrobacterium* in chloroplasts morphology. The control chloroplast presented an average degree of atypical morphology of 0.17, being the lowest. Chloroplasts transformed with NpHR got the higher level of atypical morphology with an average of 0.80. Chloroplasts transformed with AE1 got a level of atypical morphology average of 0.57. Finally, chloroplasts expressing AE1 and NpHR got an average level of affection of 0.49 respectively. The averages in all the cases were lower than 1, indicating a very low number of chloroplasts found with a level of atypical morphology 2. After doing the one-way ANOVA analysis ($p<0.05$) it was observed that all of the different values were statistically different among themselves. The chloroplasts expressing NpHR were the most affected by atypical morphology, however, when expressing both proteins together the affection got decreased.

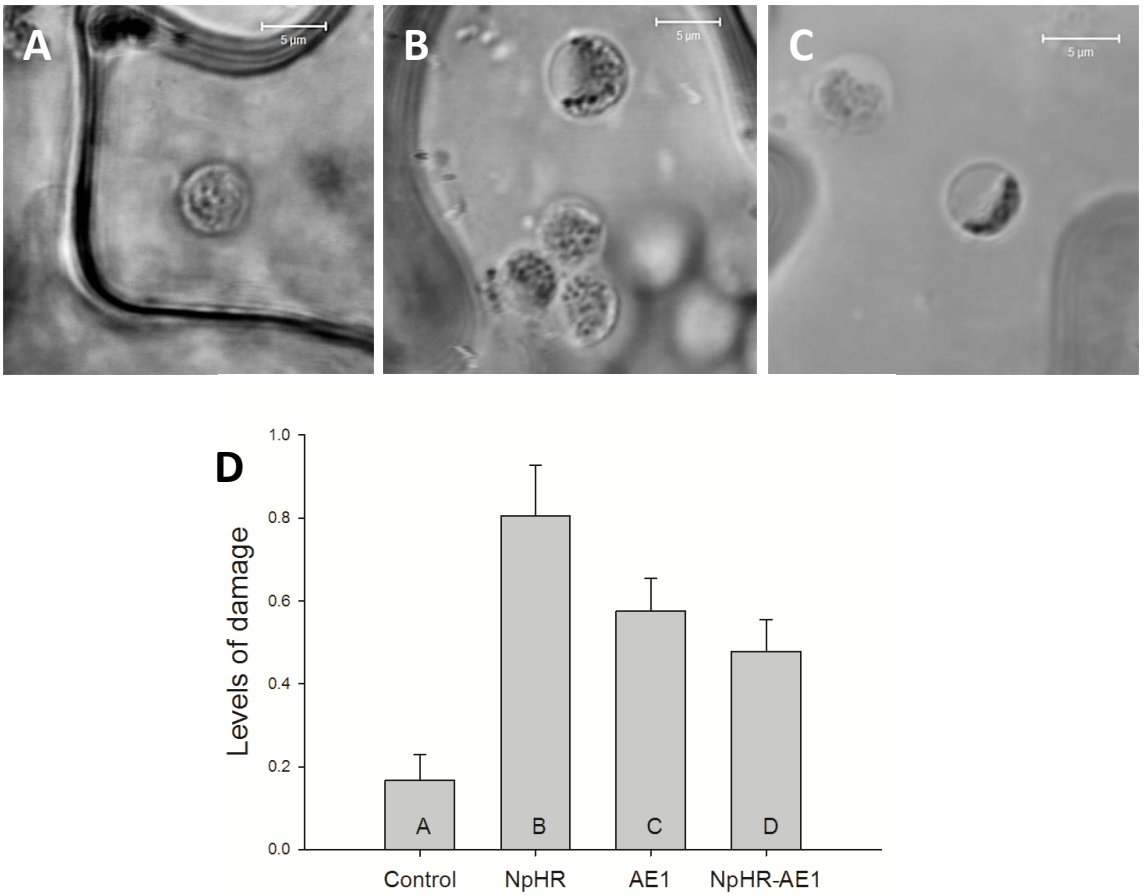

Figure 5.1.27. (A-C) Different levels of atypical morphology established in relation to the atypical morphology obtained between the analysed chloroplasts. A-C are bright field confocal microscopy images from chloroplasts of transiently transformed tobacco. A, B and C show an example of chloroplasts of a level of atypical morphology equal to 0, 1 and 2 respectively. A is a 3D reconstruction image from 24-slices Z-stack through the chloroplasts with a 0.75 µm interval between slices. B is a 3D reconstruction image from 12-slice Z-stacks through the chloroplasts with a 0.8 µm interval between slices. C is a 3D reconstruction image from 11-slices Z-stacks through the chloroplasts with a 0.75 µm interval between slices. In all figures the scale bar is 5 µm. D shows the analysis of the different degrees of atypical morphology in the chloroplasts transformed with different constructs and compared with the control. Control: cells infiltrated with non-transformed *Agrobacterium*. Lettering indicates significant differences after one-way ANOVA ($p<0.05$) as determined by Holm-Sidak test.

To check for bCMO1 protein activity high-performance liquid chromatography (HPLC) was performed by a colleague of the MAGIC project in Penn State University, Bryan Ferlez. In this analysis the levels of β-carotene between chloroplasts expressing bCMO1 and control chloroplasts from a wild type tobacco plant were compared. I prepared chloroplast fractions from a wild type tobacco plant, to be used as a control,

and from transiently transformed leaf tissues expressing the construct 35S::RbcL-bCMO1. The results from the HPLC showed that the levels of β-carotene were 50 % lower in the chloroplasts expressing bCMO1 in comparison with the control (Figure 5.1.28), indicating the functionality of the protein. The HPLC analysis also detected other pigments such as chlorophyll A and unidentified carotenoids, which shown no difference between the control and the bCMO1 transformed chloroplasts.

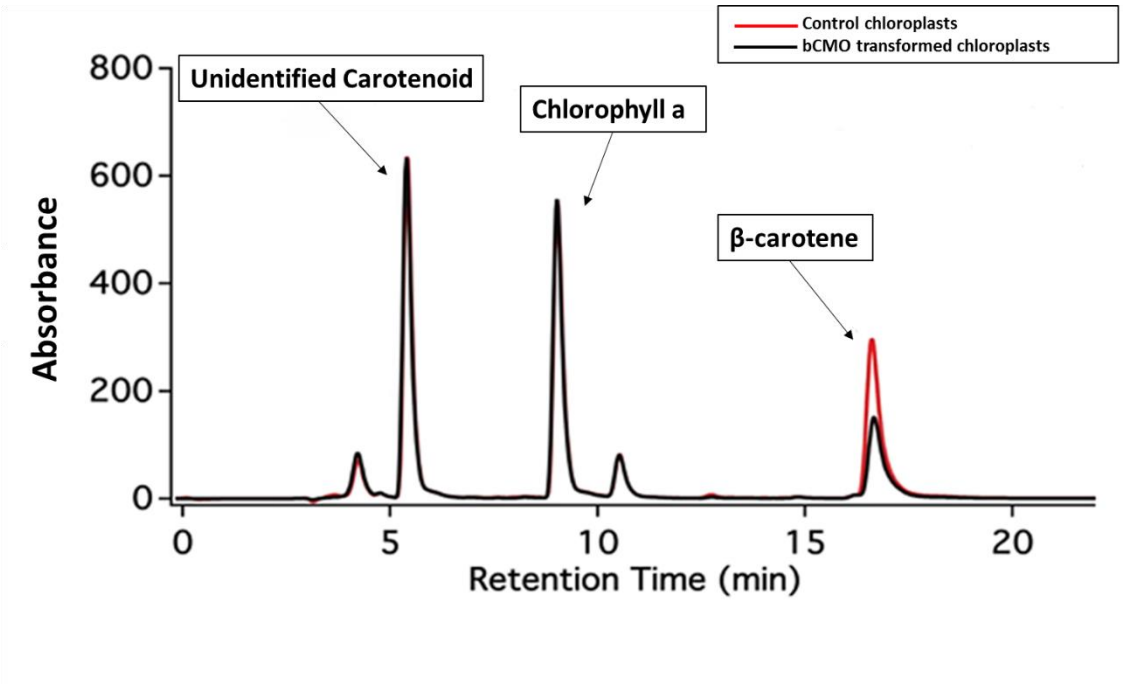

Figure 5.1.28. High-performance liquid chromatography (HPLC) analysis of β-carotene and other pigments content of isolated chloroplasts solutions. Black line: analysis on wild type chloroplasts solution, control. Red line: analysis on isolated chloroplasts expressing bCMO1 solutions. HPLC analysis shows the absorbance by retention time. The level of β-carotene from chloroplasts transformed with bCMO1 is 51 % of control chloroplasts.

In conclusion, I found an effect on the chloroplasts caused by the expression of the different proteins. NpHR as well as AE1 expression caused an atypical morphology of the chloroplasts characterised by more swollen shape and a shift of the chlorophyll to one side of the chloroplasts. bCMO1 activity was demonstrated under HPLC analysis.

5.1.3. Gas exchange measurements

In order to test the impact of the different proteins in the whole plant level I generated stable Arabidopsis transgenic lines with some of the constructs previously mentioned. In total, six different constructs were selected (Table 5.1.6) for Arabidopsis transformation by the *Agrobacterium* floral dipping method. All the constructs contained a BASTA resistance gene incorporated in the vector, which allowed the selection of transformed Arabidopsis plants.

Table 5.1.6. Selected constructs to get stable Arabidopsis lines

Construct number	Gene of expression	Expression construct
1	NpHR	35S::TPT-NpHR-RFP
2	AE1	35S::TPT-AE1-RFP
3	bCMO1	35S::RbcL-bCMO1-6His
4	bCMO1 NpHR	35S::RbcL-bCMO1-mCherry 35S::TPT-NpHR-GFP
5	AE1 NpHR	35S::TPT-AE1-mCherry 35S::TPT-NpHR-GFP
6	AE1 bCMO1 NpHR	35S::TPT-AE1-mCherry 35S::RbcL-bCMO1-6His 35S::TPT-NpHR-GFP

Arabidopsis stable lines were obtained from all of the constructs selected as at least three independent transformants. Plants expressing single genes were useful to assess the effect of each protein separately. The combination of bCMO1 with NpHR was useful for testing the influence of bCMO1 in NpHR. The expression of AE1 together with NpHR, with and without bCMO1, was the combination of proteins expected to increase the HCO_3^- in the chloroplasts stroma.

Gas exchange measurements were carried out on T3 generation Arabidopsis transgenic plants transformed with the 6 different selected constructs. Three different transgenic lines from each construct were selected to realise the experiments. I undertook A/Ci analysis using a LI-COR 6400XT infrared gas analyzer (LI-COR Bioscience GmbH, Bad Homburg, Germany) with plants grown under low light (70 µmol m^{-2} s^{-1})

and high light (300 µmol m^{-2} s^{-1}) conditions from every construct and line. Values of A_{sat}, A_{max}, $V_{c\,max}$ and g_s from transgenic line 1, line 2 and line 3 are shown in Figures 5.1.29, 5.1.30 and 5.1.31 respectively. These parameters were defined as follows: A_{sat} was calculated as the light saturated rates of CO_2 assimilation; A_{max} was calculated as the light- and carbon-saturated rates of CO_2 assimilation, $V_{c\,max}$ was determined as the maximum carboxylation velocity of Rubisco; and g_s was determined as the stomatal conductance under steady-state conditions at saturating light intensity and ambient CO_2.

Figure 5.1.28 shows gas exchange measurements results from the first line of stable transgenic Arabidopsis plants analysed. There were statistically significant differences between the plants grown in low light conditions expressing bCMO1 compared to the rest of them in all the factors analysed (figure 1, A). Which showed higher levels of A_{max}, $V_{c\,max}$, A_{sat} as well as g_s. However, phenotypically, the plants that had a difference respect the others, in this case being smaller, were the ones expressing NpHR an AE1 together, independently if bCMO1 was expressed. For the plants grown at high light the most remarkable difference is that the plant expressing the three genes together had lower levels of A_{max}, $V_{c\,max}$, A_{sat} and g_s.

Figure 5.1.29 shows gas exchange measurements from the second line of Arabidopsis transgenic plants. The results observed did not coincide with the ones from the 1st line. Nevertheless, it has to be taken into account that the number of samples analysed is too little for a proper statistical analysis. Figure 5.1.30 shows gas exchange measurements form the last line of Arabidopsis plants analysed (3rd line). The number of samples analysed for plants grown at high light conditions was too little to do statistical analysis. Not the case with the plants grown at low light conditions, which main differences are that the control has higher values of A_{max}, $V_{c\,max}$, A_{sat} and g_s compared to most of the transgenic plants.

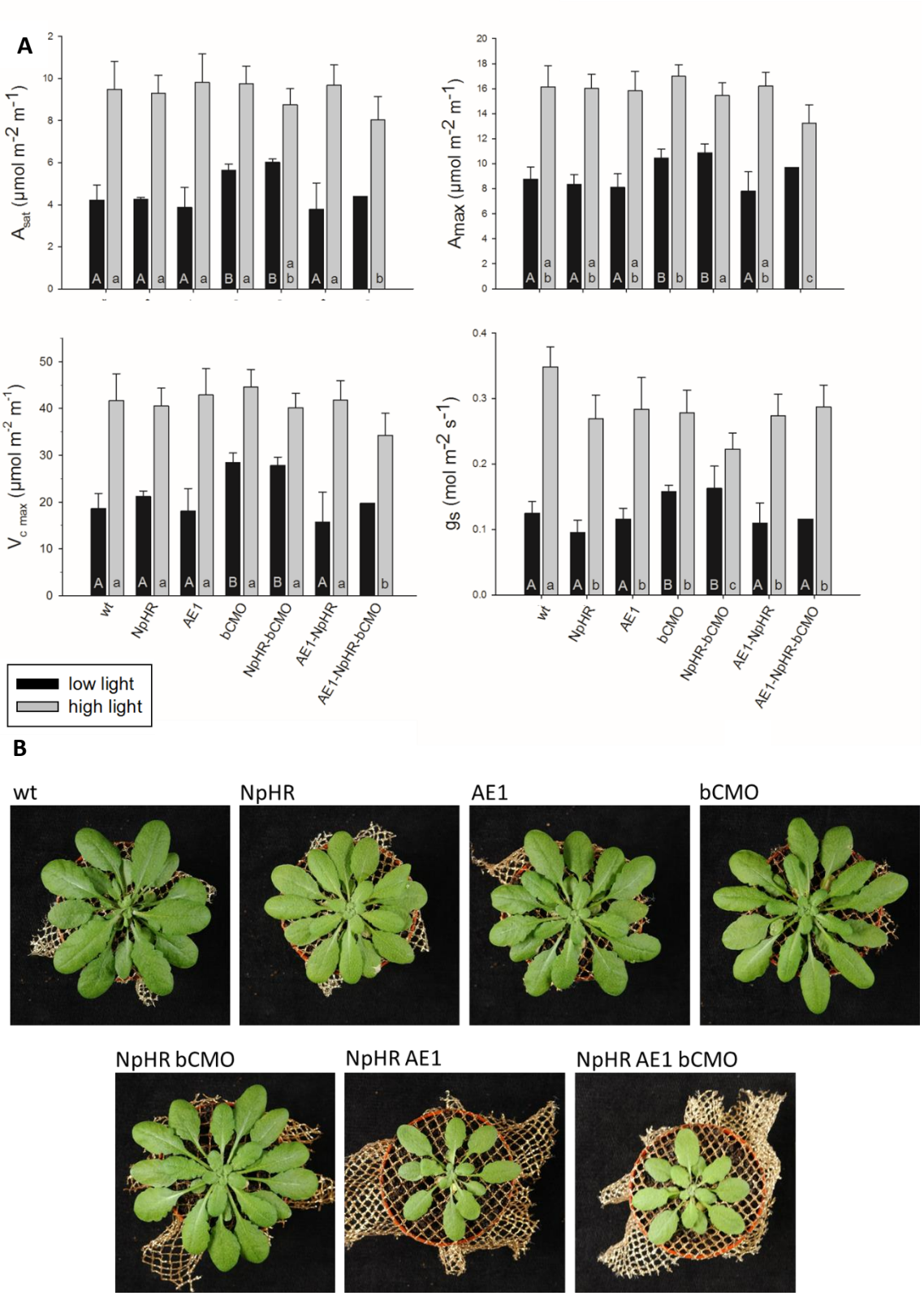

Figure 5.1.29. (A) Gas exchange measurement values for the line 1 of transgenic Arabidopsis plants. Values of light saturated rate of CO_2 assimilation (Asat), light and carbon saturated rate of CO_2 assimilation (Amax), maximum carboxylation velocity of Rubisco (Vc max) and stomatal conductance (gs) of the six different selected transgenic plants compared with a wild-type (wt) plant. The plants were grown under low (70

µmol m^{-2} s^{-1}) or high (300 µmol m^{-2} s^{-1}) light conditions. Experiments were carried out with saturating light at 500 µmol m^{-2} s^{-1} (10 % Blue). Leaf temperature was maintained at 22°C. Data are means of different replicates. Lettering indicates significant differences after one-way ANOVA ($p<0.05$) as determined by Holm-Sidak test, performed between plants grown at low light and high light conditions. (B) Plant phenotype from the line 1 of transgenic Arabidopsis plants. Pictures of Col-0 Arabidopsis (wt) and six different plants expressing the six different constructs selected for Arabidopsis transformation (NpHR, AE1, bCMO1, NpHR-bCMO1, NpHR-AE1 and NpHR-AE1-bCMO1).

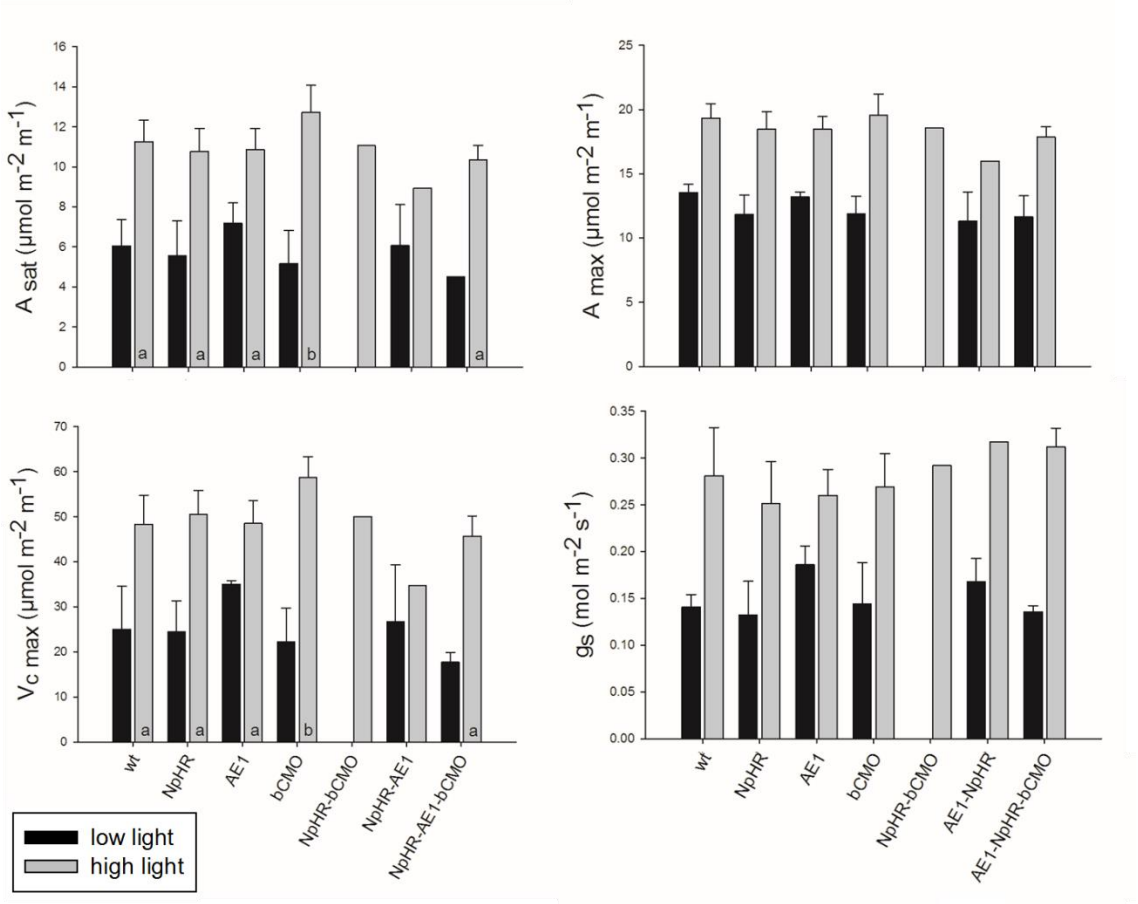

Figure 5.1.30. Gas exchange measurement values for the line 2 of transgenic Arabidopsis plants. Values of light saturated rate of CO2 assimilation (Asat), light and carbon saturated rate of CO2 assimilation (Amax), maximum carboxylation velocity of Rubisco (Vc max) and stomatal conductance (gs) of the six different selected transgenic plants compared with a wild-type (wt) plant. The plants were grown under low (70 µmol m^{-2} s^{-1}) or high (300 µmol m^{-2} s^{-1}) light conditions. Experiments were realised with saturating light at 500 µmol m^{-2} s^{-1} (10 % Blue). Leaf temperature was maintained at 22°C. Data are means of different replicates. Lettering indicates significant differences after one-way ANOVA ($p<0.05$) as determined by Holm-Sidak test, performed between plants grown at low light and high light conditions.

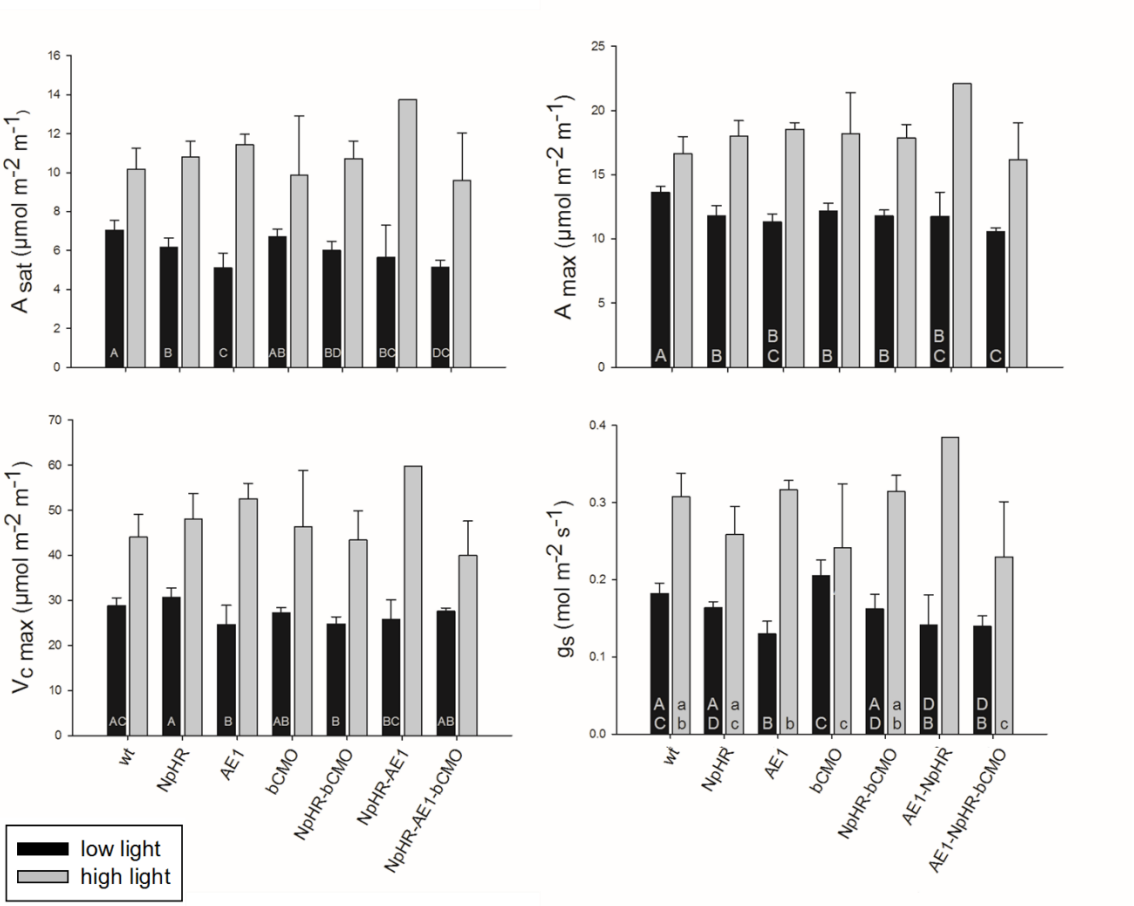

Figure 5.1.31. Gas exchange measurement values for the line 3 of transgenic Arabidopsis plants. Values of light saturated rate of CO2 assimilation (Asat), light and carbon saturated rate of CO2 assimilation (Amax), maximum carboxylation velocity of Rubisco (Vc max) and stomatal conductance (gs) of the six different selected transgenic plants compared with a wild-type (wt) plant. The plants were grown under low (70 µmol m^{-2} s^{-1}) or high (300 µmol m^{-2} s^{-1}) light conditions. Experiments were realised with saturating light at 500 µmol m^{-2} s^{-1} (10 % Blue). Leaf temperature was maintained at 22°C. Data are means of different replicates. Lettering indicates significant differences after one-way ANOVA ($p<0.05$) as determined by Holm-Sidak test, performed between plants grown at low light and high light conditions.

5.2. Manipulation of stomatal kinetics

5.2.1 KAT1

This chapter arose following the idea that manipulating stomatal kinetics, in order to better align stomatal conductance with mesophyll demand for CO_2, may be a way of improving photosynthesis and water use efficiency (Lawson, Kramer et al. 2012, Lawson and Blatt 2014). According to Wang *et al.* (2014), manipulating the gating properties of the guard cell K^+ channels is likely to be the most effective method to

achieve this aim. Indeed, the sites involved in the gating properties of KAT1 channel have been identified and mutants which have gating properties shifted to more positive or more negative values have been created (Lefoulon, Karnik et al. 2014).

5.2.1.1. Modelling

I used the OnGuard model to simulate how manipulating the gating properties of the K_{in} channels may affect the stomatal response to transitions between light and dark that will affect photosynthetic demand for CO_2. The model was run simulating separately two different conditions of the K_{in} channels gating properties. Such conditions implied tuning K_{in} channel gating, that is the value for $V_{1/2}$ which is the voltage at half-maximal activation of the channel, to more positive or more negative values. Considering normal values of K_{in} channels $V_{1/2}$ of -180 mV, the model was run at $V_{1/2}$ of -120 mV and -160 mV to simulate a displace of the gating to more positive values, and $V_{1/2}$ of -200 mV and -240 mV to simulate a displace of the gating to more negative values.

In this chapter I present the data from the modelling for variations of $V_{1/2}$ at -120 mV (Figures 5.2.1-5.2.6) and -240 mV (Figures 5.2.7-5.2.12). Simulations were carried out first with the full complement of membrane transporters under normal conditions, and then with K_{in} channels $V_{1/2}$ modified to more positive or negative values as indicated in each figure. In all the cases the model was run on a standard diurnal cycle of 12 h light followed by 12 h of dark, with 10 mM KCl, 1 mM $CaCl_2$ and pH 6.5 outside (Chen, Hills et al. 2012, Wang, Papanatsiou et al. 2012, Wang, Hills et al. 2014). The modelling data I am presenting shows the macroscopic outputs from the OnGuard model (Figures 5.2.1 and 5.2.7); the K^+ contents and analysis of K^+ fluxes at the plasma membrane and tonoplast (Figures 5.2.2 and 5.2.8); cytosolic and vacuolar pH and H^+ fluxes across the plasma membrane and tonoplast (Figures 5.2.3 and 5.2.9); chloride contents and analysis of Cl^- fluxes at the plasma membrane and tonoplast (Figures 5.2.4 and 5.2.10); malic acid synthesis, total malate (Mal) contents and analysis of Mal^{2-} fluxes at the plasma membrane and tonoplast (Figures 5.2.5 and 5.2.11); and finally, cytosolic and vacuolar [Ca^{2+}], cytosolic-free [Ca^{2+}] and analysis of Ca^{2+} fluxes across the plasma membrane and tonoplast (Figures 5.2.6 and 5.2.11). The simulation was initiated with

wild-type parameters and K_{in} $V_{1/2}$ was modified at the beginning of day 3, yielding a new stable cycle from day 4 onwards. Thus, the data shown is from day 2 for the wild-type and day 5 for the modified conditions, at which point both cycles were stable.

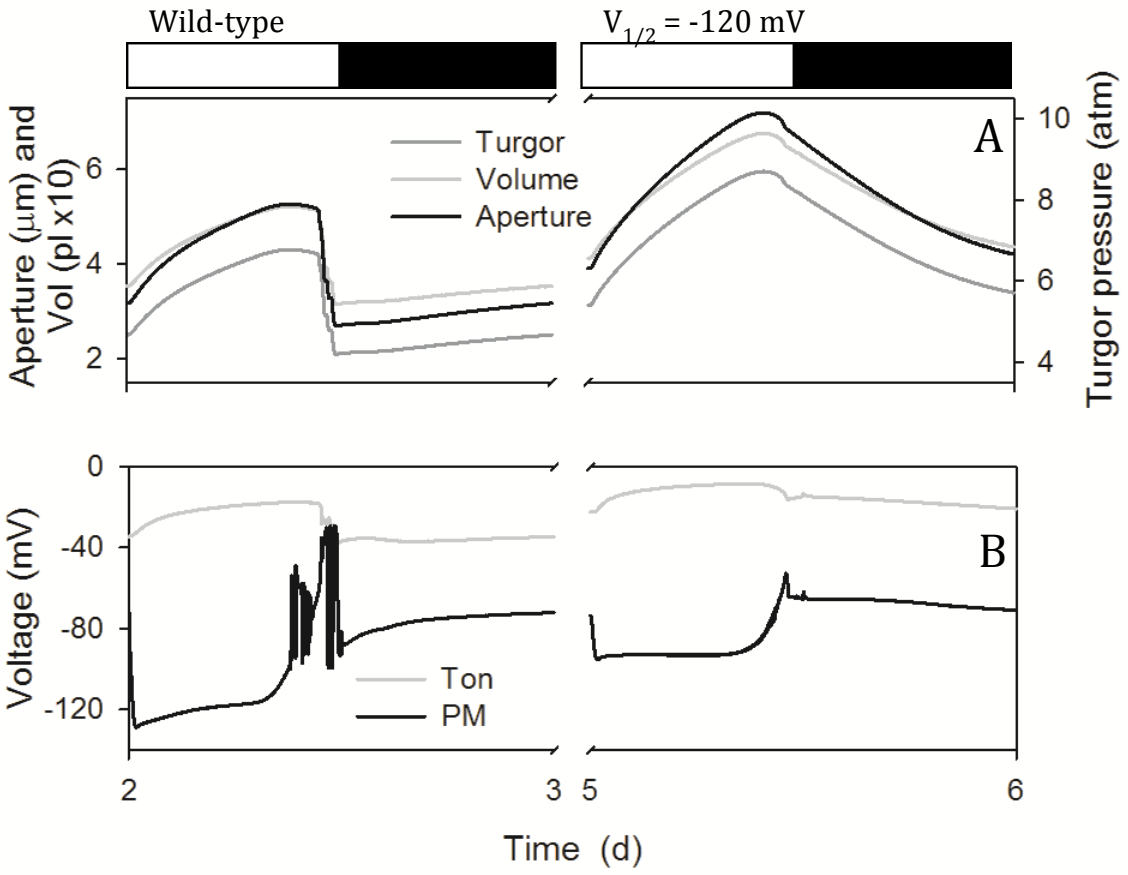

Figure 5.2.1. Macroscopic outputs from the OnGuard model. Outputs resolved over a standard diurnal cycle (12 h light:12 h dark, indicated by bars above) with 10 mM KCl, 1 mM $CaCl_2$ and pH 6.5 outside (Chen, Hills et al. 2012). Representative diurnal cycles are shown for the wild-type (control, left) and the manipulation of K_{in} channels $V_{1/2}$ to -120 mV from -180 mV (right). For the results in this and the subsequent figures, the simulation was initiated with wild-type parameters (Wang, Papanatsiou et al. 2012) and the K_{in} $V_{1/2}$ was manipulated at the start of day 3, yielding a new stable cycle from day 4 onwards. A summary analysis is provided with each of the subsequent figures; further details will be found in Chen, et al. (2012). Shown are (A) stomatal aperture, turgor pressure and total guard cell volume, and (B) plasma membrane and tonoplast voltages. Stomatal apertures varied over a physiological range between roughly 3 µm and 6 µm in the wild-type and from 3 µm to 8 µm when K_{in} $V_{1/2}$ was modified. Stomatal apertures were paralleled by physiologically sensible changes in guard cell volume and turgor. Following stomatal closure at the end of the day, the model generated a small and gradual rise in aperture and the associated outputs that anticipated the start of the next day, much as has been observed in vivo (Gorton, Williams et al. 1993,

Meidner and Willmer 1993). The start of the day was associated with hyperpolarisation of the plasma membrane to voltages near -130 mV and the dark period was accompanied by depolarisation of the plasma membrane to voltages near the equilibrium voltage for K^+, consistent with the diurnal cycle in energetic outputs of the ATP-driven pumps (Spanswick 1981, Blatt 1987, Blatt and Clint 1989, Clint and Blatt 1989, McClure, Shaff et al. 1989, Kinoshita, Nishimura et al. 1995). Voltage oscillations at the end of the daylight period are detailed by Chen, et al. (2012) and mark periods of substantial K^+ and anion efflux that drive stomatal closure. When K_{in} $V_{1/2}$ was shifted to more positive values the model predicted a bigger aperture of the stomata during daylight period with a slower and non-complete closure during the night (A). The start of the day presented a very small hyperpolarisation of the plasma membrane reaching voltages near -100 mV. Consequently, oscillations on voltage disappear at the end of the daylight period (B).

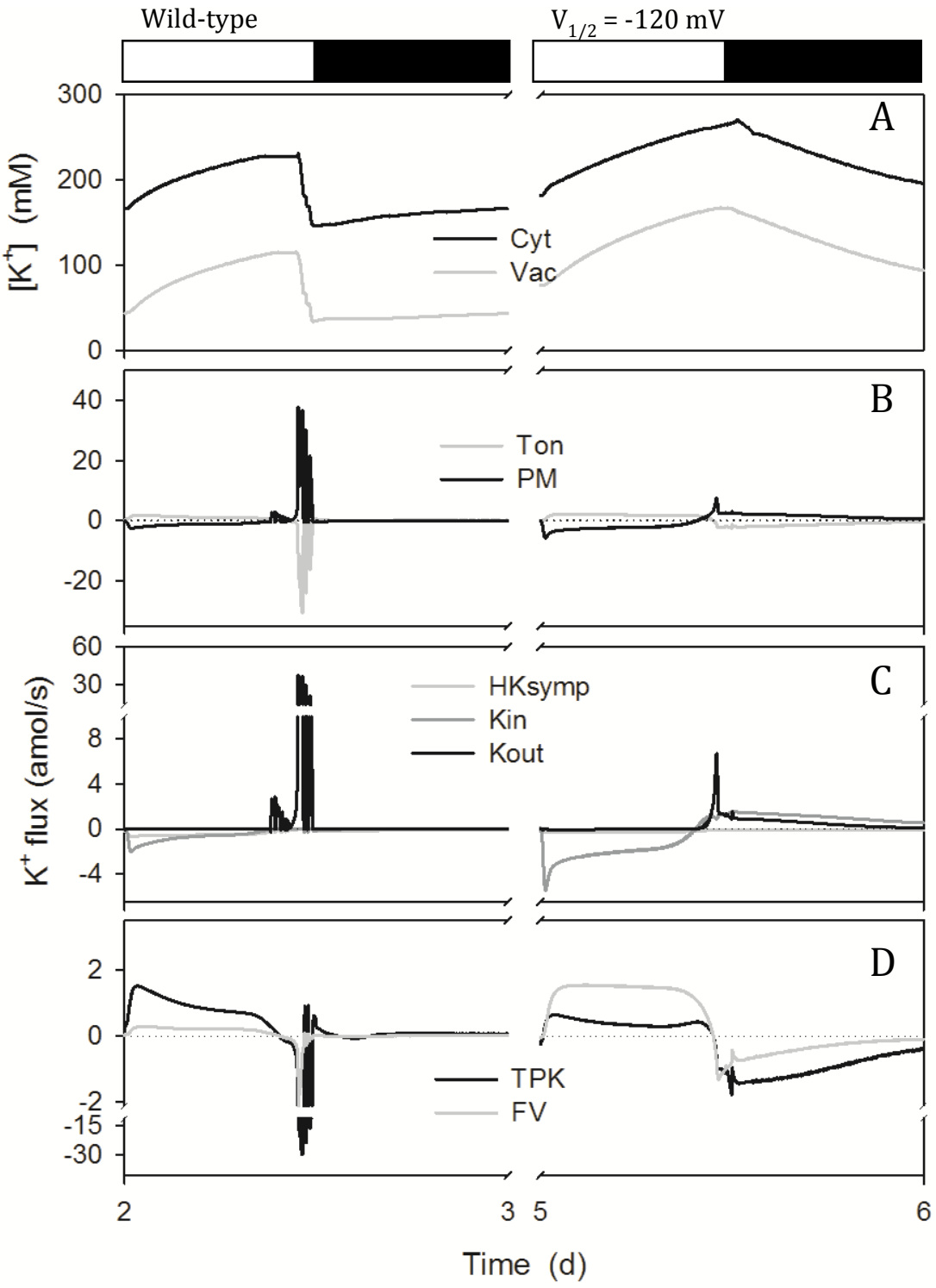

Figure 5.2.2. K^+ contents and analysis of K^+ fluxes at the plasma membrane and tonoplast resolved over a standard diurnal cycle (12 h light:12 h dark, indicated by bars above) (Chen, Hills et al. 2012) for the wild-type (left) and the manipulation of K_{in} channels $V_{1/2}$ to -120 mV from -180 mV (right) as described in Figure 5.2.1. Shown are (A) cytosolic and vacuolar [K^+], (B) the net K^+ flux across the plasma membrane and tonoplast, (C) the K^+ flux through the K^+-permeable transporters at the plasma membrane, comprising the two K^+ channels and the H^+-K^+ symporter, and (D) the K^+

flux through the K^+ permeable transporters at the tonoplast, comprising the TPK and FV channels. K^+ flux through the TPC channel accounted for less than one percent of either of the other channel fluxes, and has therefore been omitted for purposes of clarity. Positive flux is defined as movement of the ionic species (not the charge) out of the cytosol, either across the plasma membrane or the tonoplast. In the wild-type, the cytosolic K^+ concentration varied between approximately 160 mM and 230 mM; in the vacuole, K^+ concentrations ranged between approximately 40 mM and 120 mM (A). The major proportion of K^+ influx across the plasma membrane was shunted across the tonoplast to the vacuole during the day and this pattern reversed in the first hours of dark, as expected from experimental observation (Chen, Hills et al. 2012, Hills, Chen et al. 2012). At the plasma membrane (C), K^+ influx was dominated by $I_{K,in}$ in the first half of the day, this flux relaxing to roughly that through the H^+-K^+ symport in the second half of the day. Closure was marked by the predominance of K^+ efflux through $I_{K,out}$, which relaxed to a near-zero value during the night. The model predicted a higher retention of K^+ in both cytosol and vacuole during daylight period (A) when the K_{in} $V_{1/2}$ was modified to more positive values, with a very slow and low decrease on K^+ retention during the dark period; the cytosolic K^+ concentration varied between approximately 190 mM and 280 mM; in the vacuole, K^+ concentrations ranged between approximately 90 mM and 150 mM (A). The model also predicted an increase of fluxes across either plasma membrane and tonoplast during the daylight period (B) with a complete lack on fluxes oscillations at the end of the daylight period; it also predicted a big increase on fluxes of K^+ through the K_{in} (C) and the FV channels (D); a remarkable increase of K^+ fluxes through the FV channels during the daylight period, which provided the major proportion of K^+ influx to the vacuole; and a remarkable efflux of K^+ from the vacuole during the dark period also through the FV channels (D). It also predicted an increase on the efflux of K^+ from the vacuole through the TPK channels during the dark period.

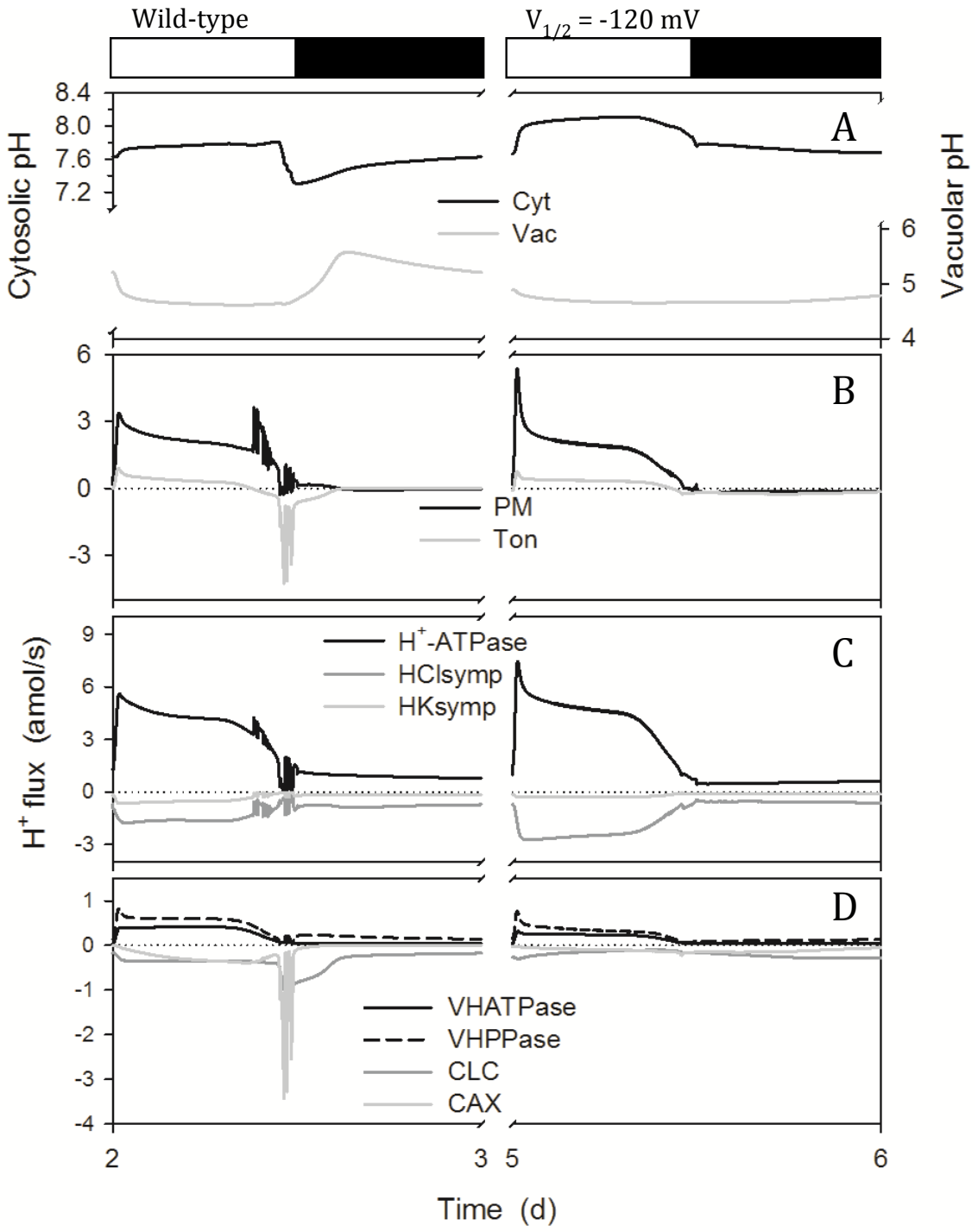

Figure 5.2.3. Cytosolic and vacuolar pH, and H^+ fluxes across the plasma membrane and tonoplast. Outputs resolved over a standard diurnal cycle (12 h light:12 h dark, indicated by bars above) (Chen, Hills et al. 2012) for the wild-type (control, left) and the manipulation of K_{in} channels $V_{1/2}$ to -120 mV from -180 mV (right) as described in Figure 5.2.1. Shown are (A) cytosolic and vacuolar pH, (B) the net H^+ flux across the plasma membrane and tonoplast, (C) the H^+ flux through the H^+-permeable transporters at the plasma membrane, comprising the H^+-ATPase, and the H^+-K^+ and H^+-Cl^- symporters, and (D) the H^+ flux through the H^+ permeable transporters at the tonoplast, comprising the VH^+-ATPase, VH^+-PPase, the CLC H^+-Cl^- antiporter and the

CAX H^+-Ca^{2+} antiporter. Positive flux is defined as movement of the ionic species (not the charge) out of the cytosol, either across the plasma membrane or the tonoplast. The bulk of H^+ production associated with daytime Mal synthesis (Figure 5) is exported via the plasma membrane H^+-ATPase, with roughly 20% transported to the vacuole (B-D). In the vacuole, Mal comprises the major pH buffer and its accumulation is associated with acidification of the vacuolar contents (Van Kirk and Raschke 1978, Talbott and Zeiger 1993, Willmer and Fricker 1996). The organic acid is thought to be transported as the fully deprotonated (Mal^{2-}) form – with the ALMT channel as the primary pathway for tonoplast Mal^{2-} flux [reviewed by Hills, et al. (2012)] – implying charge balance via the tonoplast VH^+-ATPase H^+-PPase (Rea and Poole 1993, Martinoia, Maeshima et al. 2007). When K_{in} $V_{1/2}$ was modified to more positive values, the model predicted a small increase in cytosolic pH, and a decrease during the night on vacuolar one (A). An increase on H^+ efflux during the daylight period through ATP pump, and an increase on H^+-Cl^- symport, while H^+-K^+ symport remained similar (C); and minimal H^+ fluxes during the dark period. Fluxes of H^+ vacuolar pumps and CLC, CAX channels were reduced (D) and oscillations on H^+ fluxes were not observable through any of the transporters.

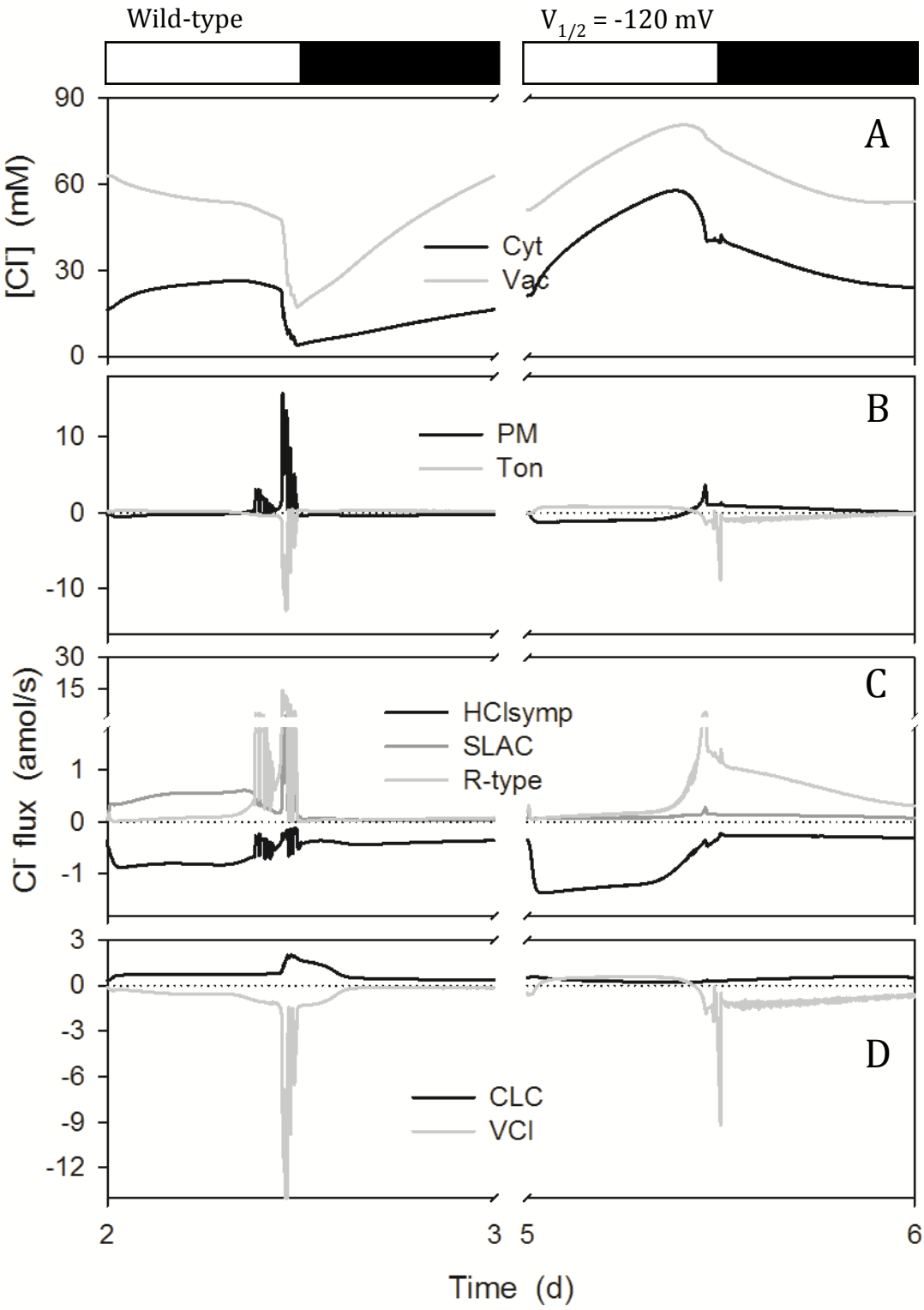

Figure 5.2.4. Chloride contents and analysis of Cl^- fluxes at the plasma membrane and tonoplast. Outputs resolved over a standard diurnal cycle (12 h light:12 h dark, indicated by bars above) (Chen, Hills et al. 2012) for the wild-type (control, left) and the manipulation of K_{in} channels $V_{1/2}$ to -120 mV from -180 mV (right) as described in Figure 5.2.1. Shown are (A) total cytosolic and vacuolar [Cl^-], (B) the net flux of Cl^- across the plasma membrane and tonoplast, (C) the flux of Cl^- through the Cl^- -permeable transporters at the plasma membrane, comprising the SLAC and R- (ALMT-)

type anion channels and H^+-Cl^- symporter, and (D) the flux of Cl^- through the Cl^- -permeable transporters at the tonoplast, comprising the VCL channel and CLC H^+-Cl^- antiporter. Positive flux is defined as movement of the ionic species (not the charge) out of the cytosol, either across the plasma membrane or the tonoplast. In the wild-type stomatal opening was accompanied by a net efflux of Cl^- from the vacuole to the cytosol and later in the daylight period from the cytosol to the apoplast. Closure was marked by much larger fluxes of Cl^- from the vacuole to the cytosol and export across the plasma membrane this pattern reversed after the first 1-2 h of dark. The rise in cytosolic Cl^- concentration during the first hours of the day arose from the rapid Cl^- efflux from the vacuole, and a slower rise in the rate of Cl^- export across the plasma membrane. When K_{in} $V_{1/2}$ was modified to more positive values the model predicted a higher retention of Cl^- either in cytosol and vacuole during the daylight as well as during the dark period (A); during the daylight period it predicted an influx of Cl^- either from the apoplast to the cytosol and from the cytosol to the vacuole (A); during the dark period there was an efflux of Cl^- from the vacuole to cytoplasm, and from cytoplasm to the apoplast, more pronounced at the end of the daylight period (A). Cl^- fluxes through both plasma membrane and cytoplasm became increased, predominantly through H^+-Cl^- symport during the daylight period, and through R-type channels during the dark period (C).

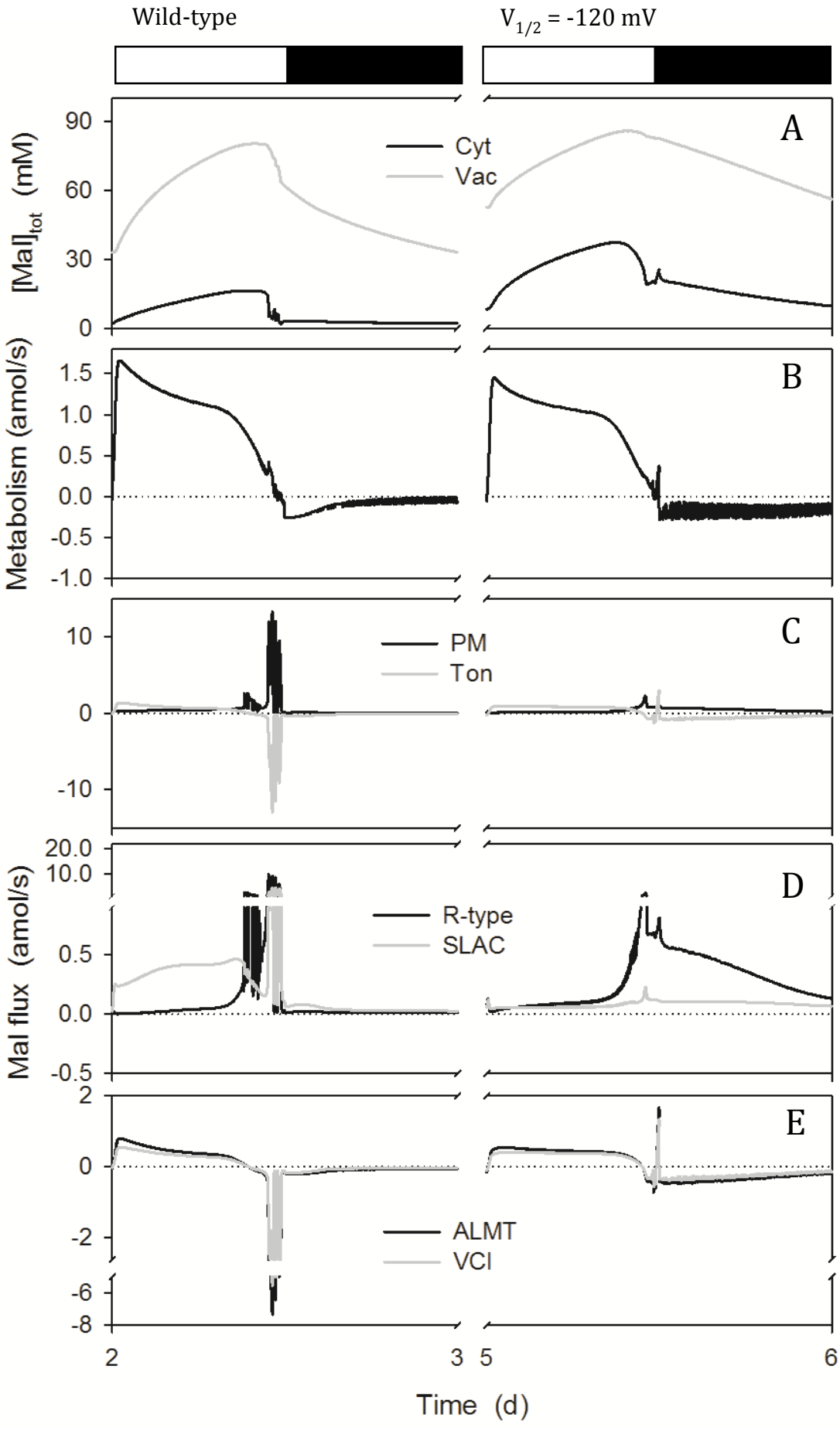
Wild-type
$V_{1/2}$ = -120 mV
A
B
C
D
E
Cyt
Vac
PM
Ton
R-type
SLAC
ALMT
VCl
$[Mal]_{tot}$ (mM)
Metabolism (amol/s)
Mal flux (amol/s)
Time (d)
90
60
30
0
1.5
1.0
0.5
0.0
-0.5
-1.0
10
0
-10
20.0
10.0
0.5
0.0
-0.5
2
0
-2
-6
-8
2
3
5
6

Figure 5.2.5. Malic acid synthesis, total malate (Mal) contents and analysis of Mal^{2-} fluxes at the plasma membrane and tonoplast resolved over a standard diurnal cycle (12 h light:12 h dark, indicated by bars above) (Chen, Hills et al. 2012) for the wild-type (control, left) and the manipulation of K_{in} channels $V_{1/2}$ to -120 mV from -180 mV (right) as described in Figure 5.2.1. Shown are (A) total cytosolic and vacuolar [Mal], (B) the rates of Mal synthesis and metabolism, (C) the net flux of Mal^{2-} across the plasma membrane and tonoplast, (D) the Mal^{2-} flux through the Mal^{2-} -permeable transporters at the plasma membrane, comprising the SLAC and R- (ALMT-) type anion channels, and (E) the Mal^{2-} flux through the Mal^{2-} -permeable transporters at the tonoplast, comprising the VMAL and VCL channels. Positive flux is defined as movement of the ionic species (not the charge) out of the cytosol, either across the plasma membrane or the tonoplast. In the wild-type, the bulk of Mal production was diverted by transport of Mal^{2-} across the tonoplast, leading to a rise in total vacuolar Mal from 30 mM at the end of the night to near 90 mM before declining at the end of the daylight period; Mal in the cytosol rose from approximately 1 mM to values near 15 mM, much as has been estimated from experimental data (Hills, Chen et al. 2012). When K_{in} $V_{1/2}$ was modified to more positive values the model predicted a higher retention of total malate either in cytosol and vacuole during the daylight as well as during the dark period (A); total vacuolar malate rise from 50 mM at the end of the dark period to 90 mM at the end of the daylight period, in the cytosol rose from approximately 5 mM to values of 30 mM Malate metabolism became shortly reduced (B). Fluxes through plasma membrane and tonoplast became reduced, however an increase of malate fluxes through R-type channels during the dark period was observed (D). Oscillations of malate fluxes were slightly existent.

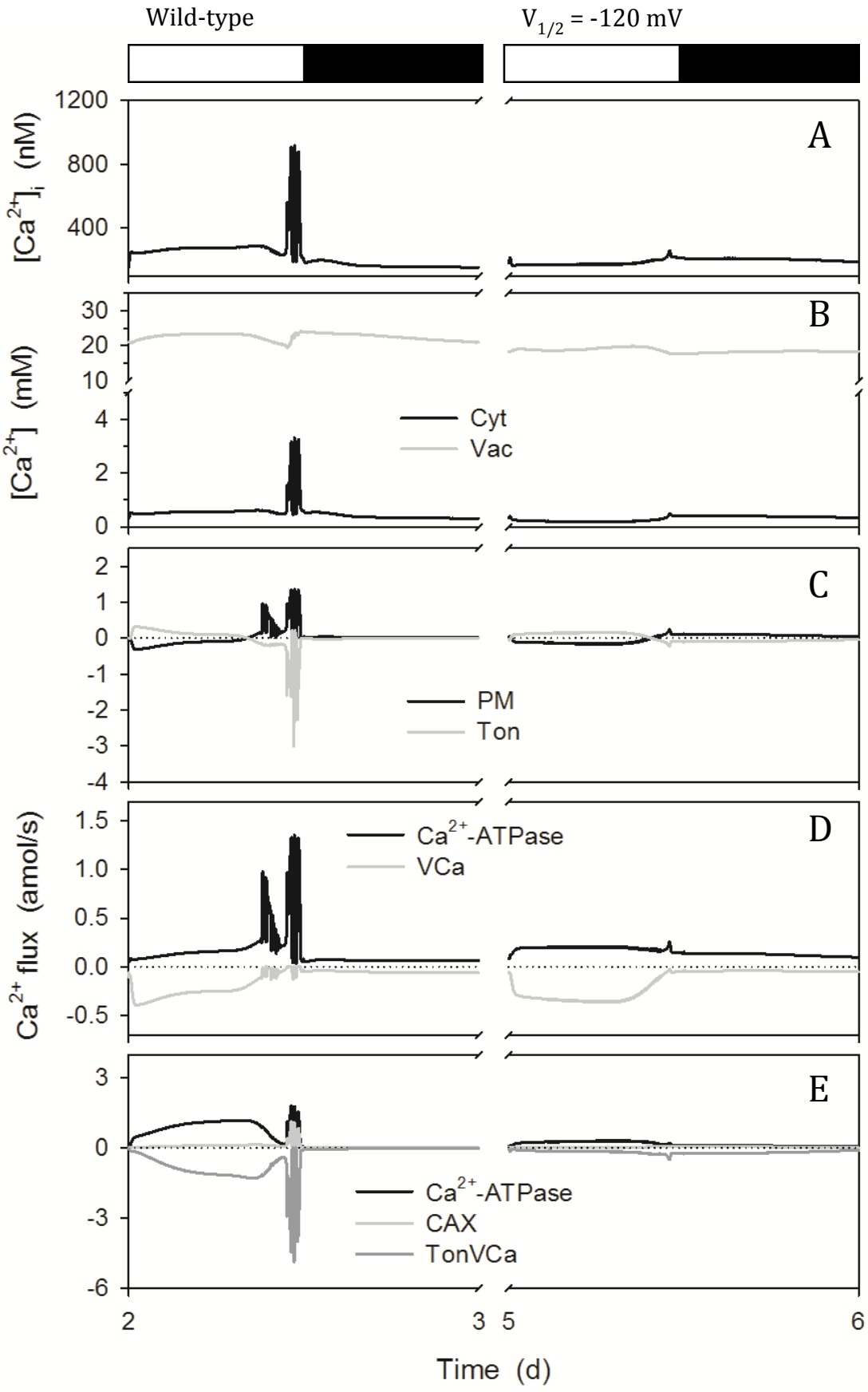
Wild-type
$V_{1/2}$ = -120 mV
A
B
C
D
E
$[Ca^{2+}]_i$ (nM)
$[Ca^{2+}]$ (mM)
Ca^{2+} flux (amol/s)
Cyt
Vac
PM
Ton
Ca^{2+}-ATPase
VCa
Ca^{2+}-ATPase
CAX
TonVCa
Time (d)

Figure 5.2.6. Total cytosolic and vacuolar [Ca^{2+}], cytosolic free [Ca^{2+}], and analysis of Ca^{2+} fluxes across the plasma membrane and tonoplast resolved over a standard diurnal cycle (12 h light:12 h dark, indicated by bars above) (Chen, Hills et al. 2012) for the wild-type (control, left) and the manipulation of K_{in} channels $V_{1/2}$ to -120 mV from -180 mV (right) as described in Figure 5.2.1. Shown are (A) the cytosolic-free [Ca^{2+}] ([Ca^{2+}]$_i$), (B) the total cytosolic and vacuolar [Ca^{2+}], (C) the net flux of Ca^{2+} across the plasma membrane and tonoplast, (D) the Ca^{2+} flux through the Ca^{2+} -permeable transporters at the plasma membrane, comprising the hyperpolarisation-activated Ca^{2+} channel and the Ca^{2+}-ATPase, and (E) the flux of Ca^{2+} through the Ca^{2+} permeable transporters at the tonoplast, comprising the Ca^{2+}-ATPase, the CAX H^{+}-Ca^{2+} antiporter, and the TonVCa Ca^{2+} channel. Flux through the TPC channel accounts for less than two percent of the total Ca^{2+} flux across the tonoplast and has therefore been omitted for purposes of clarity. Positive flux is defined as movement of the ionic species (not the charge) out of the cytosol, either across the plasma membrane or the tonoplast. For the wild-type, the OnGuard model predicted [Ca^{2+}]$_i$ to decrease from a value near 200 nM in the daylight period to a resting value near 100 nM in the dark period (A). Stomatal closure was accompanied by a series of voltage (Figure 1) and [Ca^{2+}]$_i$ oscillations that drive K^{+} and anion efflux for stomatal closure (Gilroy, Fricker et al. 1991, Irving, Gehring et al. 1992, McAinsh, Brownlee et al. 1992, Thiel, MacRobbie et al. 1992). When K_{in} $V_{1/2}$ was modified to more positive values the model predicted a decrease on the Ca^{2+} levels in both cytosol and vacuole (B), which concentration varied from 100 nM to 150 nM between daylight and dark period. Ca^{2+} oscillations disappeared completely at the beginning of the dark period. Fluxes of Ca^{2+} through VCa channels became increased during the daylight period (D).

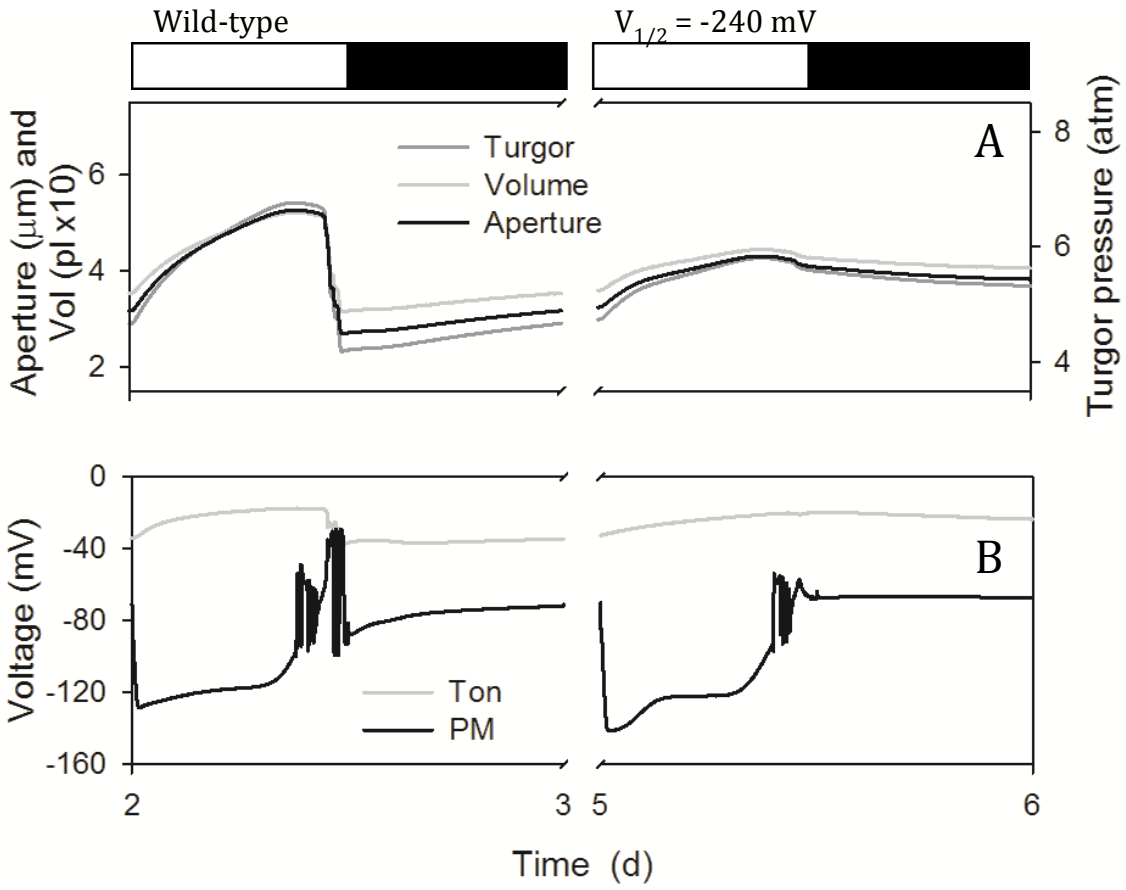

Figure 5.2.7. Macroscopic outputs from the OnGuard model. Outputs resolved over a standard diurnal cycle (12 h light:12 h dark, indicated by bars above) with 10 mM KCl, 1 mM $CaCl_2$ and pH 6.5 outside (Chen, Hills et al. 2012). Representative diurnal cycles are shown for the wild-type (control, left) and the manipulation of K_{in} channels $V_{1/2}$ to -240 mV from -180 mV (right). Shown are (A) stomatal aperture, turgor pressure and total guard cell volume, and (B) plasma membrane and tonoplast voltages. Stomatal apertures varied over a physiological range between roughly 3 µm and 6 µm in the wild-type and approximately from 3 µm to 4 µm when K_{in} $V_{1/2}$ was modified. Stomatal apertures were paralleled by physiologically sensible changes in guard cell volume and turgor. Following stomatal closure at the end of the day, the model generated a small and gradual rise in aperture and the associated outputs that anticipated the start of the next day, much as has been observed in vivo (Gorton, Williams et al. 1993, Meidner and Willmer 1993). The start of the day was associated with hyperpolarisation of the plasma membrane to voltages near -130 mV and the dark period was accompanied by depolarisation of the plasma membrane to voltages near the equilibrium voltage for K^+, consistent with the diurnal cycle in energetic outputs of the ATP-driven pumps (Spanswick 1981, Blatt 1987, Blatt and Clint 1989, Clint and Blatt 1989, McClure, Shaff et al. 1989, Kinoshita, Nishimura et al. 1995). Voltage oscillations at the end of the daylight period are detailed by Chen, et al. (2012) and mark periods of substantial K^+ and anion efflux that drive stomatal closure. When K_{in} $V_{1/2}$ was shifted to more negative values the model predicted a minimal aperture of the stomata during the daylight period (A). Membrane voltage suffered a bigger hyperpolarisation during

the daylight period reaching voltages near -150 mV, causing les pronounced oscillations at the beginning of the dark period (B).

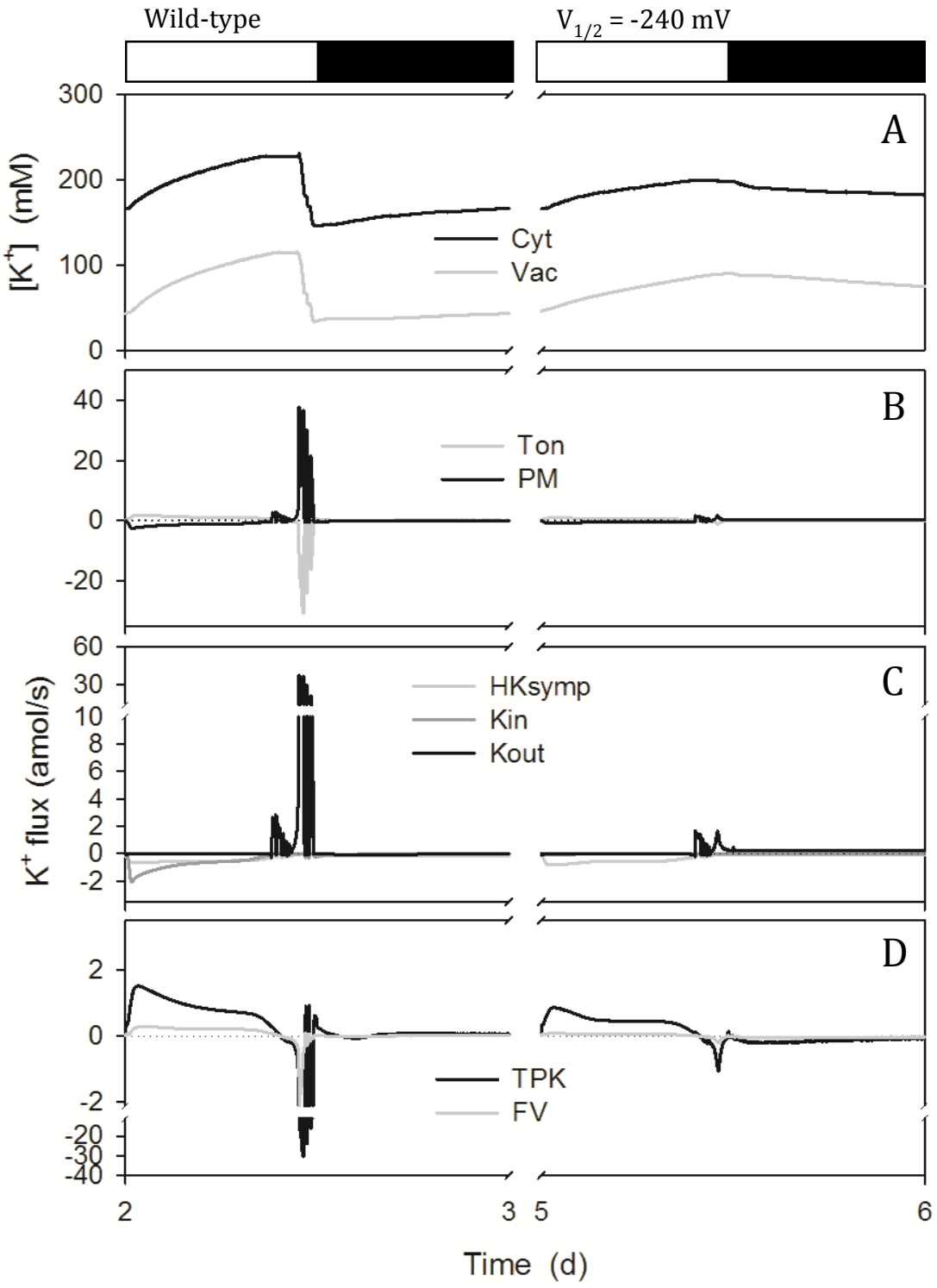

Figure 5.2.8. K^+ contents and analysis of K^+ fluxes at the plasma membrane and tonoplast resolved over a standard diurnal cycle (12 h light:12 h dark, indicated by bars above) (Chen, Hills et al. 2012) for the wild-type (left) and the manipulation of K_{in} channels $V_{1/2}$ to -240 mV from -180 mV (right) as described in Figure 5.2.7. Shown are (A) cytosolic and vacuolar [K^+], (B) the net K^+ flux across the plasma membrane and tonoplast, (C) the K^+ flux through the K^+-permeable transporters at the plasma membrane, comprising the two K^+ channels and the H^+-K^+ symporter, and (D) the K^+

flux through the K^+ permeable transporters at the tonoplast, comprising the TPK and FV channels. K^+ flux through the TPC channel accounted for less than one percent of either of the other channel fluxes, and has therefore been omitted for purposes of clarity. Positive flux is defined as movement of the ionic species (not the charge) out of the cytosol, either across the plasma membrane or the tonoplast. In the wild-type, the cytosolic K^+ concentration varied between approximately 160 mM and 230 mM; in the vacuole, K^+ concentrations ranged between approximately 40 mM and 120 mM (A). The major proportion of K^+ influx across the plasma membrane was shunted across the tonoplast to the vacuole during the day and this pattern reversed in the first hours of dark, as expected from experimental observation (Chen, Hills et al. 2012, Hills, Chen et al. 2012). At the plasma membrane (C), K^+ influx was dominated by $I_{K,in}$ in the first half of the day, this flux relaxing to roughly that through the H^+-K^+ symport in the second half of the day. Closure was marked by the predominance of K^+ efflux through $I_{K,out}$, which relaxed to a near-zero value during the night. When K_{in} $V_{1/2}$ was modified to more negative values the model predicted a decrease on K^+ retention in both plasma membrane and cytoplasm compared to the wild-type (A); the cytosolic K^+ concentration varied between approximately 160 mM and 190 mM; in the vacuole, K^+ concentrations ranged between approximately 40 mM and 100 mM (A). K^+ fluxes either through plasma membrane and tonoplast decreased, and K^+ fluxes oscillations were not appreciable (B, C, D).

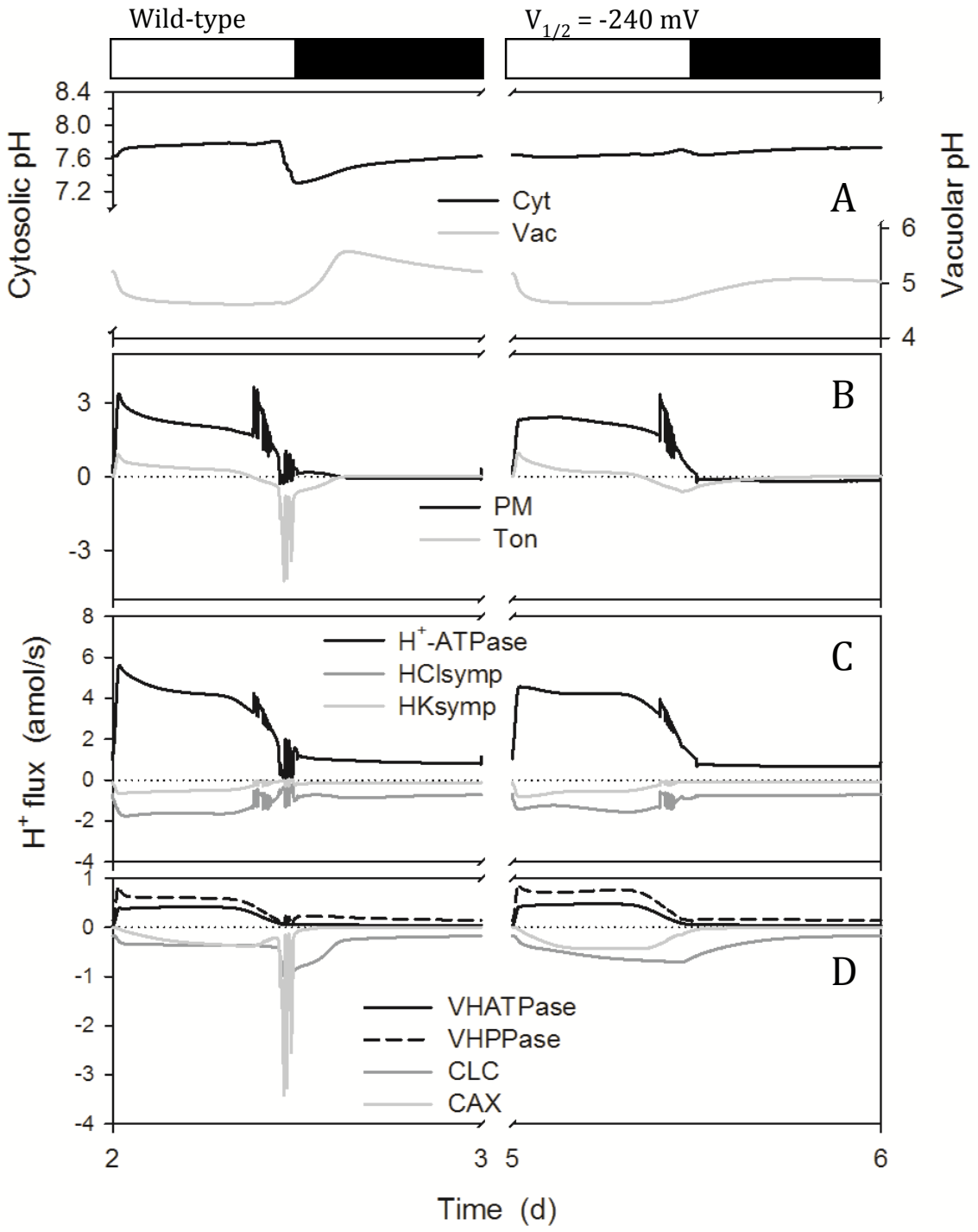

Figure 5.2.9. Cytosolic and vacuolar pH, and H^+ fluxes across the plasma membrane and tonoplast. Outputs resolved over a standard diurnal cycle (12 h light:12 h dark, indicated by bars above) (Chen, Hills et al. 2012) for the wild-type (control, left) and the manipulation of K_{in} channels $V_{1/2}$ to -240 mV from -180 mV (right) as described in Figure 5.2.7. Shown are (A) cytosolic and vacuolar pH, (B) the net H^+ flux across the plasma membrane to and tonoplast, (C) the H^+ flux through the H^+-permeable transporters at the plasma membrane, comprising the H^+-ATPase, and the H^+-K^+ and H^+-Cl^- symporters, and (D) the H^+ flux through the H^+ permeable transporters at the tonoplast, comprising the VH^+-ATPase, VH^+-PPase, the CLC H^+-Cl^- antiporter and the

CAX H^+-Ca^{2+} antiporter. Positive flux is defined as movement of the ionic species (not the charge) out of the cytosol, either across the plasma membrane or the tonoplast. The bulk of H^+ production associated with daytime Mal synthesis (Figure 10) is exported via the plasma membrane H^+-ATPase, with roughly 20% transported to the vacuole (B-D). In the vacuole, Mal comprises the major pH buffer and its accumulation is associated with acidification of the vacuolar contents (Van Kirk and Raschke 1978, Talbott and Zeiger 1993, Willmer and Fricker 1996). The organic acid is thought to be transported as the fully deprotonated (Mal^{2-}) form – with the ALMT channel as the primary pathway for tonoplast Mal^{2-} flux [reviewed by Hills, et al. (2012)] – implying charge balance via the tonoplast VH^+-ATPase and H^+-PPase (Rea and Poole 1993, Martinoia, Maeshima et al. 2007). When K_{in} $V_{1/2}$ was modified to more negative values the model predicted a small decrease on cytosolic pH showing no difference between the daylight and the dark periods; and it predicted a decrease on vacuolar pH during the dark period. Fluxes of H^+ in general were reduced in exception of fluxes through CLC and CAX which became slightly increased (D). Minimal H^+ fluxes oscillations were observed.

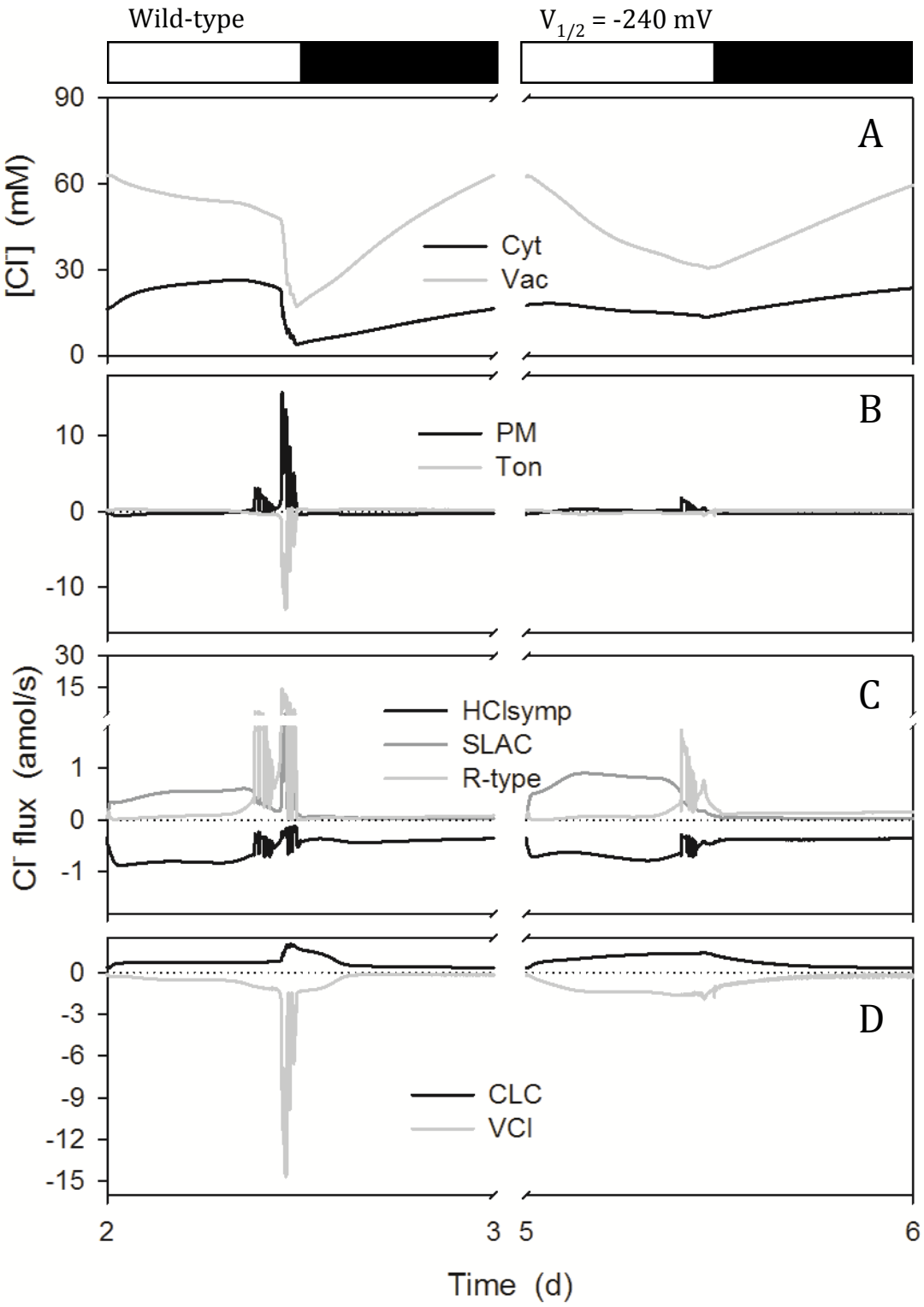

Figure 5.2.10. Chloride contents and analysis of Cl^- fluxes at the plasma membrane and tonoplast. Outputs resolved over a standard diurnal cycle (12 h light:12 h dark, indicated by bars above) (Chen, Hills et al. 2012) for the wild-type (control, left) and the manipulation of K_{in} channels $V_{1/2}$ to -240 mV from -180 mV (right) as described in Figure 5.2.7. Shown are (A) total cytosolic and vacuolar [Cl^-], (B) the net flux of Cl^- across the plasma membrane and tonoplast, (C) the flux of Cl^- through the Cl^- -permeable transporters at the plasma membrane, comprising the SLAC and R- (ALMT-)

type anion channels and H^+-Cl^- symporter, and (D) the flux of Cl^- through the Cl^- -permeable transporters at the tonoplast, comprising the VCL channel and CLC H^+-Cl^- antiporter. Positive flux is defined as movement of the ionic species (not the charge) out of the cytosol, either across the plasma membrane or the tonoplast. In the wild-type stomatal opening was accompanied by a net efflux of Cl^- from the vacuole to the cytosol and later in the daylight period from the cytosol to the apoplast. Closure was marked by much larger fluxes of Cl^- from the vacuole to the cytosol and export across the plasma membrane this pattern reversed after the first 1-2 h of dark. The rise in cytosolic Cl^- concentration during the first hours of the day arose from the rapid Cl^- influx across the tonoplast, and a slower rise in the rate of Cl^- export across the plasma membrane. When K_{in} $V_{1/2}$ was modified to more negative values the model predicted a reduction on cytosolic and vacuolar Cl^- levels (A), and a lightly increase on Cl^- fluxes through CLC and VCl channels.

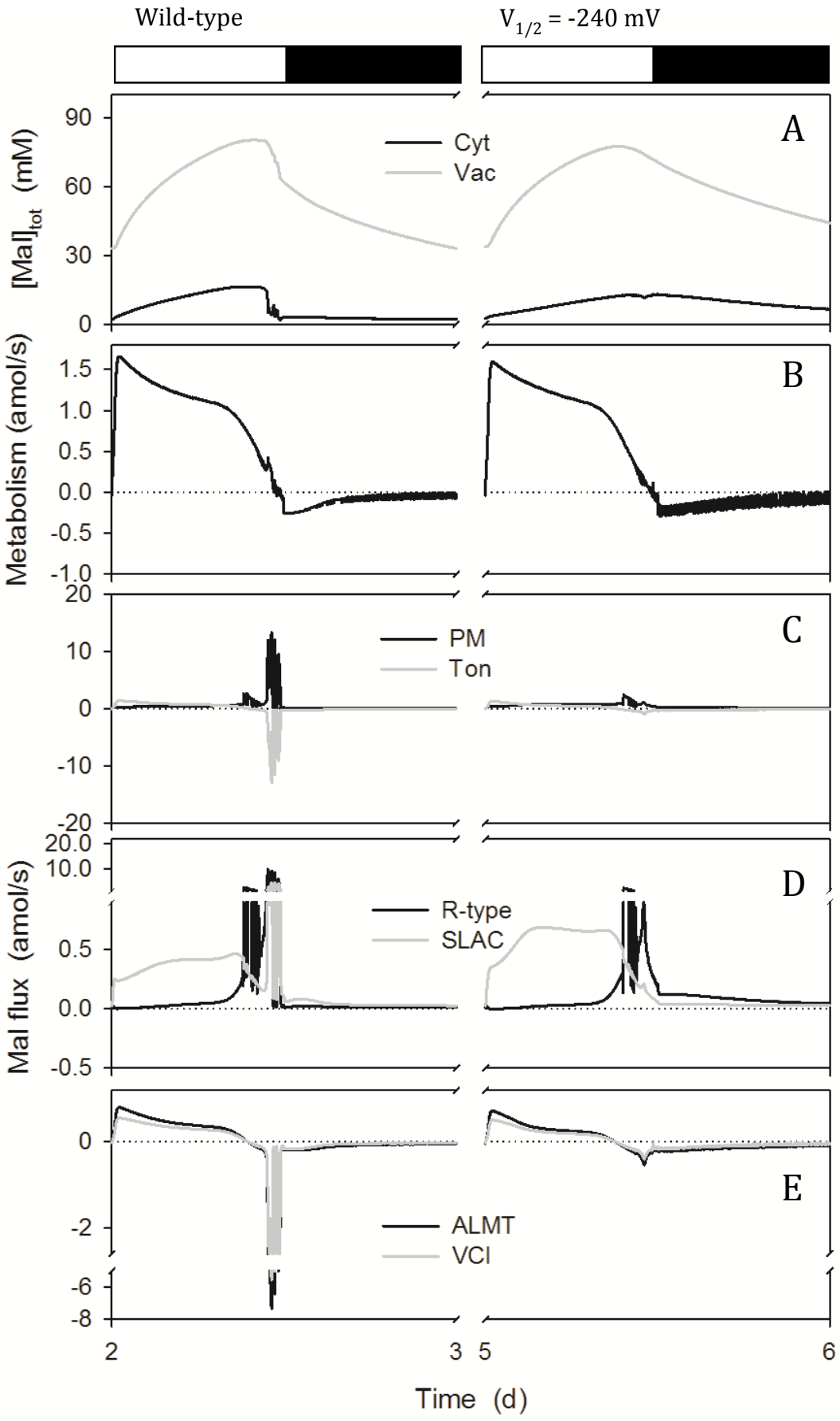
Wild-type
$V_{1/2}$ = -240 mV
A
Cyt
Vac
$[Mal]_{tot}$ (mM)
90
60
30
0
B
Metabolism (amol/s)
1.5
1.0
0.5
0.0
-0.5
-1.0
C
PM
Ton
20
10
0
-10
-20
D
R-type
SLAC
Mal flux (amol/s)
20.0
10.0
0.5
0.0
-0.5
E
ALMT
VCl
0
-2
-6
-8
2
3
5
6
Time (d)

Figure 5.2.11. Malic acid synthesis, total malate (Mal) contents and analysis of Mal^{2-} fluxes at the plasma membrane and tonoplast resolved over a standard diurnal cycle (12 h light:12 h dark, indicated by bars above) (Chen, Hills et al. 2012) for the wild-type (control, left) and the manipulation of K_{in} channels $V_{1/2}$ to -240 mV from -180 mV (right) as described in Figure 5.2.7. Shown are (A) total cytosolic and vacuolar [Mal], (B) the rates of Mal synthesis and metabolism, (C) the net flux of Mal^{2-} across the plasma membrane and tonoplast, (D) the Mal^{2-} flux through the Mal^{2-} -permeable transporters at the plasma membrane, comprising the SLAC and R- (ALMT-) type anion channels, and (E) the Mal^{2-} flux through the Mal^{2-} -permeable transporters at the tonoplast, comprising the VMAL and VCL channels. Positive flux is defined as movement of the ionic species (not the charge) out of the cytosol, either across the plasma membrane or the tonoplast. In the wild-type, the bulk of Mal production was diverted by transport of Mal^{2-} across the tonoplast, leading to a rise in total vacuolar Mal from 30 mM at the end of the night to near 90 mM before declining at the end of the daylight period; Mal in the cytosol rose from approximately 1 mM to values around 15 mM, much as has been estimated from experimental data (Hills, Chen et al. 2012). When K_{in} $V_{1/2}$ was modified to more negative values the model predicted a little reduction of the levels of malate in both cytosol and vacuole during the daylight period; varying from 30 mM to 80 mM in the vacuole between the end of the dark period to the end of the daylight period, and from 1 mM to 10 mM in the cytosol (A). Fluxes of malate get reduced in almost all of the channels except the SLAC which presented a higher fluxes of malate during the daylight period (D). Fluxes oscillations were just observed through the R-type channels (D).

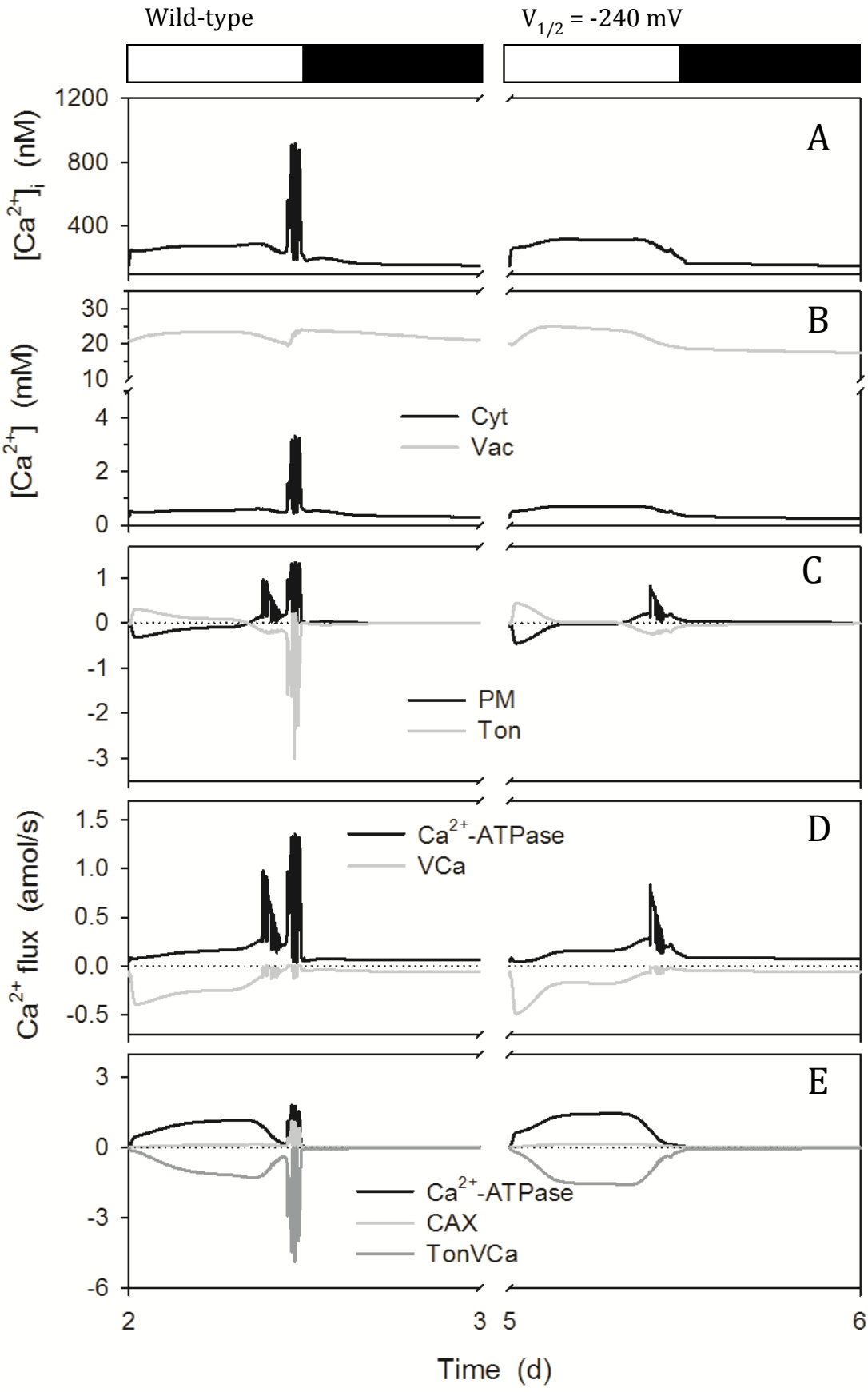
Wild-type
$V_{1/2}$ = -240 mV
A
B
C
D
E
$[Ca^{2+}]_i$ (nM)
1200
800
400
$[Ca^{2+}]$ (mM)
30
20
10
4
2
0
Cyt
Vac
1
0
-1
-2
-3
PM
Ton
Ca^{2+} flux (amol/s)
1.5
1.0
0.5
0.0
-0.5
Ca^{2+}-ATPase
VCa
3
0
-3
-6
Ca^{2+}-ATPase
CAX
TonVCa
2
3
5
6
Time (d)

Figure 5.2.12. Total cytosolic and vacuolar [Ca^{2+}], cytosolic free [Ca^{2+}], and analysis of Ca^{2+} fluxes across the plasma membrane and tonoplast resolved over a standard diurnal cycle (12 h light:12 h dark, indicated by bars above) (Chen, Hills et al. 2012) for the wild-type (control, left) and the manipulation of K_{in} channels $V_{1/2}$ to -240 mV from -180 mV (right) as described in Figure 5.2.7. Shown are (A) the cytosolic-free [Ca^{2+}] ([$Ca^{2+}]_i$), (B) the total cytosolic and vacuolar [Ca^{2+}], (C) the net flux of Ca^{2+} across the plasma membrane and tonoplast, (D) the Ca^{2+} flux through the Ca^{2+}-permeable transporters at the plasma membrane, comprising the hyperpolarisation-activated Ca^{2+} channel and the Ca^{2+}- ATPase, and (E) the flux of Ca^{2+} through the Ca^{2+} permeable transporters at the tonoplast, comprising the Ca^{2+}-ATPase, the CAX H^{+}-Ca^{2+} antiporter, and the TonVCa Ca^{2+} channel. Flux through the TPC channel accounts for less than two percent of the total Ca^{2+} flux across the tonoplast and has therefore been omitted for purposes of clarity. Positive flux is defined as movement of the ionic species (not the charge) out of the cytosol, either across the plasma membrane or the tonoplast. For the wild-type, the OnGuard model predicted $[Ca^{2+}]_i$ to decrease from a value near 200 nM in the daylight period to a resting value near 100 nM in the dark period (A). Stomatal closure was accompanied by a series of voltage (Figure 7) and $[Ca^{2+}]_i$ oscillations that drive K^{+} and anion efflux for stomatal closure (Gilroy, Fricker et al. 1991, Irving, Gehring et al. 1992, McAinsh, Brownlee et al. 1992, Thiel, MacRobbie et al. 1992). When K_{in} $V_{1/2}$ was modified to more negative values the model predicted a lack on Ca^{2+} oscillations at the beginning of the dark period, and a reduction on Ca^{2+} fluxes from the middle of the daylight period (C). $[Ca^{2+}]_i$ increased to 300 nM during the daylight period and decrease to 100 nM during the dark period. Fluxes of Ca^{2+} through the Ca^{2+}-ATPase and TonVCa became slightly increased.

As shown in Figures 5.2.1 to 5.2.12, the model predicted a big variation in both the macroscopic variables of aperture, turgor, volume and membrane voltage, as well as the underlying microscopic variables when gating properties of K_{in} channels were modified either to the two extremes. When $V_{1/2}$ of K_{in} channels was displaced to more positive values (-120 mV), the aperture rose more quickly at the start of the day and achieved greater final values. Nevertheless, the stomata remained opened during the dark period (Figure 5.2.1). Changing $V_{1/2}$ to more negative values (-240 mV) led to the opposite response. In this case, the stomata aperture remained nearly closed during the whole of the diurnal cycle (Figure 5.2.7). The differences in the output variables and their association with the gating changes between the wild-type and the modified $V_{1/2}$ are detailed in each of the figures and explored further in the discussion below.

5.2.1.2. Cloning and confocal imaging

To validate the model predictions, stable Arabidopsis transformed plants presenting such modifications on the KAT1 gating properties were generated. $KAT1^{F102W}$ mutant

has been found to shift the $V_{1/2}$ of KAT1 strongly negative whereas KAT1^{D105E} mutant has been found to displace $V_{1/2}$ of KAT1 to more positive values (Lefoulon, Karnik et al. 2014, Grefen, Karnik et al. 2015). I used these two KAT1 mutants to generate stable Arabidopsis transformants, in order to examine the effects on gas exchange and compare stomata response in vivo with the model predictions. I generated six different constructs by gateway cloning (Table 5.2.1) and used these to generated different lines of Arabidopsis transformed plants. I expressed KAT1^{wt} protein and the mutants in Arabidopsis under control of the 35S promoter and of the guard cell promoter (GCP) AtMYB60 (Cominelli, Galbiati et al. 2011). For protein expression under the GCP, I generated a destination vector (Figure 5.2.13), which contained the GCP and a C-terminal RFP marker to enable localisation of the protein under confocal microscopy.

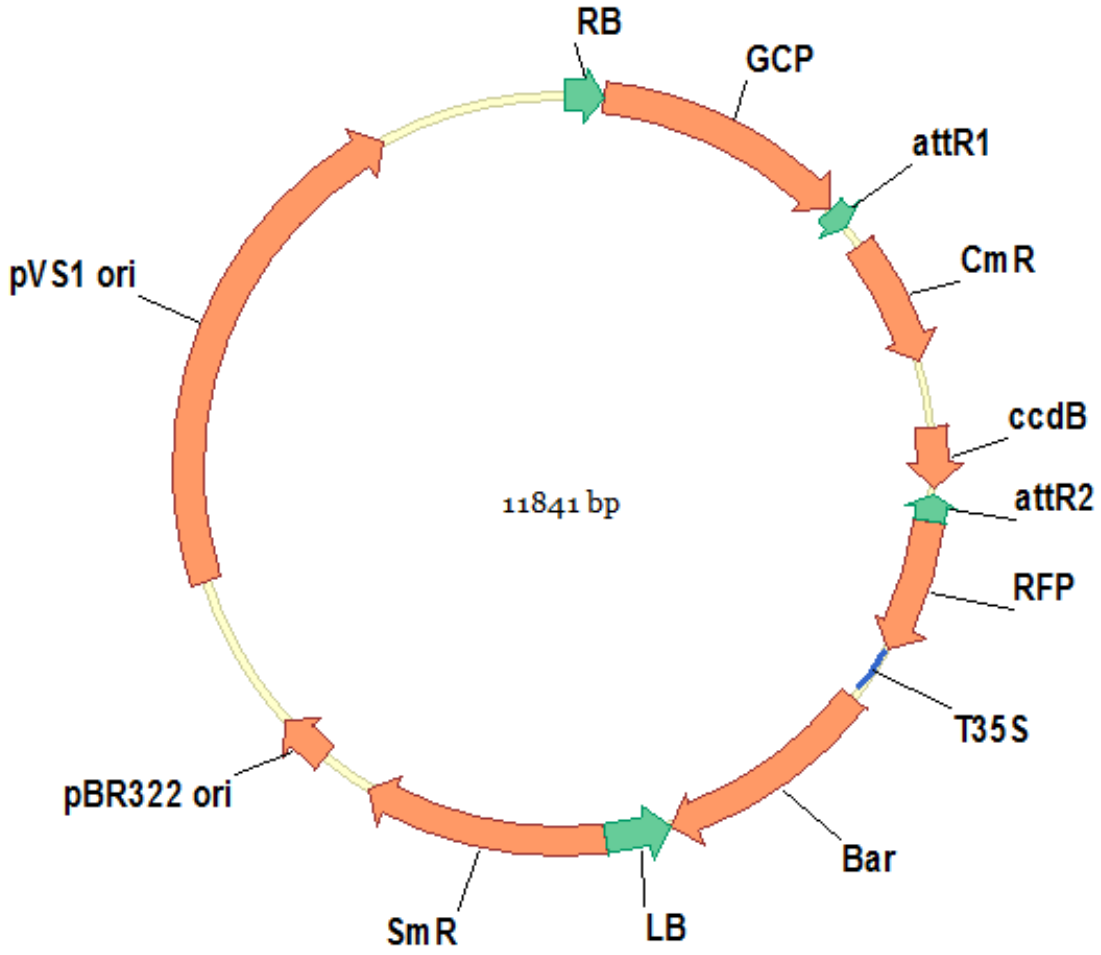

Figure 5.2.13. Gateway vector containing one cassette under the expression of a GCP (guard cell promoter and RFP marker. From the background of pB7RWG2 (Karimi, Depicker et al. 2007). pBR322ori/pVS1ori: replication origins. RB/LF: right/left border. SmR: Spectinomycin resistance. CmR: Cloramphenicol resistance. BarR: BASTA resistance.T35S: 35S terminator. 35S: 35S strong promoter. pUBQ10: UBQ10 promoter. RFP: red fluorescent marker. *ccd*B: *ccd*B toxic gene. *att*R1/*att*R2: recombination sites. The vector size is 11841 bp.

Expression construct	Entry clone (All in pDONR207)	Destination vector	SM
35S::KAT1^{wt}-RFP	KAT1^{wt}-wo	pUBC-GFP-Dest	S.10.14
35S::KAT1^{F102W}-RFP	KAT1^{F102W}-wo	pUBC-RFP-Dest	S.10.14
35S::KAT1^{D105E}-RFP	KAT1^{D105E}-wo	pUBC-GFP-Dest	S.10.14
GCP::KAT1^{wt}-RFP	KAT1^{wt}-wo	pB7RWG2-GCP	S.10.15
GCP::KAT1^{F102W}-RFP	KAT1^{F102W}-wo	pB7RWG2-GCP	S.10.15
GCP::KAT1^{D105E}-RFP	KAT1^{D105E}-wo	pB7RWG2-GCP	S.10.15
GCP::GFP	GFP-st	pB7RWG2-GCP	S.10.15

Table 5.2.1. Expression constructs expressing KAT1^{wt}, KAT1^{F102W} and KAT1^{D105E} under the expression of 35S and GC promoters, with a C-terminal RFP tag. Entry clones and destination vectors used for their production, with the respective promoter. pB7RWG2 (Karimi, Depicker et al. 2007) is a Gateway-compatible vector with C-terminal fluorescent RFP tag and incorporating the 35S promoter. pB7RWG2-GCP (Figure 12) is a Gateway-compatible vector with C-terminal fluorescent RFP tag and incorporating the GCP AtMYB60. pDONR207 is an entry vector from Gateway technology (Life Technologies) containing the *att*B1 and *att*B2 recombination sites. wo: without stop codon. st: with stop codon. SM: supplemental material.

All the constructs from Table 5.2.1 were used to transform Arabidopsis wild-type plants (Col0) as well as Arabidopsis plants which had the KAT1 channel knock-out (KAT1-KO) by the *Agrobacterium* floral dipping procedure (Zhang, Henriques et al. 2006), except GCP::GFP expression construct, which was introduced only in Col0. In total, 13 different Arabidopsis transgenic lines were generated. Arabidopsis Col0 plants expressing GFP in the guard cells under the GCP expression were generated as a control to verify the proper functionality of the GCP. Figure 5.2.14 shows a confocal image of from an Arabidopsis leaf stably transformed with GCP::GFP and demonstrates, as expected of the GCP, that protein localisation was found exclusively in the guard cells. GFP is a soluble protein, so its localisation was expected in the cytoplasm, as characterized by the presence of the protein within the nucleus and in cytoplasmic strands. Figure 5.2.14, not only demonstrates the correct expression under control of the GCP, but also its capacity to drive a strong expression of the protein.

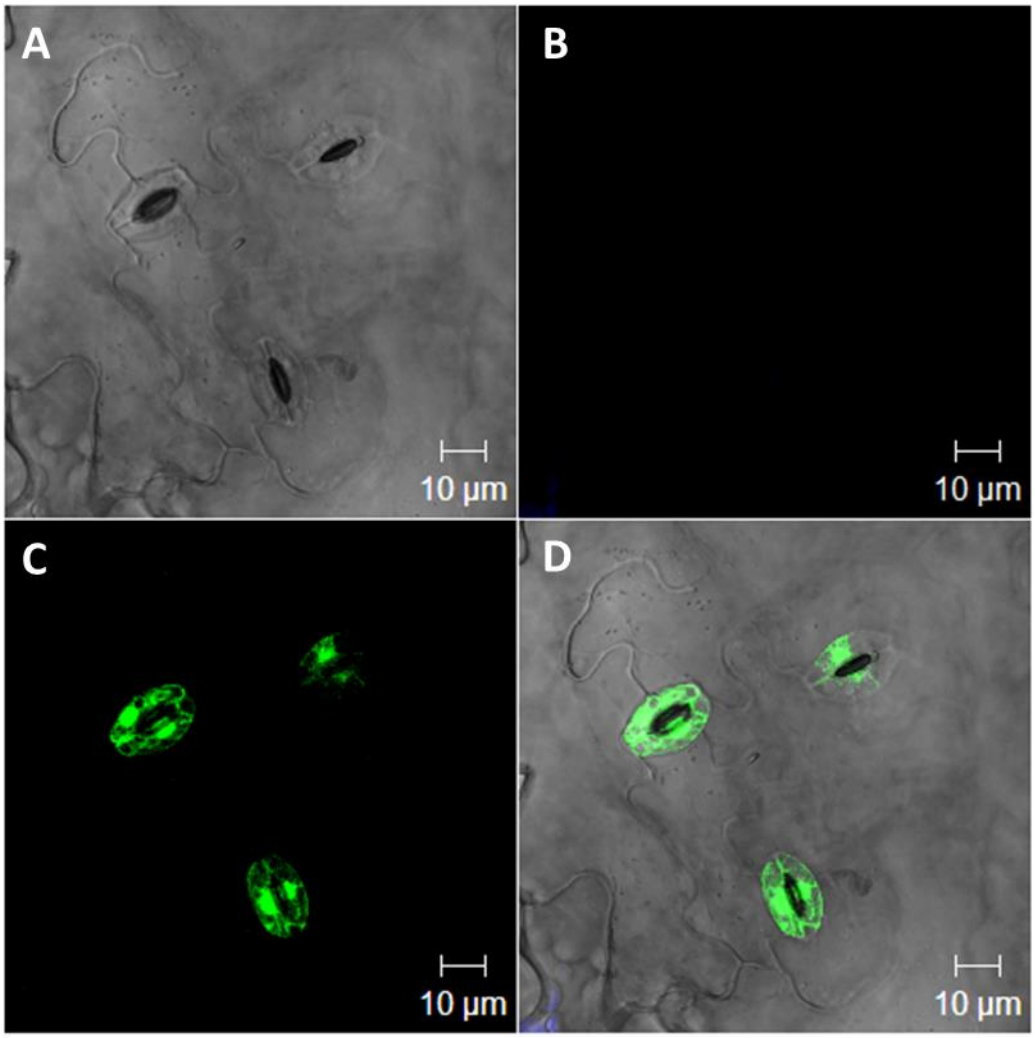

Figure 5.2.14. Expression of the construct GCP::GFP in transient transformed tobacco leaves after 3 days of transformation. GFP fluorescence indicates cytosolic localisation of GFP in the guard cells (green C, D). The chlorophyll autofluorescence is shown in blue (B, D) indicating the localisation of the chloroplasts. A is the bright field image, and D shows a merged image. The images are from 18 slice-Z-stack through the epidermal cell with a 0.75 µm interval between slices. In all the images the scale bar is 10 µm.

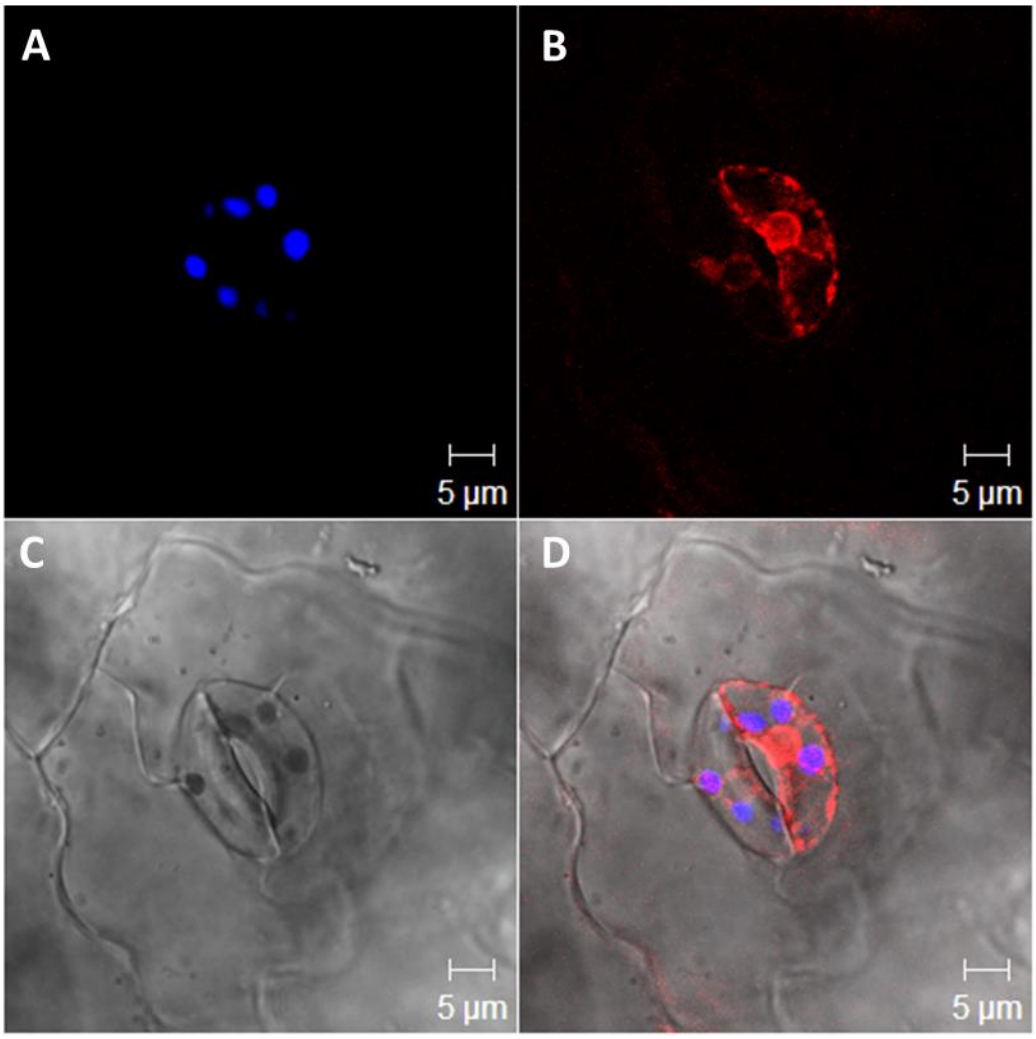

Figure 5.2.15. Expression of the construct GCP::KAT1^{D105E}-RFP in transient transformed tobacco leaves after 3 days of transformation. RFP fluorescence indicates ER and plasma membrane localisation of KAT1^{D105E} in the guard cells (red B, D). The chlorophyll autofluorescence is shown in blue (A, D) indicating the localisation of the chloroplasts. C is the bright field image, and D shows a merged image. The images are from 15 slice-Z-stack through the epidermal cell with a 0.7 µm interval between slices. In all the images the scale bar is 5 µm.

Figure 5.2.15 is a representative image of an Arabidopsis plant expressing one of the KAT1 mutants in the guard cells. Specifically, it shows a confocal microscopy image of an Arabidopsis Col0 stable transformed with the construct GCP::KAT1^{D105E}-RFP. Expression is evident both in both plasma membrane and ER. Of ER localisation, it is typical to find protein localised in a ring around the nucleus and nets within the cytoplasm. The fact that it was seen ER expression of KAT1 channels is because during the secretory pathway the channel is transported to the plasma membrane via the ER

and Golgi (Reuff, Mikosch et al. 2010). Typical of plasma membrane localisation for KAT1 is to find expression of the protein at the periphery of the cell in puncta.

5.2.1.3. Gas exchange measurements

The purpose of generating stable Arabidopsis transformants was to use T1 generation for gas exchange measurements. Plants from Arabidopsis Col0 as well as KAT1-KO, expressing all the constructs shown in Table 5.2.1, were used for gas exchange measurements. However, some of the transformed plants, mostly the KAT1-KO, had very low transformation efficiency ratio, which made difficult to produce enough plants for the gas exchange measurements analysis.

For gas exchange measurements values of A_{sat}, A_{max}, $V_{c\,max}$ and g_s were analysed on T1 generation Arabidopsis transformed plants using the LI-COR 6400XT. The first transformed plants obtained and analysed were grown under low light (70 µmol m^{-2} s^{-1}) conditions. However, it was decided to change the plants growing conditions to high light (300 µmol m^{-2} s^{-1}) for a better appreciation on changes on photosynthesis. Under high light conditions the photosynthesis is higher, allowing a better appreciation on the differences between the plants that have low photosynthesis and the ones with high photosynthetic capacity. Thus, the first T1 generation plants obtained – wild-type Arabidopsis plants expressing the constructs under GCP control - were grown under low light conditions (Figure 5.2.16). Figure 5.2.17 shows the results on gas exchange measurements done in Arabidopsis Col0 plants expressing all the different constructs generated and grown under high light (300 µmol m^{-2} s^{-1}) conditions. Figure 5.2.18 shows the results on gas exchange measurements done in KAT1-KO transformed plants and grown under high light conditions. Unfortunately, the transformation efficiency of KAT1-KO plants was very poor, and just few transformed plants were obtained.

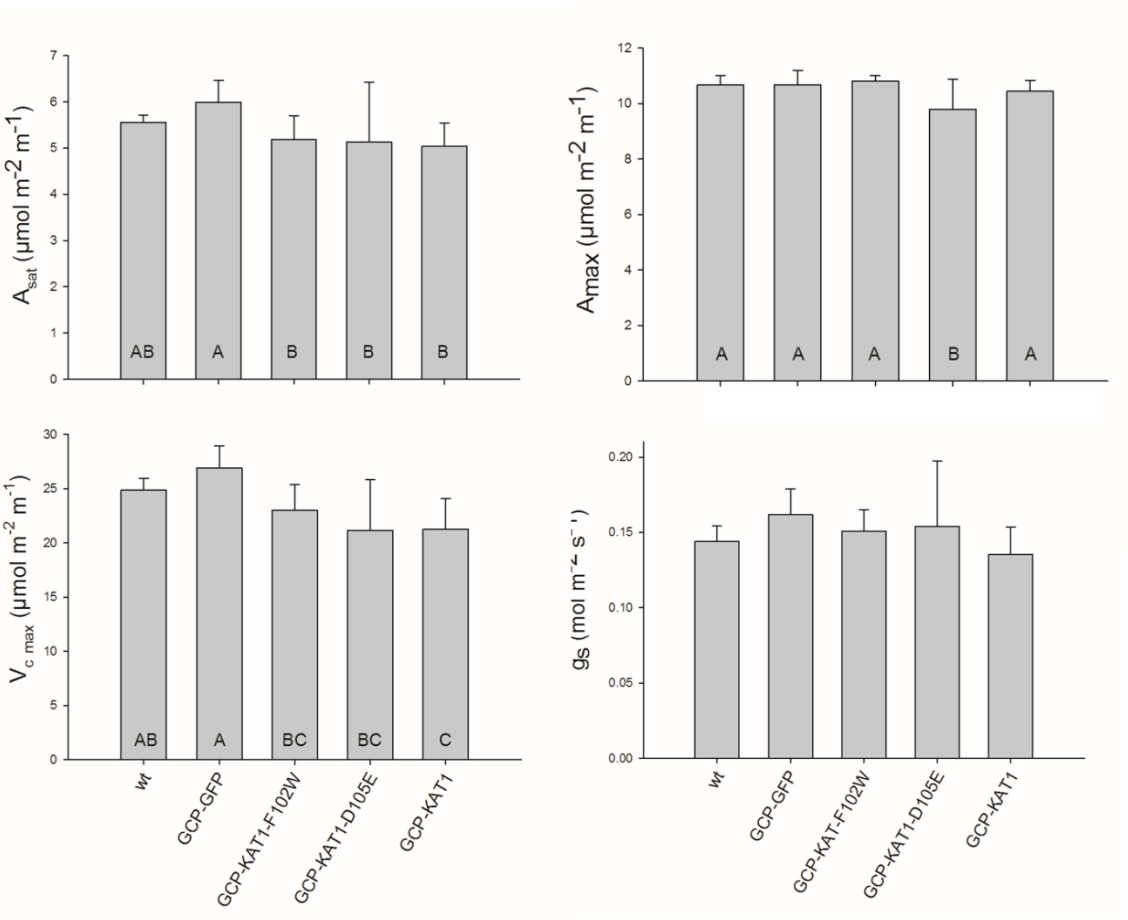

Figure 5.2.16. Gas exchange measurement values from Arabidopsis Col0 plants expressing the constructs GCP::GFP, GCP::KAT1D105E, GCO::KAT1 and wild-type. Values of light saturated rate of CO_2 assimilation (A_{sat}), light and carbon saturated rate of CO_2 assimilation (A_{max}), maximum carboxylation velocity of Rubisco ($V_{c\ max}$) and stomatal conductance (g_s). The plants were grown under low light (70 µmol m^{-2} s^{-1}) conditions. Experiments were realised with saturating light at 500 µmol m^{-2} s^{-1} (10 % Blue). Leaf temperature was maintained at 22°C. Data are means of different replicates. Lettering indicates significant differences after one-way ANOVA ($p<0.05$) as determined by Holm-Sidak test.

Figure 5.2.16 shows the gas exchange measurements data from Arabidopsis Col0 transformed plants grown in low light conditions expressing just the constructs under the GCP expression. I observed significant differences in A_{max} for the $KAT1^{D105E}$ mutant, which showed lower photosynthesis rates compared to the rest of the plants analysed. Also the plant expressing KAT1 wild-type had significant differences in $V_{c\ max}$ compared to the wild-type.

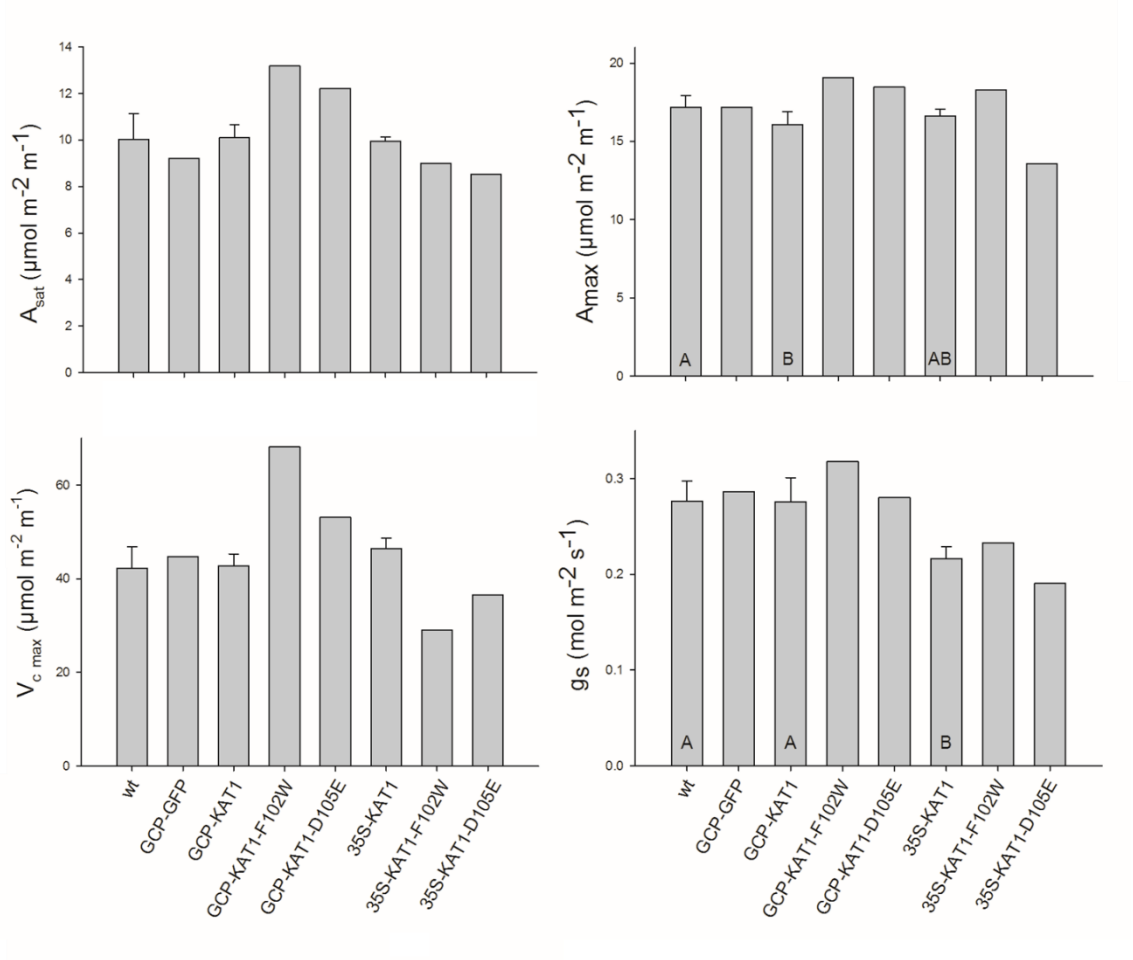

Figure 5.2.17. Gas exchange measurement values from Arabidopsis col0 plants expressing the constructs GCP::GFP, GCP::KAT1, GCP::KAT1^{F102W}, GCP::KAT1^{D105E}, 35S::KAT1, 35S::KAT1^{F102W}, 35S::KAT1^{D105E} and wild-type. Values of light saturated rate of CO_2 assimilation (A_{sat}), light and carbon saturated rate of CO_2 assimilation (A_{max}), maximum carboxylation velocity of Rubisco ($V_{c\ max}$) and stomatal conductance (g_s). The plants were grown under high light (300 µmol m^{-2} s^{-1}) conditions. Experiments were realised with saturating light at 500 µmol m^{-2} s^{-1} (10 % Blue). Leaf temperature was maintained at 22°C. Data are means of different replicates. Lettering indicates significant differences after one-way ANOVA ($p<0.05$) as determined by Holm-Sidak test. Columns with no error bars indicate just one sample analysed, thus statistical analysis was not done on them.

The plants grown under high light conditions did not show a lot of statistically significant differences. In fact, no differences were appreciated on A_{sat} and $V_{c\ max}$ analysis. Statistically significant differences were just sown on plants expressing KAT1 under GCP, which had a lower A_{max}; and plants expressing KAT1 under 35S promoter, which had lower stomatal conductance.

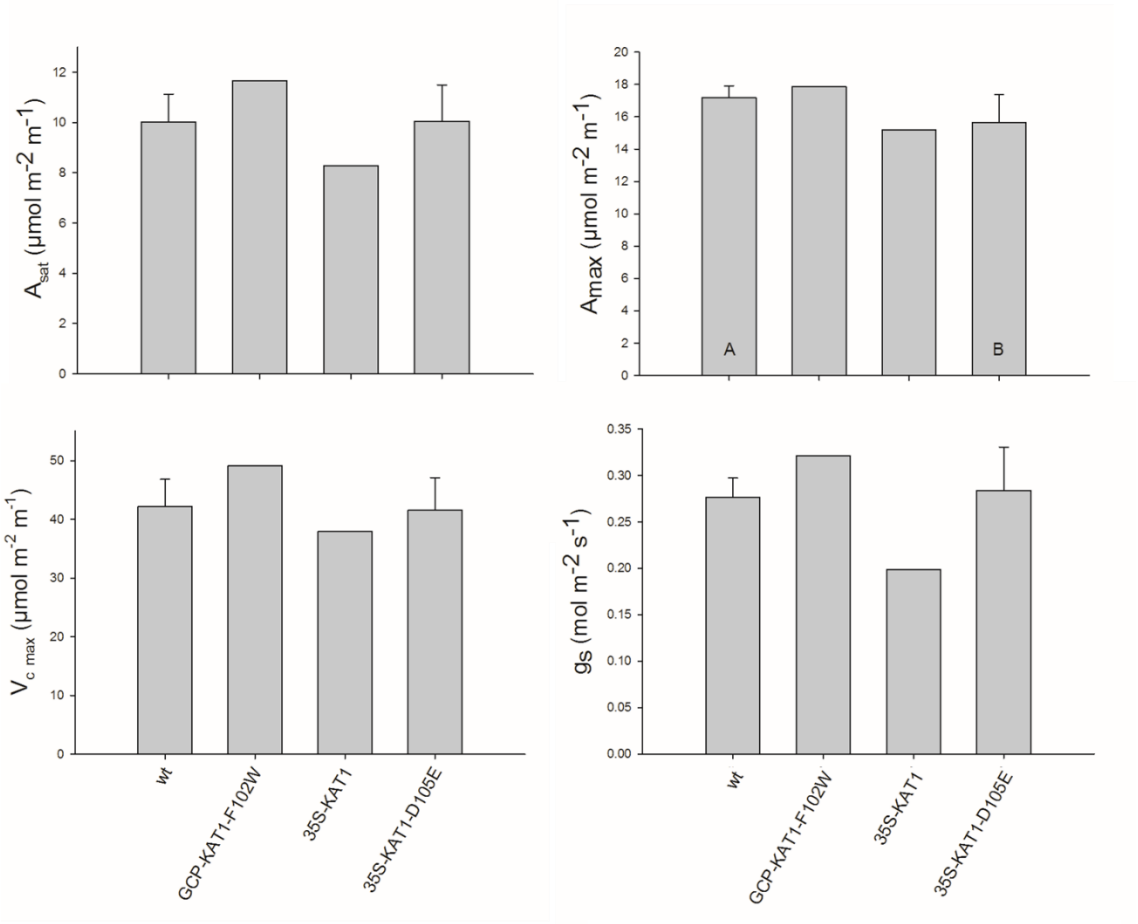

Figure 5.2.18. Gas exchange measurement values from Arabidopsis KAT1-KO plants expressing the constructs GCP::GFP, GCP::KAT1^{F102W}, 35S::KAT1^{D105E}, 35S::KAT1 and wild-type. Values of light saturated rate of CO_2 assimilation (A_{sat}), light and carbon saturated rate of CO_2 assimilation (A_{max}), maximum carboxylation velocity of Rubisco ($V_{c\ max}$) and stomatal conductance (g_s). The plants were grown under high light (300 µmol m^{-2} s^{-1}) conditions. Experiments were realised with saturating light at 500 µmol m^{-2} s^{-1} (10 % Blue). Leaf temperature was maintained at 22°C. Data are means of different replicates. Lettering indicates significant differences after one-way ANOVA ($p<0.05$) as determined by Holm-Sidak test. Columns with no error bars indicate just one sample analysed, thus statistical analysis was not done on them.

For KAT1-KO plants expressing the different constructs it was only possible to compare the 35S::KAT1^{D105E} mutant with the control (wt), due to there were not enough plans analysed from the other constructs to statistically compare between them all. The mutant also showed statistically significant lower values of Amax.

5.2.2. NpHR

The use of synthetic biology should be considered as an alternative for stomatal kinetics manipulation. It can even represent an advantage considering that external changes in guard cell membrane transport may not change the overall properties of the transport. Since the OnGuard model is not limited on the natural guard cell transporters but allows the incorporation of new ones, it was worth to try how an external transporter might influence stomatal behaviour. The use of NpHR was considered again for this project due to its regulating mechanism, light, is a main stimuli for stomatal opening, and also because NpHR pumps one of the two main ions, Cl^-, involved in the stomatal aperture movements.

5.2.2.1 Modelling

The OnGuard model was used to simulate how the incorporation of NpHR in the plasma membrane and in the tonoplast of the guard cells would affect stomatal kinetics. In the model, different amount of NpHR were simulated in one or the other of these two membranes. In all the cases the model was run on a standard diurnal cycle of 12 h light followed by 12 h of dark, with 10 mM KCl, 1 mM $CaCl_2$ and pH 6.5 outside (Chen, Hills et al. 2012). The complete parameter set used as the equivalent of the wild-type background is published in Wang, et al. (2012). Additions of NpHR were made to this background to simulate the effects of this light-driven pump. A series of trials were run with different pump densities, starting with 0.1 million (M) pumps up to a total value of 5 M pumps per cell, in total six different conditions on each membrane were run in the model (0.1 M, 0.2 M, 0.5 M, 1 M, 2 M, 5 M NpHR).

In this chapter I present representative data extract from the model, which shows the stomatal response when 2 M pumps are expressed in plasma membrane and the same conditions for tonoplast. The modelling data I am presenting shows the macroscopic outputs from the OnGuard model (Figures 5.2.19 and 5.2.25); the K^+ contents and analysis of K^+ fluxes at the plasma membrane and tonoplast (Figures 5.2.20 and 5.2.26); cytosolic and vacuolar pH and H^+ fluxes across the plasma membrane and tonoplast (Figures 5.8.21 and 5.8.27); chloride contents and analysis of Cl^- fluxes at the

plasma membrane and tonoplast (Figures 5.2.22 and 5.2.28); malic acid synthesis, total malate (Mal) contents and analysis of Mal^{2-} fluxes at the plasma membrane and tonoplast (Figures 5.2.23 and 5.2.29); and finally, cytosolic and vacuolar [Ca^{2+}], cytosolic-free [Ca^{2+}] and analysis of Ca^{2+} fluxes across the plasma membrane and tonoplast (Figures 5.2.24 and 5.2.30). The simulation was initiated in each case with the wild-type parameters and NpHR was added at the beginning of day 3, yielding a new stable cycle from day 4 onwards. Thus, the data shown is from day 2 for the wild-type and day 5 for the modified conditions, where both cycles were stable.

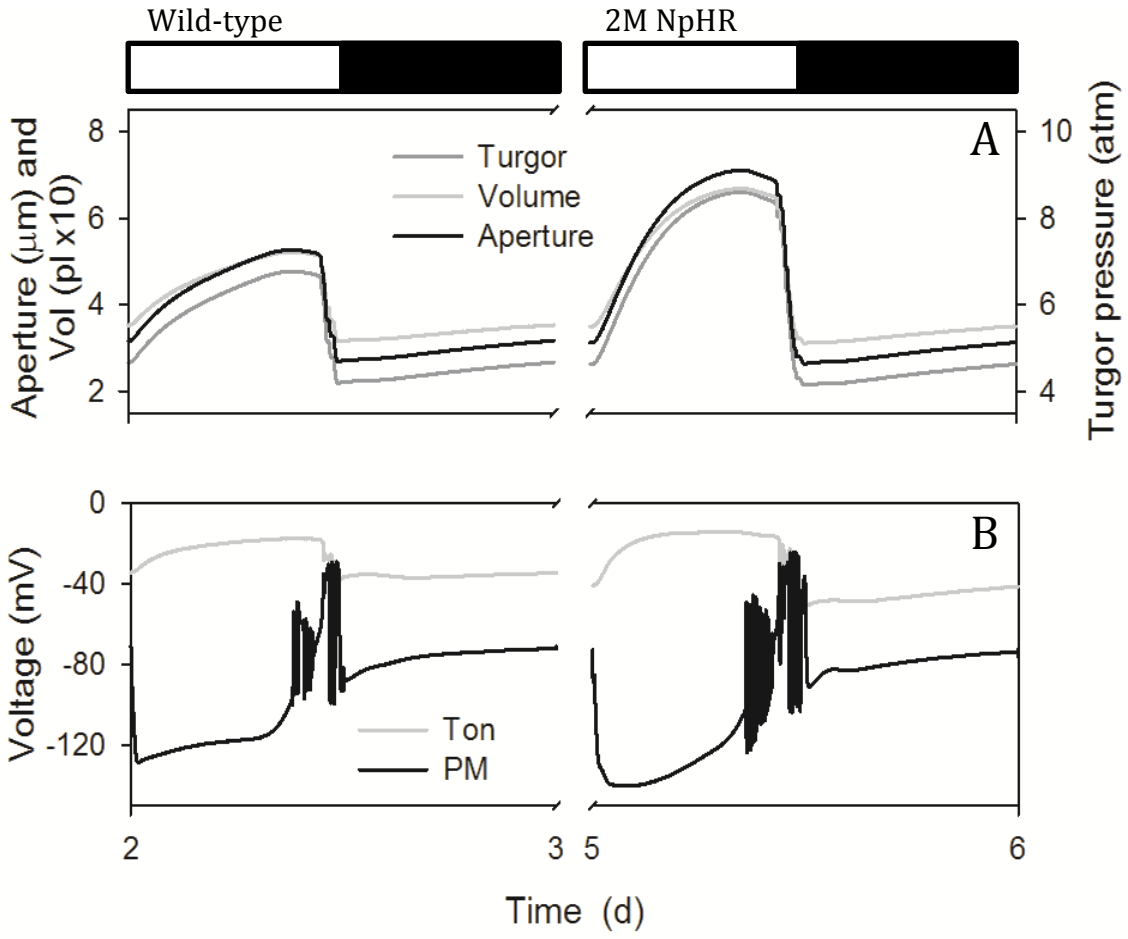

Figure 5.2.19. Macroscopic outputs from the OnGuard model. Outputs resolved over a standard diurnal cycle (12 h light:12 h dark, indicated by bars above) with 10 mM KCl, 1 mM $CaCl_2$ and pH 6.5 outside (Chen, Hills et al. 2012). Representative diurnal cycles are shown for the wild-type (control, left) and when 2 million NpHR pumps were added in the plasma membrane. For the results in this and the subsequent figures, the simulation was initiated with wild-type parameters (Wang, Papanatsiou et al. 2012)

and the 2M NpHR added in plasma membrane at the start of day 3, yielding a new stable cycle from day 4 onwards. A summary analysis is provided with each of the subsequent figures; further details will be found in Chen, et al. (2012). Shown are (A) stomatal aperture, turgor pressure and total guard cell volume, and (B) plasma membrane and tonoplast voltages. Stomatal apertures varied over a physiological range between roughly 3 µm and 6 µm in the wild-type and from 3 µm to 8 µm when NpHR is added. Stomatal apertures were paralleled by physiologically sensible changes in guard cell volume and turgor. Following stomatal closure at the end of the day, the model generated a small and gradual rise in aperture and the associated outputs that anticipated the start of the next day, much as has been observed in vivo (Gorton, Williams et al. 1993, Meidner and Willmer 1993). The start of the day was associated with hyperpolarisation of the plasma membrane to voltages near -130 mV and the dark period was accompanied by depolarisation of the plasma membrane to voltages near the equilibrium voltage for K^+, consistent with the diurnal cycle in energetic outputs of the ATP-driven pumps (Spanswick 1981, Blatt 1987, Blatt and Clint 1989, Clint and Blatt 1989, McClure, Shaff et al. 1989, Kinoshita, Nishimura et al. 1995). Voltage oscillations at the end of the daylight period are detailed by Chen, et al. (2012) and mark periods of substantial K^+ and anion efflux that drive stomatal closure. When 2 million NpHR pumps were added in the plasma membrane the model predicted a much quicker and bigger aperture of the stomata (A) during the daylight period with a higher hyperpolarisation of the plasma membrane (B), and a quicker stomatal closure response at the beginning of the dark period (A).

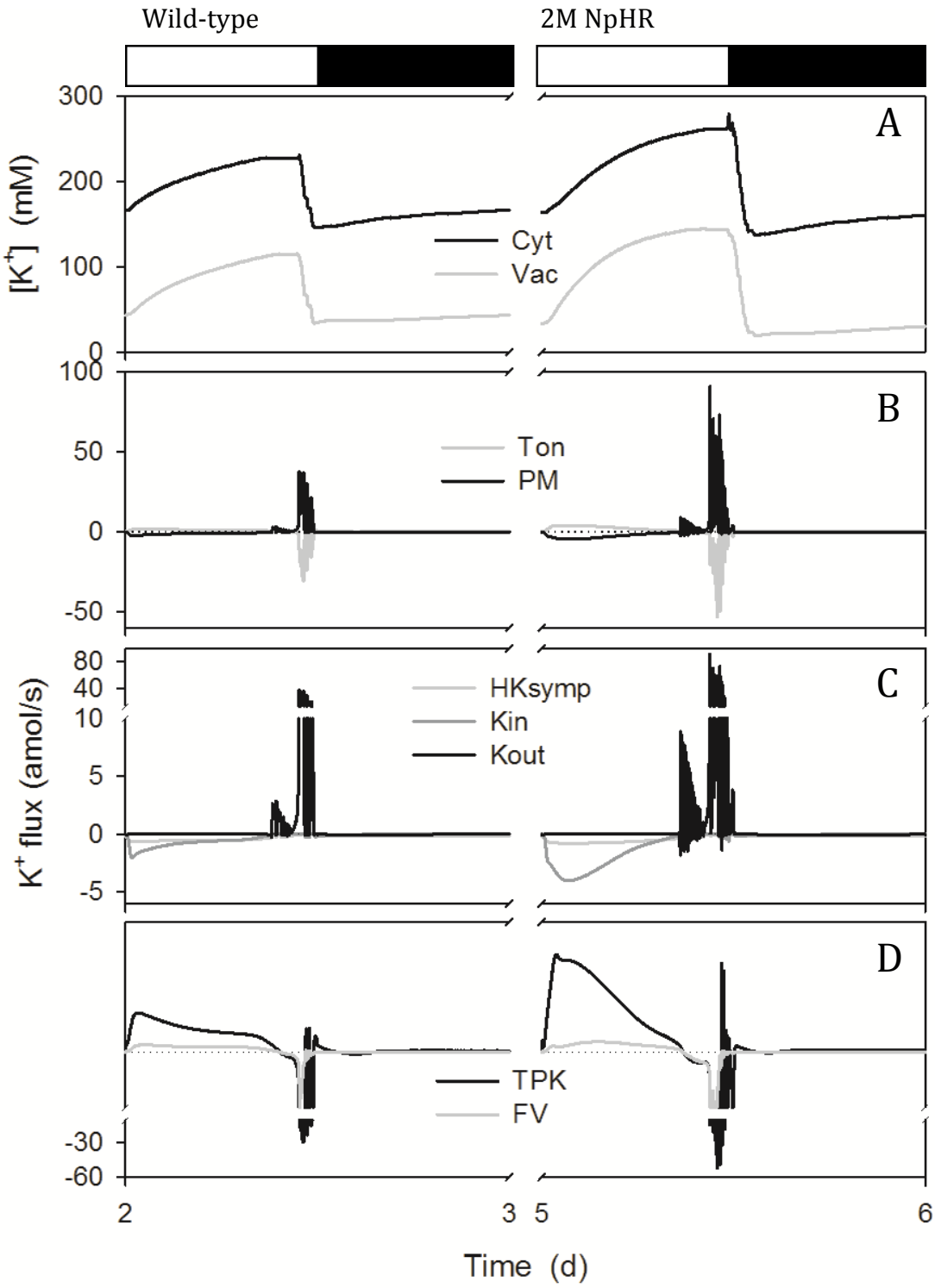

Figure 5.2.20. K^+ contents and analysis of K^+ fluxes at the plasma membrane and tonoplast resolved over a standard diurnal cycle (12 h light:12 h dark, indicated by bars above) (Chen, Hills et al. 2012) for the wild-type (left) and when 2 million NpHR pumps are added in the plasma membrane (right) as described in Figure 5.2.19. Shown are (A) cytosolic and vacuolar [K^+], (B) the net K^+ flux across the plasma membrane and tonoplast, (C) the K^+ flux through the K^+-permeable transporters at the plasma membrane, comprising the two K^+ channels and the H^+-K^+ symporter, and (D) the K^+

flux through the K^+ permeable transporters at the tonoplast, comprising the TPK and FV channels. K^+ flux through the TPC channel accounted for less than one percent of either of the other channel fluxes, and has therefore been omitted for purposes of clarity. Positive flux is defined as movement of the ionic species (not the charge) out of the cytosol, either across the plasma membrane or the tonoplast. In the wild-type, the cytosolic K^+ concentration varied between approximately 160 mM and 230 mM; in the vacuole, K^+ concentrations ranged between approximately 40 mM and 120 mM (A). In contrast, when 2 million NpHR were added in the plasma membrane the K^+ concentration was higher than in the wild-type reaching values from 160 mM to approximately 260 mM in the cytosol and from 40 mM to 150 mM in the vacuole with a much quicker increase than the wild-type. The major proportion of K^+ influx across the plasma membrane was shunted across the tonoplast to the vacuole during the day and this pattern reversed in the first hours of dark, as expected from experimental observation (Chen, Hills et al. 2012, Hills, Chen et al. 2012). At the plasma membrane (C), K^+ influx was dominated by $I_{K,in}$ in the first half of the day, this flux relaxing to roughly that through the H^+-K^+ symport in the second half of the day. Closure was marked by the predominance of K^+ efflux through $I_{K,out}$, which relaxed to a near-zero value during the night. The model predicted a much retention of K^+ in both cytosol and vacuole (A) when 2 million NpHR were added in the plasma membrane; an increase of fluxes across either plasma membrane and tonoplast during the daylight period with major fluxes oscillations at the beginning of the dark period (B); and a high increase on fluxes of K^+ through the K_{in} channel (C) and the TPK channel (D).

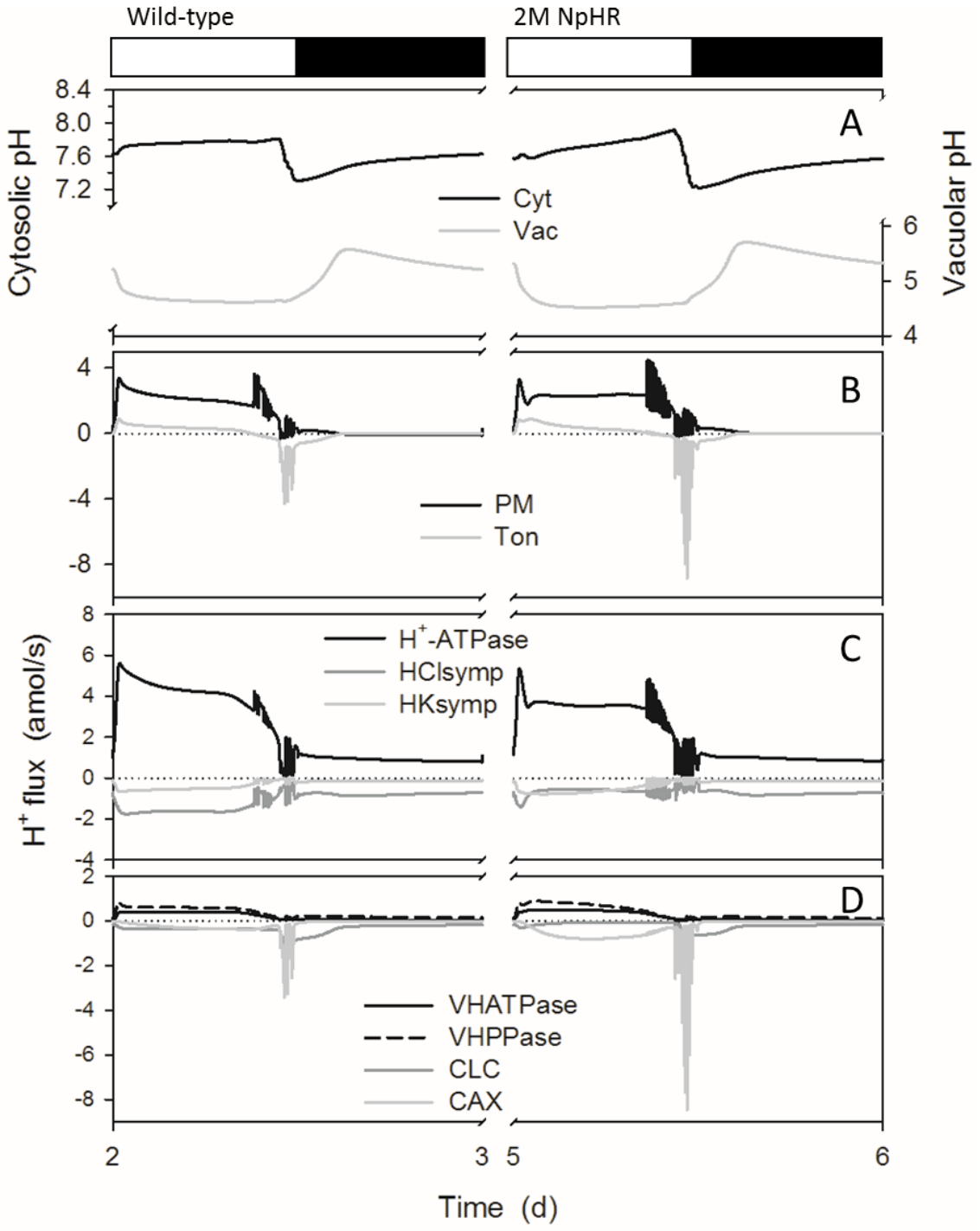

Figure 5.2.21. Cytosolic and vacuolar pH, and H^+ fluxes across the plasma membrane and tonoplast. Outputs resolved over a standard diurnal cycle (12 h light:12 h dark, indicated by bars above) (Chen, Hills et al. 2012) for the wild-type (control, left) and when 2 million NpHR pumps are added in the plasma membrane (right) as described in Figure 5.2.19. Shown are (A) cytosolic and vacuolar pH, (B) the net H^+ flux across the plasma membrane to and tonoplast, (C) the H^+ flux through the H^+-permeable transporters at the plasma membrane, comprising the H^+-ATPase, and the H^+-K^+ and H^+-Cl^- symporters, and (D) the H^+ flux through the H^+ permeable transporters at the tonoplast, comprising the VH^+-ATPase, VH^+-PPase, the CLC H^+-Cl^- antiporter and the

CAX H^+-Ca^{2+} antiporter. Positive flux is defined as movement of the ionic species (not the charge) out of the cytosol, either across the plasma membrane or the tonoplast. The bulk of H^+ production associated with daytime Mal synthesis (Figure 5) is exported via the plasma membrane H^+-ATPase, with roughly 20% transported to the vacuole (B-D). In the vacuole, Mal comprises the major pH buffer and its accumulation is associated with acidification of the vacuolar contents (Van Kirk and Raschke 1978, Talbott and Zeiger 1993, Willmer and Fricker 1996). The organic acid is thought to be transported as the fully deprotonated (Mal^{2-}) form – with the ALMT channel as the primary pathway for tonoplast Mal^{2-} flux [reviewed by Hills, et al. (2012)] – implying charge balance via the tonoplast VH^+-ATPase H^+-PPase (Rea and Poole 1993, Martinoia, Maeshima et al. 2007). Adding 2 million NpHR pumps in the plasma membrane leads to a lower flux of H^+ through the H^+-ATPase and less H^+-Cl^- symport (C), and major fluxes of H^+ through the CAX channels in the tonoplast (D). H^+ fluxes oscillations are more pronounced at the beginning of the dark period in comparison with the wild-type.

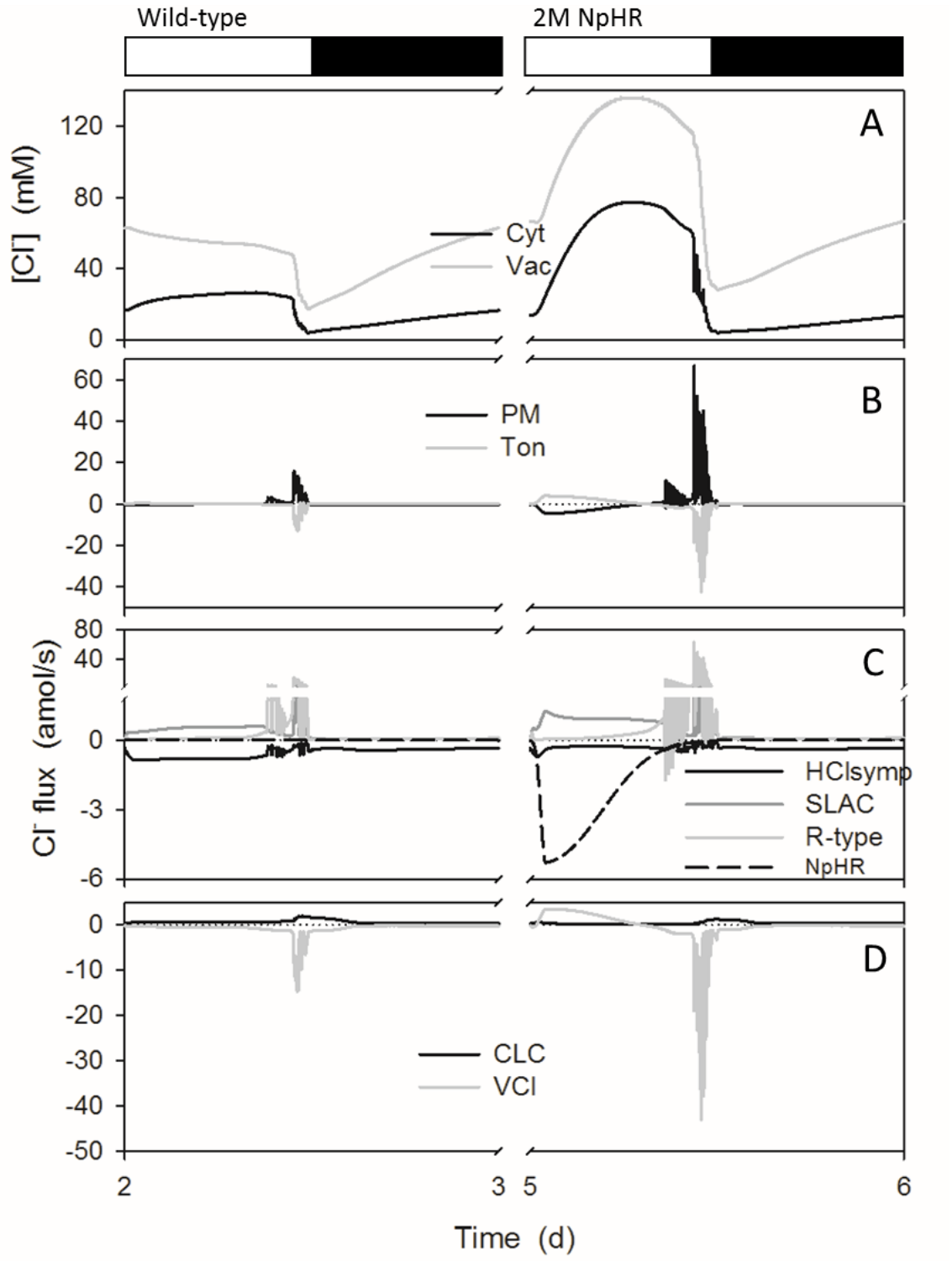

Figure 5.2.22. Chloride contents and analysis of Cl^- fluxes at the plasma membrane and tonoplast. Outputs resolved over a standard diurnal cycle (12 h light:12 h dark, indicated by bars above) (Chen, Hills et al. 2012) for the wild-type (control, left) and when 2 million NpHR pumps were added in the plasma membrane (right) as described in Figure 5.2.19. Shown are (A) total cytosolic and vacuolar [Cl^-], (B) the net flux of Cl^- across the plasma membrane and tonoplast, (C) the flux of Cl^- through the Cl^- -

permeable transporters at the plasma membrane, comprising the SLAC and R- (ALMT-) type anion channels and H^+-Cl^- symporter, and (D) the flux of Cl^- through the Cl^- -permeable transporters at the tonoplast, comprising the VCL channel and CLC H^+-Cl^- antiporter. Positive flux is defined as movement of the ionic species (not the charge) out of the cytosol, either across the plasma membrane or the tonoplast. In the wild-type stomatal opening was accompanied by a net efflux of Cl^- from the vacuole to the cytosol and later in the daylight period from the cytosol to the apoplast. Closure was marked by much larger fluxes of Cl^- from the vacuole to the cytosol and export across the plasma membrane this pattern reversed after the first 1-2 h of dark. The rise in cytosolic Cl^- concentration during the first hours of the day arose from the rapid Cl^- influx across the tonoplast. And a slower rise in the rate of Cl^- export across the plasma membrane. Adding 2 million NpHR pumps in the plasma membrane leads to an enhanced Cl^- accumulation in the cytoplasm as well as the vacuole (A), the fluxes of Cl^- in both plasma membrane and tonoplast are enhanced as well as are the fluxes oscillations at the end of the daylight period (B). The main Cl^- fluxes goes through the NpHR pump. H^+-Cl^- symport gets reduced while Cl^- fluxes through SLAC and R-type channels gets increased (C), there is a big increase on Cl^- fluxes through VCl channel (D).

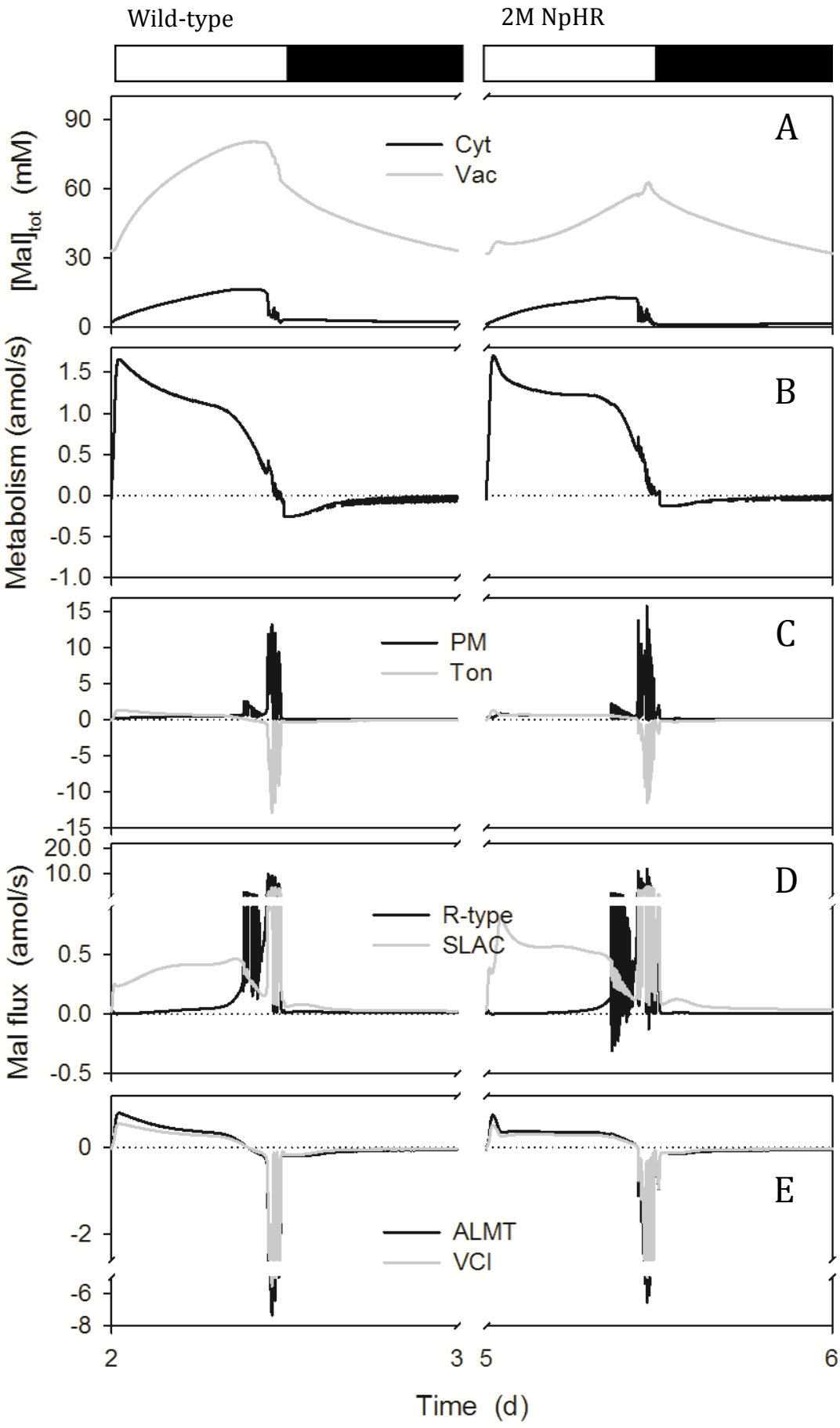
Wild-type
2M NpHR
A
B
C
D
E
Cyt
Vac
PM
Ton
R-type
SLAC
ALMT
VCl
[Mal]tot (mM)
Metabolism (amol/s)
Mal flux (amol/s)
Time (d)
90
60
30
0
1.5
1.0
0.5
0.0
-0.5
-1.0
15
10
5
0
-5
-10
-15
20.0
10.0
0.5
0.0
-0.5
0
-2
-6
-8
2
3
5
6

Figure 5.2.23. Malic acid synthesis, total malate (Mal) contents and analysis of Mal^{2-} fluxes at the plasma membrane and tonoplast resolved over a standard diurnal cycle (12 h light:12 h dark, indicated by bars above) (Chen, Hills et al. 2012) for the wild-type (control, left) and when 2 million NpHR pumps are added in the plasma membrane (right) as described in Figure 5.2.19. Shown are (A) total cytosolic and vacuolar [Mal], (B) the rates of Mal synthesis and metabolism, (C) the net flux of Mal^{2-} across the plasma membrane and tonoplast, (D) the Mal^{2-} flux through the Mal^{2-} -permeable transporters at the plasma membrane, comprising the SLAC and R- (ALMT-) type anion channels, and (E) the Mal^{2-} flux through the Mal^{2-} -permeable transporters at the tonoplast, comprising the VMAL and VCL channels. Positive flux is defined as movement of the ionic species (not the charge) out of the cytosol, either across the plasma membrane or the tonoplast. In the wild-type, the bulk of Mal production was diverted by transport of Mal^{2-} across the tonoplast, leading to a rise in total vacuolar Mal from 30 mM at the end of the night to near 90 mM before declining at the end of the daylight period; Mal in the cytosol rose from approximately 1 mM to values near 15 mM, much as has been estimated from experimental data (Hills, Chen et al. 2012). With the addition of 2 million NpHR pumps in the plasma membrane Mal accumulation was reduced in both cytosol and mainly in vacuole during the daylight period (A) and Mal synthesis (B) was shortly reduced. Fluxes of Mal through the plasma membrane became increased mediated largely by the SLAC-type anion channel during daylight period. Mal fluxes through ALMT and VCl became slightly reduced during the daylight period (E).

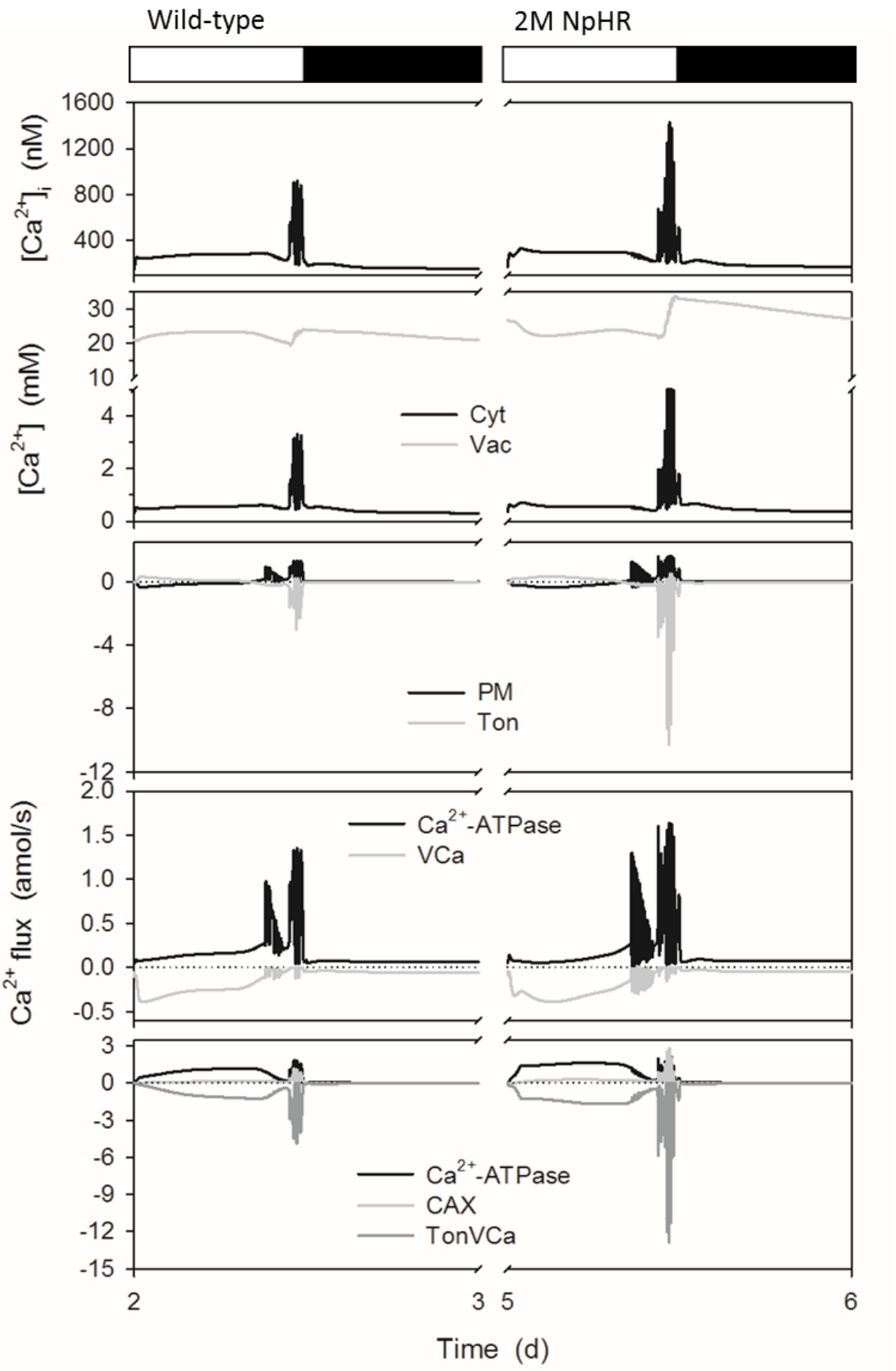
Wild-type
2M NpHR
[Ca2+]i (nM)
1600
1200
800
400
[Ca2+] (mM)
30
20
10
4
2
0
Cyt
Vac
0
-4
-8
-12
PM
Ton
Ca2+ flux (amol/s)
2.0
1.5
1.0
0.5
0.0
-0.5
Ca2+-ATPase
VCa
3
0
-3
-6
-9
-12
-15
Ca2+-ATPase
CAX
TonVCa
2
3
5
6
Time (d)

Figure 5.2.24. Total cytosolic and vacuolar [Ca^{2+}], cytosolic free [Ca^{2+}], and analysis of Ca^{2+} fluxes across the plasma membrane and tonoplast resolved over a standard diurnal cycle (12 h light:12 h dark, indicated by bars above) (Chen, Hills et al. 2012) for the wild-type (control, left) and when 2 million NpHR pumps are added in the plasma membrane (right) as described in Figure 5.2.19. Shown are (A) the cytosolic-free [Ca^{2+}] ([Ca^{2+}]$_i$), (B) the total cytosolic and vacuolar [Ca^{2+}], (C) the net flux of Ca^{2+} across the plasma membrane and tonoplast, (D) the Ca^{2+} flux through the Ca^{2+} -permeable transporters at the plasma membrane, comprising the hyperpolarisation-activated Ca^{2+} channel and the Ca^{2+}-ATPase, and (E) the flux of Ca^{2+} through the Ca^{2+} permeable transporters at the tonoplast, comprising the Ca^{2+}-ATPase, the CAX H^{+}-Ca^{2+} antiporter, and the TonVCa Ca^{2+} channel. Flux through the TPC channel accounts for less than two percent of the total Ca^{2+} flux across the tonoplast and has therefore been omitted for purposes of clarity. Positive flux is defined as movement of the ionic species (not the charge) out of the cytosol, either across the plasma membrane or the tonoplast. For the wild-type, the OnGuard model predicted [Ca^{2+}]$_i$ to decrease from a value near 200 nM in the daylight period to a resting value near 100 nM in the dark period (A). Stomatal closure was accompanied by a series of voltage (Figure 1) and [Ca^{2+}]$_i$ oscillations that drive K^{+} and anion efflux for stomatal closure (Gilroy, Fricker et al. 1991, Irving, Gehring et al. 1992, McAinsh, Brownlee et al. 1992, Thiel, MacRobbie et al. 1992). Adding 2 million NpHR pumps in the plasma membrane leaded to a slightly increase on [Ca^{2+}]$_i$ (A). There was also an increase on vacuolar [Ca^{2+}], increase on the fluxes and especially increase on Ca^{2+} oscillations at the end of the daylight period. Most of the transporters also increased their Ca^{2+} fluxes (B, C).

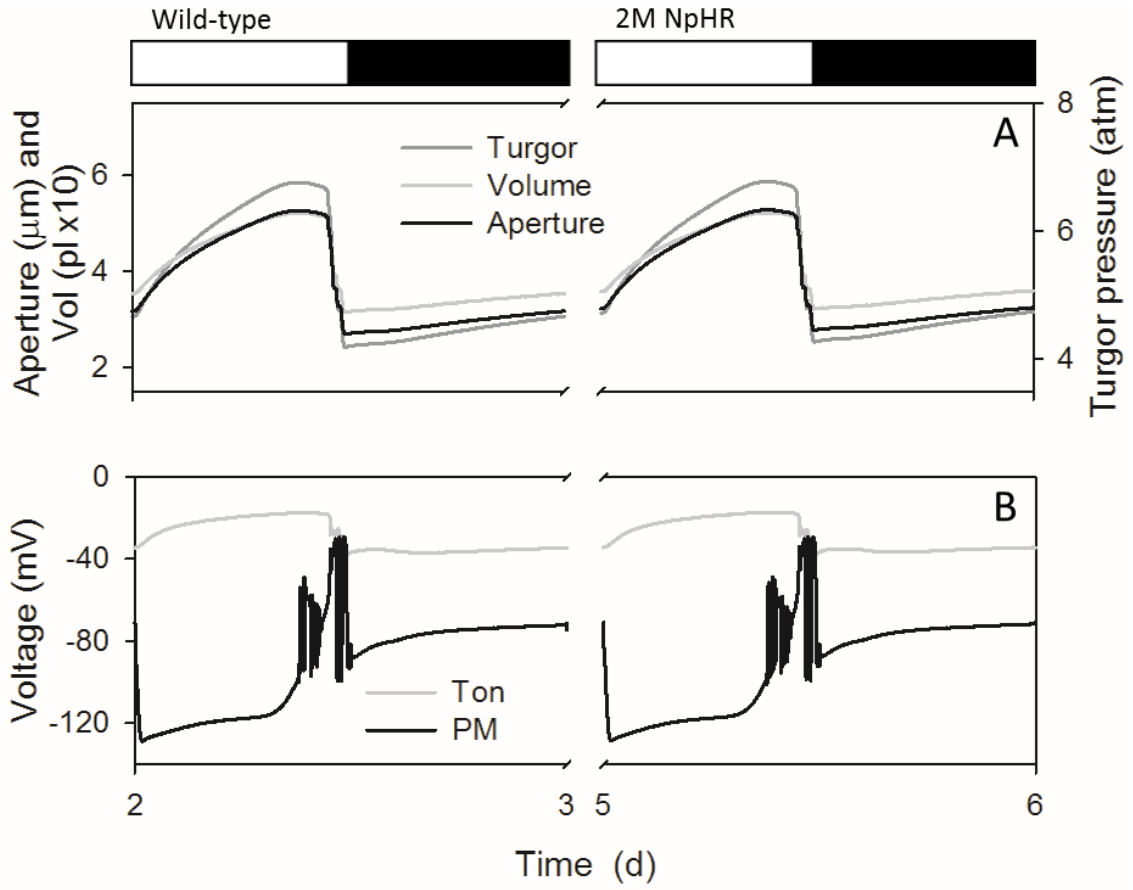

Figure 5.2.25. Macroscopic outputs from the OnGuard model. Outputs resolved over a standard diurnal cycle (12 h light:12 h dark, indicated by bars above) with 10 mM KCl, 1 mM $CaCl_2$ and pH 6.5 outside (Chen, Hills et al. 2012). Representative diurnal cycles are shown for the wild-type (control, left) and when 2 million NpHR pumps were added in the tonoplast. For the results in this and the subsequent figures, the simulation was initiated with wild-type parameters (Wang, Papanatsiou et al. 2012) and the 2M NpHR added in plasma membrane at the start of day 3, yielding a new stable cycle from day 4 onwards. A summary analysis is provided with each of the subsequent figures; further details will be found in Chen, et al. (2012). Shown are (A) stomatal aperture, turgor pressure and total guard cell volume, and (B) plasma membrane and tonoplast voltages. Stomatal apertures varied over a physiological range between roughly 3 µm and 6 µm in the wild-type and from 3 µm to 8 µm when NpHR is added. Stomatal apertures were paralleled by physiologically sensible changes in guard cell volume and turgor. Following stomatal closure at the end of the day, the model generated a small and gradual rise in aperture and the associated outputs that anticipated the start of the next day, much as has been observed in vivo (Gorton, Williams et al. 1993, Meidner and Willmer 1993). The start of the day was associated with hyperpolarisation of the plasma membrane to voltages near -130 mV and the dark period was accompanied by depolarisation of the plasma membrane to voltages near the equilibrium voltage for K^+, consistent with the diurnal cycle in energetic outputs of the ATP-driven pumps (Spanswick 1981, Blatt 1987, Blatt and Clint 1989, Clint and Blatt 1989, McClure, Shaff et al. 1989, Kinoshita, Nishimura et al. 1995). Voltage oscillations

at the end of the daylight period are detailed by Chen, et al. (2012) and mark periods of substantial K^+ and anion efflux that drive stomatal closure. When 2 million NpHR pumps were added in the tonoplast the model didn't predict any substantial difference between the two simulations.

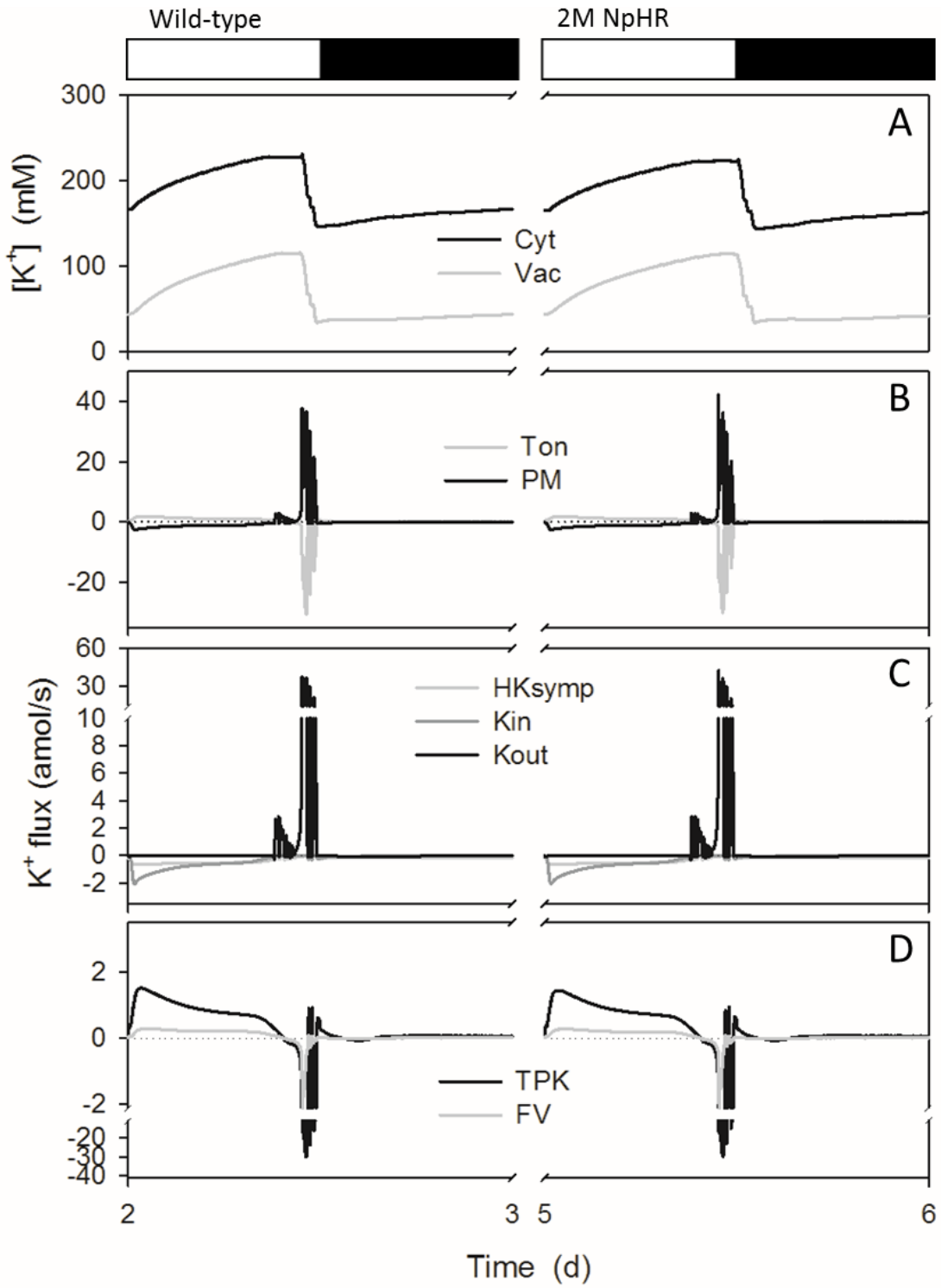

Figure 5.2.26. K^+ contents and analysis of K^+ fluxes at the plasma membrane and tonoplast resolved over a standard diurnal cycle (12 h light:12 h dark, indicated by bars above) (Chen, Hills et al. 2012) for the wild-type (left) and when 2 million NpHR pumps were added in the tonoplast (right) as described in Figure 5.2.25. Shown are (A) cytosolic and vacuolar [K^+], (B) the net K^+ flux across the plasma membrane and tonoplast, (C) the K^+ flux through the K^+-permeable transporters at the plasma membrane, comprising the two K^+ channels and the H^+-K^+ symporter, and (D) the K^+

flux through the K^+ permeable transporters at the tonoplast, comprising the TPK and FV channels. K^+ flux through the TPC channel accounted for less than one percent of either of the other channel fluxes, and has therefore been omitted for purposes of clarity. Positive flux is defined as movement of the ionic species (not the charge) out of the cytosol, either across the plasma membrane or the tonoplast. In the wild-type, the cytosolic K^+ concentration varied between approximately 160 mM and 230 mM; in the vacuole, K^+ concentrations ranged between approximately 40 mM and 120 mM (A). In contrast, when 2 million NpHR were added in the plasma membrane the K^+ concentration was higher than in the wild-type reaching values from 160 mM to approximately 260 mM in the cytosol and from 40 mM to 150 mM in the vacuole with a much quicker increase than the wild-type. The major proportion of K^+ influx across the plasma membrane was shunted across the tonoplast to the vacuole during the day and this pattern reversed in the first hours of dark, as expected from experimental observation (Chen, Hills et al. 2012, Hills, Chen et al. 2012). At the plasma membrane (C), K^+ influx was dominated by $I_{K,in}$ in the first half of the day, this flux relaxing to roughly that through the H^+-K^+ symport in the second half of the day. Closure was marked by the predominance of K^+ efflux through $I_{K,out}$, which relaxed to a near-zero value during the night. When 2 million NpHR pumps were added in the tonoplast the model didn't predict any substantial difference between the two simulations.

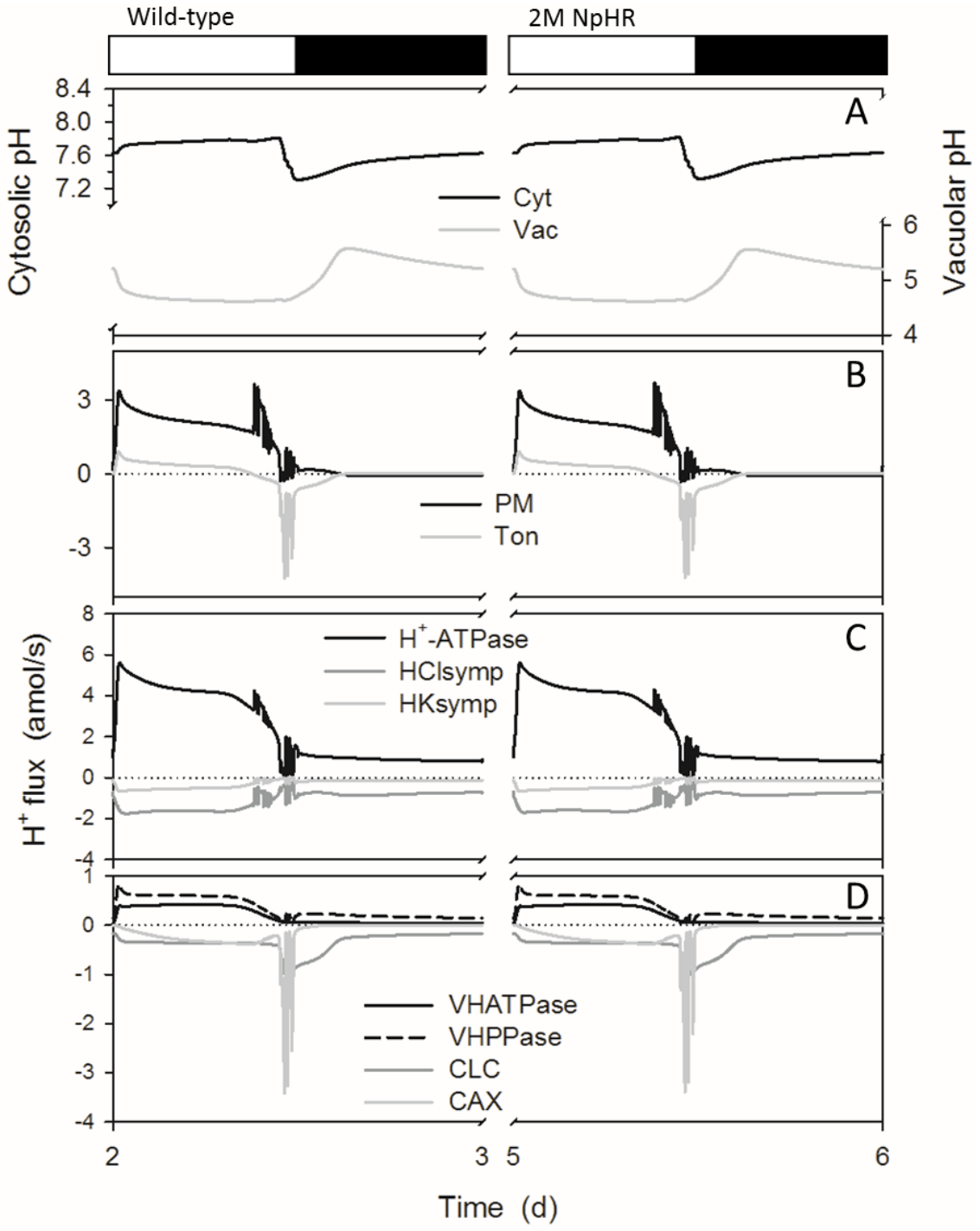

Figure 5.2.27. Cytosolic and vacuolar pH, and H^+ fluxes across the plasma membrane and tonoplast. Outputs resolved over a standard diurnal cycle (12 h light:12 h dark, indicated by bars above) (Chen, Hills et al. 2012) for the wild-type (control, left) when 2 million NpHR pumps were added in the tonoplast (right) as described in Figure 5.2.25. Shown are (A) cytosolic and vacuolar pH, (B) the net H^+ flux across the plasma membrane to and tonoplast, (C) the H^+ flux through the H^+-permeable transporters at the plasma membrane, comprising the H^+-ATPase, and the H^+-K^+ and H^+-Cl^- symporters, and (D) the H^+ flux through the H^+ permeable transporters at the tonoplast, comprising

the VH^+-ATPase, VH^+-PPase, the CLC H^+-Cl^- antiporter and the CAX H^+-Ca^{2+} antiporter. Positive flux is defined as movement of the ionic species (not the charge) out of the cytosol, either across the plasma membrane or the tonoplast. The bulk of H^+ production associated with daytime Mal synthesis (Figure 5) is exported via the plasma membrane H^+-ATPase, with roughly 20% transported to the vacuole (B-D). In the vacuole, Mal comprises the major pH buffer and its accumulation is associated with acidification of the vacuolar contents (Van Kirk and Raschke 1978, Talbott and Zeiger 1993, Willmer and Fricker 1996). The organic acid is thought to be transported as the fully deprotonated (Mal^{2-}) form – with the ALMT channel as the primary pathway for tonoplast Mal^{2-} flux [reviewed by Hills, et al. (2012)] – implying charge balance via the tonoplast VH^+-ATPase H^+-PPase (Rea and Poole 1993, Martinoia, Maeshima et al. 2007). When 2 million NpHR pumps were added in the tonoplast the model didn't predict any substantial difference between the two simulations.

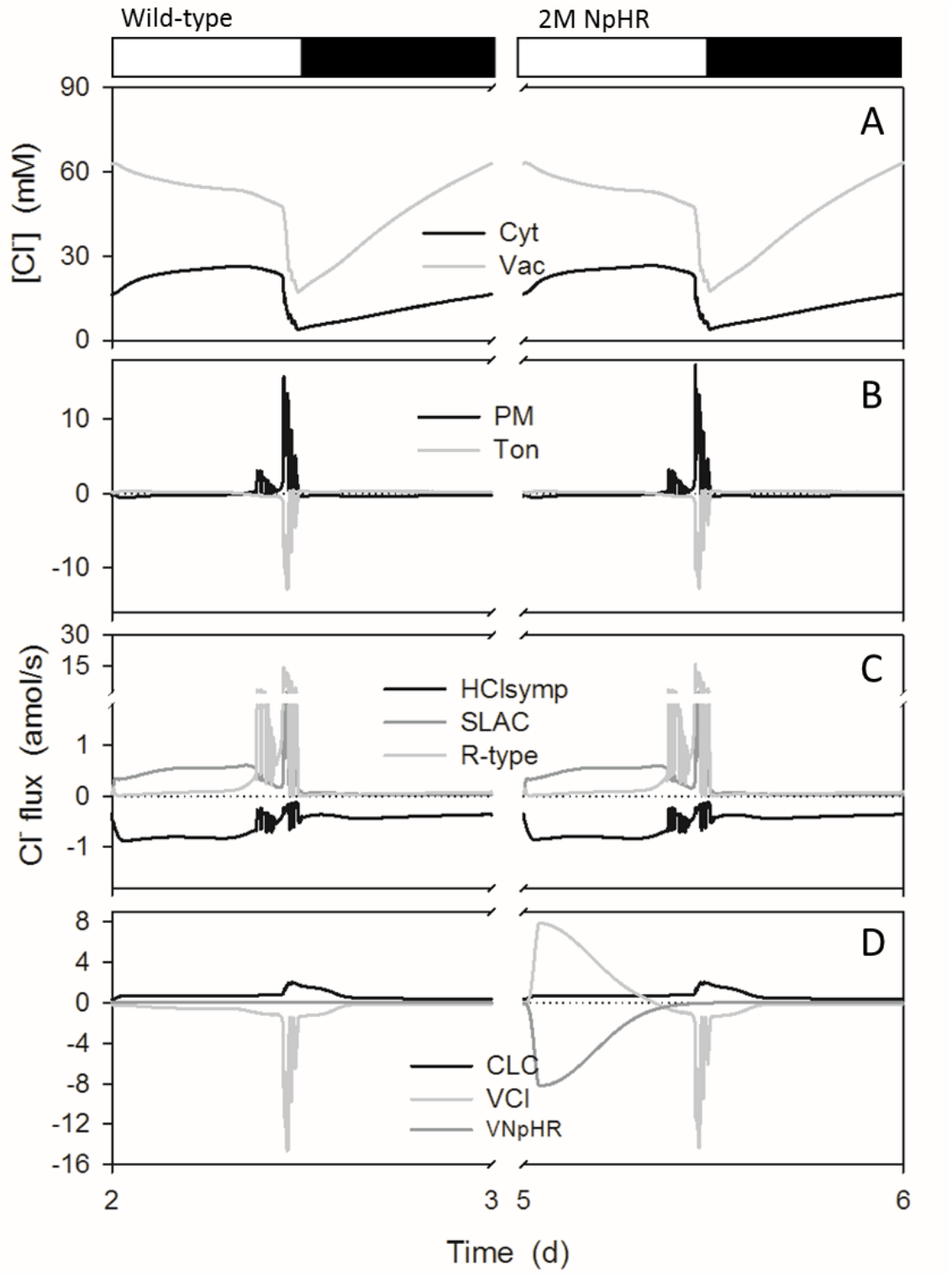

Figure 5.2.28. Chloride contents and analysis of Cl^- fluxes at the plasma membrane and tonoplast. Outputs resolved over a standard diurnal cycle (12 h light:12 h dark, indicated by bars above) (Chen, Hills et al. 2012) for the wild-type (control, left) and when 2 million NpHR pumps were added in the tonoplast (right) as described in Figure 5.2.25. Shown are (A) total cytosolic and vacuolar [Cl^-], (B) the net flux of Cl^- across the plasma membrane and tonoplast, (C) the flux of Cl^- through the Cl^- -permeable transporters at the plasma membrane, comprising the SLAC and R- (ALMT-) type anion

channels and H^+-Cl^- symporter, and (D) the flux of Cl^- through the Cl^- -permeable transporters at the tonoplast, comprising the VCL channel and CLC H^+-Cl^- antiporter. Positive flux is defined as movement of the ionic species (not the charge) out of the cytosol, either across the plasma membrane or the tonoplast. In the wild-type stomatal opening was accompanied by a net efflux of Cl^- from the vacuole to the cytosol and later in the daylight period from the cytosol to the apoplast. Closure was marked by much larger fluxes of Cl^- from the vacuole to the cytosol and export across the plasma membrane this pattern reversed after the first 1-2 h of dark. The rise in cytosolic Cl^- concentration during the first hours of the day arose from the rapid Cl^- influx across the tonoplast. And a slower rise in the rate of Cl^- export across the plasma membrane. The only change that the model predicted when 2 M NpHR were added in the tonoplast is that the VCl channel compensated the fluxes of Cl^- caused by NpHR, thus not affecting the total fluxes through plasma membrane and tonoplast.

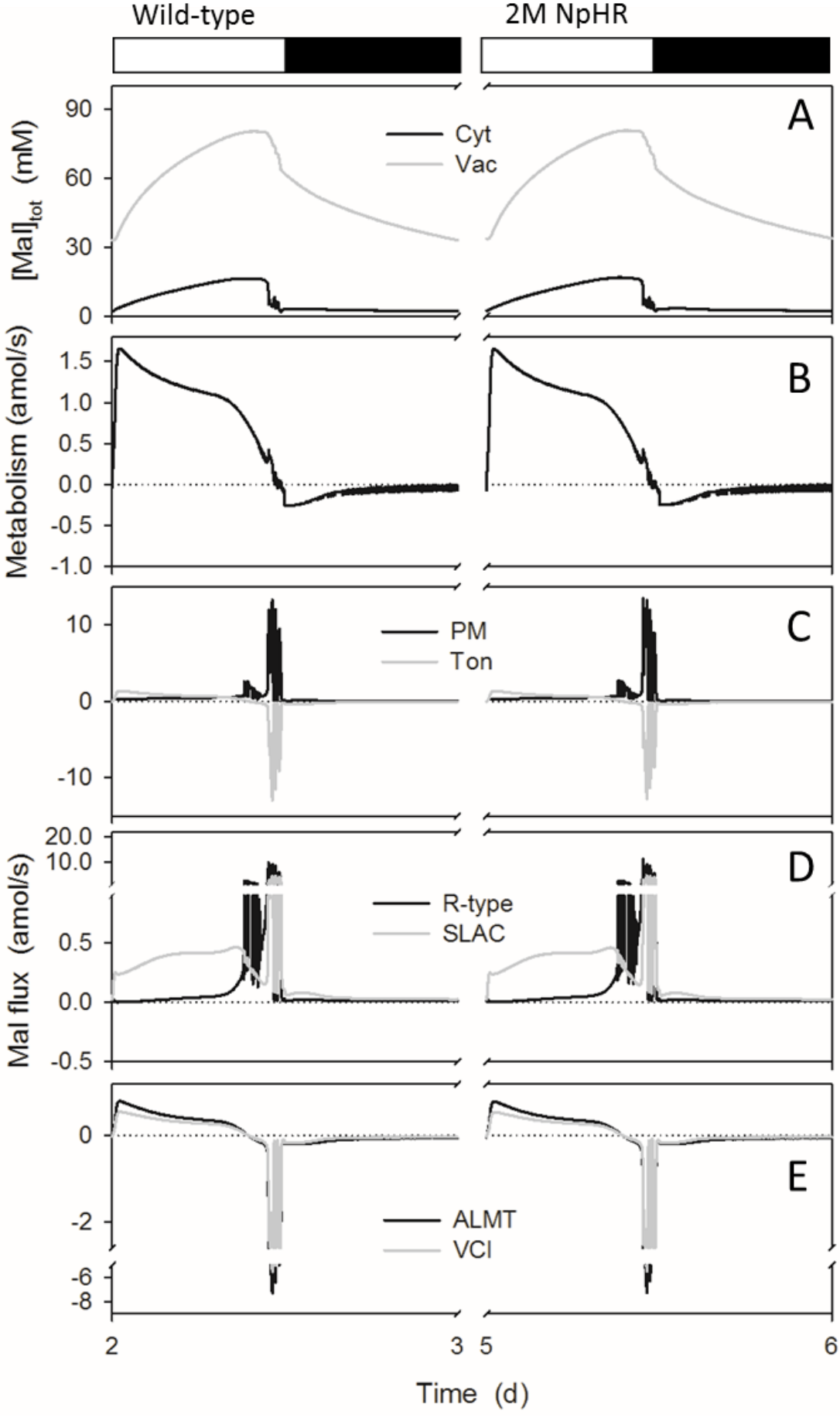
Wild-type
2M NpHR
A
B
C
D
E
Cyt
Vac
PM
Ton
R-type
SLAC
ALMT
VCl
[Mal]tot (mM)
Metabolism (amol/s)
Mal flux (amol/s)
Time (d)
90
60
30
0
1.5
1.0
0.5
0.0
-0.5
-1.0
10
0
-10
20.0
10.0
0.5
0.0
-0.5
0
-2
-6
-8
2
3
5
6

Figure 5.2.29. Malic acid synthesis, total malate (Mal) contents and analysis of Mal^{2-} fluxes at the plasma membrane and tonoplast resolved over a standard diurnal cycle (12 h light:12 h dark, indicated by bars above) (Chen, Hills et al. 2012) for the wild-type (control, left) and when 2 million NpHR pumps were added in the tonoplast (right) as described in Figure 5.2.25. Shown are (A) total cytosolic and vacuolar [Mal], (B) the rates of Mal synthesis and metabolism, (C) the net flux of Mal^{2-} across the plasma membrane and tonoplast, (D) the Mal^{2-} flux through the Mal^{2-} -permeable transporters at the plasma membrane, comprising the SLAC and R- (ALMT-) type anion channels, and (E) the Mal^{2-} flux through the Mal^{2-} -permeable transporters at the tonoplast, comprising the VMAL and VCL channels. Positive flux is defined as movement of the ionic species (not the charge) out of the cytosol, either across the plasma membrane or the tonoplast. In the wild-type, the bulk of Mal production was diverted by transport of Mal^{2-} across the tonoplast, leading to a rise in total vacuolar Mal from 30 mM at the end of the night to near 90 mM before declining at the end of the daylight period; Mal in the cytosol rose from approximately 1 mM to values near 15 mM, much as has been estimated from experimental data (Hills, Chen et al. 2012). When 2 million NpHR pumps were added in the tonoplast the model didn't predict any substantial difference between the two simulations.

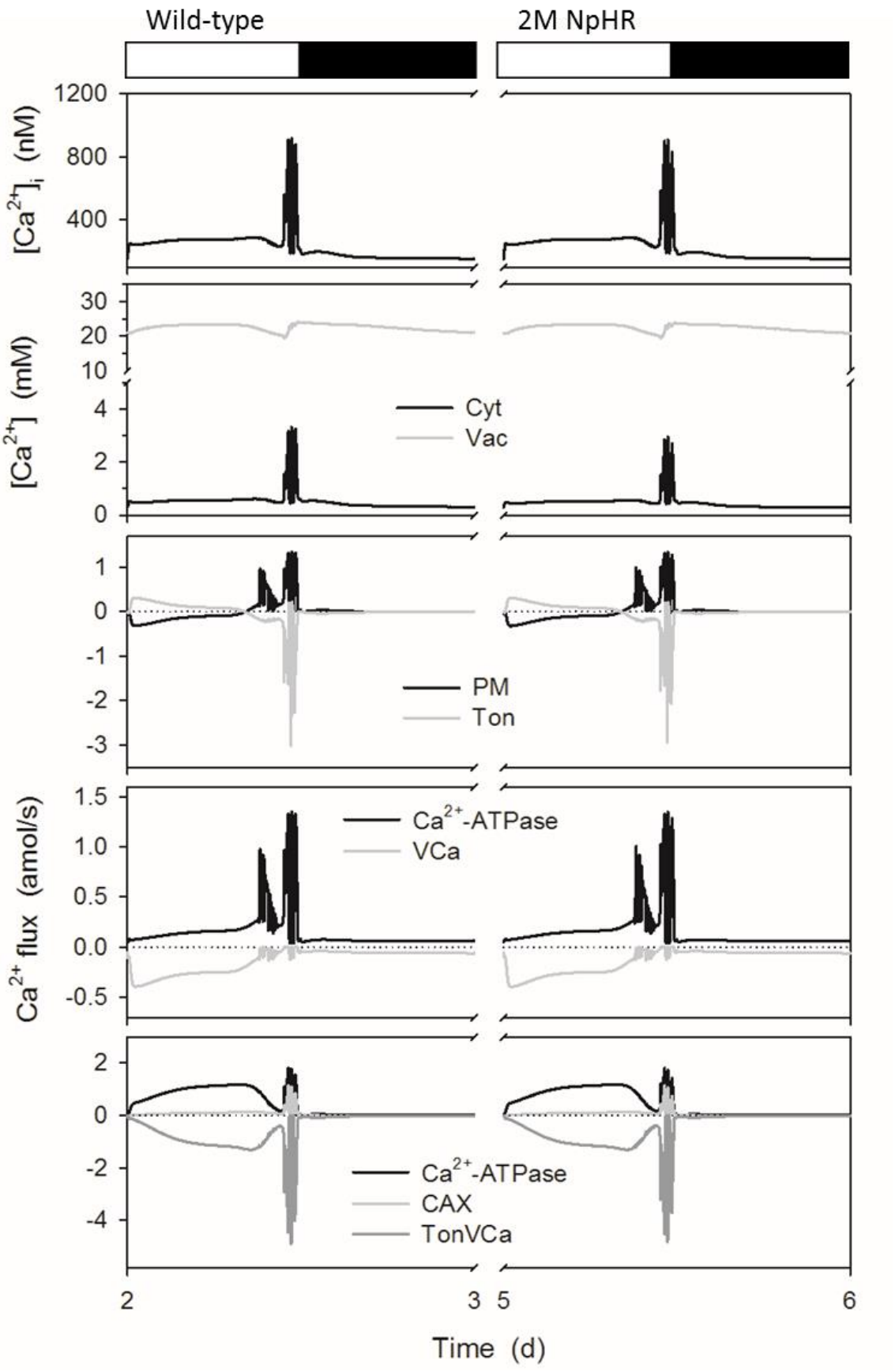
Wild-type
2M NpHR
1200
800
400
[Ca2+]i (nM)
30
20
10
4
2
0
[Ca2+] (mM)
Cyt
Vac
1
0
-1
-2
-3
PM
Ton
1.5
1.0
0.5
0.0
-0.5
Ca2+ flux (amol/s)
Ca2+-ATPase
VCa
2
0
-2
-4
Ca2+-ATPase
CAX
TonVCa
2
3
5
6
Time (d)

Figure 5.2.30. Total cytosolic and vacuolar [Ca^{2+}], cytosolic free [Ca^{2+}], and analysis of Ca^{2+} fluxes across the plasma membrane and tonoplast resolved over a standard diurnal cycle (12 h light:12 h dark, indicated by bars above) (Chen, Hills et al. 2012) for the wild-type (control, left) when 2 million NpHR pumps were added in the tonoplast (right) as described in Figure 5.2.25. Shown are (A) the cytosolic-free [Ca^{2+}] ([Ca^{2+}]$_i$), (B) the total cytosolic and vacuolar [Ca^{2+}], (C) the net flux of Ca^{2+} across the plasma membrane and tonoplast, (D) the Ca^{2+} flux through the Ca^{2+} -permeable transporters at the plasma membrane, comprising the hyperpolarisation-activated Ca^{2+} channel and the Ca^{2+}-ATPase, and (E) the flux of Ca^{2+} through the Ca^{2+} permeable transporters at the tonoplast, comprising the Ca^{2+}-ATPase, the CAX H^+-Ca^{2+} antiporter, and the TonVCa Ca^{2+} channel. Flux through the TPC channel accounts for less than two percent of the total Ca^{2+} flux across the tonoplast and has therefore been omitted for purposes of clarity. Positive flux is defined as movement of the ionic species (not the charge) out of the cytosol, either across the plasma membrane or the tonoplast. For the wild-type, the OnGuard model predicted [Ca^{2+}]$_i$ to decrease from a value near 200 nM in the daylight period to a resting value near 100 nM in the dark period (A). Stomatal closure was accompanied by a series of voltage (Figure 1) and [Ca^{2+}]$_i$ oscillations that drive K^+ and anion efflux for stomatal closure (Gilroy, Fricker et al. 1991, Irving, Gehring et al. 1992, McAinsh, Brownlee et al. 1992, Thiel, MacRobbie et al. 1992). When 2 million NpHR pumps were added in the tonoplast the model didn't predict any substantial difference between the two simulations.

The primary effect predicted by the model, when expressing 2M NpHR in the plasma membrane of the guard cells, was the big increase on Cl^- accumulation both in the cytosol as well as in the vacuole. The Cl^- influx from the apoplast to the cytosol was mainly through the NpHR (Figure 5.2.22C). The influx of Cl^- from the cytoplasm to the vacuole was mainly through the VCl channels (Figure 5.2.22D). Simultaneously, the increase on Cl^- accumulation caused associated effects such as a big increase on K^+ accumulation in the cytosol and vacuole; and a decrease on the levels of malate mainly in the vacuole. The K^+ influx happened mainly through K_{in} channels in the plasma membrane (Figure 5.2.20C) and through TPK channels in the vacuole (Figure 5.2.20D). Malate efflux was observed to occur through SLAC channels. In contrast, there were no big differences observed on pH changes (Figure 5.2.21), or Ca^{2+} fluxes (Figure 5.2.24).

Not many differences were observed when the model simulated the expression of 2M NpHR in the tonoplast. In fact, the only changes predicted by the model were in relation to Cl^- (Figure 5.2.28). Indeed, the same amount of Cl^- pumped out of the vacuole by the NpHR (Figure 5.2.28C), was transported back to the vacuole through the VCl channels (Figure 5.2.28D).

Overall, the model predicted a change on the stomatal kinetics when NpHR was expressed in the plasma membrane but no effect when expressed in the tonoplast membrane. Indeed, adding NpHR in the plasma membrane caused a major increase and quicker change in aperture of the stomata at the beginning of the daylight period, and a more rapid and complete closure at the beginning of the dark period (Figure 1 A). If the stomata really reproduce the same response in vivo, we are facing a new possibility to improve photosynthesis and WUE.

5.2.2.2. Cloning and Confocal Imaging for plasma membrane expression of NpHR

Based on the OnGuard predictions of expressing NpHR in the plasma membrane, it was decided to express the protein in plants and verify if the same effects can be reproducible in vivo. From the experience out of the chloroplasts project (Chapter 5.1) it was known that NpHR could be expressed in plants, however its localisation was seen in the tonoplast, but not in the plasma membrane. Even so, it was decided to express again NpHR without any target sequence, but just changing the position of the fluorescent tag, to verify again its localisation under confocal microscopy. Thus, I created new constructs (Table 5.2.2) expressing NpHR under the 35S promoter expression, with an N-terminal or C-terminal RFP fluorescent tags.

Table 5.2.2. List of the expression constructs expressing full length NpHR.

Expression construct	Entry clone (All in pDONR207)	Destination vector	SM
35S::NpHR-RFP	NpHR-wo	pB7RWG2	S.10.16
35S::RFP-NpHR	NpHR-st	pB7WGR2	S.10.16

Table 1. Expression constructs expressing NpHR with N-terminal or C-terminal RFP tag under the 35S promoter expression. Entry clones and destination vector used for the production of the expression constructs and site localisation of the RFP fluorescent tag. pB7RWG2 (Karimi, Depicker et al. 2007) is a Gateway-compatible vector with C-terminal fluorescent RFP tag and incorporating the 35S promoter. pB7WGR2 (Karimi, Depicker et al. 2007) is a Gateway-compatible vector with N-terminal fluorescent RFP tag and incorporating the 35S promoter. pDONR207 is an entry vector from Gateway

technology (Life Technologies) containing the *att*B1 and *att*B2 recombination sites. wo: without stop codon, st: with stop codon. SM: supplemental material.

I transformed tobacco transiently with the two expression constructs from Table 5.2.2. I used the *Agrobacterium*-mediated gene transfer by the leave infiltration method. Three days after transformation, I examined the expression of the proteins under confocal microscopy. Figure 5.2.31 and 5.2.32 show the expression in tobacco of the constructs 35S::NpHR-RFP and 35S::RFP-NpHR respectively. From the confocal images I concluded that the localisation of the protein changes depending of the position of the RFP tag in the protein. The protein was observed in the tonoplast when expressed with C-terminal RFP tag, whereas when expressed with N-terminal RFP tag the localisation was in the ER. Typical for tonoplast localisation is the observation of fluorescent signal in the tonoplast invaginations, also when a protein is expressed in the tonoplast the fluorescent signal doesn't reach the edges of the cell completely. Whereas, when a protein is expressed in the ER the fluorescent signal is localised surrounding the nucleus, as well as showing the nets of the ER network in the cytoplasm. These results are consistent with the data from the chapter 5.1, which shows tonoplast expression of NpHR when expressed with a C-terminal GFP tag (Figure 5.1.1).

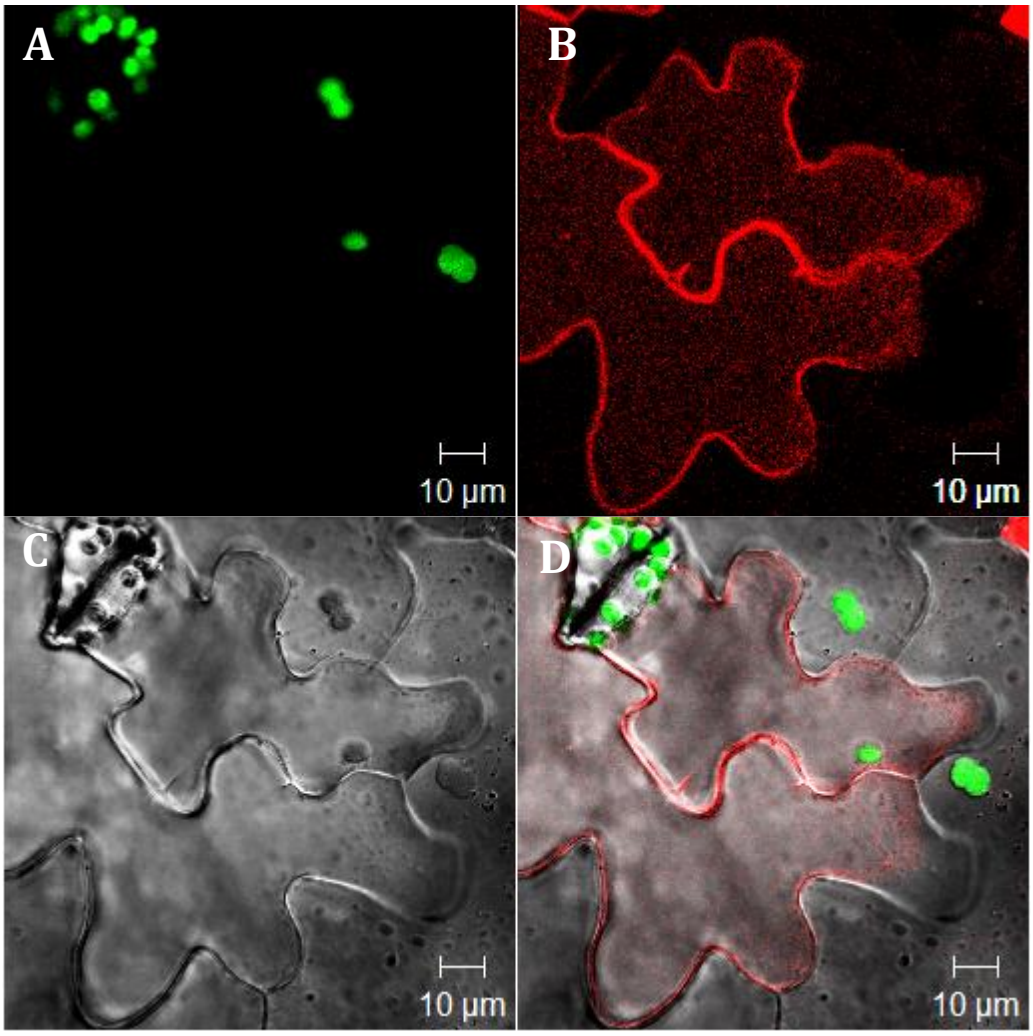

Figure 5.2.31. Expression of the construct 35S::NpHR-RFP in transient transformed tobacco leaves after 3 days of transformation. RFP fluorescence indicates tonoplast localisation of NpHR in the epidermal cells (red B, D). The chlorophyll *autofluorescence* is shown in green (A, D). C is the bright field image, and D shows a merged image. The images are from 25-slice Z-stack through the epidermal cell with a 0.75 µm interval between slices. In all the images the scale bar is 10 µm.

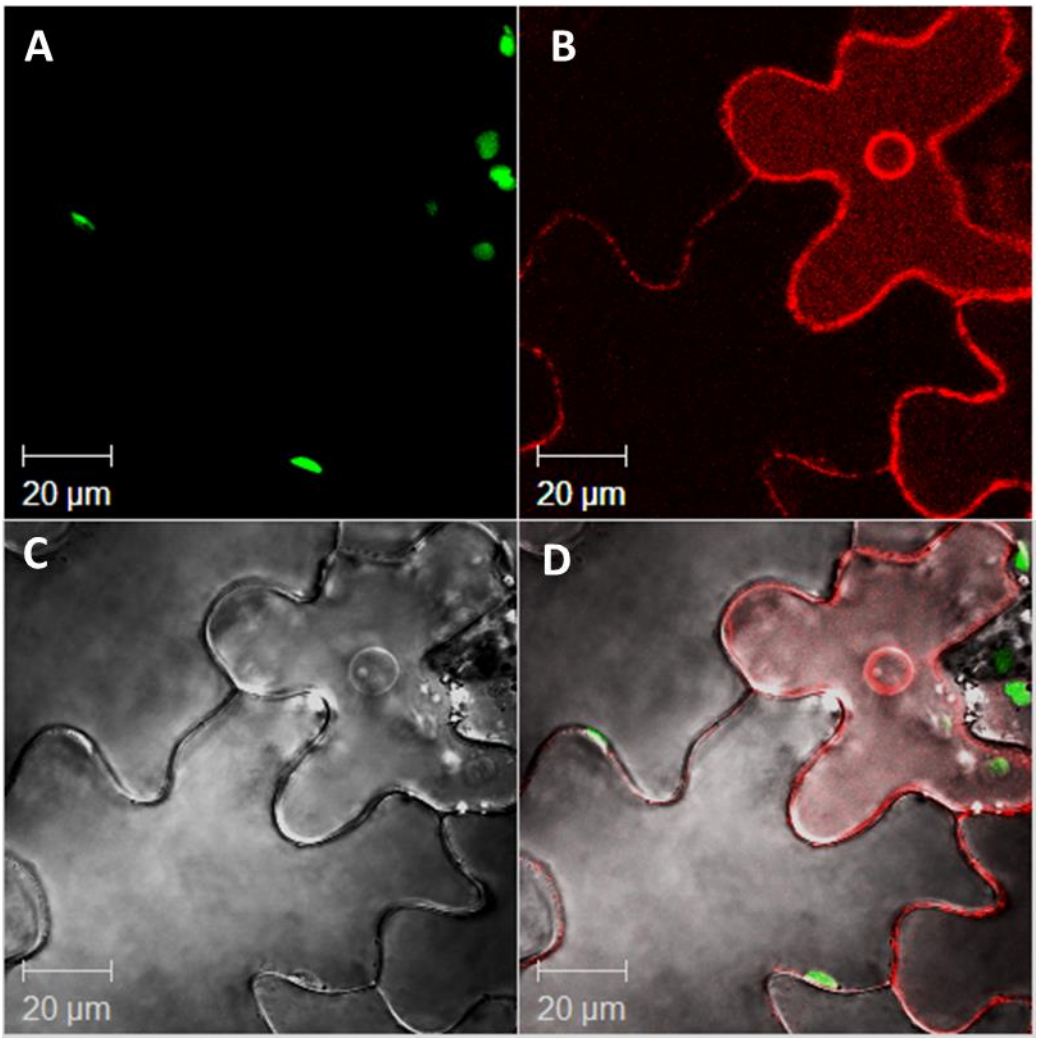

Figure 5.2.32. Expression of the construct 35S::RFP-NpHR in transient transformed tobacco leaves after 3 days of transformation. RFP fluorescence indicates ER localisation of NpHR in the epidermal cells (red B, D). The chlorophyll *autofluorescence* is shown in green (A, D). C is the bright field image, and D shows a merged image. The images are from 18-slice Z-stack through the epidermal cell with a 0.75 µm interval between slices. In all the images the scale bar is 20 µm.

These findings also underlined the challenge of targeting the protein to the plasma membrane. No target sequence is currently known and described to drive plasma membrane localisation of proteins, although clearly these most likely exist. Indeed, firstly it was thought that plasma membrane was a destination by default, however this has not been demonstrated yet (Vitale and Raikhel 1999). Initially, an analysis of the NpHR protein sequence was carried out to discard the possibility that it contains a retention site, which could stop transfer of NpHR from the endoplasmic reticulum to

the plasma membrane. No obvious retention sequences were identified. However, the N-terminus of the NpHR incorporates some hydrophobic residues within the first 17 amino acid residues followed by an amphipathic sequence over the next 15 amino acids. Because the N-terminus of NpHR is localised to the extracellular space in bacteria, it was thought that these hydrophobic and amphipathic sequences might pose difficulties in targeting for a plasma membrane localisation in the plant. Thus, I created new constructs lacking the first 17 and 32 amino acids of NpHR (Table 5.2.3) to test the possibility that these sequences were hampering plasma membrane localisation.

Table 5.2.3. List of the expression constructs expressing ^{1_17del}NpHR and ^{1_32del}NpHR.

Expression construct	Entry clone (All in pDONR207)	Destination vector	SM
35S::^{1_17del}NpHR-RFP	^{1_17del}NpHR-wo	pB7RWG2	S.10.1/10.16
35S::RFP-^{1_17del}NpHR	^{1_17del}NpHR-st	pB7WGR2	S.10.2/10.16
35S::^{1_32del}NpHR-RFP	^{1_32del}NpHR-wo	pB7RWG2	S.10.3/10.16
35S:: RFP-^{1_32del}NpHR	^{1_32del}NpHR-st	pB7WGR2	S.10.4/10.16

Table 2. Expression constructs expressing NpHR lacking the first 17 amino acids (^{1_17del}NpHR) and the first 32 amino acids (^{1_32del}NpHR). All with N-terminal or C-terminal RFP tag under the 35S promoter expression. Entry clones and destination vector used for the production of the expression constructs and site localisation of the RFP fluorescent tag. pB7RWG2 (Karimi, Depicker et al. 2007) is a Gateway-compatible vector with C-terminal fluorescent RFP tag and incorporating the 35S promoter. pB7WGR2 (Karimi, Depicker et al. 2007) is a Gateway-compatible vector with N-terminal fluorescent RFP tag and incorporating the 35S promoter. pDONR207 is an entry vector from Gateway technology (Life Technologies) containing the *att*B1 and *att*B2 recombination sites. wo: without stop codon, st: with stop codon. SM: supplemental material.

Transient transformations in tobacco were done with all the constructs shown in Table 5.2.3. I used the *Agrobacterium*-mediated gene transfer by leave infiltration method to transform tobacco. After three days of transformation I was examined the expression of the proteins under confocal microscopy. The confocal microscope images showing the constructs on table 2 are shown in the annex (S.10.1 to S.10.4). No differences

from when expressing full length NpHR were found between the different constructs. In all the cases NpHR with an N-terminus RFP tag showed ER localisation of the protein, and NpHR with a C-terminus RFP tag showed tonoplast localisation, independently of the length of the sequence. Due to cutting the amino acids length of NpHR made no difference on protein localisation it was decided to work with the full length protein from now on.

As a different option for plasma membrane targeting of NpHR, I followed the strategy that Gradinaru et al (2008) used in order to promote membrane localisation and ER export of NpHR when expressed in neurons. They used a combination of two export motifs, an N-terminal signal peptide form nAChR, for membrane insertion, and a C-terminal ER export sequence from Kir2.1, to improve export NpHR to the plasma membrane. Following the same strategy, and without any guarantee that it could be functional in plants I reproduced exactly the same strategy to express NpHR in the plasma membrane. Thus, I created 4 different vectors (Figure 5.2.33) in order to express NpHR using their same signal peptide (SP) and ER export (ERexp) signal together with a fluorescent tag. It was decided to try again with UBQ10 promoter as well as 35S promoter. The choice of trying again with the UBQ10 was made because the strong expression of 35S promoter could raise the risk of mislocalization of the protein.

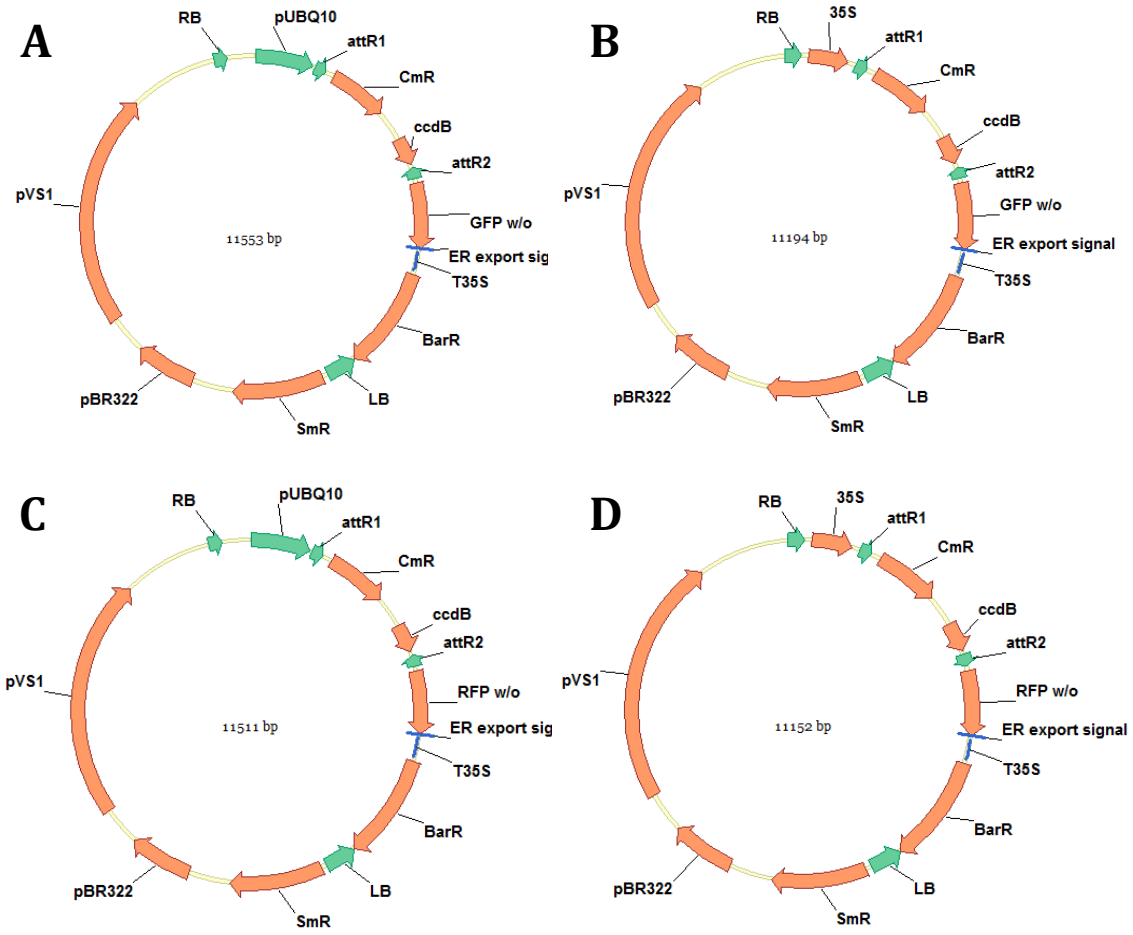

Figure 5.2.33. Four different destination vectors expressing the ER export signal. Two of the vectors contain UBQ10 promoter (A, C), and the other two contain the 35S promoter (B, D). Expressing C-terminal RFP (C, D) or GFP (A, B) fluorescent markers. pBR322ori/pVS1ori: replication origins. RB/LF: right/left border. SmR: spectinomycin resistance. BarR: BASTA resistance. T35S: 35S terminator. 35S: 35S strong promoter. pUBQ10: UBQ10 promoter. RFP/GFP: red/green fluorescent marker. *ccd*B: *ccd*B toxic gene. *att*R1/*att*R2: recombination sites. The vector sizes are 11553 bp (A), 11194 bp (B), 11511 bp (C) and 11152 bp (D).

As described in Gradinaru's paper, I expressed the SP in the N-terminal of the protein and the ERexp signal in the C-terminal, following the fluorescent tag (RFP/GFP). After transient transformation of tobacco, confocal images showed tonoplast localisation of the protein (Figure 5.2.34). Besides, when the protein was under the expression of the UBQ10 promoter the signal was too low to proper identify localisation of the NpHR. From here it was decided to work just with the 35S promoter. Because of no success on plasma membrane localisation when expressing NpHR with SP and ERexp signal, I decided to express the protein just with SP or with ERexp, but not with both together

(Table 5.2.4). Again, localisation of the protein appeared in the tonoplast (Figure 5.2.35 and 5.2.36).

Table 5.2.4. List of the expression constructs expressing NpHR with SP and ERexp.

Expression construct	Entry clone (pDONR207)	Destination vector	SM
pUBQ::SP-NpHR-GFP-ERexp	NpHR-wo	pUBQ::GFP-DEST-ERexp	S.10.17
pUBQ::SP-NpHR-RFP-ERexp	NpHR-wo	pUBQ::RFP-DEST-ERexp	S.10.17
35S::SP-NpHR-GFP-ERexp	NpHR-wo	35S::GFP-DEST-ERexp	S.10.17
35S::SP-NpHR-RFP-ERexp	NpHR-wo	35S::RFP-DEST-ERexp	S.10.17
35S::SP-NpHR-GFP	NpHR-wo	pH7FWG2	S.10.18
35S::SP-NpHR- RFP	NpHR-wo	pB7RWG2	S.10.18
35S::NpHR-ERexp-GFP	NpHR-wo	pH7FWG2	S.10.18
35S::NpHR-ERexp-RFP	NpHR-wo	pB7RWG2	S.10.18

Table 5.2.4. Expression constructs expressing NpHR with SP and/or ERexp, under the espression of UBQ10 or 35S promoter, and tag to a RFP or GFP fluorescent marker. All the entry clones are made in pDONR207, an entry vector from Gateway technology (Life Technologies) containing the *att*B1 and *att*B2 recombination sites. pH7FWG2 and pB7RWG2 (Karimi, Depicker et al. 2007) are Gateway-compatible vectors with C-terminal fluorescent tags incorporating the 35S promoter. pUBQ::GFP-DEST-ERexp, pUBQ::RFP-DEST-ERexp, 35S::GFP-DEST-ERexp and 35S::RFP-DEST-ERexp are new vectors created from the background vectors pUBQ::GFP-DEST and pUBQ::RFP-DEST (Grefen, Donald et al. 2010) which are Gateway-compatible vectors with C-terminal fluorescent tags. wo: without stop codon. SM: supplemental material.

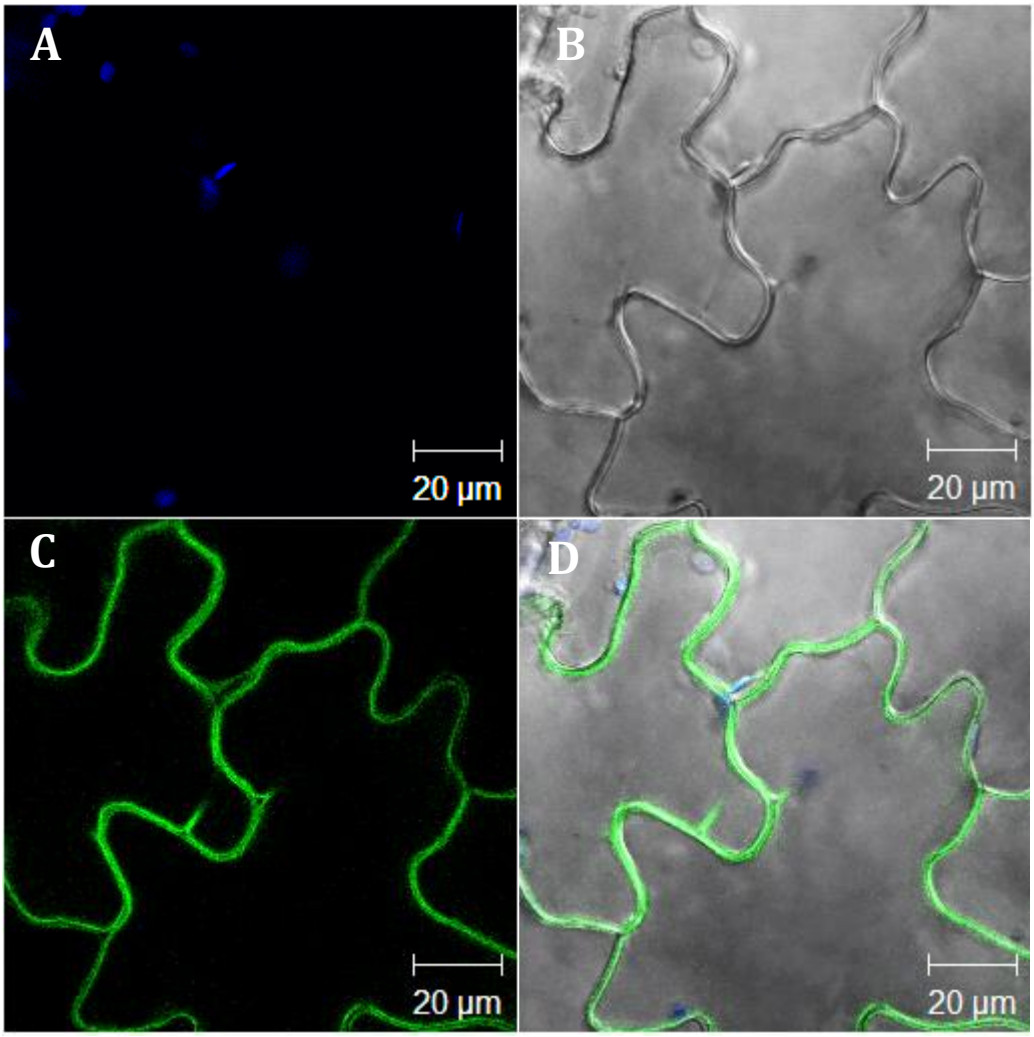

Figure 5.2.34. Expression of the construct 35S::SP-NpHR-GFP-ERexp in transient transformed tobacco leaves after 3 days of transformation. GFP fluorescence indicates tonoplast localisation of NpHR in the epidermal cells (green C, D). The chlorophyll *autofluorescence* is shown in blue (A, D). B is the bright field image, and D shows a merged image. The images are from 35-slice Z-stack through the epidermal cell with a 1.2 µm interval between slices. In all the images the scale bar is 20 µm.

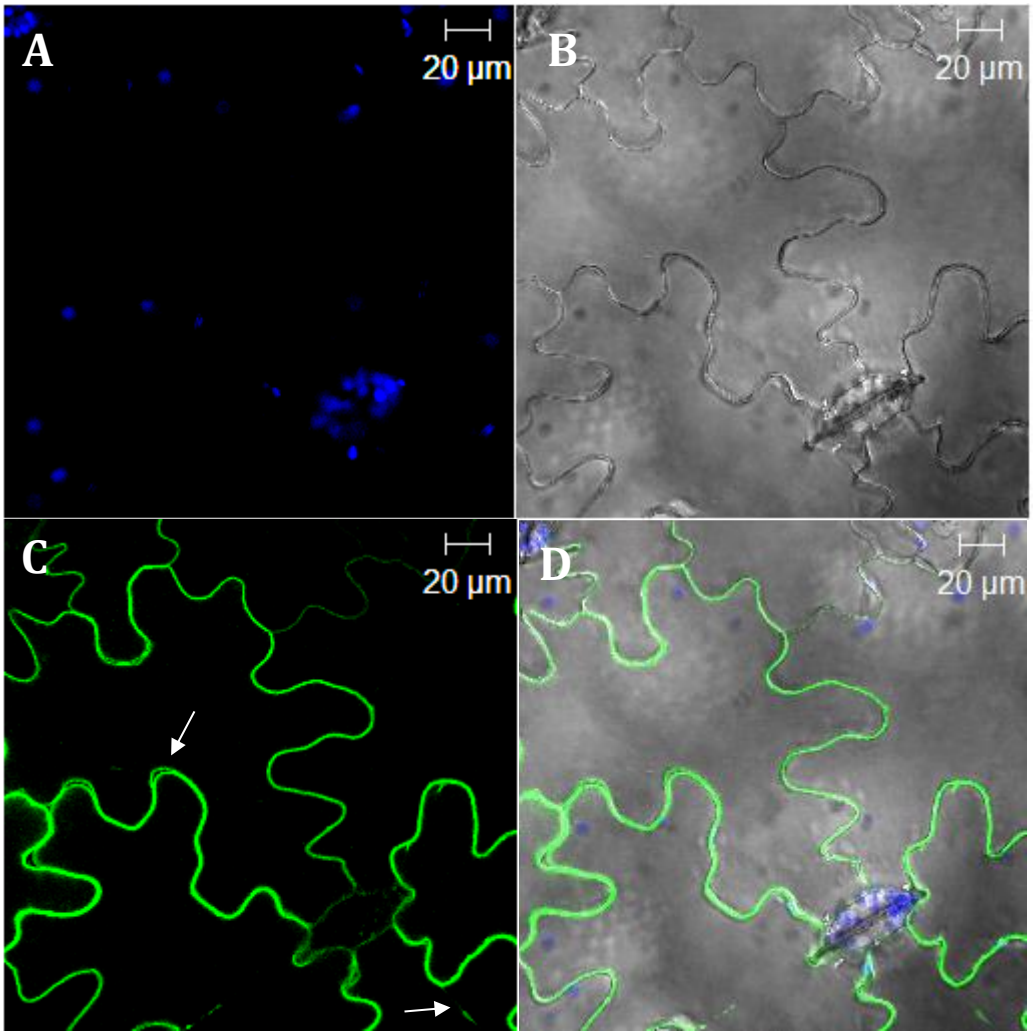

Figure 5.2.35. Expression of the construct 35S::SP-NpHR-GFP in transient transformed tobacco leaves after 3 days of transformation. GFP fluorescence indicates tonoplast localisation of NpHR in the epidermal cells (green C, D). The chlorophyll *autofluorescence* is shown in blue (A, D). B is the bright field image, and D shows a merged image. The white arrows indicate typical characteristics of tonoplast protein localisation, in this case characterised by not reaching the edges of the cell completely. The images are from a single scan of the epidermal cell. In all the images the scale bar is 20 µm.

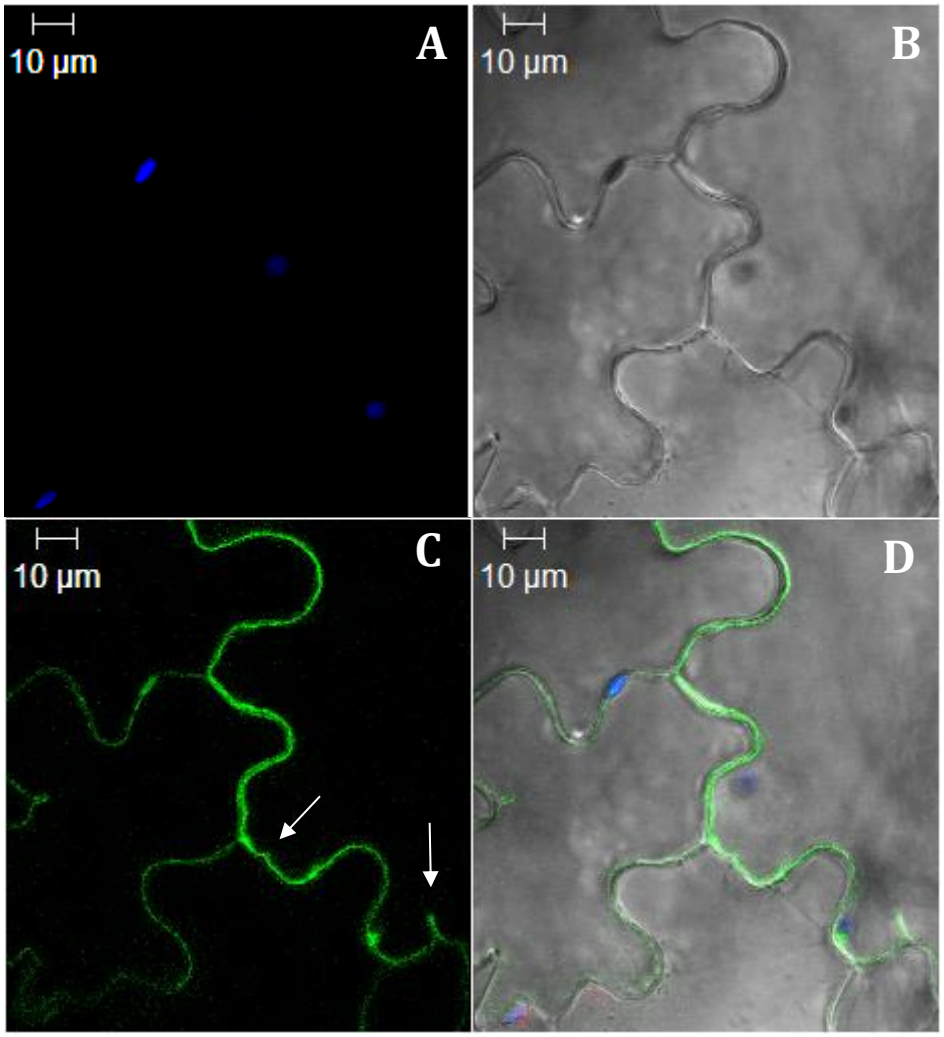

Figure 5.2.36. Expression of the construct 35S::NpHR-GFP in transient transformed tobacco leaves after 3 days of transformation. GFP fluorescence indicates tonoplast localisation of NpHR in the epidermal cells (green C, D). The chlorophyll *autofluorescence* is shown in blue (A, D) indicating the localisation of the chloroplasts. B is the bright field image, and D shows a merged image. The white arrows indicate typical characteristics of tonoplast protein localisation, in this case characterised by not reaching the edges of the cell completely. The images are from 30-slice Z-stack through the epidermal cell with a 1.1 µm interval between slices. In all the images the scale bar is 10 µm.

A third strategy was also pursued due to none of the strategies previously described worked out to drive the NpHR to the plasma membrane. It has been shown previously that tethering two proteins together can be used to 'drag' a protein of interest to the normal destination of the tethered partner. This approach was recently adapted in work by Kleinlogel, et al. (2011) who used the method to generate functional 1:1

fusions between NpHR and ChR2 (channelrhodopsin-2) for expression of these proteins in the membrane of neurons. Their interest was to ensure a direct correspondence between the activities of the two proteins, but the application also showed the potential for directing proteins to different target membranes. Thus, I reasoned that driving NpHR to the plant plasma membrane might be possible by linking it with a naturally expressed plasma membrane protein in the plant.

Initially I trialled linking NpHR with the SNARE protein SYP121, a membrane fusion protein involved in vesicle-mediate transport for intracellular protein transport, as this protein is routinely used in the lab and suitable constructs were readily available (Leyman, Geelen et al. 1999, Leyman, Geelen et al. 2000)**.** Another advantage of SYP121 is that its C-terminus is normally localised outside the cell (Blatt, Leyman et al. 1999, Jahn and Scheller 2006, Lipka, Kwon et al. 2007) and therefore could be coupled directly to the N-terminus of NpHR. The different constructs made combining SYP121 and NpHR are shown in Table 4. I created two different constructs where NpHR was linked in the N-terminal of SYP121 under the expression of UBQ10 and 35S promoter. For these constructs an RFP fluorescent tag was incorporated in between the two proteins, as a linker function to provide enough mobility between the two proteins. For these cloning it was used a destination vector, pUB-DEST (Grefen, Donald et al. 2010), containing the UBQ10 promoter and no fluorescent marker. Moreover, I created a new vector (35S::DEST) based on the background of the pUB-DEST in which I exchanged the UBQ10 promoter for the 35S, again without incorporating a fluorescent marker (Table 5.2.5). A third expression construct was created in which NpHR was linked in the C-terminus of the SYP121 protein, and expressed under the 35S promoter expression.

Table 5.2.5. List of the expression constructs expressing NpHR linked to SYP121.

Expression construct	Entry clone (All in pDONR207)	Destination vector	SM
UBQ10::NpHR-RFP-SYP121	NpHR-RFP-SYP121-st	pUB-DEST	S.10.19
35S::NpHR-RFP-SYP121	NpHR-RFP-SYP121-st	35S::DEST	S.10.19
35S::SYP121-2xHA-NpHR-RFP	SYP121-2xHA-NpHR-wo	pB7RWG2	S.10.19

Table 5.2.5. Expression constructs expressing NpHR linked with SYP121, under the expression of UBQ10 or 35S promoter, and tag to a RFP fluorescent marker. All the entry clones are made in pDONR207, an entry vector from Gateway technology (Life Technologies) containing the *att*B1 and *att*B2 recombination sites. pB7RWG2 (Karimi, Depicker et al. 2007) is a Gateway-compatible vector with C-terminal RFP fluorescent tag incorporating the 35S promoter. pUB-DEST (Grefen, Donald et al. 2010) is a Gateway-compatible vectors with no fluorescent tags containing the UBQ10 promoter. 35S::DEST is a new vector, created from the background vector pUB-DEST, which is Gateway-compatible, without any fluorescent tag and containing the 35S promoter. HA: hemagglutinin tag. wo: without stop codon. st: with stop codon. SM: supplemental material.

None of the three constructs shown in Table 5.2.5 yielded protein expression in the plasma membrane once transiently expressed in tobacco epidermal cells. Again the expression of the construct containing the UBQ10 promote was too low to show localisation of the protein. An example of the construct 35S::NpHR-RFP-SYP121 is shown in Figure 5.2.37 where it can be seen ER localisation of the proteins.

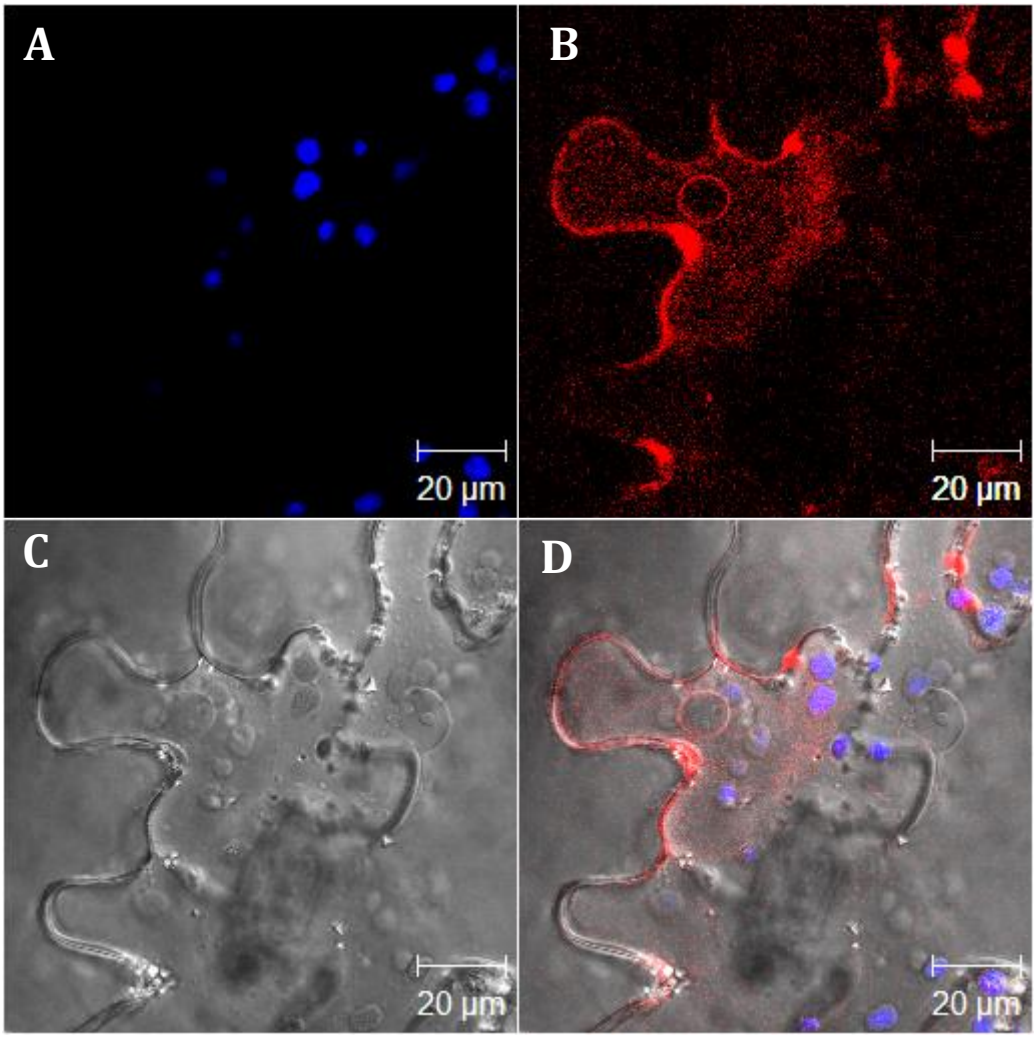

Figure 5.2.37. Expression of the construct 35S::NpHR-RFP-SYP121 in transient transformed tobacco leaves after 3 days of transformation. RFP fluorescence indicates ER localisation of NpHR-SYP121 in the epidermal cells (red B, D). The chlorophyll *autofluorescence* is shown in blue (A, D) indicating the localisation of the chloroplasts. C is the bright field image, and D shows a merged image. The images are from 25-slice Z-stack through the epidermal cell with a 1.2 µm interval between slices. In all the images the scale bar is 20 µm.

I next linked NpHR with the longin domain of VAMP721 (LD_VAMP721). VAMP721 is a vesicle-associated membrane protein that associates with the plasma membrane, and its longin domain includes a determinant for protein location (Uemura, Sato et al. 2005, Zhang, Karnik et al. 2015). Although the exact residues are not known that determine this characteristic, I tested whether the LD_VAMP721 linked to NpHR would be able to drive as well the NpHR to the plasma membrane. I created a new construct linking the LD_VAMP721 with NpHR. Its localisation was analysed under confocal

microscopy and the protein expression was seen in the ER of transient transformed tobacco epidermal cells (Figure 5.2.38).

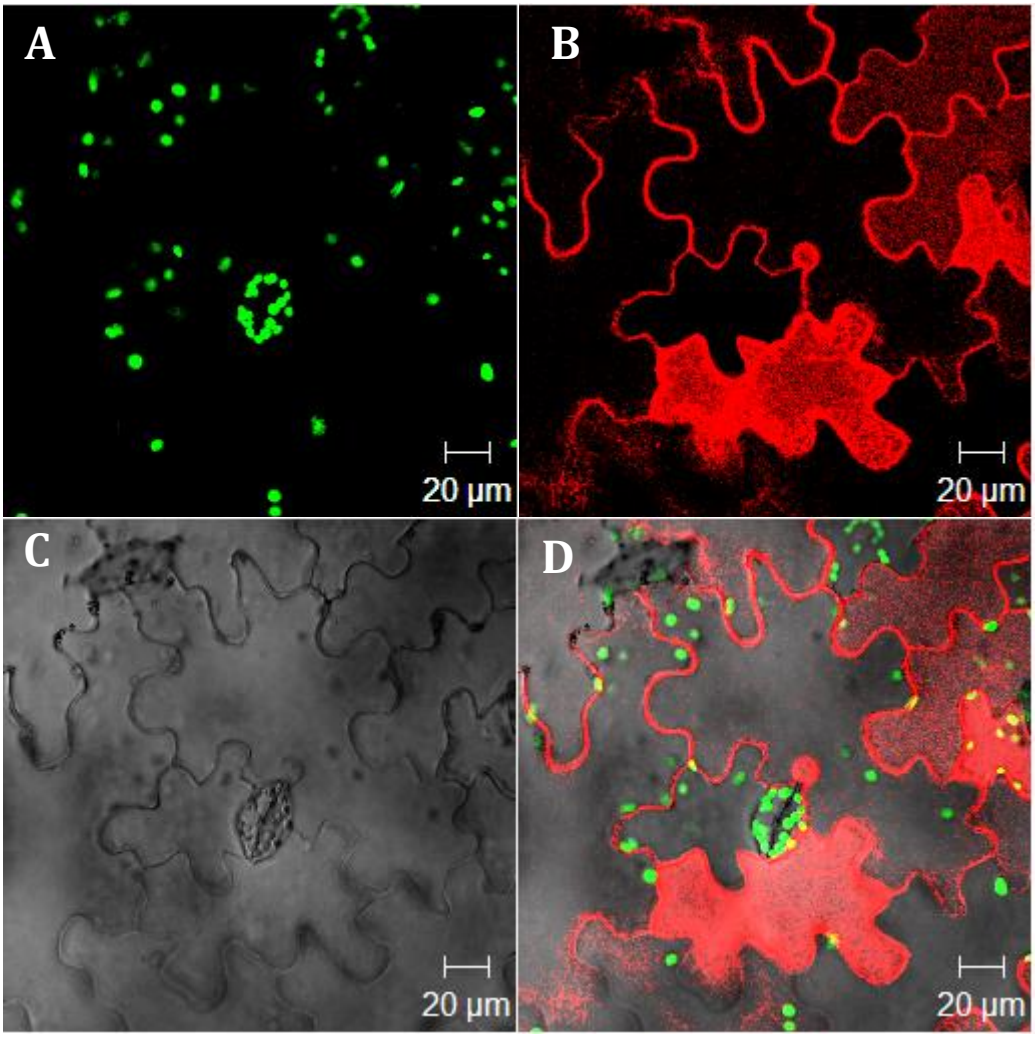

Figure 5.2.38. Expression of the construct 35S::NpHR-LD_VAMP721-RFP in transient transformed tobacco leaves after 3 days of transformation. RFP fluorescence indicates ER localisation of NpHR-LD_VAMP721 in the epidermal cells (red B, D). The chlorophyll *autofluorescence* is shown in green (A, D) indicating the localisation of the chloroplasts. C is the bright field image, and D shows a merged image. The images are from 12-slice Z-stack through the epidermal cell with a 2.75 µm interval between slices. In all the images the scale bar is 20 µm.

My third approach to coupling proteins focused on two integral, multidomain transmembrane proteins that normally are directed to the plasma membrane, the aquaporins or PIPs and the plasma membrane H^+-ATPases or AHAs. The PIPs (plasma membrane intrinsic protein) are well-characterised and abundant at the plasma

membrane, like the Arabidopsis H^+-ATPases. From PIP and AHA family proteins were selected PIP 2;1, PIP 2;7, AHA1 and AHA2.

First of all I created constructs expressing the 4 different proteins selected (PIP 2;1, PIP 2;7, AHA1 and AHA2) to check for plasma membrane localisation. The proteins were expressed in different constructs with N-terminal and C-terminal RFP marker (Table 5.2.6)

Table 5.2.6. List of the expression constructs expressing PIP 2;1, PIP 2;7, AHA1 and AHA2.

Expression construct	Entry clone (All in pDONR207)	Destination vector	SM.
35S::PIP2;1-RFP	PIP2;1-wo	pB7RWG2	S.10.20
35S:: RFP-PIP2;1	PIP2;1-st	pB7WGR2	S.10.20
35S::PIP2;7-RFP	PIP2;7-wo	pB7RWG2	S.10.20
35S:: RFP-PIP2;7	PIP2;7-st	pB7WGR2	S.10.20
35S::AHA1-RFP	AHA1-wo	pB7RWG2	S.10.21
35S:: RFP-AHA1	AHA1-st	pB7WGR2	S.10.21
35S::AHA2-RFP	AHA2-wo	pB7RWG2	S.10.21
35S:: RFP-AHA2	AHA2-st	pB7WGR2	S.10.21

Table 5.2.6. Expression constructs expressing PIP 2;1, PIP 2;7, AHA1 and AHA2, under the expression 35S promoter, and tag to a N-terminal or C-terminal RFP fluorescent marker. All the entry clones are made in pDONR207, an entry vector from Gateway technology (Life Technologies) containing the *att*B1 and *att*B2 recombination sites. pB7RWG2 (Karimi, Depicker et al. 2007) is a Gateway-compatible vector with C-terminal fluorescent RFP tag and incorporating the 35S promoter. pB7WGR2 (Karimi, Depicker et al. 2007) is a Gateway-compatible vector with N-terminal fluorescent RFP tag and incorporating the 35S promoter. wo: without stop codon. st: with stop codon. SM: supplemental material.

Of the constructs from Table 5, when transiently expressed in tobacco only AHA2 localisation was seen in the plasma membrane (Figure 5.2.42). The localisation of PIPs was in the ER (Figure 5.2.39 and 5.2.40) whereas AHA1 localisation was seen in the tonoplast (Figure 5.2.41). No difference on protein localisation was observed depending on the position of the RFO marker. Figures 5.2.39 to 5.2.42 are representative images of the constructs containing the different proteins.

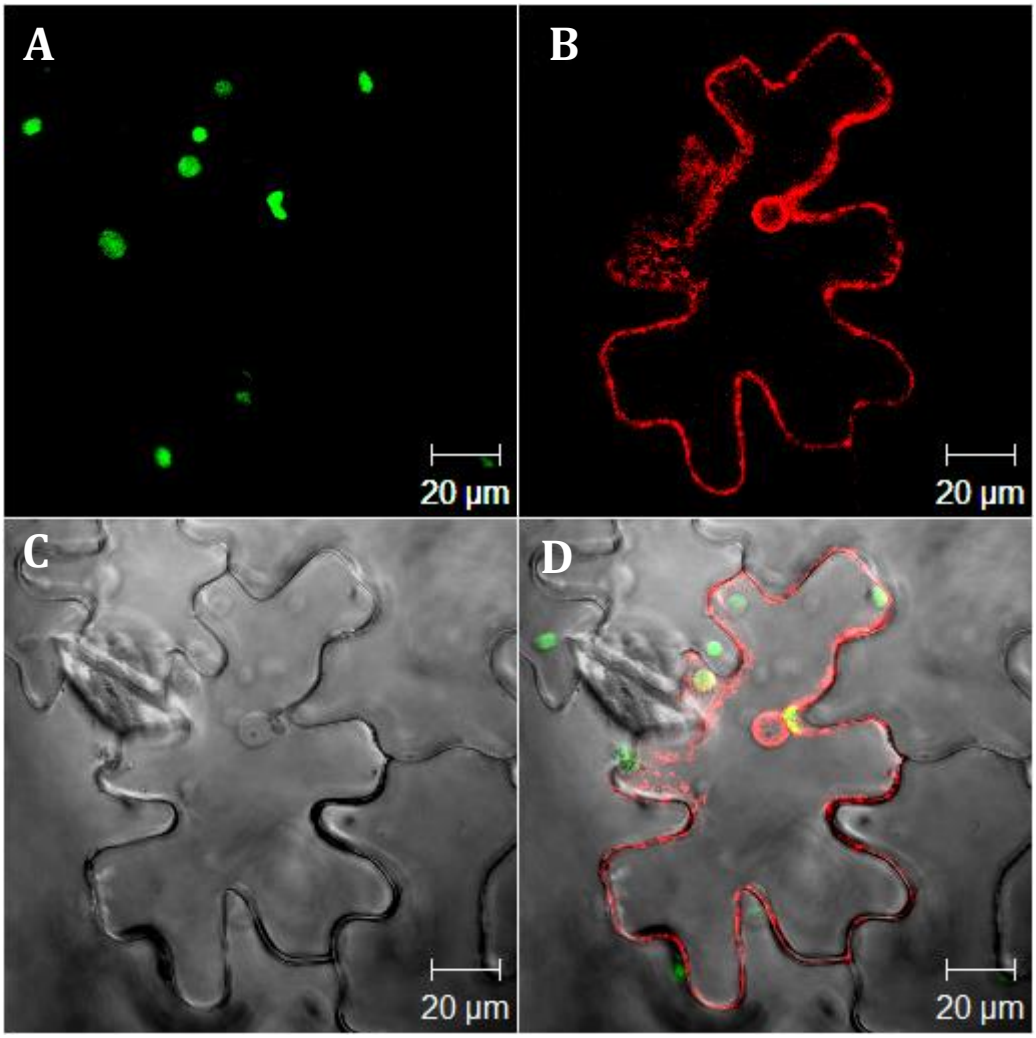

Figure 5.2.39. Expression of the construct 35S::RFP-PIP2,1 in transient transformed tobacco leaves after 3 days of transformation. RFP fluorescence indicates ER localisation of PIP2,1 in the epidermal cells (red B, D). The chlorophyll *autofluorescence* is shown in green (A, D) indicating the localisation of the chloroplasts. C is the bright field image, and D shows a merged image. The images are from 38-slice Z-stack through the epidermal cell with a 0.75 µm interval between slices. In all the images the scale bar is 20 µm.

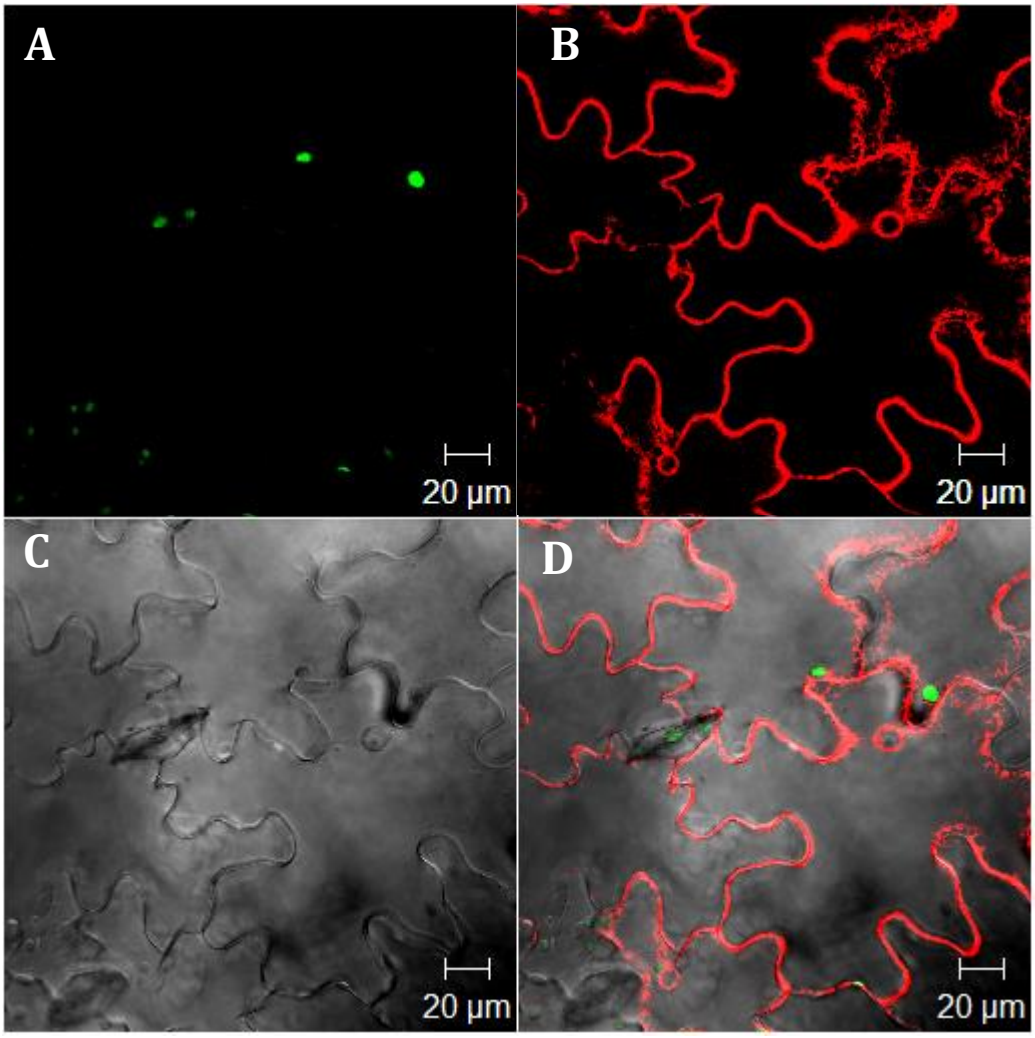

Figure 5.2.40. Expression of the construct 35S::RFP-PIP2,7 in transient transformed tobacco leaves after 3 days of transformation. RFP fluorescence indicates ER localisation of PIP2,7 in the epidermal cells (red B, D). The chlorophyll *autofluorescence* is shown in green (A, D) indicating the localisation of the chloroplasts. C is the bright field image, and D shows a merged image. The images are from 23-slice Z-stack through the epidermal cell with a 0.75 µm interval between slices. In all the images the scale bar is 20 µm.

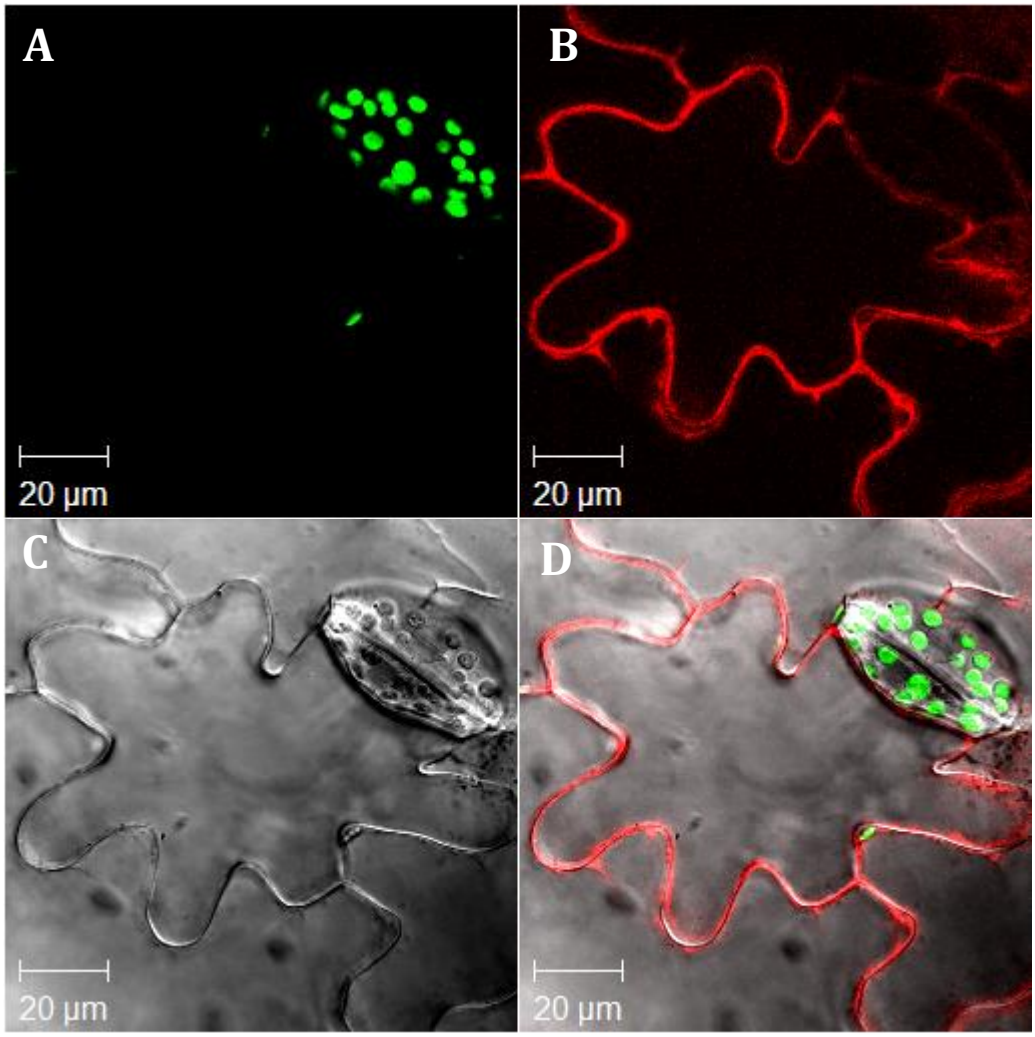

Figure 5.2.41. Expression of the construct 35S::AHA1-RFP in transient transformed tobacco leaves after 3 days of transformation. RFP fluorescence indicates tonoplast localisation of AHA1 in the epidermal cells (red B, D). The chlorophyll *autofluorescence* is shown in green (A, D) indicating the localisation of the chloroplasts. C is the bright field image, and D shows a merged image. The images are from 38-slice Z-stack through the epidermal cell with a 0.75 µm interval between slices. In all the images the scale bar is 20 µm.

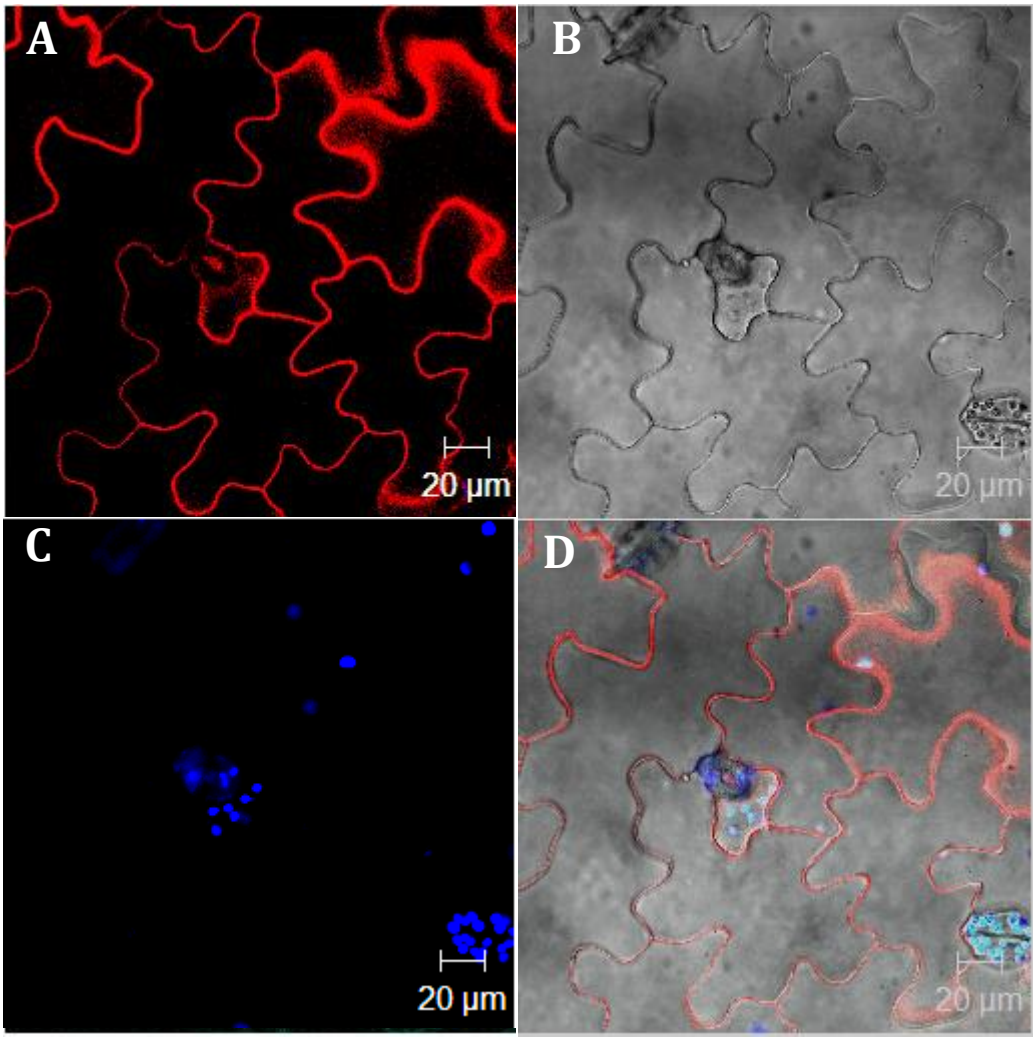

Figure 5.2.42. Expression of the construct 35S::AHA2-RFP in transient transformed tobacco leaves after 3 days of transformation. RFP fluorescence indicates plasma membrane localisation of AHA2 in the epidermal cells (red A, D). The chlorophyll *autofluorescence* is shown in blue (C, D) indicating the localisation of the chloroplasts. B is the bright field image, and D shows a merged image. The images are from a single scan through the epidermal cell. In all the images the scale bar is 20 µm.

Given that AHA2 was the only protein that expressed and localised in the plasma membrane of tobacco, it was selected to be linked with NpHR. The advantage of AHA2 versus SYP121 or LD_VAMP721 was that while these last are firstly synthetized and secondly driven and inserted to the plasma membrane, AHA2 is inserted into the plasma membrane at the same time that is being synthetized. AHA2 is a big protein, it has 10 transmembrane domains and a molecular weight of approximately 104 KDa. Due to its size, I considered expressing just a part of AHA2 instead of the full length

protein. Groves et al. (1998) showed that after cutting the AE1 protein in some of the loops and co-expressing the different fragments, the protein was still able to co-assemble and get expressed in the membrane. Another advantage of expressing just part of the protein instead of the full length is that the protein has less possibilities to be functional, this way could only make the function of driving NpHR into the plasma membrane. I started making constructs expressing different parts of the AHA2 protein without the NpHR attached. Cuts were made in locations within either intracellular or extracellular loops, following the observations of Groves & Tanner (1998). I also created constructs linking some of these fragments of the AHA2 protein with the NpHR. All of the constructs of AHA2 with or without NpHR are shown in Table 6.

Table 6. List of the expression constructs expressing fragments of AHA2 with or without NpHR.

Expression construct	Entry clone (All in pDONR207)	Destination vector	SM
35S::RFP-1TMD_AHA2	1TMD_AHA2-st	pB7WGR2	S.10.22
35S::RFP-3TMD_AHA2	3TMD_AHA2-st	pB7WGR2	S.10.22
35S::GFP-5TMD_AHA2	5TMD_AHA2-st	pH7WGF2	S.10.22
35S::GFP-7TMD_AHA2	7TMD_AHA2-st	pH7WGF2	S.10.22
35S::GFP-9TMD_AHA2	9TMD_AHA2-st	pH7WGF2	S.10.22
35S::GFP-3_5TMD_AHA2	3_5TMD_AHA2-st	pH7WGF2	S.10.22
35S::1TMD-AHA2-2xHA-NpHR-RFP	1TMD-AHA2-2xHA-NpHR-wo	pB7RWG2	S.10.23
35S::3TMD-AHA2-2xHA-NpHR-RFP	3TMD-AHA2-2xHA-NpHR-wo	pB7RWG2	S.10.23
35S::3_5TMD-AHA2-2xHA-NpHR-GFP	3_5TMD-AHA2-2xHA-NpHR-wo	pH7FWG2	S.10.23
35S::7TMD-AHA2-2xHA-NpHR-GFP	7TMD-AHA2-2xHA-NpHR-wo	pH7FWG2	S.10.23
35S::9TMD-AHA2-2xHA-NpHR-GFP	9TMD-AHA2-2xHA-NpHR-wo	pH7FWG2	S.10.24

Table 6. Expression constructs expressing fragments of AHA2 with or without NpHR, under the expression 35S promoter, and tag to a N-terminal or C-terminal RFP or GFP fluorescent marker. All the entry clones are made in pDONR207, an entry vector from Gateway technology (Life Technologies) containing the *att*B1 and *att*B2 recombination sites. pB7RWG2 (Karimi, Depicker et al. 2007) is a Gateway-compatible vector with C-

terminal fluorescent RFP tag and incorporating the 35S promoter. pB7WGR2 (Karimi, Depicker et al. 2007) is a Gateway-compatible vector with N-terminal fluorescent RFP tag and incorporating the 35S promoter. pH7WGF2 (Karimi, Depicker et al. 2007) is a Gateway-compatible vector with N-terminal fluorescent GFP tag and incorporating the 35S promoter. pH7FWG2 (Karimi, Depicker et al. 2007) is a Gateway-compatible vector with C-terminal fluorescent GFP tag and incorporating the 35S promoter. HA: hemagglutinin tag. wo: without stop codon. st: with stop codon. SM: supplemental material.

I transiently expressed in tobacco all the constructs from Table 6 and checked the localisation of the expressed proteins under confocal microscopy. None of these proteins localised to the plasma membrane. Figures 5.2.43 and 5.2.44 show ER localisation of AHA2 when the 1st and the 1st nine transmembrane domains of AHA2 are expressed in tobacco. From these results I concluded that full length AHA2 was necessary for plasma membrane localisation of the protein. Thus, I created a construct where I linked the full lenght AHA2 with the full lenght NpHR (Table 5.2.8).

Table 5.2.8. Expression construct expressing full length AHA2 linked to full length NpHR.

Expression construct	Entry clone (All in pDONR207)	Destination vector	SM
35S::2xHA-NpHR-link-AHA2-GFP	2xHA-link-NpHR-link-AHA2-wo	pH7FWG2	S.10.24

Table 5.2.8. Expression construct expressing full length NpHR linked with full length AHA2, under the expression of 35S promoter and tag to a GFP fluorescent marker. pDONR207 is an entry vector from Gateway technology (Life Technologies) containing the *att*B1 and *att*B2 recombination sites. wo: without stop codon, st: with stop codon. pH7FWG2 (Karimi, Depicker et al. 2007) is a Gateway-compatible vector with C-terminal fluorescent GFP tag and incorporating the 35S promoter. HA: hemagglutinin tag. wo: without stop codon. SM: supplemental material.

Plasma membrane localisation of NpHR was achieved (Figure 5.2.45) by linking it with full length AHA2. To verify plasma membrane localisation of NpHR under confocal microscopy, I co-expressed the construct from Table 5.2.8 with a construct expressing full length AHA2 and check for co-localisation of the proteins. Each of the constructs

was tag to a different fluorescent marker for its proper differentiation of the proteins. Figure 5.2.46 shows plasma membrane co-localisation of full length AHA2 tag to a RFP marker, with NpHR link to AHA2 tag to a GFP marker.

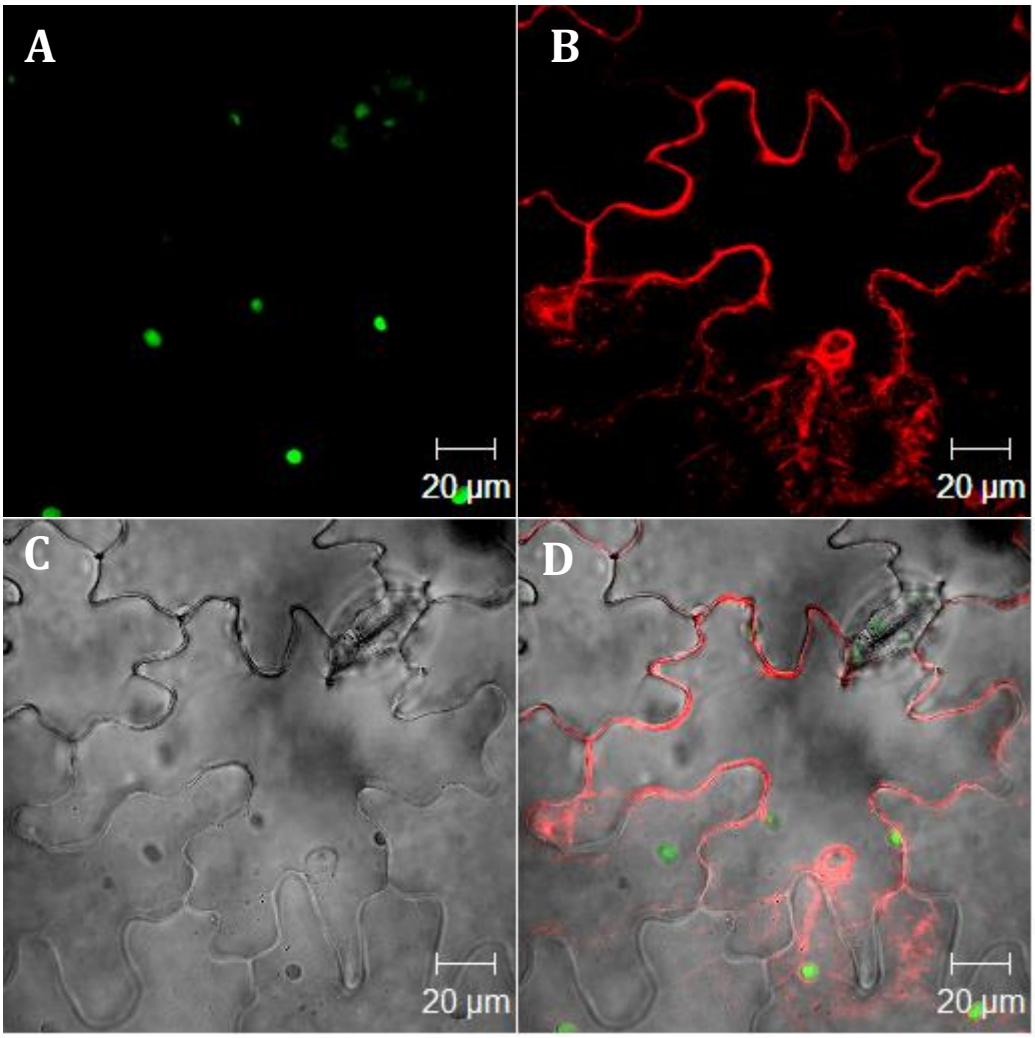

Figure 5.2.43. Expression of the construct 35S::RFP-1TMD_AHA2 in transient transformed tobacco leaves after 3 days of transformation. RFP fluorescence indicates ER localisation of 1TMD_AHA2 in the epidermal cells (red B, D). The chlorophyll *autofluorescence* is shown in green (A, D) indicating the localisation of the chloroplasts. C is the bright field image, and D shows a merged image. The images are from 37-slice Z-stack through the epidermal cell with a 0.75 µm interval between slices. In all the images the scale bar is 20 µm.

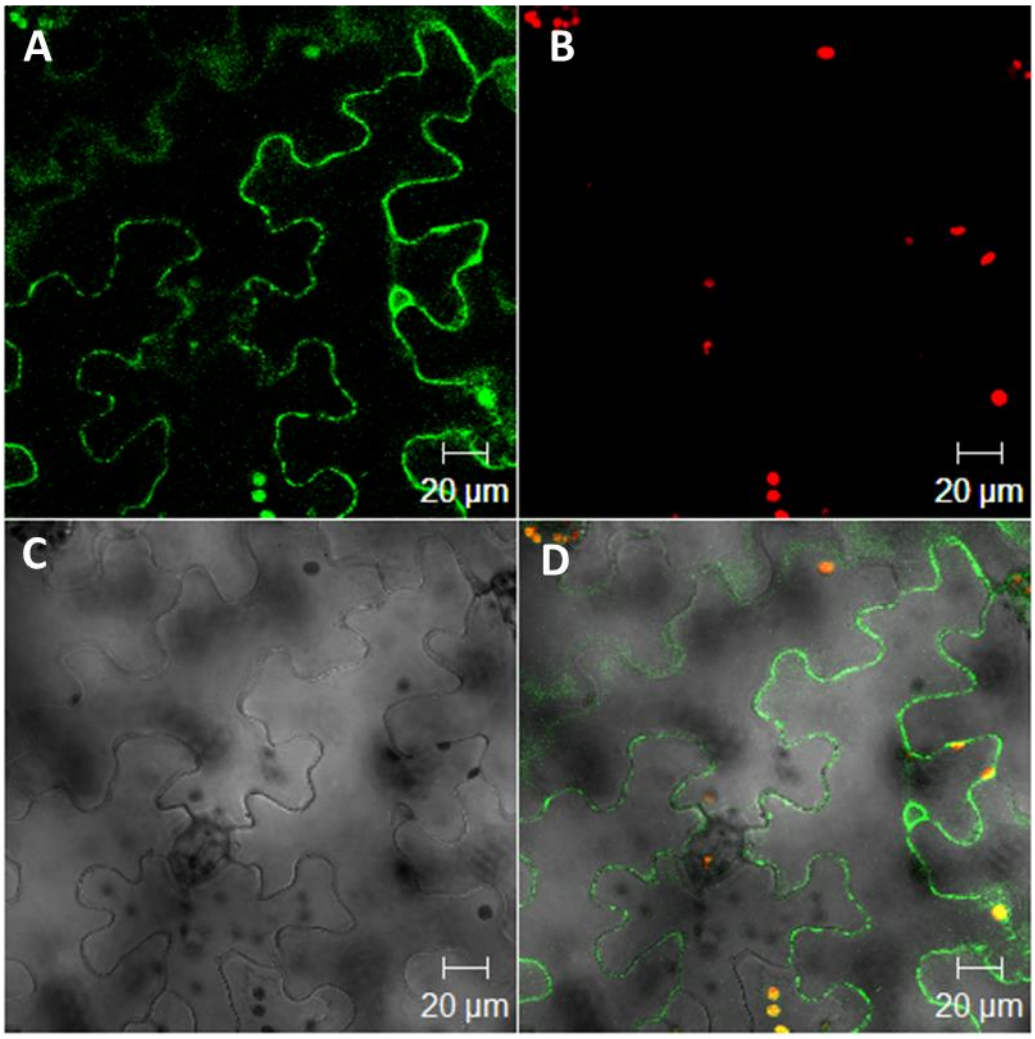

Figure 5.2.44. Expression of the construct 35S::GFP-9TMD_AHA2 in transient transformed tobacco leaves after 3 days of transformation. GFP fluorescence indicates ER localisation of 9TMD_AHA2 in the epidermal cells (green A, D). The chlorophyll *autofluorescence* is shown in red (B, D) indicating the localisation of the chloroplasts. C is the bright field image, and D shows a merged image. The images are from 26-slice Z-stack through the epidermal cell with a 1.5 µm interval between slices. In all the images the scale bar is 20 µm.

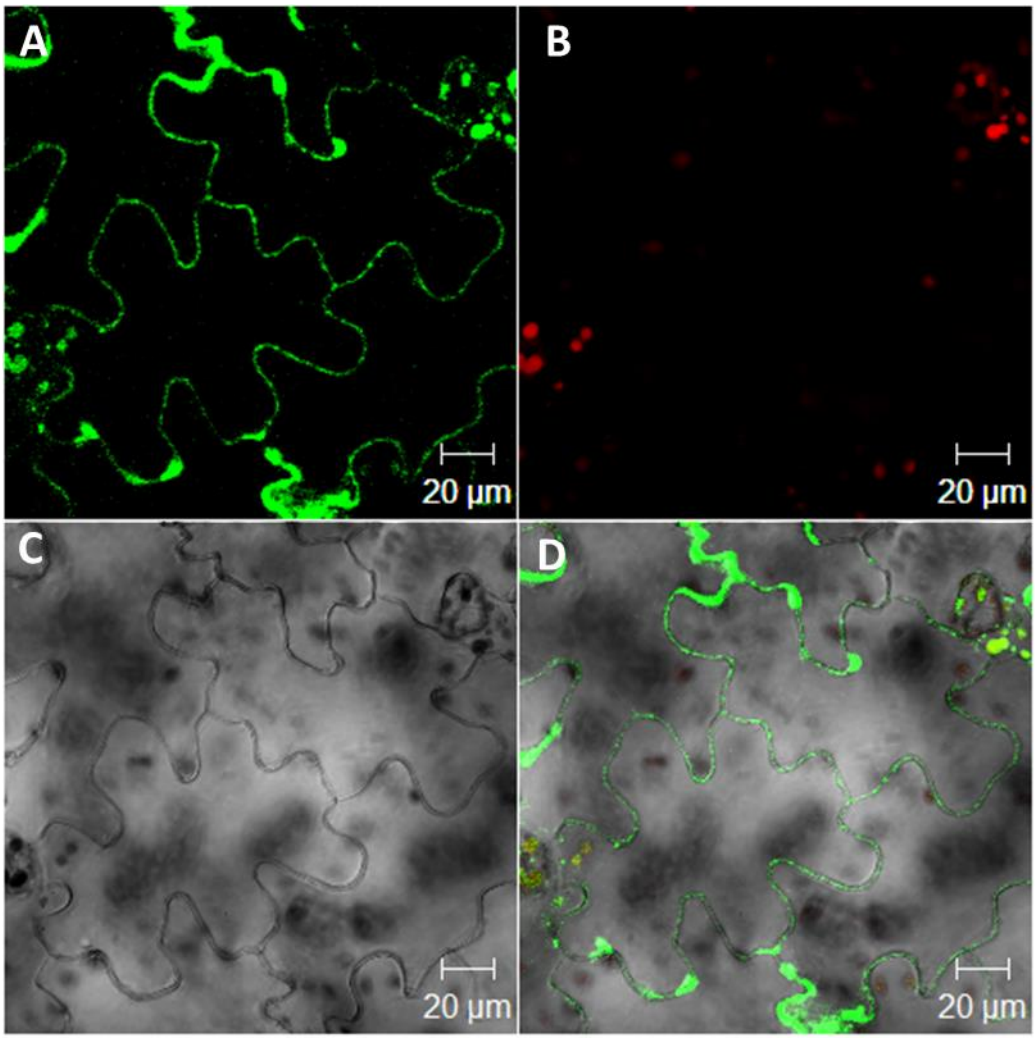

Figure 5.2.45. Expression of the construct 35S::NpHR-AHA2-GFP in transient transformed tobacco leaves after 3 days of transformation. GFP fluorescence indicates plasma membrane localisation of NpHR-AHA2 in the epidermal cells (green A, D). The chlorophyll *autofluorescence* is shown in red (B, D) indicating the localisation of the chloroplasts. C is the bright field image, and D shows a merged image. The images are from 11-slice Z-stack through the epidermal cell with a 2.25 µm interval between slices. In all the images the scale bar is 20 µm.

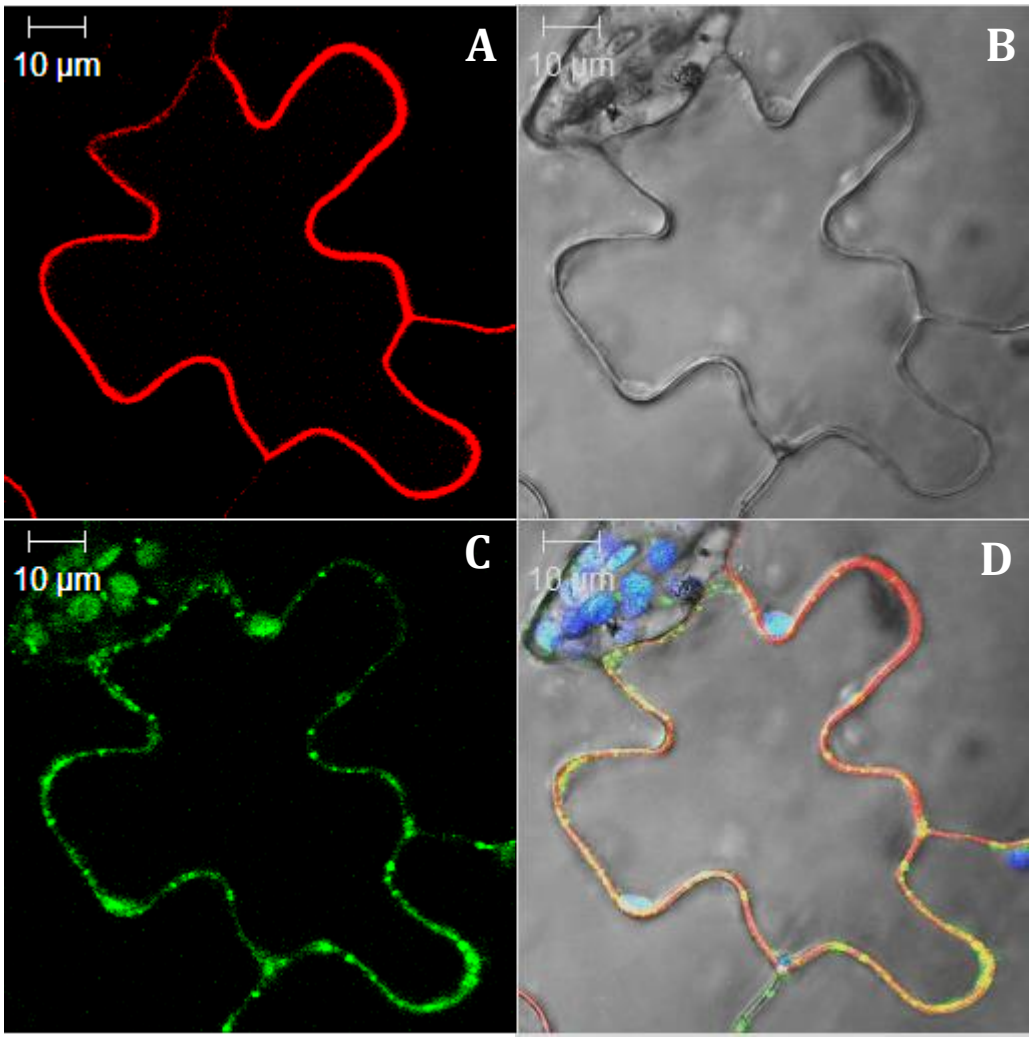

Figure 5.2.46. Expression of the construct 35S::NpHR-AHA2-GFP co-localised with the construct 35S::AHA2-RFP in transient transformed tobacco leaves after 3 days of transformation. RFP fluorescence indicates plasma membrane localisation of AHA2 in the epidermal cells (red A, D). GFP fluorescence indicates plasma membrane localisation of NpHR-AHA2 in the epidermal cells (green C, D). The chlorophyll *autofluorescence* is shown in blue (D) indicating the localisation of the chloroplasts. B is the bright field image, and D shows a merged image. The images are from 21-slice Z-stack through the epidermal cell with a 1.5 µm interval between slices. In all the images the scale bar is 10 µm.

Once achieved plasma membrane localisation of NpHR protein, it was decided to create stable Arabidopsis plants expressing the construct. It was decided to create transgenic plants expressing NpHR in the plasma membrane but also expressing it in the ER and tonoplast, and both under the 35S and the GC promoters. Because it is not known if it is really necessary to provide retinal to NpHR once expressed in plants it was also decided to create some constructs combining the NpHR with the bCMO1. For

these, it was created a new vector based on the 2in1 vector used in chapter 5.1. The new vector also contains two cassettes, but the first one has a GC promoter instead of the 35S (Figure 5.2.47), in order to localise NpHR exclusively in the plasma membrane. Table 8 shows the new constructs I made to transform Arabidopsis by the floral dipping method.

Table 5.2.9. List of the new expression constructs created expressing NpHR in tonoplast and plasma membrane under the 35S or GCP.

Expression construct	Entry clone	Destination vector	Expected NpHR localisation	SM
Cassette 1: 35S::NpHR-mCherry Cassette 2: 35S::bCMO1-GFP	NpHR-wo (in pDONR221-P1P4) bCMO1-wo (in pDONR221-P3P2)	pFRETgc-2in1-CC	Tonoplast	S.10.25
GCP::NpHR-RFP	NpHR-wo (in pDONR207)	pB7RWG2-GCP	GC-tonoplast	S.10.25
Cassette 1: GCP::NpHR-mCherry Cassette 2: 35S::bCMO1-GFP	NpHR-wo (in pDONR221-P1P4) bCMO1-wo (in pDONR221-P3P2)	pFRETcg-2in1-CC-GCP	GC-tonoplast	S.10.25
Cassette 1: 35S::NpHR-AHA2-mCherry Cassette 2: 35S::bCMO1-GFP	NpHR-AHA2-wo (in pDONR221-P1P4) bCMO1-wo (in pDONR221-P3P2)	pFRETgc-2in1-CC	Plasma membrane	S.10.25
Cassette 1: GCP::NpHR-AHA2-mCherry Cassette 2: 35S::bCMO1-GFP	NpHR-AHA2-wo (in pDONR221-P1P4) bCMO1-wo (in pDONR221-P3P2)	pFRETcg-2in1-CC-GCP	GC-plasma membrane	S.10.25
GCP::NpHR-AHA2-RFP	NpHR-AHA2-wo (in pDONR207)	pB7RWG2-GCP	GC-plasma membrane	S.10.25

Table 5.2.9. Expression constructs expressing NpHR in tonoplast and plasma membrane under the 35S or GC promoter expression. pDONR207 is an entry vector from Gateway technology (Life Technologies) containing the *att*B1 and *att*B2 recombination sites. pDONR221-P1P4 and pDONR221-P3P2 are entry vectors from Gateway technology containing the *att*B1-*att*B4 and *att*B3-*att*B2 recombination sites respectively. pFRETgc-2in1-CC (Hecker, Wallmeroth et al. 2015) is a Gateway compatible vector, It contains a 35S promoter for each cassette, *att*B1-*att*B4 recombination sites and C-terminal mCherry in the first cassette, and *att*B2-*att*B3 recombination sites and C-terminal GFP in the second cassette. pB7RWG2 (Karimi, Depicker et al. 2007) is a Gateway-compatible vector with C-terminal fluorescent RFP tag and incorporating the 35S promoter. GC: guard cell. wo: without stop codon. SM: supplemental material.

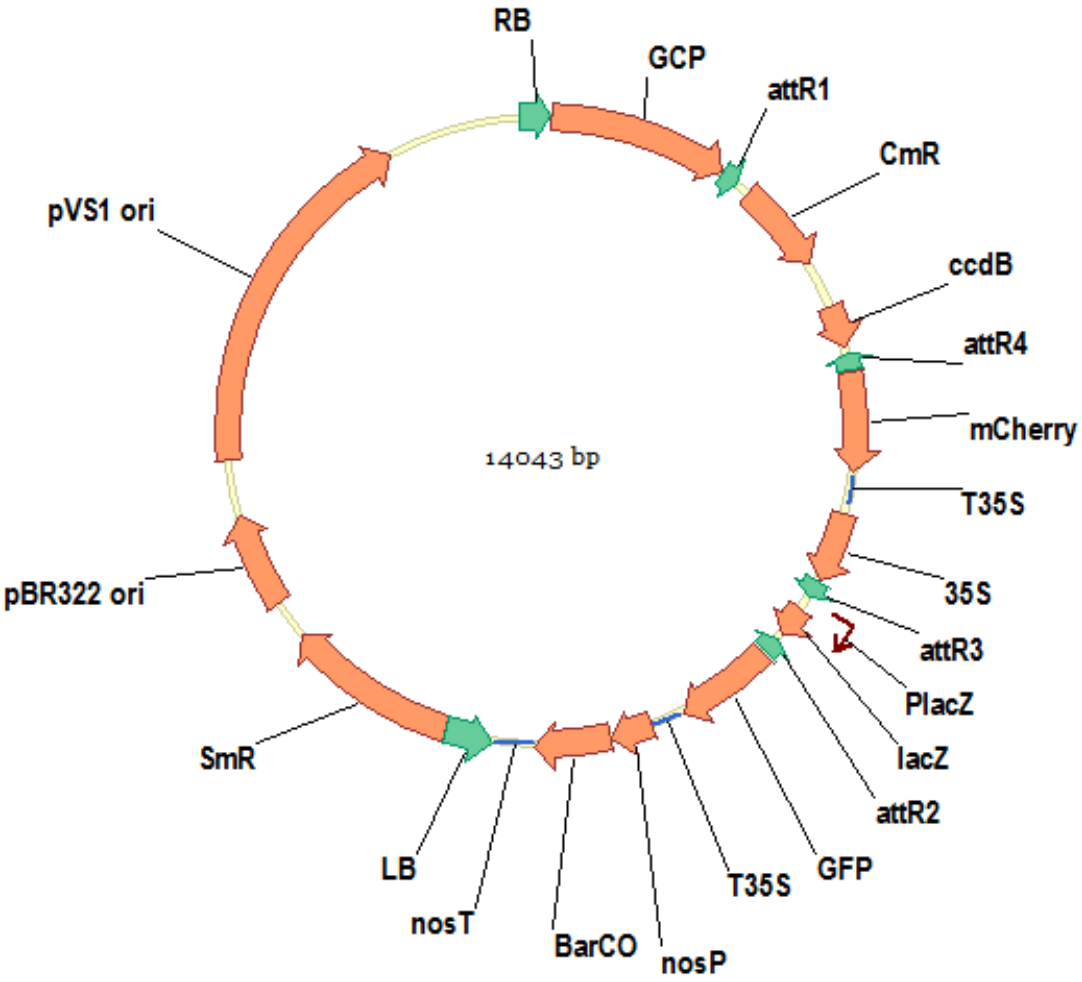

Figure 5.2.47. 2in1 Gateway vector containing one cassette under the expression of a GCP (guard cell promoter) and C-terminal mCherry fluorescent marker, and a second cassette under the expression of 35S promoter and C-terminal GFP fluorescent marker. pBR322ori/pVS1ori: replication origins. RB/LF: right/left border. SmR: Spectinomycin resistance. CmR: Cloramphenicol resistance. nosP/nosT: nos promoter/nos terminator. BarR: BASTA resistance.T35S: 35S terminator. GCP: AtMYB60 promoter. 35S: 35S strong promoter. pUBQ10: UBQ10 promoter. PlacZ: lacZ gene promoter. lacZ: lacZ gene for selection. mCherry/GFP: red/green fluorescent marker. *ccd*B: *ccd*B toxic gene. *att*B1/*att*B2/*att*B3/*att*B4: recombination sites. The vector size is 11841 bp.

I used the constructs in Table 5.2.9 to transform Arabidopsis by the floral dipping method(Zhang, Henriques et al. 2006). I also transformed Arabidopsis plants with some constructs mentioned before such as 35S::NpHR-RFP, 35S::RFP-NpHR, and 35S::NpHR-AHA2-GFP, which were expected to give tonoplast, ER and plasma membrane expression of NpHR respectively. T1 seeds containing these constructs

were obtained and experiments including gas exchange measurements were carried out on T1 to T4 generations.

6. Discussion

6.1 Engineering a CCM in the chloroplast

The property of C4 plants of presenting CCMs give them the advantage of having a higher rate of photosynthesis, however they achieve this advantage with the extra cost of ATP needed to cycle 3- and 4-carbon moieties (Ehleringer and Cerling 2002). Thus, engineering CCM mechanisms in C_3 plants powered by an external power source may increase photosynthesis without requiring any extra energy cost for the plant. Furthermore, nowadays science can profit of synthetic biology, which permits to combine different modules of nature in a way that new modules can be created (Liu and Stewart 2015). By combining the engineering capacity of synthetic biology and the optogenetics approach arose the possibility of using light-driven pumps on plants, not being reported in the literature yet. Thus, this thesis describes the use of light-driven pumps in plants for the first time. And not only that, furthermore for the first time light-driven pumps are being used not to manipulate membrane voltage, but to manipulate transport ion fluxes.

Much remains unknown about the chloroplasts membrane transport, and even more is unknown about how the incorporation of external proteins might affect the natural functioning of the chloroplast. In a way, these unknowns makes it worthwhile to carry out projects like MAGIC which, even if they do not provide more photosynthesis for the plant, provide knowledge of synthetic biology and of chloroplast behaviour.

The use of a light-driven pump such as halorhodopsin is an advantageous choice to power a CCM in the chloroplasts. Halorhodopsin will be active only during photosynthesis, that is only when light is on. Furthermore, its light absorption wavelength is around 588 nm (Schobert and Lanyi 1982) gives rise to some overlap with photosynthesis, it does not compete over the shorter range of wavelengths with the light absorbed by the plant in carrying out photosynthesis. NpHR pumps Cl^-, and this behaviour is well suited to a combination with an anion exchanger. The fact that AE1 is a well-known protein from mammals has enabled the identification of the C-terminal part of the protein as the only requirement for the protein functionality,

not being necessary the full length protein and facilitating its use for cloning (Kopito 1985, Lux, John et al. 1989, Sahr, Taylor et al. 1994). AE1 also has the advantage of transporting C in the HCO_3^- form, which is the most abundant form of inorganic carbon dissolved in water.

Tobacco and Arabidopsis plants were selected for the expression of the proteins as these plant model systems are commonly used for genome modifications (Koornneef and Meinke 2010). In this study, transient expression of proteins was carried out in tobacco leaves simply because of its speed, requiring only 2-4 days from *Agrobacterium* infiltration to protein expression. Transient transformation was exclusively realised in tobacco cells due to the frequency of transformation is higher compared to infiltration of *Arabidopsis*. In contrast, Arabidopsis plants were used for the generation of stable transgenic lines. It is also possible to obtain transgenic tobacco plants using a culture approach from a transformed tissue (Sparkes, Runions et al. 2006), however this technique was not used for this study as it requires much more time than Arabidopsis from transformation to homozygous lines.

6.1.2 Cloning strategies

Two different constitutive promoters were used to get expression of the proteins, UBQ10 and 35S. The UBQ10 (polyubiquitin 10) is an Arabidopsis promoter and gives modest expression. However, proteins under its control were difficult to detect in tobacco transient transformation. The 35S promoter is originally from cauliflower mosaic virus (CaMV), which is a pararetrovirus from the genus *Caulimovirus* that infects plants (Pringle 1999). The 35S promoter is used in almost all the genetic modified crops and allows a strong expression of proteins. After verifying under confocal microscopy that the promoter which provided the stronger signal was 35S all the genes in these studies were cloned under its control. The tags RFP and GFP were used for protein localisation under confocal microscopy. Their different emission wavelengths made it easy to differentiate between them when expressing two proteins in the same plant sample. GFP emission was collected between 505 and

530 nm, and RFP emission was collected between 560 and 615 nm, both of them differ from chlorophyll fluorescence, which was collected from 630 nm.

The expression of the transmembrane proteins NpHR and AE1 under the 35S promoter and with a C-terminal fluorescent tag, was localised in the tonoplast from epidermal tobacco cells (Figures 5.1.1, 5.1.2). The tonoplast localisation can be easily differentiated from the plasma membrane because its signal surrounds the nucleus to the inside away from the plasma membrane and the signal does not reach completely the entire shape of the cell but is localised more internally. The TPT leader sequence used as a signal peptide to target proteins for the inner envelope of the chloroplast. TPT is an integral membrane protein found in the inner envelope of the chloroplasts and its sequence has been widely used for chloroplasts localisation of proteins. Under confocal microscopy it was possible to verify the localisation of NpHR and AE1 proteins in the chloroplasts envelope both in epidermal (Figures 5.1.3 and 5.1.5) as well as in mesophyll cells (Figures 5.1.4 and 5.1.6) from transient tobacco transformations. It was of crucial importance in this project to achieve transformation of the chloroplasts from mesophyll cells, because these are the main sites for photosynthetic activity. However, confocal imaging of mesophyll cells is always a bit tricky, as it requires scanning deeper in the tissue where there is a loss of fluorescent signal. So the loss of signal in this case does not imply that a protein is not expressed. Thus, to analyse the localisation of the proteins, my work focused primarily on the signal for protein expression in epidermal cells.

The addition of bCMO1 in the system when expressing NpHR arose from knowledge of the properties of NpHR and its requirement of all-trans retinal as a cofactor for protein activity (Fenno, Yizhar et al. 2011). However, since this was, to my knowledge, the first time NpHR was expressed in a plant system, it was not clear whether it was really essential to provide an external source of retinal or whether NpHR might use a different cofactor for its activity in the plant. As a fallback approach, the idea of using bCMO1 enzyme to provide retinal from the hydrolysis of carotenoids appeared as a excellent candidate to be used in plants. bCMO1 catalyses

the oxidative cleavage of beta-carotene, an abundant molecule in plants, into two all-trans retinal molecules, the final substrate required.

As bCMO1 was considered a complementary protein in this project, its cloning was not started until NpHR and AE1 expression in the cells was confirmed. As previously mentioned, in order to get a strong expression of the protein it was necessary to drive expression under the 35S promoter. bCMO1 localisation in transient transformed epidermal tobacco cells was in the cytoplasm and inside the nucleus (Figure 5.1.8). To localise the protein into the chloroplast stroma it was cloned with the RbcL as a target sequence (Figure 5.1.9).

It was observed that to assess consistently co-expression of protein combinations it was necessary to clone them together in the same vector. Thus, a 2in1 vector was used (Grefen, Donald et al. 2010), with the advantage of allowing individual protein identification under confocal microscopy (Figures 5.1.16, 5.1.18, 5.1.20). A 3in1 vector was generated for the co-expression of the three proteins together. In this case, the bCMO1 was added in the 2in1 vector by classical cloning, and it was tag to a 6-Histidine sequence, which allowed identification of the protein by western blot analysis.

6.1.3 Protein activity

From the expression of the different proteins in transient tobacco cells it was observed that some of the chloroplasts expressing NpHR or AE1 proteins, and also the two together, had what it was called an atypical morphology. This morphology was characterised in the chloroplasts by a swollen morphology compared with the chloroplasts from non-transformed cells. The grana was “pushed” to one site of the stroma instead of being well distributed in the interior of the chloroplasts (Figures 5.1.3, 5.1.23 and 5.1.24). This behaviour was observed in 39.5 % of cells examined and both when NpHR and/or AE1 were expressed in the cells. It is difficult to know if the expression of the proteins itself in the membrane was already affecting its morphology, or whether the effect on chloroplast morphology was a result of the activity of these proteins. There are several approaches to addressing this question.

Among others, experiments with non-functional NpHR might be trialled in order to test whether the presence of the proteins itself was the cause. However, the swollen shape might also be due to osmotic changes due to the change of ion concentrations caused by the protein activities leading to a passive influx of water and expansion of the organelle. Analysed this way, the accumulation of ions in the chloroplasts stroma, caused by the activity of NpHR, is also suggesting the correct orientation of the protein in the chloroplasts envelope.

It has to be considered that most of the chloroplasts analysed by confocal microscopy were from epidermal cells. As noted before, with deeper confocal scans within the tissue the marker fluorescence signal was commonly lost. However, it would be necessary an analysis of the chloroplasts from transformed mesophyll cells to verify if it was also observed that mesophyll chloroplasts showed the same atypical morphology. Nonetheless, from all of the images analysed, it was more common to find atypical morphology in chloroplasts from epidermal cells than in chloroplasts from the mesophyll.

Analysis of enzyme activity was easier to detect experimentally in chloroplasts transformed with bCMO1. HPLC carried out on bCMO1-transformed chloroplasts, work completed by another research group involved in the MAGIC project, showed a reduction in the levels of b-carotene. The analysis was done in isolated chloroplasts from transient transformed tobacco leaves. The results showed that the chloroplasts expressing bCMO1 had half levels of b-carotene in comparison with chloroplasts from non-transformed leaves. From this result several conclusions can be drawn. Firstly, the lower levels of b-carotene may be due to the activity of the enzyme, which consists on breaking b-carotene molecules to create two retinal molecules. Secondly, the fact that it was possible to see a difference on the levels of b-carotene between the two samples may indicate that most of the chloroplasts were expressing the protein. Thus, indicating that the chloroplasts from mesophyll cells were transformed, something difficult to demonstrate just by the confocal images. And finally, there is sufficient protein expression capable of catalyse b-carotene of the chloroplasts, but without ending its existences. Again, it is difficult to know if the

amount of retinal that should be produced by bCMO1 is enough for the amount of NpHR pumps that are being expressed in the envelope. Mainly because it is still not know if the NpHR really needs this extra source of retinal in plants.

However, when expressing proteins in transient transformation it has to be considered that it is difficult to get same levels of expression in all cells, and that the expression varies by timing. It is necessary to get stable lines of transgenic plants, where the expression of the proteins will be stable, and this will allow to calculate the activity of the proteins in a more accurate way.

6.1.5 Consequences in the whole plant level

Stable Arabidopsis transgenic plants were generated from the constructs showed in Table 5.1.6. From the first line of transgenic Arabidopsis plants analysed it was observed a higher photosynthesis in plants expressing bCMO1, also combined with NpHR, when grown under low light conditions. However, this pattern was not consistent with the data obtained from the other two more lines analysed. Moreover, out of gas exchange measurements analysis for the first line of transgenic plants analysed it was observed a reduction on photosynthesis when the three proteins were expressed together. It also was observed a plant phenotype that shows lower growth on the plants expressing the combination of AE1 and NpHR with and without bCMO1. From the other two more lines analysed it was difficult to have proper statistically analysis due to the low amount of samples available to be analysed. However, in some of the cases, it was also observed a decrease on photosynthesis on plants transformed with the different proteins in relation to the wild type.

The fact that it was not possible to obtain plants with higher photosynthesis can be due to different reasons. It has to be considered the possibility that the system was working as expected, however, the CO_2 diffused to quickly in order for the Rubisco to be able to fix it. In this case, being part of the second half of the MAGIC project, it would be necessary to create a mechanism that helps to retain the CO_2 next to Rubisco. Another possibility would be that the atypical morphology previously

described in the chloroplast made them less functional, thus affecting the photosynthetic ratio. One more reason could be that the proteins expression had a negative impact to the chloroplasts even if the morphology of them was not affected by the presence of the proteins. To reach proper conclusions out of this data it should be considered to do molecular experiments in order to check the expression levels of the proteins into the chloroplast, as well as the activity.

6.2. Manipulation of stomatal kinetics

6.2.1. KAT1

6.2.1.1. Model predictions

Using OnGuard model to manipulate the voltage gating properties of guard cells K_{in} channels was fundamental to understand the relationships between the different transporters activities, ion fluxes, membrane voltage and stomatal aperture.

When simulating, in the OnGuard software, a change of the K_{in} channels $V_{1/2}$ to more positive values of -120 mV, the model predicted a higher and faster stomatal aperture. The main effect of changing the $V_{1/2}$ to more positive values is the increase on K^+ flux capacity of the channels within the physiological voltage range. Thus, the K_{in} channels allow more K^+ ions to enter the cytoplasm thought the plasma membrane. Once in the cytosol, the K^+ ions are transported to the vacuole mainly through the FV channels. Thus, the $[K^+]$ increases both in the cytosol as well as in the vacuole. The change in the gating properties of KAT1 also affects the membrane voltage, due to the variations in total charge flux balance. The membrane voltage becomes more positive during the daylight period to reach the balance point were the total charge flux is equal and its sum is zero across the membrane. Because the H^+-ATPase activity is limited by its voltage dependent kinetics, and the voltage is turn more positive, the pump activity increases and the number of H^+ pumped out of the cytoplasm is elevated. This increase on H^+ efflux from the cytosol causes an increase on the cytosolic pH from values of 7.7 in the wild-type to pH values approaching 8.2.

Such effects on pH are extreme, but are nonetheless realistic and have been observed previously, for example in the *slac1* mutant (Wang, et al. 2012).

The effects of a more positive $V_{1/2}$ do not stop here, however. Due to a reduced hyperpolarisation of the plasma membrane, there is less activation of Ca^{2+} channels at the plasma membrane and consequently a decrease in Ca^{2+} influx which in turn affects the $[Ca^{2+}]_i$ in comparison with the wild-type. One of the knock-on effects that is most noticeable is a lack of Ca^{2+} oscillations at the beginning of dark period. These oscillations fail primarily because the enhanced K^+ channel activity suppresses voltage oscillations. Without an increase in $[Ca^{2+}]_i$ there is no Ca^{2+} inactivation of the K_{in} channels and no Ca^{2+} inactivation of the Cl^- channels to promote Cl^- efflux. As a consequence there is no membrane depolarisation at the end of the daylight period. Because the Cl^- channels that promote Cl^- efflux are not activated, $[Cl^-]$ remains high both in the cytosol as well as in the vacuole. Cl^- enters the cytosol mainly through H^+-Cl^- symport, and goes to the vacuole through the VCl channels. At the end of the daylight period there are few small Cl^- flux oscillations, which drive a slow Cl^- efflux through R-type and VCl channels.

In short, the lack of membrane voltage oscillations and lack of Ca^{2+} oscillations does not promote ion and organic molecules efflux from the cytosol and the stomata does not close during the night. Finally, the accumulation of malate in the vacuole during the dark period maintains an acid vacuolar pH, which remains largely constant during the whole cycle. So, while stomatal aperture with $V_{1/2}$ = -120 mV is predicted to be bigger than in the wild type due to the major accumulation of ions and organic molecules, but it is also predicted to remain open longer and close more slowly than the wild-type. Again, there are precedents for some aspects of these predictions, notably in the behaviour of the *slac1* and *gork* mutants of Arabidopsis (Wang, et al. 2012; Hosy, et al. 2003), but I note that these are both knock-out mutants which do not affect channel gating per se.

When simulating a change of the K_{in} channels $V_{1/2}$ to more negative values of -240 mV, the model predicted a small stomatal aperture that remained nearly unchanged

during the whole day cycle. The principal effect of changing K_{in} $V_{1/2}$ to more negative values was to decrease the channel capacity to transport K^+ within the physiological voltage range. K^+ fluxes through both tonoplast and plasma membrane were reduced. There was almost no flux of K^+ through K_{in} channel; the only K^+ that entered the cytoplasm was predicted to do that through H^+-K^+ symport. The flux of K^+ from the cytosol to the vacuole through FV channels was almost zero, and K^+ ions entered almost entirely through the vacuole TPK channels, for which the flux was also reduced compared with the wild-type. The membrane voltage became more negative during the daylight period in order to reach the balance point at which the total charge flux summed to zero. This change in voltage towards a hyperpolarisation of the membrane, affected the H^+-ATPase by limiting its activity. As a consequence of the reduced activity of H^+-ATPase cytosolic pH decreased during the daylight period. The pH in the vacuole remains roughly constant during the daylight period, but it decreased during the dark period compared to the wild-type. Again, this decrease in vacuolar pH can be ascribed to the accumulation of Mal in the vacuole during the dark period. Total levels of Mal were lower during the daylight period due to the plasma membrane hyperpolarisation activated SLAC channels, which also transport Mal outside the cell. However, during the dark period the concentration of Mal in the vacuole was higher, because the Mal oscillations at the end of the daylight period were insufficient to enhance Mal release from the vacuole.

Other predictions of the model include an increase in $[Ca^{2+}]_i$ during the daylight period. This increase was promoted by plasma membrane hyperpolarisation, which enhanced Ca^{2+} influx through Ca^{2+} channels at the plasma membrane. The increase in cytosolic $[Ca^{2+}]_i$ as well as membrane hyperpolarisation enhanced Cl^- efflux, thus reducing the levels of Cl^- both in cytosol as well as in the vacuole. The main efflux of Cl^- occurred through SLAC channels in the plasma membrane, activated by the membrane hyperpolarisation, and through the VCl channels in the tonoplast. Like the effect of shifting the K^+ channel $V_{1/2}$ positive, the effect in suppressing Ca^{2+} flux and membrane voltage oscillations were sufficient to reduce the a difference in the stomatal aperture during the closure period.

6.2.1.2. Consequences for stomatal physiology

From the model predictions, varying the gating properties of K_{in} channels did modify the kinetics of stoma. In fact, changing K_{in} $V_{1/2}$ to more positive values did allow a quicker and also bigger stomatal aperture at the beginning of the daylight period. The fact that stoma opened quicker, may enable a better concordance between the mesophyll demand for CO_2 and stomata conductance for the first hours of light at the beginning of the day (Lawson, Kramer et al. 2012, Lawson and Blatt 2014). In this context, varying KAT1 gating properties by changing its $V_{1/2}$ to more positives values may have a positive effect on photosynthesis due to it can maximise CO_2 uptake. However, modifying KAT1 $V_{1/2}$ to more positive values also meant that the stoma did not close rapidly at the end of the day. Of course, these are predictions only. Nonetheless, if stomata were to remain open during the night, there would not be a minimisation of water loss through transpiration when photosynthesis is not active, and the time-averaged WUE over the entire diurnal cycle will be greatly reduced. In general terms, by varying $V_{1/2}$ to more positive values the stomata efficiency was enhanced, but just during the daylight period, and it was worsened during the dark period.

By contrast, changing the $V_{1/2}$ of the K_{in} channels to more negative values hindered the stomatal opening. As a consequence the stomata remained almost completely closed during the whole day cycle. With almost closed stomata, we can anticipate that it would limit the CO_2 uptake, thus limiting photosynthesis, however WUE would be high, due to a reduction on conductance. Despite the negative effects for the plant of having the stomata open during the whole day cycle, the results out of the model were interesting enough for trying it in vivo. The modelling results were showing a possibility of changing stomatal kinetics and enhancing photosynthesis, even if for the expensive cost of water loose.

For Arabidopsis transformation, $KAT1^{wt}$ and two mutants ($KAT1^{D105E}$ / $KAT1^{F102W}$) were selected to be driven both with a guard cell and the 35S promoters (Table 5.2.1). The two KAT1 mutants were previously shown to affect the $V_{1/2}$ value, shifting

this some 40-60 mV either positive or negative of the wild type (Lefoulon, et al. 2014), so roughly consistent with the model parameters I used in the simulations. The guard cell promoter (GCP) used, the *At*MYB60 promoter (Cominelli, Galbiati et al. 2011), incorporates an ABA response element and is suppressed by ABA. I reasoned that if the plant were to suffer stress conditions, this construct might be important to control expression and thereby reduce the activity of the transgenic KAT1 constructs. By contrast, the 35S promoter ensured same level of expression in all the cells, not just guard cells and no matter whether the plant was under stress or not. In addition, Arabidopsis plants were also transformed with a construct containing exclusively GFP protein under the expression of GCP to have a control for GCP activity. GFP allowed to identify the proper localisation of a protein under the GCP as well as how powerful was its expression (Figure 5.2.14). It was decided to use the GCP::GFP as a control for further experiments, together with a wild-type control plant, to discard the possible effects of expressing the construct with the GCP could have in the guard cell.

The transformation of Arabidopsis was done in Col0 plants as well as KAT1-KO plants. KAT1-KO plants were selected in order to discard any effect of KAT1 overexpression. However, the transformation efficiency of KAT1-KO plants was very low, and as a consequence, few transformed plants were obtained. Thus, it was difficult to compare the results of gas exchange measurements with the Col0 transformed plants due to the small number of plants that could be analysed.

Gas exchange measurements were carried on plants from the T1 generation for several reasons, primarily because it shortened the time needed to validate the effects of transgene expression and because it was not essential to ensure homozygosity for the purposes of these experiments. I note too that in T1 generation there was less of a chance that plants would show gene silencing.

Measurements of assimilation and stomatal conductance were carried out on these KAT1-transgenic lines by gas exchange measurements. CO_2 assimilation at saturating light conditions (A_{sat}), the maximum photosynthetic rates at saturating CO_2 (A_{max})

and the maximum carboxylation velocity of Rubisco ($V_{c\,max}$) were calculated to check differences in photosynthesis assimilation between the different Arabidopsis transformed plants. g_s was calculated to have values of stomatal conductance in the steady state. Time did not permit measurements of stomatal conductance kinetics, although these measurements might have given further information about the effects of the transgenes. Despite all the parameters calculated, the amount of plant replicates analysed was too low to be confident of the effects. Overall, the transformed plants did not show evidence of enhanced assimilation compared to the controls, but indeed showed lower assimilation rates. Values of assimilation as well as conductance were calculated to be compared ones with the others. It was expected that the plants with higher stomatal conductance would have higher photosynthetic assimilation, and the opposite. However this cannot be demonstrated yet and further experiments have to complement this data. Moreover, further experiments with plants grown under drought and well-watered conditions may be considered, mostly for the water not to be a limiting factor for the plants, which are supposed to have open stomata during the whole day cycle ($KAT1^{D105E}$).

6.2.2 NpHR

6.2.2.1 Model predictions

One of the advantages of working in a model is the capacity to simulate new situations that would not occur naturally. Here the model allowed to simulate the addition of a foreign pump in the guard cell tonoplast and plasma membrane and predicted how it would affect the natural transport operations that promote stomatal movement.

The principal effect predicted by the model when simulating the addition of 2 M NpHR in the plasma membrane was the big increase on Cl^- flux through both plasma membrane and tonoplast and a higher Cl^- accumulation in both cytosol and vacuole. Cl^- ions entered the cytosol mainly through NpHR, while Cl^- influx through H^+-Cl^- symport was reduced. Despite the location of NpHR at the plasma membrane, most

of the Cl^- ions entering the cytoplasm moved into the vacuole through VCl channels, effectively demonstrating an indirect coupling between the two membranes. The influx of Cl^- also provoked a change in total charge flux, which led to a hyperpolarisation of the plasma membrane voltage, as expected for the physical principles of charge balance. One knock-on effect of this hyperpolarization was that ATPase activity was reduced due to the pump dependence on voltage. Thus, as pumping of H^+ to the apoplast was reduced, cytosolic pH was elevated.

NpHR activity also led to a number of other consequences for the guard cell. Hyperpolarisation of the plasma membrane promoted K^+ influx to the cytosol mainly through K_{in} channels, and to the vacuole through TPK channels. Plasma membrane hyperpolarisation also activated SLAC channels, increasing the efflux of malate and Cl^-. As a consequence, the levels of malate in the cytosol and vacuole decreased mostly during the daylight period. By contrast, the efflux of Cl^- was not enough to compensate the big influx through NpHR. The reduced accumulation of Mal in the vacuole during the daylight was due to a reduction on the Mal flux through ALMT and VCl channels. Membrane hyperpolarisation also increased $[Ca^{2+}]_i$ in the cytoplasm during the daylight period, which promoted Cl^- efflux through R-type channels, facilitating membrane depolarisation and promoting K^+ efflux especially at the end of the daylight period. Oscillations of all the different ion flux analysed in the model were increased by the enhanced electrical driving force. Thus, overall the model showed an increase in the rate of stomatal opening at the start of the day and a similar increase in the rate of closure at the end of the day.

I also introduced NpHR into the tonoplast membrane. These simulations showed that an addition of 2 M NpHR in the guard cell tonoplast did not affect the stomatal behaviour, although adding the pump in the tonoplast promoted the efflux of Cl^- from the vacuole to the cytoplasm. This efflux was compensated by VCl, which transported the same amount of Cl^- back into the vacuole, effectively short-circuiting the action of the pump.

The model predictions show plasma membrane expression of NpHR as a perfect approach to change stomatal kinetics in order to increase stomatal efficiency (Lawson and Blatt 2014)**.** NpHR is a perfect candidate for several reasons. It pumps one of the most important ions involved in stomatal movements (Essen 2002) and it is just active during the daylight period (Schobert and Lanyi 1982).

Different quantities of NpHR were tested in the model both in plasma membrane and tonoplast to have an estimation of how many pumps would be necessary to really make a difference on transport. Effects on guard cell behaviour started appearing when 0.5 M pumps of NpHR were expressed in the plasma membrane, however the most remarkable effects were seen when expressing 2 M pumps (Figures 1-6). The maximum number of pumps simulated in the model in both tonoplast and plasma membrane was 5 M NpHR. Once again, expressing the pumps in the tonoplast had no appreciable effect on transport or stomatal behaviour. However, the model crashed when 5 M pumps were expressed in the plasma membrane. It might be that the huge change in total charge flux provoked by the addition of 5 M NpHR was to extreme for the plasma membrane voltage to reach the balance point were the net flux was zero.

6.2.2.2 Cloning strategies

Based on these simulations, I proceeded to express NpHR in guard cells in order to confirm the predictions. However, the complications came when trying to express NpHR in the plasma membrane of plant cells. Plasma membrane targeting of proteins in plant cells is still poorly understood, and no specific target sequence for plasma membrane localisation has yet to be identified. Even suggestion of the plasma membrane as a default final destination of polytopic proteins are not consistently supported by experimental evidence (Vitale and Raikhel 1999). When NpHR was expressed in the plant cell without any target sequence, its localisation was either in tonoplast or ER (Figures 13, 14). However, analysis on the amino acids sequence of the protein didn't provide any clues to why the protein was retained in the ER or trafficked to the tonoplast. To assess its possible contribution, the length of

NpHR transmembrane domains was also estimated to discard the possibility that it might prevent proper plasma membrane targeting or insertion (Masibay, Balaji et al. 1993, Munro 1995, Watson and Pessin 2001). Indeed, its transmembrane domains are of such a length that this cannot be an explanation; these sequences are between 21 and 23 residues long and therefor are longer than the ones from naturally occurring plasma membrane proteins such as AHA2 (predictions were done with UniProt "www.uniprot.org" and ΔGpredictor "http://dgpred.cbr.su.se" web tools).

A review of the literature on halorhodopsin membrane insertion only turns up information about expressing NpHR in organisms such as bacteria, cyanobacteria and in mammals, not in plant cells. Following the mammalian literature, I reproduced the approach of Gradinaru *et al.* (2008) to express NpHR in the plasma membrane of neurons. Again, this approach had no effect on NpHR localisation or targeting to the plasma membrane in plants.

After analysing the paper of Kleinlogel *et al*. (2011) in nature methods, the option of linking NpHR to another plasma membrane protein was settled on as feasible to try. The authors of this paper linked NpHR to ChR2, thus ensuring one-to-one expression of the proteins. Their purpose was to control and compare the levels of activity with a confirmed balance of the two proteins at the membrane. Linking a plasma membrane protein to NpHR in order to drive the NpHR to the plasma membrane followed the logic that if a plasma membrane protein contains the necessary sequences for plasma membrane targeting, it might draw NpHR to the same membrane site.

Choosing a candidate to drive NpHR into the plasma membrane was not straightforward, in part because the characteristics for plasma membrane localisation of a protein remain unknown. The first proteins to be linked with NpHR were SYP121 and the longin domain of VAMP721, LD_VAMP721. SYP121 is a well-known SNARE protein, proven of a strong expression in the plasma membrane of plant cells, and has the advantage that its C-terminus is located to the outside when

situated in the plasma membrane (Geelen, Leyman et al. 2002). After the unsuccessful attempts to link SYP121 to NpHR, the idea of using the longin domain of VAMP721 (LD_VAMP721) seemed more promising. LD_VAMP721 has been reported to determine the plasma membrane localisation of VAMP721 (Uemura, Sato et al. 2005), a vesicle-associated membrane protein, and recent studies from this laboratory have indicated that a small number of amino acid residues at the center of this domain are important for delivery to the plasma membrane (Zhang, et al. 2015). Thus, it was considered as a possibility to drive NpHR in the plasma membrane. Once again, the attempt failed (Figure 5.2.38).

Both the SNAREs are type II proteins and therefore are inserted into the membrane after translation. Therefore, still with the aim of linking NpHR with a plasma membrane protein, I decided to try plasma membrane proteins that are inserted in the membrane during translation. Members of the plasma membrane intrinsic protein family (so-called PIPs), and Arabidopsis H^+-ATPases (AHAs) were selected as the best candidates as, again, both protein groups are generally found in high abundance. From the PIP family I selected PIP2;1 and PIP2;7, and from the AHA family I selected AHA1 and AHA2. First the 4 different proteins were expressed transiently in tobacco and the protein with the best plasma membrane expression, AHA2, was selected for the linking approach.

A concern was that expressing a proton pump would, itself, affect membrane transport independent of the NpHR. Therefore, AHA2 was cut into different fragments in order to identify the minimum length of the protein necessary for plasma membrane targeting and to ensure that a fully-functional AHA was not included in the fusion. As already mentioned in the results, the advantages of expressing just a fragment of AHA2 instead of the full length are several. However, it was not possible to obtain plasma membrane localisation of the protein unless the full length AHA2 was expressed.

Thus, as a final resort I selected the full length AHA2 protein to be linked with NpHR. I reasoned that if this strategy worked, it might then be possible to introduce

mutations in AHA2 in order to prevent its functional activity. AHA2 was linked via the C-terminus of NpHR in order to combine both cytosolic extremes together. This construct gave expression of both proteins together and it was identified at the plasma membrane under confocal microscopy. The new complication now was that there was not just NpHR expression in the plasma membrane but probably also overexpression of AHA2. From recent literature it has been reported that plants overexpressing AHA2 in the guard cells present an enhanced stomatal opening contributing to an enhanced photosynthesis (Wang, Noguchi et al. 2014b). Thus, the next task for the future will be to introduce mutations in AHA2 affecting its function. These are well-characterised and should not pose difficulty.

Interestingly, it was observed that the expression of both proteins linked together (see Figure 5.2.46C) did not follow the same pattern as when the proteins were expressed individually (see Figure 5.2.31 for NpHR, Figure 5.2.46A for AHA2). Normally AHA2 expression gives a uniform labelling of the plasma membrane. The distribution of the proteins linked together presented small punctate domains instead. Taking in account that NpHR forms trimers (Kolbe, Besir et al. 2000, Sasaki, Kubo et al. 2009, Sasaki, Aizawa et al. 2009b, Kouyama, Kanada et al. 2010) and AHA2 hexamers (Palmgren 2001, Ottmann, Marco et al. 2007, Pedersen, Buch-Pedersen et al. 2007), the puncta may be the result of the complex formation between the two proteins giving rise to cross-linked complexes when expressed together in the membrane. Again, exploring this possibility is a challenge for the future.

It was decided to transform Arabidopsis plants expressing the NpHR protein in all the different places where it was possible to get its expression. Even if the place of interest was to have NpHR in the plasma membrane, it was thought that it could be interesting to see its expression also in the tonoplast and the ER. As the model predicts, expression of NpHR in the tonoplast would not make any effect in stomata behaviour (Figures 5.2.25-5.2.30). Thus, plants expressing NpHR in the tonoplast can be used as a control, as well as to prove the validity of the model. The effects of having expression of NpHR in the ER are still unpredicted.

Further experiments on Arabidopsis plants can be determinant to test if the model predictions of NpHR expression in the plasma membrane are correct. It will be important to have an approximation of the expression level of NpHR in the plasma membrane and relate it with the model predictions. Experiments on isolated guard cells as well as gas exchange measurements in the whole plant level need to be done. Experiments on isolated guard cells could confirm the relations between the different ion movements across the plasma membrane, as well as predict the stomatal aperture ration depending on the levels of NpHR expression. Experiments in the whole plant level, such as gas exchange measurements, will be important to relate how the stomatal behaviour is connected to photosynthesis. Moreover, if finally it can be demonstrated an increase on photosynthesis and WUE it would be a very important achievement in plant sciences.

6.3. Overview

The work in this thesis focused on two of the different strategies for improving photosynthesis. The first strategy was to increase photosynthesis through the creation of a CCM in the chloroplasts stroma in order to increase carboxylation activity of Rubisco (Furbank and Hatch 1987, Ehleringer and Cerling 2002, CARMO‐SILVA, Powers et al. 2008). The second strategy was to modify stomatal kinetics in order to align stomatal conductance with the mesophyll demand for CO_2, which may not increase photosynthesis but is directed to improving WUE (Wong, Cowan et al. 1979, Lawson, Kramer et al. 2012, Lawson and Blatt 2014). A novel feature of the work was the use of synthetic manipulations with light-driven pumps in plants, an approach incorporated to accomplish different purposes in the two different projects exposed in this thesis. Thus, predominant throughout this research was the introduction of new technologies to engineer innovative techniques overstepping the limits of nature.

6.3.1. Engineering a CCM in the chloroplasts

The objective of this project was to create an artificial transport system in the inner envelope of the chloroplasts in order to increase HCO_3^- in the chloroplast stroma.

The main advantage of the engineered artificial transport system was the fact that it was driven with external energy and therefore did not impose an extra energetic cost for the plant. The transport system was powered with the light-driven pump NpHR and was complemented with the antiporter AE1. The NpHR provided the energy to power the system, using the pumping of Cl^- into the chloroplast to provide the driving force for the AE1 to exchange Cl^- with HCO_3^-.

Expression of both proteins and their correct targeting into the inner envelope of the chloroplasts was realised in this thesis. Additionally, bCMO1 was expressed in the chloroplasts stroma and its function, necessary for retinal production was confirmed. bCMO1 is an enzyme capable of breaking the plant b-carotene to create 2 molecules of all-trans retinal (Devery and Milborrow 1994), indispensable molecule for the NpHR activity. Furthermore, it was possible to combine the different proteins in single vectors and demonstrate its co-expression in the chloroplast of transiently transformed tobacco plants.

Activity of the proteins was more difficult to demonstrate in the case of NpHR and AE1. However, some of the chloroplasts transformed with both proteins, either separately or co-expressed together, showed what I denoted as an “atypical morphology” pattern. The chloroplasts presenting this atypical morphology were characterised by a swollen shape: the chloroplasts were larger and the grana were pushed to one site instead of being well distributed among the chloroplasts stroma.

It remains to ascertained if the atypical morphology pattern was due to the activity of the proteins, which could cause osmotic imbalances in the chloroplasts, or if it was due to the physical presence of the proteins. The atypical morphology was mostly seen in chloroplasts from epidermal cells and was more difficult to detect in the mesophyll cells. However, image collection and protein fluorescence presents a challenge in the mesophyll cells under confocal microscopy, which is best suited to relatively thin tissue samples. Moreover it is uncertain if the atypical morphology observed would have negative values on chloroplasts activity, for example by

interfering with Rubisco activity and electron transport which takes place in the chloroplast thylakoid.

A semi-quantitative analysis of the atypical morphology and its distribution among the chloroplasts showed that there was a significant variation that depended on which protein was expressed. NpHR was most effective in causing the atypical morphology whereas AE1 was less effective. Curiously, the effects chloroplast morphology decreased when both proteins were expressed together. Several conclusions can be extracted of this data, however all remain hypotheses that will have to be consolidated with a functional data.

It would be necessary to demonstrate protein activity by calculating ion fluxes through the chloroplasts envelope. However, it is not under our knowledge how all the different transporters in the chloroplast envelope are interconnected, and even less how an external change caused by the introduction of an external protein would affect the relationship between them. Thus, in order to prove protein activity on a molecular level and its relationships with the other transporters it was necessary to face a complex set of experiments that could not fit given the time available for this research. Despite this, I did an attempt to calculate the levels of O_2 on isolations of tobacco chloroplasts, transiently expressing AE1 and NpHR, by using an oxygen electrode. The idea was to calculate the O_2 differences produced by photosynthetic activity, and to determinate the effects of NpHR by providing a light source. However and as expected, working with chloroplasts isolations required a big amount of time of which I lacked in order to finish the research on time. Thus, it was decided to leave a part the experiments on chloroplasts isolations and to focus the research on elaborating Arabidopsis stable transgenic plants. At this point, having the calculations of photosynthesis in the whole plant level was a more direct step to determine the effects of the expression of the different proteins in the chloroplasts.

Fortunately, the activity of bCMO1 could be easily detected by an analysis on the levels of b-carotene from the chloroplasts. As shown in Figure 5.1.28 chloroplasts expressing bCMO1 had half levels of b-carotene than the wild-type chloroplasts.

From this data it was assumed that the difference on b-carotene was due to the activity of the enzyme. Because it is not known yet if it is indispensable to provide external retinal for the proper activity NpHR in plants, it was decided to generate stable Arabidopsis plants combining the NpHR with and without bCMO1.

Unsuccessfully, the results on gas exchange measurements were not consistent between the different lines of transgenic Arabidopsis plants analysed. Thus, making it difficult to reach proper conclusions on the effect of the proteins in the plant photosynthesis. However, it was not surprising that no higher photosynthesis was achieved with the transgenic plants. Further experiments have to focus on verifying the activity of the proteins and search for an increase on HCO_3^- in the chloroplasts. Once it is demonstrated an increase on HCO_3^- is when the second part of the MAGIC projects starts, with the aim of concentrate CO_2 next to Rubisco.

Further experiments will need to include protein activity calculations on isolated chloroplasts. It will be important to do this type of experiments in chloroplasts from Arabidopsis stable lines to ensure stable levels of protein expression. In transient transformed tobacco, protein expression levels vary and are also dependent on timing post-transformation. Different methods can be used to check the effects of the proteins in the isolated chloroplasts. For example, the use of ion dyes techniques to identify the directions of specific ions movements, pH calculations in chloroplasts solutions or O_2 electrode experiments as already mentioned before. Furthermore, with the advantage that NpHR is activated by light, thus allowing the possibility to calculate the differences on ion fluxes between the activated and deactivated state of the pump.

6.3.2. Manipulation of stomatal kinetics

Two different approaches were followed with the aim of manipulating stomatal kinetics. The first approach was to modify the gating properties of one of the main channels from the guard cells involved in stomatal opening, KAT1. The second was to add the light driven pump, NpHR, in the guard cell plasma membrane. Both

approaches were first simulated using the OnGuard model, and both predicted a set of well-defined changes in stomatal behaviour.

Simulations using the model were very useful to understand the relationship between the different transporters and ion fluxes involved in stomatal movement. In the case of KAT1, OnGuard was used to simulate a change in the $V_{1/2}$ of the K_{in} channels to either more positive or more negative values relative to the wild-type. The model predicted a major increase in the capacity of the K_{in} channels within the physiological voltage range when its $V_{1/2}$ was shifted to more positive values, and the opposite result when the $V_{1/2}$ was shifted to more negative values. Overall, the main predictions for stomatal kinetics were that in the first case the K_{in} channels enhanced K^+ influx, aperture and opening kinetics during the daylight period, with the disadvantage that the stomata did not close as effectively during the dark period. By contrast, reducing the capacity to drive K^+ influx was predicted to suppress the stomatal aperture, with only minor changes between daylight and dark periods.

The advantages of adding NpHR in the guard cell plasma membrane versus changing the gating properties of KAT1 channels were notable. The model predicted faster opening and bigger apertures of the stomata when NpHR was activated in the light, as well as a faster rate of closure and total closure of the stomata when NpHR was deactivated at the beginning of the dark period. By contrast, the simulations showed that expression in the tonoplast should have no appreciable effect on stomatal behaviour, either in the kinetics of movement or the dynamic range of apertures.

It was decided to carry out both approaches experimentally in order to verify if the model predictions were reproducible in vivo. For KAT1, two different mutants of KAT1 were selected to create stable Arabidopsis lines. These two mutants, $KAT1^{D105E}$ and $KAT1^{F102W}$, were available in the laboratory and had been shown to shift the $V_{1/2}$ to more positive and more negative values, respectively (Lefoulon, Karnik et al. 2014, Grefen, Karnik et al. 2015). Thus the challenge in this case was to establish stable transgene expression in the wild-type and *kat1* mutant Arabidopsis for analysis. For NpHR, the challenges were greater in that it was necessary to establish correct

targeting of a foreign protein as well as expression of the transgene, and here the things became complicated. I undertook several different strategies to achieve the correct targeting of NpHR, before I was able to successfully drive the expression of the protein targeted to the plasma membrane. The only successful strategy in this case was to link the protein to AHA2. In addition, for exclusive guard cell localisation of the proteins, I generated vectors containing the MYB60 promoter specific for expression in the guard cells.

It was possible to generate Arabidopsis plants transformed with all the selected constructs for the KAT1 approach as well as for the NpHR approach. However, due to the time required to localise NpHR in the plasma membrane, plants expressing this protein were not ready yet for gas exchange analysis at the end of this thesis. Therefore, gas exchange analysis was only realised with the plants transformed with the KAT1 protein and its mutants. An added complication proved to be that some of the Arabidopsis lines generated with the KAT1 approach showed poor expression. Thus, the number of lines recovered with good expression was insufficient to get meaningful data out of the gas exchange measurements, either to support or refute the model predictions.

Further experiments could be divided into two different sets of experiments for each approach. The first one may include gas exchange measurements on Arabidopsis plants expressing the different proteins in order to calculate conductance as well as photosynthesis activity, and relate the dependence of one to the other. The second set of experiments may include an analysis on transporters behaviour when the guard cell is isolated. Patch clamp experiments may be useful to directly link the model prediction with the real impact of the proteins in plants, as well as to detect the proper function of NpHR in the plasma membrane of the guard cells.

7. Conclusions

7.1 Engineering a CCM in the chloroplast

1. It has been possible to express bCMO1, NpHR and AE1 in the plant cell.

2. It has been possible to target the transmembrane proteins NpHR and AE1 in the inner envelope of chloroplasts with the signal peptide TPT; and to target bCMO1 in the chloroplasts stroma driven by the RbcL.

3. It has been possible to express different combinations of the proteins in the chloroplasts with co-localisation.

4. It has been possible to co-express different combinations of the proteins in a single vector.

5. Some of the chloroplasts expressing NpHR and AE1 presented a phenotype.

6. Activity of bCMO1 could be demonstrated in transient transformed chloroplasts.

7. Transgenic plants expressing different combinations of the proteins were obtained.

8. Stable lines of transgenic plants expressing different combinations of the three proteins did not have an increase on photosynthesis yet.

7.2 Manipulation of stomatal kinetics

1. It has been possible to simulate in the OnGuard model a change on the K_{in} channels $V_{1/2}$ to more positive and more negative values related to the wild-type.

2. It has been possible to simulate in the OnGuard model the introduction of the external pump NpHR both in tonoplast and plasma membrane.

3. The model predicted a change on the stomatal kinetics when K_{in} channels $V_{1/2}$ was shifted to more positive and more negative values in relation to the wild-type; as

well as, a change on the stomatal kinetics when NpHR was added in the plasma membrane of the guard cells.

4. The model predicted a typical response expected of an efficient stoma when NpHR was expressed in the plasma membrane of the guard cells.

5. NpHR targeting to the plasma membrane was achieved in transiently transformed tobacco by fusing NpHR with the plasma membrane protein AHA2. It was also achieved NpHR targeting to the tonoplast and ER, depending on the position of the fluorescent tag.

6. A vector containing a specific promoter for the guard cells (AtMYB60) was generated and KAT1, KAT1 mutants and NpHR were cloned under its expression, as well as under the expression of the promoter 35S.

7. Transgenic Arabidopsis plants were generated with all the created constructs.

8. It was possible to do gas exchange measurements on plants expressing KAT1 and its mutants, but not consistent data was obtained to make proper comparisons of the results with the model predictions.

8. Summary in Catalan

8.1 Introducció

8.1.1 Fent front a l'augment de la població mundial

El ràpid increment de la població mundial, sobretot als països subdesenvolupats, està amenaçant la seguretat alimentària. Es calcula que la població mundial podria augmentar de 7 bilions de persones actualment a 9 bilions de persones al 2050, superant els 10 bilions al 2100 (UN 2013). Dades de la FAO estimen que al 2014 el nombre de persones sofrint malnutrició ja arribava 805 milions (FAO 2014). Així doncs, per poder alimentar a aquesta població creixent i poder combatre el problema de la fam al món, es prediu que la producció d'aliments s'hauria d'incrementar un 70 % en els pròxims 30-50 anys (FAO 2009).

Un creixement en l'agricultura genera un creixement econòmic global i condueix a la reducció de la pobresa (FAO 2014). Avui en dia però, l'agricultura està amenaçada per varis factors com el canvi climàtic (Easterling 2007, Kurukulasuriya and Rosenthal 2003, Rosenzweig, Tubiello et al. 2002), la creixent escassetat d'aigua (Sauer, Havlík et al. 2010), la falta de terra disponible (FAO 2012, FAO 2010) i l'ús de cultius per a la creació de biocombustibles (FAO 2013, FAO 2009). Dins d'aquest context, la millora en la producció de cultius es planteja com un dels grans reptes d'aquest segle.

Un increment en la producció de cultius reduiria l'efecte negatiu que la producció de biocombustibles està tenint en la disponibilitat d'aliments, com també reduiria l'alta demanda per terres forestals (FAO2009). A més a més, la recerca científica enfocada en incrementar la biomassa dels cultius i en desenvolupar plantes amb alta eficiència en l'ús de l'aigua és essencial per tal d'augmentar la producció agrícola i fer front a la baixa disponibilitat d'aigua dolça. El pròxim pas a seguir per tal d'augmentar el potencial del rendiment dels cultius és una millora en la fotosíntesi (Zhu, Long et al. 2010).

8.1.2 Millorant l'eficiència fotosintètica

Durant els últims anys, la fotosíntesi s'ha convertit en un tòpic de gran interès en el món científic degut al seu potencial per a augmentar la producció d'aliments. Avui en dia, gran part de la investigació entorn la fotosíntesi està centrada en millorar els punts crítics que en limiten el procés, per tal d'augmentar l'eficiència fotosintètica.

La majoria de plantes del planeta, incloent la majoria dels cultius, depenen de la fotosíntesi C_3. Aquest procés consisteix en la incorporació d'una molècula de CO_2 a la ribulosa bisfosfat (RuBP) per tal de crear dues molècules de 3-fosfoglicerat (3-PGA) (molècula de 3C) durant la via metabòlica coneguda com a Cicle de Calvin (Ehleringer and Cerling 2002). La ribulosa bisfosfat carboxilasa/oxigenasa (Rubisco) és l'enzim que catalitza la incorporació de CO_2 en aquest procés. En total, per cada molècula de CO_2 fixada es necessiten 3 ATP i 2 molècules NADPH.

El CO_2 entra a través de l'estoma i difon a través dels espais intercel·lulars fins a l'estroma del cloroplast, a on es troba la Rubisco (Evans and Von Caemmerer 1996). Per entrar al cloroplasts, el CO_2 ha de travessar les dues membranes. La membrana externa té una gran permeabilitat a molècules petites degut a la presència de porines. Per contra, la membrana interna és més selectiva, actuant de barrera entre l'estroma i el citosol (Block, Douce et al. 2007). Una vegada a l'estroma, la pressió parcial del CO_2 (pCO_2) és menor que la pCO_2 a l'atmosfera (Ca) degut a l'activitat carboxilasa de la Rubisco (Evans, Kaldenhoff et al. 2009).

Un dels factors que limita la fotosíntesi és la baixa eficiència de la Rubisco. Aquest enzim té una taxa catalítica molt lenta, que acostuma a ser d'entre 5 a 6 cicles per segon. Una segona complicació és la poca afinitat de la Rubisco envers CO_2, ja que també pot incorporar O_2 a través d'un procés anomenat fotorespiració (Spreitzer and Slavucci 2002). La fotorespiració té lloc quan la Rubisco fixa una molècula d'O_2 en comptes de CO_2 i catalitza l'oxigenació de la RuBP en comptes de la carboxilació (Wingler, Lea et al. 2000). Així doncs, una de les possibilitats d'augmentar la capacitat fotosintètica és millorant l'eficiència de la Rubisco.

En general, es considera que són dues les maneres principals d'augmentar la fotosíntesi a través de modificacions implicant la Rubisco. Una forma, no treballada en aquesta tesis, seria modificant el lloc actiu de la Rubisco per tal de millorar la seva eficiència catalítica. La segona forma seria creant un mecanisme de concentració del carboni (MCC) per augmentar la pCO_2 al lloc actiu de la Rubisco, reduint així la fotorespiració.

Una de les característiques principals de les plantes que depenen en fotosíntesi C_4 és la seva capacitat de concentrar carboni dins la cèl·lula, on es troba la Rubisco, gràcies als MCCs que conté de manera natural. Aquesta característica li proporciona a la Rubisco un ambient ric en CO_2, augmentant la taxa de carboxilació versus la d'oxigenació, i així augmentant la fotosíntesi. Actualment però, només el 3 % de totes les plantes del planeta depèn de la fotosíntesi C_4 (Sage 2004). Alguns exemples de cultius C_4 serien el panís, la melca i la canya de sucre, no obstant la majoria de plantes C_4 no són utilitzades per conrear.

El primer acceptor del CO_2 en una planta C_4 és l'enzim fosfoenolpiruvat (PEP) carboxilasa (PEPC) en comptes de la Rubisco. Aquest CO_2 és fixat en forma de $HCO3^-$, per tant, les anhidrases carbòniques (AC) tenen un paper molt important facilitant el ràpid equilibri entre CO_2 i HCO_3^-. La carboxilació del PEP crea oxalacetat (OAA), un àcid orgànic de 4C, i té lloc a les cèl·lules del mesòfil. Aquest OAA difon a un compartiment separat on és descarboxilat per alliberar el CO_2 i una molècula de piruvat. Aquest compartiment separat comprèn cèl·lules especialitzades, cèl·lules de la beina, on es troba la Rubisco, i és on té lloc la fixació del CO_2 a través del Cicle de Calvin. La gran activitat catalítica del PEPC permet concentrar el CO_2 a les cèl·lules de la beina d'una manera efectiva. A més a més aquesta separació física de la Rubisco permet que la proporció CO_2/O_2 a les cèl·lules de la beina sigui elevada, així limitant la fotorespiració (Ehleringer and Cerling 2002). Durant tot el procés, per cada molècula de CO_2 fixada es necessiten 5 ATP i 2 molècules NADPH. Així doncs, les plantes amb fotosíntesi C_4, tenen un consum addicional de 2 ATP respecte a les plantes amb fotosíntesi C_3.

Per tant, enginyar MCC en una planta C_3 donaria la possibilitat d'augmentar la fotosíntesi i així el rendiment dels cultius. També seria important aconseguir un augment de fotosíntesi sense requerir cap extra cost d'energia per les plantes. Per sort, hi ha també altres maneres d'augmentar la fotosíntesi, com per exemple millorant la velocitat del moviment estomàtic.

8.1.3 El paper de l'estoma en la fotosíntesi

Els estomes són petits porus a l'epidermis de les diferents parts aèries de les plantes, per on té lloc l'entrada principal del CO_2 a la planta i també per on es perd fins al 70 % d'aigua de la planta (Willmer and Fricker 1996). Així doncs, el seu paper és fonamental tant en la fotosíntesi com en la transpiració. Els estomes estan formats per un parell de cèl·lules especialitzades anomenades cèl·lules de guarda. Aquestes cèl·lules actuen com a vàlvules dependents de turgència que poden obrir i tancar segons els estímuls hormonals endògens i les diferents condicions ambientals. L'obertura estomàtica està induïda per unes condicions d'humitat elevada i baix CO_2, per tal de potenciar l'entrada de CO_2. La llum blava i vermella indueixen obertura estomàtica en plantes C_3 i C_4 mentre que el tancament estomàtic està induït per foscor (Zeiger and Helper 1977). Altres factors que indueixen el tancament estomàtic són les altes concentracions de CO_2, les altes concentracions d'ozó, i els inductors de patògens (Assmann 1999, Torsethaugen, Pell et al. 1999, Lee, Choi et al. 1999). La sequera promou la producció de l'hormona àcid abscísic (ABA) que també causa el tancament estomàtic. Altres hormones com les auxines, les citocinines, l'etilè, els brasinoesteroides i els jasmonats també estan involucrats en els moviments estomàtics (Acharya and Assmann 2009).

L'obertura i el tancament estomàtic depèn d'uns mecanismes que afecten la pressió de turgència causant la inflor o l'encongiment de les cèl·lules de guarda. Aquests canvis de volum, a la vegada, afecten la mida del porus estomàtic. Els canvis en turgència són el resultats dels canvis en els continguts osmòtics de salts seguits per una retenció o alliberament d'aigua de les cèl·lules de guarda. Durant l'obertura estomàtica hi ha una entrada principalment de ions de K^+, anions i soluts orgànics

que causen un augment en la pressió de turgència. Durant el tancament, hi ha l'alliberament de K^+ i anions des de les cèl·lules de guarda el qual deriva a una reducció de la pressió de turgència (Blatt 2000b, Maser et al. 2009). Per tant, el transport a traves d'ambdues membranes de les cèl·lules de guarda, membrana plasmàtica i tonoplast, és el motor que condueix l'obertura i el tancament estomàtic. Els vacúols de les cèl·lules de guarda ocupen del 80 al 90 % del volum total de la cèl·lula, per tant la majoria dels flux iònics que passen a través de la membrana plasmàtica també passen a través del tonoplast (Blatt 2000b).

8.1.3.1 Bombes iòniques, transportadors i canals

A les membranes s'hi troben diferents bombes iòniques, transportadors i canals encarregats de permetre el moviment dels diferents ions, principalment K^+ i Cl^-, i soluts orgànics tals com el malat i la sucrosa. Al mateix temps, els flux dels diferents ions depenen dels seus gradients electroquímics. A la membrana plasmàtica hi ha una família de bombes de protons que són les H^+-ATPases, formades per 11 diferents membres anomenats del AHA1 al AHA11 (Axelsen and Palmgren 2001). Són bombes energitzades per la hidròlisi d'ATP i el seu paper principal és bombardejar H^+ a fora la cèl·lula, causant un gradient de pH d'1,5 a 2 unitats alcalí a l'interior, creant una hiperpolarització de membrana. Com a resultat causen un gradient electroquímic de protons a traves de la membrana plasmàtica necessari per l'activació del transport de ions i metabòlits, i proveeixen l'energia per l'absorció de nutrients de les plantes (Serrano 1989, Morsomme and Boutry 2000). Les més abundants i presents en tots els òrgans i teixits de les plantes són AHA1 i AHA2. En canvi, al tonoplast hi ha dos famílies diferents de bombes de protons, les V-ATPases i les V-PPases, les quals bombegen els protons des del citoplasma fins al vacúol. El seu paper principal és crear un gradient de protons que proporcioni l'energia pel transport dels diferents ions i metabòlits (Sze, Schumacher et al. 2002). Una altra bomba iònica comuna a les dues membranes és la Ca^{2+}-ATPasa, composa de deu membres diferents anomenats ACA1 fins ACA10. La seva funció principal és la de mantenir baixos els nivells de Ca^{2+} lliure al citosol i participar amb els senyals per les oscil·lacions de Ca^{2+}.

Tant al tonoplast com a la membrana plasmàtica s'hi troben transportadors de ions acoblats a protons. Aquests utilitzen els gradients electroquímics dels protons per a transportar un segon solut. Aquests transportadors fan possible el transport de H^+ acompanyat d'anions, cations o sucres (Chen and Blatt 2010), facilitant així el transport d'aquestes molècules en contra el seu gradient electroquímic. També contribueixen a mantenir el pH del citosol i permeten l'influx de diferents soluts durant l'obertura estomàtica així com el flux de sortida d'aquestes molècules durant el tancament de l'estoma.

Finalment trobem els canals, els quals permeten el pas de diferents cations i anions tan a través de la membrana plasmàtica com del tonoplast. A la membrana plasmàtica trobem els canals de K^+, Ca^{2+} i d'anions. Els canals de K^+ tenen un paper molt important durant l'obertura i el tancament estomàtic, ja que permeten l'entrada i sortida dels majors flux de K^+ de la cèl·lula de guarda (Schroeder 1988). Els canals de K^+ de la membrana plasmàtica estan dividits entre els d'entrada (K_{in}) i els de sortida (K_{out}) de K^+ (Blatt 2008, Dreyer and Blatt 2009, Ward, Maser et al. 2009, Chen and Blatt 2010). Ambdós pertanyen a la família de canals Kv-like, i són dependents del voltatge de la membrana (Blatt 1991). Els canals K_{in} són activats per la hiperpolarització de la membrana plasmàtica durant l'obertura estomàtica (Schroeder, Raschke et al. 1987, Schachtman, Schroeder et al. 1992). A les cèl·lules de guarda d'Arabidopsis se'n troben cinc membres diferents anomenats KAT1, KAT2, AKT1, AKT2 i KC1. Essent KAT1 i KAT2 els més abundants. De fet, KAT1 representa la major entrada de K^+ a la cèl·lula de guarda i és activat a voltatges de membrana negatius per sota -100 mV. En canvi, els canals K_{out} són activats per la despolarització de la membrana plasmàtica durant el tancament estomàtic (Ache, Becker et al. 2000). L'únic canal K_{out} conegut fins al moment és el GORK.

A la membrana plasmàtica també s'hi troben els canals de Ca^{2+}, els quals permeten l'entrada de Ca^{2+} i són activats per la hiperpolarització de membrana i per l'ABA (Hamilton, Hills et al. 2000, Pei, Murata et al. 2000). Aquests canals són inactivats per altes concentracions citosòliques de Ca^{2+} lliure en un mecanisme d'autolimitació. Aquest mecanisme d'autolimitació és un prerequisit per la cèl·lula de guarda per tal

de general el comportament oscil·latori en les concentracions de Ca^{2+} citosòlic durant el tancament estomàtic (Minguet-Parramona, Wang et al. 2015). Per altra banda, també hi ha canals d'anions, classificats segons si la taxa d'activació i desactivació és ràpida (canals de tipus R) o lenta (canals de tipus S). Aquests canals permeten el flux de sortida dels diferents anions de la cèl·lula de guarda, i promouen la despolarització de la membrana plasmàtica contribuint també a l'activació dels K_{out} participant així en el tancament estomàtic (Roelfsema, Hedrich et al. 2012).

Al tonoplast també s'hi troben canals de cations i anions els quals també tenen un paper important durant el moviment de l'estoma. Els canals de cations es poden dividir en tres tipus, que són canal vacuolar ràpid (FV), canal vacuolar de K^+ (VK) i canal vacuolar lent (SV). Són sensibles al voltatge i activats per l'alcalinització del citosol. Permeten una entrada passiva i no selectiva de cations quan els nivells de $[Ca^{2+}]_i$ són en repòs, i s'inactiven quan els nivells de $[Ca^{2+}]_i$ són elevats (Allen and Sanders 1996, Ward, Maser et al. 2009, Chen and Blatt 2010).

8.1.3.2 Coordinació del transport de membrana

Els processos de tancament i obertura estomàtica estan altament coordinats, involucrant la regulació de múltiples transportadors en ambdues membranes. L'obertura de l'estoma depèn de l'activació de les H^+-ATPases de la membrana plasmàtica, les quals bombegen protons cap a l'exterior de la cèl·lula de guarda. D'aquesta manera promouen la hiperpolarització de la membrana plasmàtica a l'hora que promouen un gradient de pH a traves de la mateixa membrana (Blatt and Thiel 1993b). La hiperpolarització de la membrana plasmàtica provoca l'activació dels canals K_{in}, causat com a resultat del canvi del potencial de membrana cap a valors més negatius als quals els canals de K^+ s'activen, i en part com a resultat de l'augment en la força motriu pel l'entrada de K^+ (Thiel, MacRobbie et al. 1992). La hiperpolarització de la membrana també energitza el transport de ions lligats a protons, principalment Cl^-, i en conjunt deriva a una acumulació de K^+ i anions dins de la cèl·lula. La llum blava i vermella també promouen la producció de sucres durant l'obertura estomàtica, els quals s'acumulen a la cèl·lula de guarda i participen

significativament en tot el procés osmòtic que permet que l'estoma s'obri (Poffenroth, Green et al. 1992). A més a més, durant l'obertura estomàtica hi ha una reducció del midó el qual és convertit en malat (Outlaw and Manchester 1979). Com a resultat, els nivells de malat incrementen dins les cèl·lules de guarda, contribuint en l'acumulació de sals orgàniques i permetent la inflor de les cèl·lules de guarda i l'obertura del porus.

Durant el tancament estomàtic hi ha oscil·lacions de Ca^{2+} dins el citoplasma, l'activitat de les H^+-ATPases queda suprimida i el K^+ i els soluts anions són alliberats de la cèl·lula de guarda, causant una pèrdua de la pressió de turgència (Blatt 2000, Chen, Hills et al. 2012, Minguet-Parramona, Wang et al. 2015). Les oscil·lacions de Ca^{2+} estan directament involucrades en el tancament estomàtic i es creu que són importants per accelerar el flux de sortida de K^+, Cl^- i malat de la cèl·lula de guarda (Chen, Hills et al. 2012, Minguet-Parramona, Wang et al. 2015). L'increment en $[Ca^{2+}]_i$ activa els canals de Cl^- per conduir el flux de sortida de Cl^-, els dos processos provoquen la despolarització de la membrana. A la vegada, la despolarització promou el flux de sortida de K^+ i altres anions de la cèl·lula de guarda (Thiel, MacRobbie et al. 1992). L'increment en $[Ca^{2+}]_i$ també inactiva els canals K_{in} (Grabov and Blatt 1999, Chen, Hills et al. 2010b). El vacúol té un paper molt important tan en l'obertura com el tancament estomàtic, ja que la majoria de ions que passen a través de la membrana plasmàtica travessen també el tonoplast.

8.1.3.3 El model de l'estoma

Els models computacionals són capaços d'integrar el comportament d'un sistema biològic complex i representar complicades cadenes d'esdeveniments mitjançant simulacions per ordinador (Fisher and Henzinger 2007). Les cèl·lules de guarda són un sistema ideal per ser reproduït mitjançant un model ja que se'n coneix una gran quantitat d'informació, i perquè la seva falta de plasmodesmes fa que puguin ser tractades com un sistema semi-tancat. Els principals transportadors involucrats en el moviment estomàtic han sigut aïllats i han pogut ser analitzats experimentalment, així com també han sigut analitzats els papers del metabolisme de la sucrosa i el

malat en aquests procés (Blatt and Thiel 1993b, Willmer and Fricker 1996, MacRobbie 1997, Thiel and Wolf 1997, Blatt 2000b, Schroeder, Allen et al. 2001b, Pandey, Zhang et al. 2007, Ward, Maser et al. 2009). D'aquests experiments se n'ha obtingut una informació detallada la qual ha permès obtenir descripcions de cada flux basades en equacions exactes delimitades per les dades experimentals i els principis físics bàsics. Hills et al. (2012) van descriure un programa computacional, anomenat OnGuard, el qual unia les característiques biofísiques, cinètiques i reguladores del transport, la senyalització i la homeostasis de les cèl·lules de guarda. El poder predictiu del model és molt acurat i ha sigut demostrat (Chen, Hills et al. 2012), així com també ha sigut demostrada la seva capacitat de reproduir comportaments inesperats i emergents que prèviament s'havien demostrat experimentalment. Així doncs, és possible utilitzar el model per a simular una varietat de condicions diferents a les cèl·lules de guarda i predir com l'estoma respondrà envers aquestes. En aquesta tesis el model OnGuard s'ha utilitzat com a eina per predir quines modificacions necessiten ser realitzades a la cèl·lula de guarda per tal d'obtenir un estoma més eficient.

Un estoma eficient és aquell que maximitza la captació de CO_2 per a la fotosíntesi al mateix temps que minimitza la quantitat d'aigua perduda en la transpiració. A la natura, amb totes les condicions climàtiques adverses, és un repte per les plantes aconseguir alts nivells de fotosíntesi i un òptim d'eficiència en l'ús de l'aigua (EUA) a la vegada. Les plantes tenen una dependència directa entre assimilació fotosintètica i conductància (Wong, Cowan et al. 1979). A més, la resposta estomàtica envers els estímuls ambientals, per exemple la llum, és molt més lenta que la resposta fotosintètica cap al mateix estímul (Pearcy 1990). Així doncs, el lent moviment de les cèl·lules de guarda durant l'obertura estomàtica limita l'assimilació fotosintètica ja que està limitant la captació de CO_2. De la mateixa manera, un moviment lent de les cèl·lules de guarda durant el tancament estomàtic degut a la foscor, representa una reducció en l'EUA, ja que disminueix l'assimilació fotosintètica mentre l'estoma va perdent aigua de forma innecessària.

Així doncs, és possible millorar l'eficiència fotosintètica modificant la velocitat de la resposta estomàtica per tal de posar en concordança la demanda de CO_2 del mesòfil amb la conductància de l'estoma. Aquesta idea de manipular la cinètica de l'estoma no és nova (Lawson, Kramer et al. 2012) i hi ha evidència experimental que demostra el potencial impacte en guanys de carboni i pèrdua d'aigua depenent de la velocitat del moviment estomàtic, especialment envers l'estímul de llum (Lawson, and Blatt 2014). Wang et al (2014) suggereixen una possible manipulació de la cinètica dels estomes mitjançant la manipulació de les propietats de voltatge dels transportadors, principalment dels canals de K^+. Davant les dificultats de canviar les propietats cinètiques dels estomes, ha de ser avaluada la idea d'utilitzar noves bombes de ions sintètiques, que permetin augmentar l'assimilació fotosintètica i l'EUA sense canviar les propietats generals del transport.

8.1.4 Biologia sintètica: enginyant transport de membrana

La biologia sintètica comprèn la combinació de la ciència i l'enginyeria per dissenyar i crear noves funcions i sistemes biològics. La biologia sintètica aplicada a la millora de cultius no només podria donar una oportunitat per a crear plantes amb majors taxes de fotosíntesi i EUA, incrementant així la biomassa, sinó que també fa possible crear plantes amb una gran varietat de característiques diferents. Fins ara, la biologia sintètica ha contribuït directament en el progrés de construcció de materials, producció d'energia, i proporcionar aliments per a millorar la salut, entre altres. No obstant, el pas de la biologia sintètica encara és molt lent, possiblement degut a la gran inversió de temps i diners que requereix, i perquè els nostres coneixement dels sistemes biològics i la complexitat de l'enginyeria dels mateixos romanen limitats.

Dins de la biologia sintètica hi ha una branca anomenada optogenètica, la qual relaciona l'expressió de gens específics que codifiquen per proteïnes sensibles a la llum, i l'ús de la llum per a promoure la funció d'aquestes proteïnes per tal d'alterar el comportament cel·lular (Pastrana 2011). Fins ara l'optogenètica ha estat utilitzada per a controlar el voltatge de membrana de les cèl·lules, així controlant l'activitat dels diferents canals iònics elèctricament actius. No obstant, encara no s'ha utilitzat

mai per a manipulat els flux iònics, ja que la input requerida per a controlar els flux iònics és ordres de magnitud major que la requerida per a modificar el voltatge de membrana.

Les proteïnes sensibles a la llum identificades fins al moment són les halorodopsines, bacteriorodopsines i les canalrodopsines. Es tracta de proteïnes amb 7 dominis transmembrana i que estan codificades per gens opsines. Les tres proteïnes estan covalentment unides a una molècula de retinal, essencial per al seu correcte funcionament. Aquesta molècula de retinal isomeritza amb l'absorció d'un fotó de llum, conduint el canvi de la conformació de la proteïna i permetent el creuament dels ions d'una banda a l'altra de la membrana (Fenno, Yizhar et al. 2011).

L'any 2011 es va començar un projecte anomenat MAGIC (Multiple Approaches to Gain Increased Carbon Dioxide) amb l'objectiu de crear un MCC en una planta C_3 fent ús de l'optogenètica. Aquest projecte està dividit en dos parts, ambdues necessàries per a incrementar la quantitat de CO_2 disponible per a la Rubisco. La primera part està enfocada en aconseguir un augment de HCO_3^- dins del cloroplasts, el qual serà convertit en CO_2 per l'AC. La segona part està enfocada en retenir aquest CO_2 on es troba la Rubisco, per tal de que aquesta sigui capaç d'utilitzar-lo i fixar-lo. Per tal d'incrementar el HCO_3^- dins del cloroplasts, els investigadors van proposar la creació d'un transport artificial a la membrana interna del cloroplasts basat en una bomba iònica en dues etapes i motoritzat per la halorodopsina de *Natronomonas pharaonis* (NpHR). Aquesta estratègia en dues etapes consisteix en la introducció de la NpHR a la membrana interna del cloroplasts per tal de crear un gradient de Cl^- cap a l'interior del cloroplasts. Juntament amb la introducció d'una segona proteïna, l'AE1 (anion exchanger 1) la qual, energitzada pel gradient de Cl^-, intercanviaria el Cl^- pel HCO_3^-, creant així un augment dels nivells de HCO_3^- dins del cloroplast.

La NpHR, igual que les altres rodopsines, conté una molècula de retinal que funciona com a cromòfor per al correcte funcionament de la proteïna. La fotoisomerització del cromòfor fa que passi de all-trans retinal a 13-cis retinal i així inicia el cicle de transport, permetent a la proteïna el moviment d'una molècula de Cl^- a traves de la

membrana des del medi extracel·lular fins a l'interior del citosol. La NpHR té tan sols un lloc d'unió a la molècula de Cl^-, transportant tan sols una molècula a cada cicle. No obstant, la NpHR és relativament poc selectiva pels anions i no només transporta Cl^- sinó que també té l'habilitat de transportar nitrat (Duschl, Lanyi et al. 1990). L'AE1, també anomenada proteïna de banda 3, és la proteïna integral més abundant a la membrana dels eritròcits humans i d'altres mamífers. Funciona com un transportador antiport catalitzant l'intercanvi del Cl^- pel HCO_3^- a traves de la membrana plasmàtica (Kopito 1985, Lux, John et al. 1989).

8.2 Objectius

L'objectiu general d'aquesta tesis consistia en desenvolupar solucions biològiques sintètiques que podrien ajudar a augmentar els rendiments fotosintètics i l'eficiència en l'ús de l'aigua de les plantes, d'aquesta manera millorant els rendiments dels cultius.

Es van seguir dues estratègies diferents amb el mateix objectiu d'augmentar la fotosíntesi i l'EUA. La primera estratègia formava part del projecte MAGIC, descrit a la introducció, amb l'objectiu d'incrementar la fotosíntesis generant un MCC al cloroplasts d'una planta C_3 així reduint l'activitat oxigenasa de la Rubisco. Es tractava d'incorporar la NpHR i la AE1 a la membrana interna del cloroplasts per tal que incrementessin el HCO_3^- a l'estroma. Una tercera proteïna, bCMO1, també va haver de ser incorporada per tal de proveir el retinal necessari per al correcte funcionament de la NpHR.

La segona estratègia consistia en augmentar l'eficiència fotosintètica i l'EUA a través de la manipulació de la cinètica de l'estoma, per tal de ficar en concordança l'obertura estomàtica amb la demanda pel CO_2 del mesòfil. Primer es va comprovar, mitjançant el model OnGuard, les possibilitats de canviar les cinètiques dels estomes quan les propietats de voltatge dels canals K_{in} van ser modificades, i també quan una proteïna externa, en aquest cas la NpHR, va ser introduïda a les membranes de les

cèl·lules de guarda. Un cop analitzats els resultats del model es va voler comprovar *in vivo* els efectes de les diferents modificacions estomàtiques.

8.3 Resultats

8.3.1. Enginyant un MCC al cloroplast

L'objectiu del treball presentat en aquest capítol era expressar les dues proteïnes transmembrana, NpHR i AE1, a la membrana interna del cloroplasts; i la proteïna soluble, bCMO1, a l'estroma del cloroplasts per tal de proveir el retinal necessari per la NpHR. Després es va comprovar la correcta localització de les proteïnes, la seva activitat i els seus efectes en assimilació fotosintètica i conductància estomàtica.

Primer es varen expressar les proteïnes de forma transient i en tabac per a comprovar si era possible la seva expressió a la cèl·lula vegetal ja que cap de les tres proteïnes és originària de plantes. La NpHR és bacteriana, la AE1 és humana i la bCMO1 utilitzada és de ratolí. Es van crear diferents plàsmids expressant les proteïnes sota l'expressió del promotor 35S i UBQ10. Tot i que els futurs experiments es van centrar només en el promotor 35S ja que és el que donava una millor expressió de les proteïnes a la cèl·lula. Mitjançant el microscopi confocal es va comprovar la localització de les proteïnes, ja que aquestes anaven lligades a una proteïna fluorescent verda o vermella indiferentment (GFP or RFP). L'expressió de la NpHR va ser observada al tonoplast de les cèl·lules de tabac. L'expressió de l'AE1 va ser observada, per contra, al reticle endoplasmàtic (RE). Finalment, l'expressió de la bCMO1 va ser observada al citosol de la cèl·lula vegetal.

Un cop verificada l'expressió de les diferents proteïnes en tabac, es va procedir a crear nou plàsmids, aquests cops amb seqüències diana per a la correcta localització de les diferents proteïnes al cloroplasts. Per a l'expressió de les proteïnes NpHR i AE1 a la membrana interna del cloroplasts es van utilitzar la seqüència diana TPT, un translocador triosafosfat indicat per a aquest tipus de localització. En canvi, per la localització a l'estroma de la proteïna bCMO1 es va utilitzar la subunitat gran de la Rubisco (RbcL) com a seqüència diana. Un cop més, utilitzant microscòpia confocal,

va ser possible verificar la correcta localització de les proteïnes. Es va analitzar la localització de les proteïnes en diferents cloroplasts de transformacions diferents i, fins i tot, es van realitzar el que anomenem "line-scan" que és una exploració en línia d'una secció específica de la imatge a analitzar. A partir del line-scan és possible calcular la quantitat de fluorescència emesa a la zona seleccionada, com també diferenciar la fluorescència entre les diferents proteïnes i l'autofluorescència de la clorofil·la, i ens permet verificar la localització de l'expressió de la proteïna.

Com que l'objectiu final del projecte és expressar les tres proteïnes juntes al cloroplast, es varen fer transformacions transients en tabac co-expressant les diferents proteïnes. Utilitzant microscòpia electrònica es va comprovar que era possible la expressió en tabac de més d'una proteïna amb co-localització. No obstant, també es va observar que, tot i que algunes cèl·lules estaven transformades amb les dues o tres proteïnes utilitzades per la transformació, algunes cèl·lules tan sols expressaven una proteïna sola. El següent pas realitzat va ser expressar les proteïnes conjuntament en un mateix vector, per tal de tenir co-localització de les proteïnes a totes les cèl·lules transformades. Per tal d'expressar dues proteïnes en un mateix vector es va utilitzar un vector 2en1 anomenat pFRETgc-2in1-CC (Hecker, Wallmeroth et al. 2015), el qual és un vector compatible amb la metodologia de clonatge Gateway. En aquest vector es van co-expressar les proteïnes NpHR amb la AE1, i també la NpHR amb la bCMO1. Per tal d'expressar les tres proteïnes al mateix vector, es va clonar la bCMO1 seguint la metodologia de clonatge clàssic, dins del plàsmid d'expressió que contenia les proteïnes NpHR i AE1, creant un nou plàsmid d'expressió el qual es va anomenar 3en1. A la figura 8.1 es pot veure una imatge de microscòpia confocal que mostra la localització de la NpHR en verd i la AE1 en vermell. L'expressió de la proteïna bCMO1 es mostra en els resultats del western blot (figura 8.1F), la qual no es veu en microscòpia confocal ja que la proteïna no anava lligada a un tag fluorescent sinó a un tag 6-His identificable per wester blot gràcies a un antibodi anti-His.

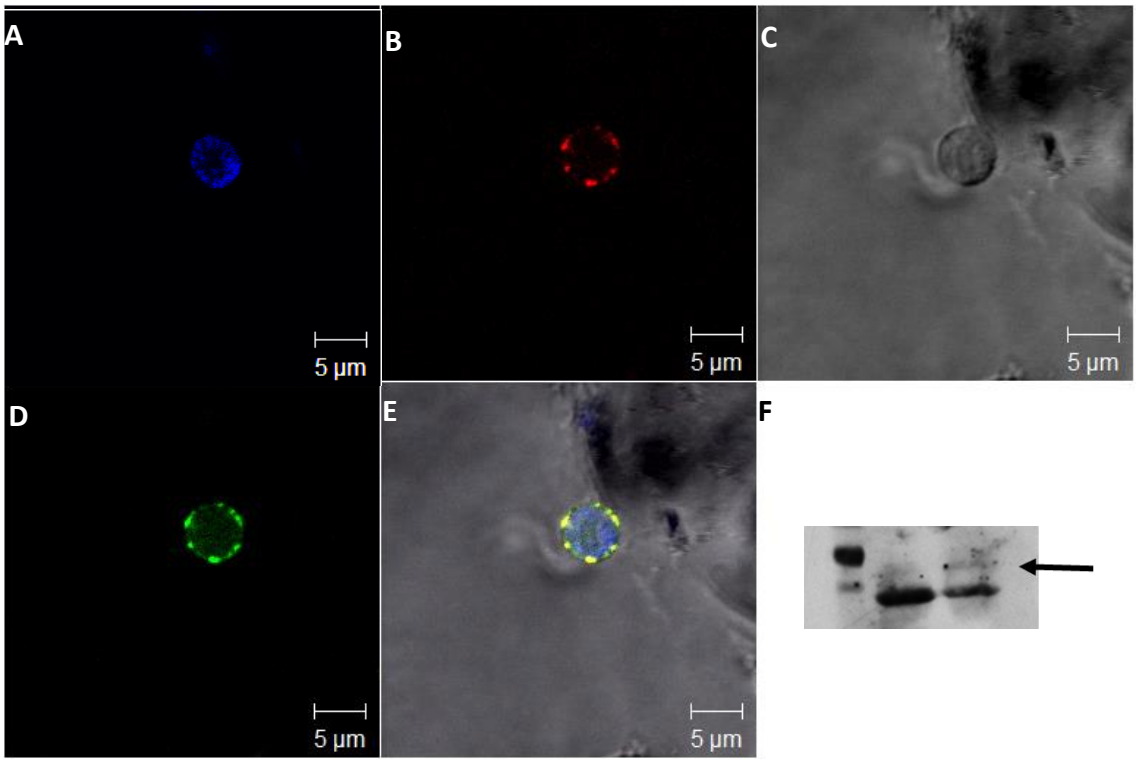

Figura 8.1. Expressió del plàsmid de destinació 3en1. El plàsmid conté 35S::TPT-AE1-mCherry, 35S::RbcL-bCMO1-6His I 35S::TPT-NpHR-GFP. L'expressió de AE1 (vermell, B) i NpHR (verd, D) es troba localitzada a la membrana interna del cloroplasts. L'autofluorescència de la clorofil·la està indicada en blau (A, E). C és la imatge en camp clar, i E mostra una imatge fusionada de tots els canals, on es possible d'observar co-localització d'ambdues proteïnes (groc). F mostra un anàlisis western blot fet amb un antibodi comercial anti-histidina, la fletxa indica la banda de la proteïna bCMO1 a 74 KDa, no expressada a la mostra del wild-type. La banda grossa de sota és l'expressió de la Rubisco. Les imatges de microscopi són d'un Z-stack de 19-talls a través de les cèl·lules de l'epidermis amb 0.75 d d'interval entre talls. A totes les imatges l'escala és de 5 µm.

A les imatges de microscopi es va observar que alguns dels cloroplasts transformats presentaven una morfologia atípica, caracteritzada per una forma més inflada dels cloroplasts i pel desplaçament de la grana cap a una sola banda de l'estroma en comptes d'estar ben repartida. Aquesta morfologia atípica es va poder observar tan sols quan hi havia expressió de la NpHR o de la AE1, i podria ser deguda a l'activitat de les proteïnes al causar flux iònic a través de la membrana i afectant l'osmolaritat del cloroplasts. No obstant, també podria ser possible que la sola presència de les proteïnes afectés al cloroplasts d'alguna manera causant aquesta atípica morfologia, sense estar relacionada amb l'activitat de les proteïnes.

Atesa aquesta atípica morfologia es va establir un mètode per a classificar els cloroplasts en diferents nivells depenent del grau de l'afectació. Es va establir el nivell 0 pels cloroplasts que no estaven afectats; el nivell 1 pels cloroplasts que presentaven una moderada morfologia atípica; finalment es va establir nivell 2 als cloroplasts que presentaven una forta afectació (Figura 8.2.). Seguint aquest criteri es va calcular quin tant era el grau d'afectació dels cloroplasts depenent de quina proteïna estaven expressant. Després de realitzar un anàlisis estadístic es va veure que realment els cloroplasts presentaven una morfologia atípica comparats amb el control.

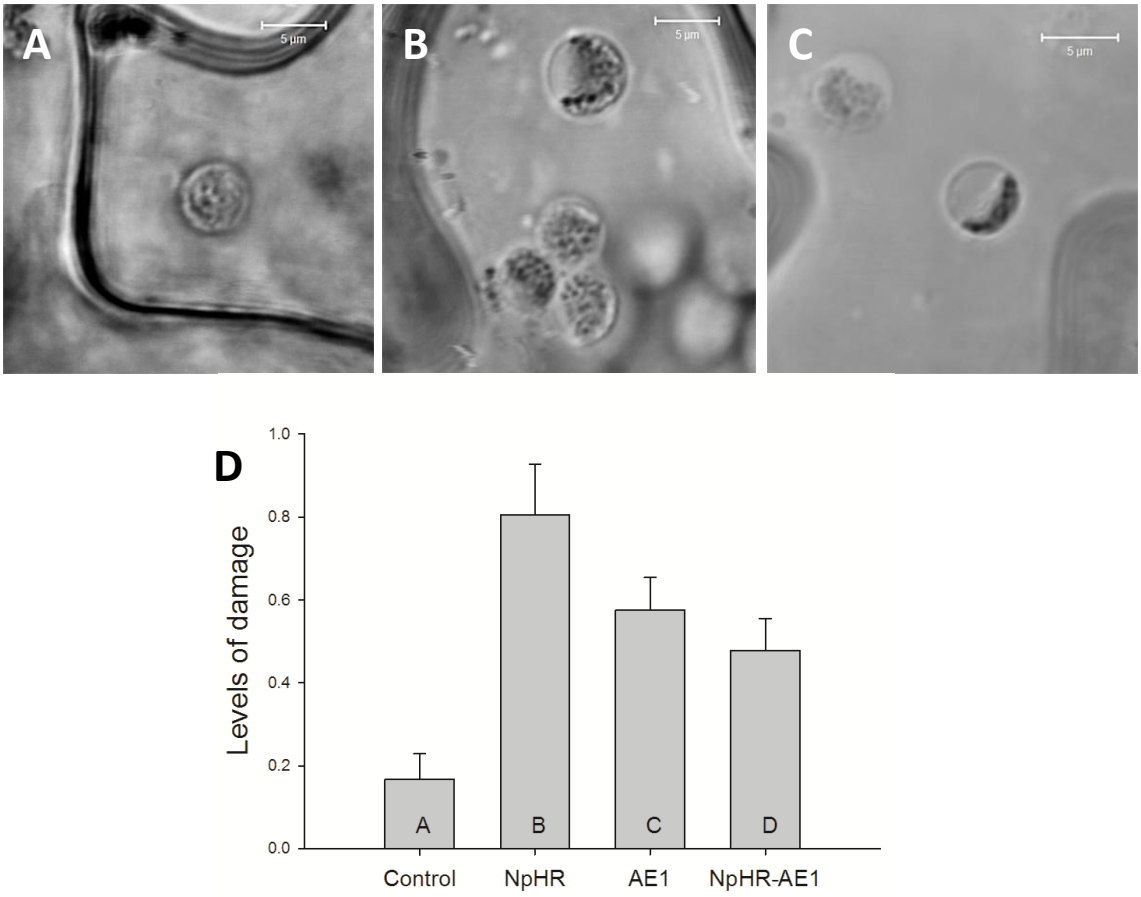

Figura 8.2. (A-C) Diferents nivells de morfologia atípica establerta, en relació a la atípica morfologia obtinguda entre els cloroplasts analitzats. A-C són imatges de camp clar fetes amb microscòpia confocal de cloroplasts de tabac transformat de forma transient. A, B i C mostren un exemple de cloroplasts de nivell de morfologia atípica igual a 0, 1 i 2 respectivament. A és una reconstrucció en 3D d'un Z-stac de 24 talls a través del cloroplast, amb un interval de 0.8 µm entre talls. En totes les figures l'escala és de 5 µm. D mostra l'anàlisi dels diferents graus de morfologia atípica en cloroplasts transformats amb els diferents plàsmids i comparats amb el control. Control: cèl·lules infiltrades amb *Agrobacterium* no transformat. Les lletres indiquen les diferències significatives analitzades per one-way ANOVA ($p<0.05$) determinades pel test de Holm-Sidak.

Per mirar l'activitat de la bCMO1 es va realitzar una cromatografia líquida d'alta resolució (HPLC) feta per un company del projecte MAGIC. Es van analitzar els cloroplasts que s'havien obtingut prèviament transformats de forma transient amb bCMO1. Als resultats de la HPLC es va observar que els nivells de b-carotè dels cloroplasts transformats eren la meitat dels nivells observats en cloroplasts no

transformats. Això indica el correcte funcionament de l'enzim bCMO1, el qual trenca les molècules de b-carotè formant dues molècules de retinal.

Finalment es van seleccionar diferents plàsmids per transformar Arabidopsis i obtenir línies estables expressant les diferents proteïnes. Un cop obtingudes les plantes es van realitzar anàlisis d'intercanvi de gasos per a veure si hi havia algun efecte en fotosíntesis produït per l'expressió de les proteïnes a la planta. A la Figura 8.3 es pot veure els resultats de la primera línia de transgènic analitzada, de tres línies analitzades en total.

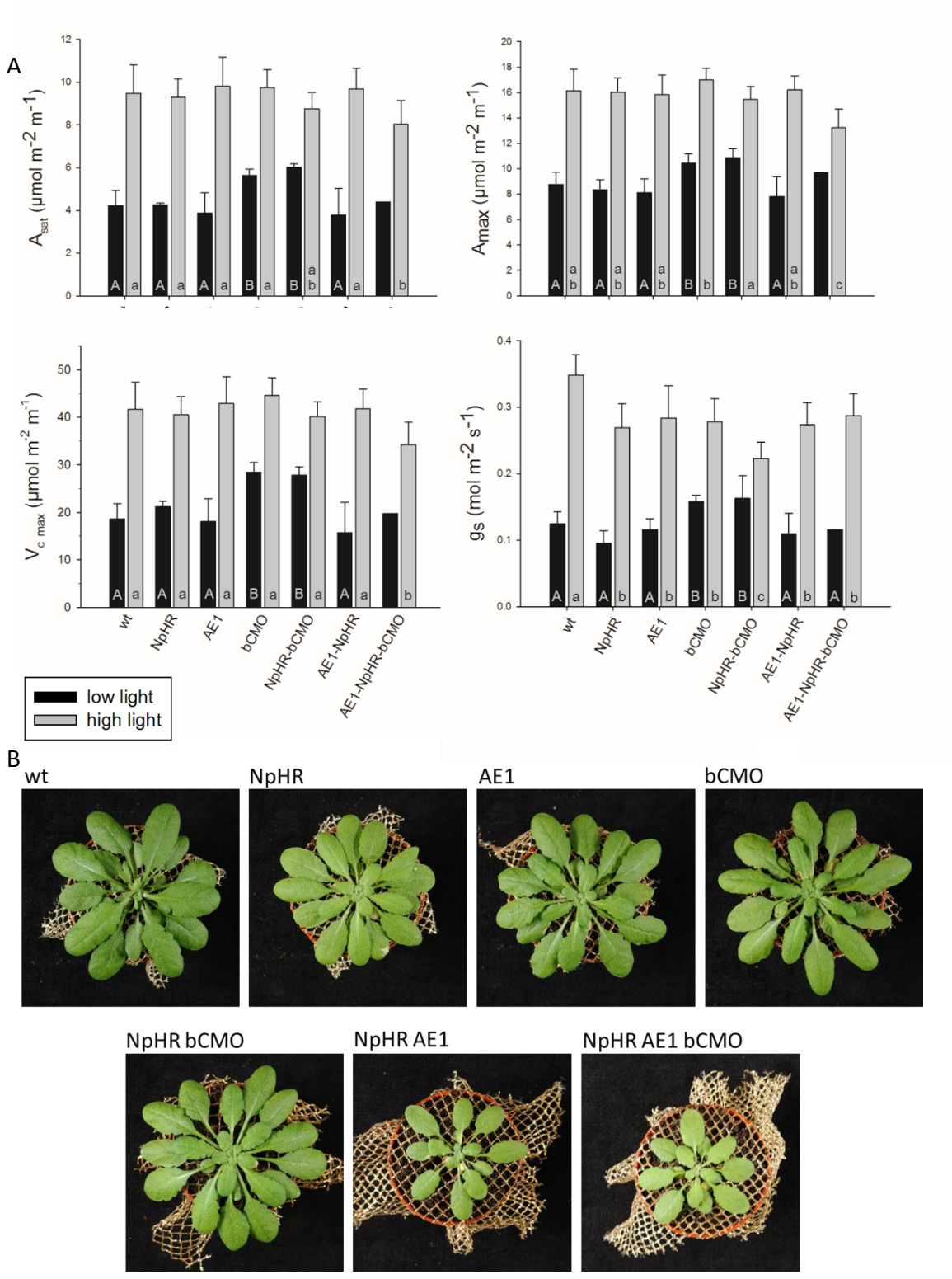

Figura 8.3. (A) Valors de mesures d'intercanvi de gasos de la 1era línia de plantes d'Arabidopsis transgèniques analitzades. Taxa d'assimilació de CO2 a llum saturada

(Asat), taxa d'assimilació de CO2 quan la llum i el carboni són saturants (Amax), velocitat màxima de carboxilació de la Rubisco (Vc max) i conductància estomàtica (gs) dels sis diferents tipus de plantes transgèniques analitzades comparades amb el wild-type. Les plantes varen créixer sota condicions de llum alta (300 µmol m-2 s-1) o baixa (70 µmol m-2 s-1). Els experiments es van realitzar a llum saturant de 500 µmol m-2 s-1 (10 % Blue). La temperatura de la fulla es va mantenir a 22°C durant la realització de l'experiment. Les dades obtingudes són les mitjanes de diferents rèpliques analitzades. Les lletres indiquen les diferències significatives analitzades per one-way ANOVA ($p<0.05$) determinades pel test de Holm-Sidak. (B) Fenotip de les plantes de la 1era línia de transgènics analitzats expressant els sis diferents plàsmids seleccionats per a transformar Arabidopsis (NpHR, AE1, bCMO1, NpHR-bCMO1, NpHR-AE1 and NpHR-AE1-bCMO1).

8.3.2 Manipulació de la cinètica de l'estoma

8.3.2.1 KAT1

Es va voler comprovar quins serien els efectes de manipular les propietats del voltatge d'un dels principals canals d'entrada de K^+ a la cèl·lula de guarda durant l'obertura estomàtica, el KAT1. Primer es va simular en el model OnGuard, com afectaria a les propietats cinètiques de l'estoma el fet de canviar la $V_{1/2}$ dels canals K_{in} cap a valors més positius i més negatius en relació als valors normals (-180 mV). Es van simular 4 situacions diferents, en dues de les quals es va canviar la $V_{1/2}$ cap a valors més positius iguals a -160 i -120 mV, i en les altres dues es va canviar cap a valors més negatius iguals a -200 i – 240 mV. En els resultats obtinguts es va poder observar que el model havia predit un canvi en la cinètica de l'estoma. El model va predir grans variacions tan en l'obertura estomàtica com en la turgència, volum i voltatge de membrana. En canviar la $V_{1/2}$ cap a valors més positius en relació a la normalitat, l'obertura succeïa més ràpidament al començament del dia i assolia valors d'obertura més elevats. Malgrat això, l'estoma es mantenia obert durant la nit. En canvi, al variar la $V_{1/2}$ cap a valors més negatius de la normalitat derivava a una resposta oposada. En aquest cas, l'obertura estomàtica es va mantenir gairebé tancada durant tot el cicle complet.

Per tal de validar les prediccions del model es van generar plantes transgèniques d'Arabidopsis presentant les modificacions descrites prèviament, en la $V_{1/2}$ del canal KAT1. S'ha trobat que el mutant $KAT1^{F102W}$ canvia les propietats de la $V_{1/2}$ cap valors

més negatius, mentre que el mutant KAT1^{D105E} canvia les propietats de la $V_{1/2}$ cap a valors més positius (Lefoulon, Karnik et al. 2014, Grefen, Karnik et al. 2015). Per tants, aquests dos mutants van ser utilitzats per a generar plantes transgèniques d'Arabidopsis per tal d'examinar els efectes en intercanvi de gasos i comparar la resposta dels estomes *in vivo* amb les prediccions del model. Es van generar diferents plàsmids expressant els diferents mutants i el gen natural del canal KAT1 (KAT1^{wt}) sota l'expressió tant del promotor 35S com d'un promotor específic per a les cèl·lules de guarda (GCP) *At*MYB60 (Cominelli, Galbiati et al. 2011). També es va unir una proteïna fluorescent juntament als gens del KAT1 per tal de poder identificar la localització a les cèl·lules de guarda un cop les línies de transgènics van ser obtingudes (Figura 8.4.).

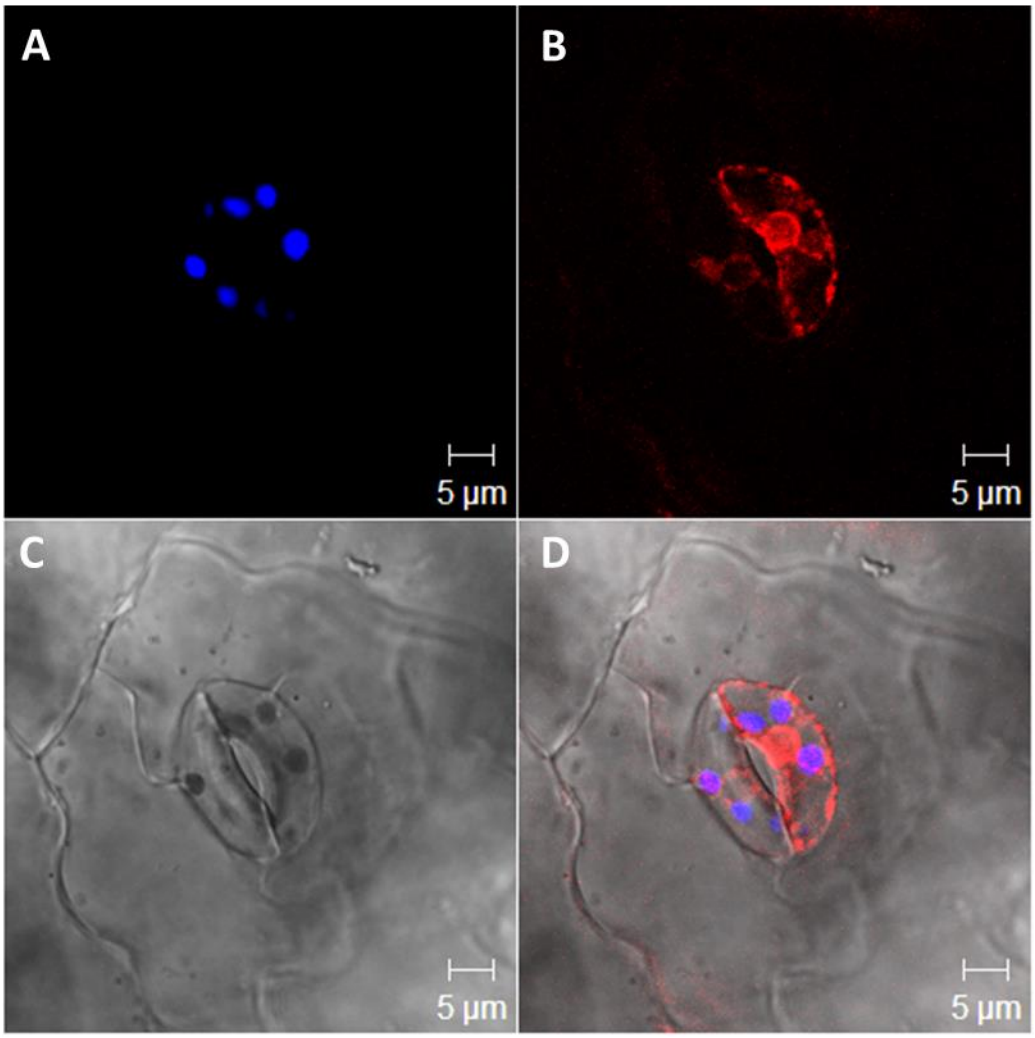

Figura 8.4. Expressió del plàsmid GCP::KAT1D105E-RFP en tabac transformat de forma transient, després de 3 dies de la transformació. La fluorescència del RFP (vermell) indica localització del KAT1D105E a la membrana plasmàtica i al RE de les cèl·lules de guarda (B, D). L'autofluorescència de la clorofil·la es mostra en blau (A, D) indicant la localització dels cloroplasts. C és la imatge de camp clar, i D mostra la imatge fusionada. Les imatges són d'un Z-stack de 15 talls a través de la cèl·lula de l'epidermis amb 0.7 µm d'interval entre els talls. A totes les imatges l'escala és 5 µm.

Es van realitzar diferents anàlisis d'intercanvi de gasos en les plantes transgèniques d'Arabidopsis obtingudes. Es van analitzar els valors de A_{sat}, A_{max}, $V_{c\,max}$ i g_s en plantes de la primera generació de transgènics. Es van fer créixer les plantes en altes (300 µmol m-2 s-1) i baixes (70 µmol m-2 s-1) condicions de llum i es van realitzar anàlisis d'intercanvi de gasos utilitzant el Li-COR 6400XT. La Figura 8.5 mostra els resultats dels anàlisis d'intercanvi de gasos realitzats en plantes d'Arabidopsis transformades amb tots els diferents plàsmids seleccionats i crescudes sota condicions de llum altes.

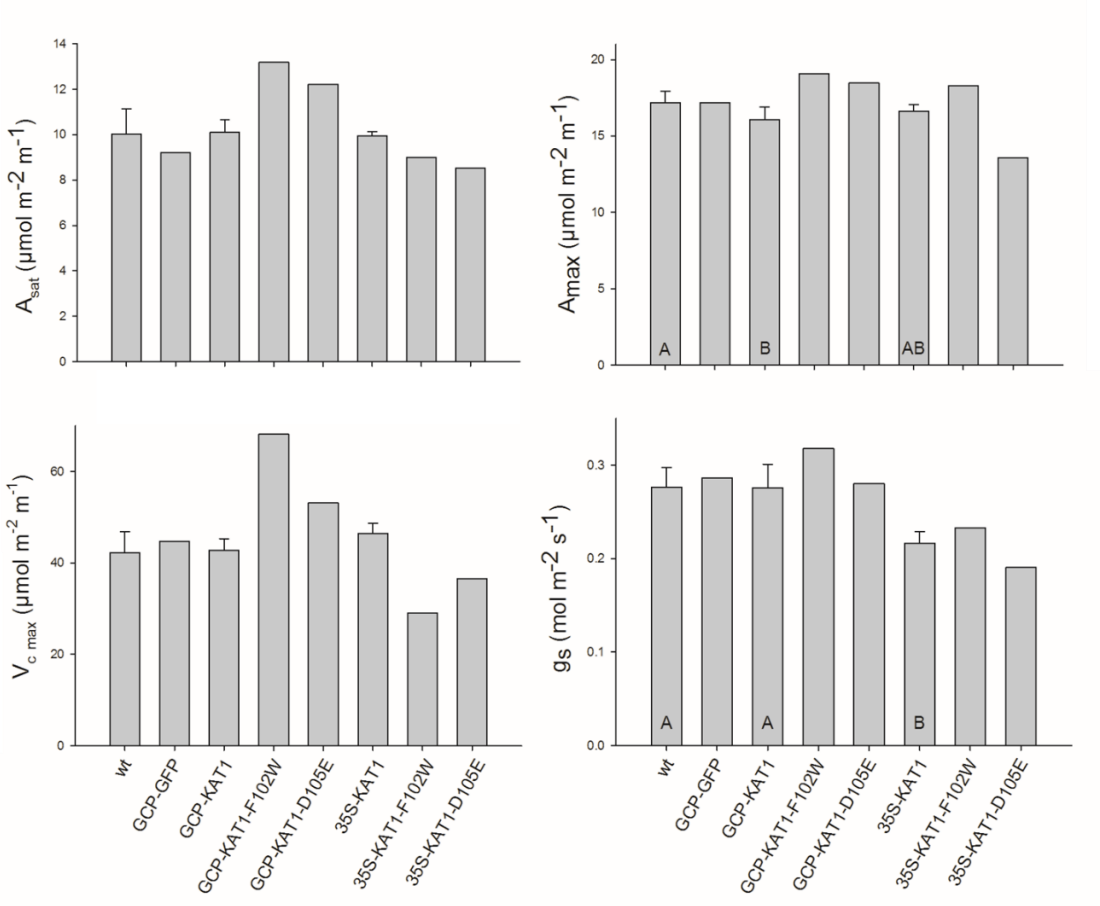

Figura 8.5. Valors de mesures d'intercanvi de gasos de plantes transgèniques d'Arabidopsis transformades amb els plàsmids GCP::GFP, GCP::KAT1, GCP::KAT1F102W, GCP::KAT1D105E, 35S::KAT1, 35S::KAT1F102W, 35S::KAT1D105E i wild-type. Taxa d'assimilació de CO2 a llum saturada (Asat), taxa d'assimilació de CO2 quan la llum i el carboni són saturants (Amax), velocitat màxima de carboxilació de la Rubisco (Vc max) i conductància estomàtica (gs). Les plantes varen créixer sota condicions de llum alta (300 µmol m-2 s-1). Els experiments es van realitzar a llum saturant de 500 µmol m-2 s-1 (10 % Blue). La temperatura de la fulla es va mantenir a 22°C durant la realització de l'experiment. Les lletres indiquen les diferències

significatives analitzades per one-way ANOVA ($p<0.05$) determinades pel test de Holm-Sidak. Les columnes sense barres d'error indiquen que només una mostra va ser analitzada, per tant no es va realitzar en aquestes l'anàlisi estadístic.

8.3.2.2 NpHR

Es va simular en el model OnGuard com afectaria a la cinètica de l'estoma la introducció d'una bomba de ions externa, en aquest cas la NpHR, introduïda a la cèl·lula de guarda de manera sintètica. Es van simular l'expressió tant a la membrana plasmàtica com al tonoplast de diferent nombres de NpHR, començant per 0.1 milions (M) de NpHR fins a arribar a un valor total de 5 M de bombes iòniques per cèl·lula. En total es van simular sis condicions diferents a cada una de les membranes (0.1 M, 0.2 M, 0.5 M, 1 M, 2 M, 5 M NpHR). Un cop analitzats els resultats predits pel model es va observar que l'expressió de NpHR al tonoplast no afectava a la cinètica de l'estoma. En canvi, expressar la mateixa proteïna a la membrana plasmàtica sí que afectava a la cinètica de l'estoma i d'una manera molt contundent. Quan la NpHR estava expressada a la membrana plasmàtica, l'estoma s'obria molt ràpidament davant l'estímul de llum i la seva obertura era molt major que sense l'expressió de la proteïna. A més a més, l'expressió de NpHR també permetia un tancament més ràpid de l'estoma al final del dia.

Es va voler comprovar si era possible de reproduir in vivo els mateixos resultats predits pel model. El primer pas a seguir va ser expressar la NpHR a la membrana plasmàtica de la cèl·lula vegetal. Sense cap seqüència diana, l'expressió de la proteïna s'observava o bé al RE, o bé al tonoplast, però mai a la membrana plasmàtica. Fins al moment, no hi ha descrita cap seqüència diana que permeti l'expressió de les proteïnes a la membrana plasmàtica. Tampoc es coneixen els mecanismes que permeten l'expressió a la membrana plasmàtica d'una proteïna. Per tant es van tenir que seguir diferents estratègies fins a trobar-ne una que permetés poder expressar la NpHR a la membrana plasmàtica en plantes. L'estratègia que va resultar ser exitosa va ser la de fusionar la NpHR amb una proteïna que s'expressés a la membrana plasmàtica de forma natural, per tal de que aquesta proteïna arrossegués amb ella la NpHR per a que ambdues quedessin expressades a la

membrana. Es van fusionar diverses proteïnes de membrana amb la NpHR, i finalment es va poder localitzar la NpHR a la membrana plasmàtica quan es va fusionar amb la AHA2. La localització de la NpHR a la membrana plasmàtica es va realitzar mitjançant microscòpia confocal en plantes de tabac transformades de forma transient amb la fusió NpHR-AHA2 (Figura 8.6).

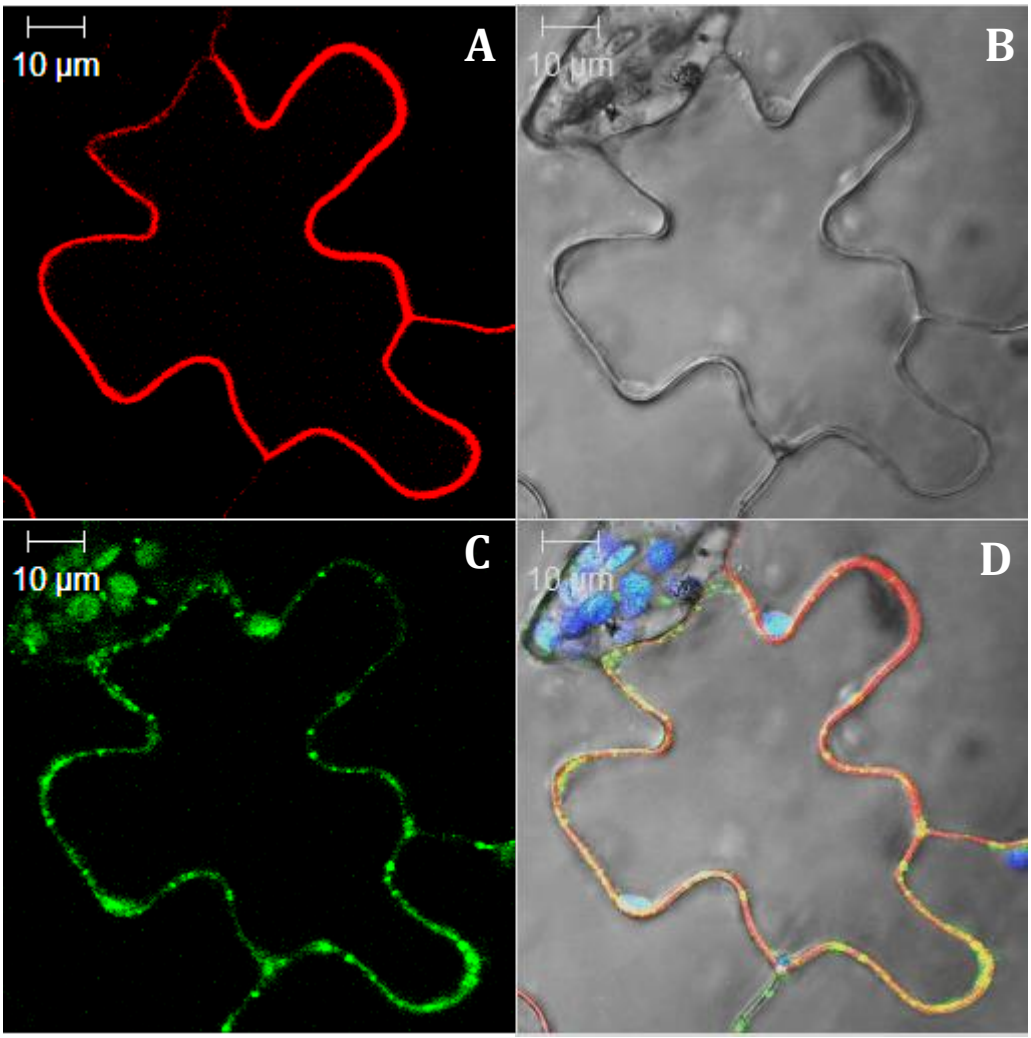

Figura 8.6. Expressió del plàsmid 35S::NpHR-AHA2-GFP co-localitzat amb el plàsmid 35S::AHA2-RFP en tabac 3 dies després d'estar transformat de forma transient. La fluorescència RFP (vermell) indica localització de la AHA2 a la membrana plasmàtica de les cèl·lules de l'epidermis (A, D). La fluorescència GFP (verd) indica localització de la fusió de proteïnes NpHR-AHA2 a la membrana plasmàtica de les cèl·lules de l'epidermis (C, D). L'autofluorescència de la clorofil·la es mostra en blau (D) indicant la localització del cloroplasts. B és la imatge de camp clar, i D és la imatge fusionada de tots els canals. Les imatges són extretes d'un Z-stack de 21 talls a traves de les

cèl·lules de l'epidermis, amb un interval d'1.5 µm entre talls. A totes les imatges l'escala és de 10 µm.

Un cop aconseguida l'expressió de la NpHR a la membrana plasmàtica es van generar plantes transgèniques d'Arabidopsis expressant la NpHR a les diferents membranes. Es van generar també plàsmids expressant la NpHR i la fusió NpHR-AHA2 juntament amb la bCMO1 en el mateix vector per tal de poder expressar les proteïnes amb co-localització a totes les cèl·lules transformades. També es van generar plàsmids expressant la NpHR i la fusió NpHR-AHA2 sota l'expressió del promotor específic per les cèl·lules de guarda. Tots aquests plàsmids van ser utilitzats per a transformar plantes d'Arabidopsis per tal de generar plantes transgèniques. Es va poder aconseguir llavors de la generació T1, en les quals s'haurà de realitzar experiments d'intercanvi de gasos per a comprovar que les prediccions del model són reproduïbles in vivo.

8.4 Discussió

8.4.1 Enginyant un MCC al cloroplast

L'expressió de les proteïnes transmembrana NpHR i AE1 a la membrana interna del cloroplast va ser possible gràcies a la seqüència diana TPT. També va ser possible localitzar la proteïna bCMO1 al cloroplasts, en aquest cas però, es va utilitzar la subunitat gran de la Rubisco (RbcL) com a seqüència diana per tal de localitzar la proteïna a l'estroma del cloroplasts, ja que es tracta d'una proteïna soluble. A més a més es va aconseguir combinar les diferents proteïnes en una mateix vector per tal d'obtenir co-localització als cloroplasts en tabac transformat de forma transient.

Es va observar que alguns dels cloroplasts transformats amb la proteïna NpHR i AE1, tant si s'expressaven juntes com per separat, produïen un fenotip als cloroplasts. Aquest fenotip es va caracteritzar com a "morfologia atípica dels cloroplasts" tot i que encara roman per saber si va ser degut a l'activitat de les proteïnes o a la presència de les proteïnes en si. També roman desconegut si la morfologia atípica afecta negativament a l'activitat dels cloroplasts. Un anàlisis semi-quantitatiu de la morfologia atípica i la seva distribució entre els cloroplasts va mostrat una variació

significativa depenent de quina de les proteïnes s'expressava. La NpHR va ser la que causava una major afectació en la morfologia dels cloroplast, mentre que els efectes de l'expressió de l'AE1 eren menors. Curiosament, els efectes en la morfologia dels cloroplasts disminuïen si les dues proteïnes estaven co-expressades. Es poden extraure diverses conclusions d'aquests anàlisis, no obstant tot serien hipòtesis que cal que siguin consolidades amb dades funcionals. Així doncs, seria necessari demostrar l'activitat de les proteïnes calculant els flux iònics a traves de la membrana del cloroplasts. Malgrat això, encara ens és desconegut com estan interconnectats els diferents transportadors de la membrana dels cloroplasts, i encara més desconegut com un canvi extern causat per la introducció d'una proteïna externa afectaria aquestes interrelacions. Es va decidir de crear plantes transgèniques expressant les proteïnes per a calcular directament els efectes en fotosíntesis a nivell de tota la planta, com un pas més directe per tal de determinar els diferents efectes de l'expressió de les proteïnes als cloroplasts. Per sort, l'activitat de la bCMO1 va ser fàcilment detectable mitjançant un anàlisis en els nivells de b-carotè dels cloroplasts.

Desafortunadament, els resultats en intercanvi de gasos no van ser consistents entre les diferents línies de transgènics analitzades. Per tant, va ser difícil d'arribar a conclusions adequades sobre els efectes que tenien les diferents proteïnes en la fotosíntesis. Tot i això, ja es contemplava la possibilitat de que encara que el sistema creat estigués funcionant correctament, i per tant incrementant els nivells de HCO_3^- a l'estroma del cloroplasts, la planta no estigués fent més fotosíntesis. Futurs experiments s'han de centrar en verificar si hi ha un augment de HCO_3^- dins de l'estroma del cloroplasts. En el cas que sí que hi hagi un augment de HCO_3^-, però això no produeixi més fotosíntesis per la planta, caldria procedir a la segona part del projecte MAGIC, encarregada de crear un sistema de retenció del CO_2 per tal de que aquest sigui assequible per la Rubisco.

8.4.2 Manipulació de la cinètica de l'estoma

Les simulacions mitjançant el model OnGuard van ser molt útils per entendre les relacions entre els diferents transportadors i els flux iònics involucrats en el moviment estomàtic. En el cas del KAT1, el model va ser utilitzat per a simular un canvi de la $V_{1/2}$ cap a valor més positius i més negatius en relació al wild-type. El model va predir un increment de la capacitat dels canals K_{in} quan la $V_{1/2}$ va ser modificada cap a valors més positius, i resultats oposats quan la $V_{1/2}$ va ser modificada cap a valors més negatius. En definitiva, les principals prediccions envers la cinètica de l'estoma en el primer cas varen ser que els canals K_{in} milloraven el flux de K^+ i l'obertura durant el dia, amb el desavantatge que l'estoma no tancava eficaçment durant la nit. Per contra, reduir la capacitat per conduir el flux d'entrada de K^+, suprimia l'obertura estomàtica, produint canvis menors entre el dia i la nit.

Els avantatges d'afegir la NpHR a la membrana plasmàtica de la cèl·lula de guarda versus canviar les propietats de voltatge dels canals KAT1 van ser notables. El model va predir una obertura més ràpida de l'estoma quan la NpHR era activada per la llum, així com també un tancament de l'estoma més ràpid que en condicions normals al principi del període de foscor. Per contra, les simulacions van mostrat que l'expressió de la NpHR al tonoplast no tenia cap efecte apreciable en relació a la cinètica de l'estoma.

Es va decidir de realitzar experimentalment el que s'havia simulat al model per verificar si les prediccions podien ser reproduïbles in vivo. En el cas del KAT1 es varen utilitzar dos mutants, $KAT1^{D105E}$ i $KAT1^{F102W}$, els quals canvien els valors de la $V_{1/2}$ cap a valors més positius i més negatius respectivament (Lefoulon, Karnik et al. 2014, Grefen, Karnik et al. 2015). El repte en aquest cas va ser aconseguir expressió dels diferents mutants en línies estables de plantes d'Arabidopsis transgèniques per poder realitzar anàlisis d'intercanvi de gasos. Per la NpHR els reptes encara van ser majors, ja que va ser necessari establir una localització correcta de la proteïna a la membrana plasmàtica, on la cosa es va complicar. Es van realitzar diferents estratègies per aconseguir la correcta expressió de la NpHR a la membrana

plasmàtica. Finalment es va aconseguir mitjançant la fusió d'aquesta proteïna amb AHA2. A més, per una exclusiva localització de les proteïnes a les cèl·lules de guarda es van generar vectors amb el promotor *At*MYB60, específic per l'expressió en aquestes cèl·lules.

Es van poder generar plantes d'Arabidopsis transformades amb tots els plàsmids seleccionats tant del KAT1 com de la NpHR. No obstant, degut a la gran quantitat de temps necessari per aconseguir localització de la NpHR a la membrana plasmàtica, les plantes expressant els diferents plàsmids de la NpHR no van estar a punt pels experiments en intercanvi de gasos. Així doncs, els experiments en intercanvi de gasos només es van realitzar en plantes transformades amb la proteïna KAT1 i els seus mutants. No obstant una complicació afegida va ser que algunes de les línies generades amb l'estratègia del KAT1 van tenir una expressió pobra. Per tant, el nombre de línies amb bona expressió de les proteïnes va ser insuficient per obtenir dades significants d'intercanvi de gasos, per tal de poder ser comparades amb les prediccions del model.

8.5 Conclusions

8.5.1 Enginyant un MCC al cloroplast

1. Possible expressió de NpHR i AE1 a la membrana interna del cloroplasts gràcies a la seqüència diana TPT.

2. Possible expressió de bCMO1 a l'estroma del cloroplasts gràcies a la seqüència diana RbcL.

3. Possible expressió de diferents combinacions de les proteïnes amb co-localització quan es varen expressar en el mateix vector.

4. Demostrable activitat de bCMO1 en cloroplasts aïllats de tabac transformat de forma transient.

5. Observació fenotípica dels cloroplasts transformats amb NpHR i AE1 analitzada i caracteritzada com a morfologia atípica. La qual disminuïa quan les dues proteïnes estaven co-expressades.

6. Obtenció de plantes transgèniques expressant diferents combinacions de les tres proteïnes, NpHR, AE1 i bCMO1.

7. Els anàlisis dels intercanvi de gasos no mostra un augment en fotosíntesis de les plantes transgèniques.

8.5.2 Manipulació de la cinètica de l'estoma

1. El model OnGuard va predir un canvi en la cinètica estomàtica al simular un canvi de la $V_{1/2}$ en els canals K_{in}. Així com també prediu un canvi en la cinètica estomàtica al simular la introducció de la proteïna NpHR a la membrana plasmàtica.

2. Expressar la NpHR en la membrana plasmàtica de les cèl·lules de guarda presenta avantatges respecte a modificar les propietats de voltatge del KAT1, ja que el model prediu una més ràpida i major obertura estomàtica sota un estímul de llum, així com també un més ràpid i complet tancament de l'estoma amb l'estímul de foscor. Obtenint amb la NpHR un perfecte exemple d'un estoma amb alta eficiència de moviment.

2. Mitjançant una estratègia de fusió de proteïnes es va aconseguir expressar la proteïna NpHR a la membrana plasmàtica amb l'objectiu de reproduir in vivo les prediccions del model.

3. Es van generar nous vectors amb el promotor específic de les cèl·lules de guarda *At*MYB60, i es van clonar les proteïnes sota l'expressió d'aquest vector del qual se'n va comprovar la seva específica localització i forta expressió de les proteïnes.

4. Es van generar plantes transgèniques d'Arabidopsis amb les dues estratègies, KAT1 i NpHR, expressant les proteïnes sota l'expressió del promotor específic de les cèl·lules de guarda, així com també del promotor 35S.

5. Es van poder analitzar plantes transgèniques d'Arabidopsis transformades amb el KAT1 i els seus mutants, tot i no haver obtingut un nombre suficient de mostres per establir relacions amb les prediccions del model OnGuard.

9. References

Acharya, B. R. and S. M. Assmann (2009). "Hormone interactions in stomatal function." Plant Mol Biol **69**(4): 451-462.

Ache, P., et al. (2000). "GORK, a delayed outward rectifier expressed in guard cells of Arabidopsis thaliana, is a K+-selective, K+-sensing ion channel." FEBS Lett **486**(2): 93-98.

Allen, G. J. and D. Sanders (1996). "Control of ionic currents in guard cell vacuoles by cytosolic and luminal calcium." The Plant Journal **10**(6): 1055-1069.

Allen, J. F. (2003). "Cyclic, pseudocyclic and noncyclic photophosphorylation: new links in the chain." Trends Plant Sci **8**(1): 15-19.

Aravanis, A. M., et al. (2007). "An optical neural interface: in vivo control of rodent motor cortex with integrated fiberoptic and optogenetic technology." Journal of neural engineering **4**(3): S143.

Assmann, S. (1999). "The cellular basis of guard cell sensing of rising CO2." Plant Cell Environ **22**(6): 629-637.

Assmann, S., et al. (1985). "Blue light activates electrogenic ion pumping in guard cell protoplasts of Vicia faba."

Atsumi, S., et al. (2008). "Non-fermentative pathways for synthesis of branched-chain higher alcohols as biofuels." Nature **451**(7174): 86-89.

Axelsen, K. B. and M. G. Palmgren (2001). "Inventory of the superfamily of P-type ion pumps in Arabidopsis." Plant Physiol **126**(2): 696-706.

Barnes, C. R. (1893). "On the food of green plants." Botanical Gazette **18**(11): 403-411.

Battisti, D. S. and R. L. Naylor (2009). "Historical warnings of future food insecurity with unprecedented seasonal heat." Science **323**(5911): 240-244.

Benner, S. A. and A. M. Sismour (2005). "Synthetic biology." Nat Rev Genet **6**(7): 533-543.

Blanck, A. and D. Oesterhelt (1987). "The halo-opsin gene. II. Sequence, primary structure of halorhodopsin and comparison with bacteriorhodopsin." EMBO J **6**(1): 265.

Blatt, M. and D. Gradmann (1997). "K+-sensitive gating of the K+ outward rectifier in Vicia guard cells." J Membr Biol **158**(3): 241-256.

Blatt, M. R. (1987). "Electrical characteristics of stomatal guard cells: The ionic basis of the membrane potential and the consequence of potassium chlorides leakage from microelectrodes." Planta **170**(2): 272-287.

Blatt, M. R. (1988). "Potassium-dependent, bipolar gating of K+ channels in guard cells." J Membr Biol **102**(3): 235-246.

Blatt, M. R. (1991). "Ion channel gating in plants: physiological implications and integration for stomatal function." J Membr Biol **124**(2): 95-112.

Blatt, M. R. (1999b). "Reassessing roles for Ca2+ in guard cell signalling." J Exp Bot **50**(Special Issue): 989-999.

Blatt, M. R. (2000). "Ca 2+ signalling and control of guard-cell volume in stomatal movements." Current Opinion in Plant Biology **3**(3): 196-204.

Blatt, M. R. (2000b). "Cellular signaling and volume control in stomatal movements in plants." Annu Rev Cell Dev Biol **16**(1): 221-241.

Blatt, M. R. (2008). "Ion Transport at the Plant Plasma Membrane." eLS.

Blatt, M. R. and F. Armstrong (1993). "K+ channels of stomatal guard cells: abscisic-acid-evoked control of the outward rectifier mediated by cytoplasmic pH." Planta **191**(3): 330-341.

Blatt, M. R. and G. M. Clint (1989). "Mechanisms of fusicoccin action: kinetic modification and inactivation of K+ channels in guard cells." Planta **178**(4): 509-523.

Blatt, M. R., et al. (1999). "Molecular events of vesicle trafficking and control by SNARE proteins in plants." New phytologist **144**(3): 389-418.

Blatt, M. R. and G. Thiel (1993b). "Hormonal control of ion channel gating." Annu Rev Plant Biol **44**(1): 543-567.

Block, M. A., et al. (2007). "Chloroplast envelope membranes: a dynamic interface between plastids and the cytosol." Photosynth Res **92**(2): 225-244.

CARMO-SILVA, A. E., et al. (2008). "Photorespiration in C4 grasses remains slow under drought conditions." Plant Cell Environ **31**(7): 925-940.

Chen, Z.-H., et al. (2012). "Systems dynamic modeling of the stomatal guard cell predicts emergent behaviors in transport, signaling, and volume control." Plant Physiol **159**(3): 1235-1251.

Chen, Z. and M. R. Blatt (2010). "Membrane transport in guard cells." Encyclopedia of life sciences.

Chen, Z. H., et al. (2012). "Systems dynamic modeling of the stomatal guard cell predicts emergent behaviors in transport, signaling, and volume control." Plant Physiol **159**(3): 1235-1251.

Chen, Z. H., et al. (2010b). "Dynamic regulation of guard cell anion channels by cytosolic free Ca2+ concentration and protein phosphorylation." The Plant Journal **61**(5): 816-825.

Cleaver, K. (2012). "Investing in agriculture to reduce poverty and hunger." Scaling Up in Agriculture, Rural Development and Nutrition **2020**.

Clint, G. M. and M. R. Blatt (1989). "Mechanisms of fusicoccin action: evidence for concerted modulations of secondary K+ transport in a higher plant cell." Planta **178**(4): 495-508.

Clough, S. J. and A. F. Bent (1998). "Floral dip: a simplified method forAgrobacterium-mediated transformation ofArabidopsis thaliana." The Plant Journal **16**(6): 735-743.

Cominelli, E., et al. (2011). "DOF-binding sites additively contribute to guard cell-specificity of AtMYB60 promoter." BMC Plant Biol **11**: 162.

De Pascalis, A. R., et al. (1993). "Binding of ferredoxin to ferredoxin: NADP+ oxidoreductase: the role of carboxyl groups, electrostatic surface potential, and molecular dipole moment." Protein Science **2**(7): 1126-1135.

Deisseroth, K. (2011). "Optogenetics." Nat Methods **8**(1): 26-29.

Deisseroth, K., et al. (2006). "Next-generation optical technologies for illuminating genetically targeted brain circuits." The Journal of Neuroscience **26**(41): 10380-10386.

Devery, J. and B. Milborrow (1994). "β-Carotene-15, 15'-dioxygenase (EC 1.13. 11.21) isolation reaction mechanism and an improved assay procedure." British Journal of Nutrition **72**(03): 397-414.

Dodd, A. N., et al. (2002). "Crassulacean acid metabolism: plastic, fantastic." J Exp Bot **53**(369): 569-580.

Dreyer, I. and M. R. Blatt (2009). "What makes a gate? The ins and outs of Kv-like K+ channels in plants." Trends Plant Sci **14**(7): 383-390.

Duschl, A., et al. (1990). "Properties and photochemistry of a halorhodopsin from the haloalkalophile, Natronobacterium pharaonis." Journal of Biological Chemistry **265**(3): 1261-1267.

Easterling, W., Aggarwal P, Batima P, Brander K, Erda L, Howden M, Kirilenko A,MortonJ,SoussanaJ-F,SchmidhuberJ,TubielloF (2007). Climate change 2007: Impacts, adaptation and vulnerability. Genebra, Suíça, Intergovernmental Panel On Climate Change, Intergovernmental Panel On Climate

Edwards, G. E., et al. (2001). "Compartmentation of photosynthesis in cells and tissues of C4 plants." J Exp Bot **52**(356): 577-590.

Ehleringer, J. and R. W. Pearcy (1983). "Variation in quantum yield for CO2 uptake among C3 and C4 plants." Plant Physiol **73**(3): 555-559.

Ehleringer, J. R. and T. E. Cerling (2002). "C3 and C4 photosynthesis." Encyclopedia of Global Environmental Change, The Earth system: biological and ecological dimensions of global environmental change **2**: 186-190.

Endy, D. (2005). "Foundations for engineering biology." Nature **438**(7067): 449-453.

Essen, L. O. (2002). "Halorhodopsin: light-driven ion pumping made simple?" Curr Opin Struct Biol **12**(4): 516-522.

Evans, J. R., et al. (2009). "Resistances along the CO2 diffusion pathway inside leaves." J Exp Bot **60**(8): 2235-2248.

Evans, J. R. and S. Von Caemmerer (1996). "Carbon dioxide diffusion inside leaves." Plant Physiol **110**(2): 339.

Evenson, R. E. and D. Gollin (2003). "Assessing the impact of the Green Revolution, 1960 to 2000." Science **300**(5620): 758-762.

FAO (2009). "How to feed the world in 2050." Food and Agriculture Organization (FAO).

FAO (2010). Global Forest Resources Assessment 2010 - main report. Rome, Food and Agriculture Organization of the United Nations.

FAO (2012). State of the World's Forests 2012 Rome, Food and Agriculture Organization of the United Nations.

FAO (2013). Biofuels and food security, The high level panel of experts on food security and nutrition.

FAO (2014). "IFAD (2012) The State of Food Insecurity in the World 2012: Economic growth is necessary but not sufficient to accelerate reduction of hunger and malnutrition." FAO, Rome.

Feng, Y. and R. E. McCarty (1990). "Subunit interactions within the chloroplast ATP synthase (CF0-CF1) as deduced by specific depletion of CF0 polypeptides." Journal of Biological Chemistry **265**(21): 12481-12485.

Fenno, L., et al. (2011). "The development and application of optogenetics." Annu Rev Neurosci **34**: 389-412

Fisher, J. and T. A. Henzinger (2007). "Executable cell biology." Nat Biotechnol **25**(11): 1239-1249.

Fraser, P. D., et al. (2009). "Genetic engineering of carotenoid formation in tomato fruit and the potential application of systems and synthetic biology approaches." Arch Biochem Biophys **483**(2): 196-204.

Freitag, H. and W. Stichler (2002). "Bienertia cycloptera Bunge ex Boiss., Chenopodiaceae, another C4 Plant without Kranz Tissues286." Plant Biol (Stuttg) **4**(1): 121-132.

Fricker, M., et al. (2006). "Quantitative fluorescence microscopy: from art to science." Annu. Rev. Plant Biol. **57**: 79-107.

Frohnmeyer, H., et al. (1998). "A role for the vacuole in auxin-mediated control of cytosolic pH by Vicia mesophyll and guard cells." The Plant Journal **13**(1): 109-116.

Furbank, R. T. and M. D. Hatch (1987). "Mechanism of C4 Photosynthesis The Size and Composition of the Inorganic Carbon Pool in Bundle Sheath Cells." Plant Physiol **85**(4): 958-964.

Gao, X. Q., et al. (2005). "The dynamic changes of tonoplasts in guard cells are important for stomatal movement in Vicia faba." Plant Physiol **139**(3): 1207-1216.

Gaxiola, R. A., et al. (2007). "Plant proton pumps." FEBS Lett **581**(12): 2204-2214.

Geelen, D., et al. (2002). "The Abscisic Acid–Related SNARE Homolog NtSyr1 Contributes to Secretion and Growth Evidence from Competition with Its Cytosolic Domain." Plant Cell **14**(2): 387-406.

Gilroy, S., et al. (1991). "Role of calcium in signal transduction of Commelina guard cells." Plant Cell **3**(4): 333-344.

Giordano, M., et al. (2005). "CO 2 concentrating mechanisms in algae: mechanisms, environmental modulation, and evolution." Annu. Rev. Plant Biol. **56**: 99-131.

Gobert, A., et al. (2007). "The two-pore channel TPK1 gene encodes the vacuolar K+ conductance and plays a role in K+ homeostasis." Proceedings of the National Academy of Sciences **104**(25): 10726-10731.

Gorton, H. L., et al. (1993). "Circadian rhythms in stomatal responsiveness to red and blue light." Plant Physiol **103**(2): 399-406.

Grabov, A. and M. R. Blatt (1999). "A steep dependence of inward-rectifying potassium channels on cytosolic free calcium concentration increase evoked by hyperpolarization in guard cells." Plant Physiol **119**(1): 277-288.

Gradinaru, D., et al. (2009). "Drug metabolizing enzyme expression in rat choroid plexus: effects of in vivo xenobiotics treatment." Arch Toxicol **83**(6): 581-586.

Gradinaru, V., et al. (2008). "eNpHR: a Natronomonas halorhodopsin enhanced for optogenetic applications." Brain Cell Biol **36**(1-4): 129-139.

Grefen, C., et al. (2010). "A ubiquitin-10 promoter-based vector set for fluorescent protein tagging facilitates temporal stability and native protein distribution in transient and stable expression studies." The Plant Journal **64**(2): 355-365.

Grefen, C., et al. (2015). "A vesicle-trafficking protein commandeers Kv channel voltage sensors for voltage-dependent secretion." Nature Plants **1**(8).

Grinstein, S., et al. (1978). "Anion transport in relation to proteolytic dissection of band 3 protein." Biochimica et Biophysica Acta (BBA)-Biomembranes **507**(2): 294-304.

Groves, J. D., et al. (1998). "Functional reassembly of the anion transport domain of human red cell band 3 (AE1) from multiple and non-complementary fragments." FEBS Lett **433**(3): 223-227.

Hamilton, D. W., et al. (2000). "Ca2+ channels at the plasma membrane of stomatal guard cells are activated by hyperpolarization and abscisic acid." Proc Natl Acad Sci U S A **97**(9): 4967-4972.

Hatch, M. D. (1987). "C 4 photosynthesis: a unique elend of modified biochemistry, anatomy and ultrastructure." Biochimica et Biophysica Acta (BBA)-Reviews on Bioenergetics **895**(2): 81-106.

Hattersley, P. and A. Browning (1981). "Occurrence of the suberized lamella in leaves of grasses of different photosynthetic types. I. In parenchymatous bundle sheaths and PCR ("Kranz") sheaths." Protoplasma **109**(3-4): 371-401.

Hecker, A., et al. (2015). "Binary 2in1 vectors improve in planta (co-) localisation and dynamic protein interaction studies." Plant Physiol: pp. 00533.02015.

Helmont, J. v. (1648). "Ortus medicinae." Amsterdam **1648**: 155.

Hetherington, A. M. and F. I. Woodward (2003). "The role of stomata in sensing and driving environmental change." Nature **424**(6951): 901-908.

Hills, A., et al. (2012). "OnGuard, a computational platform for quantitative kinetic modeling of guard cell physiology." Plant Physiol **159**(3): 1026-1042.

IPCC (2007). Climate change 2007: Impacts, adaptation and vulnerability. Genebra, Suíça, Intergovenrnamental Panel on Climate Change.

Irving, H. R., et al. (1992). "Changes in cytosolic pH and calcium of guard cells precede stomatal movements." Proceedings of the National Academy of Sciences **89**(5): 1790-1794.

Jahn, R. and R. H. Scheller (2006). "SNAREs—engines for membrane fusion." Nature reviews Molecular cell biology **7**(9): 631-643.

Jensen, P. E. and D. Leister (2014). "Chloroplast evolution, structure and functions." F1000Prime Rep **6**: 40.

Karimi, M., et al. (2007). "Recombinational cloning with plant gateway vectors." Plant Physiol **145**(4): 1144-1154.

Karimi, M., et al. (2007). "Recombinational cloning with plant gateway vectors." Plant Physiol **145**(4): 1144-1154.

Kinoshita, T., et al. (1995). "Cytosolic concentration of Ca2+ regulates the plasma membrane H+-ATPase in guard cells of fava bean." Plant Cell **7**(8): 1333-1342.

Kinoshita, T. and K. i. Shimazaki (1999). "Blue light activates the plasma membrane H+-ATPase by phosphorylation of the C-terminus in stomatal guard cells." EMBO J **18**(20): 5548-5558.

Kleinlogel, S., et al. (2011). "A gene-fusion strategy for stoichiometric and co-localized expression of light-gated membrane proteins." Nat Methods **8**(12): 1083-1088.

Kolbe, M., et al. (2000). "Structure of the light-driven chloride pump halorhodopsin at 1.8 Å resolution." Science **288**(5470): 1390-1396.

Koornneef, M. and D. Meinke (2010). "The development of Arabidopsis as a model plant." The Plant Journal **61**(6): 909-921.

Kopito, R. R. L., H. F. (1985). "Primary structure and transmembrane orientation of the murine anion exchange protein" Nature **316**: 234-238.

Kouyama, T., et al. (2010). "Crystal structure of the light-driven chloride pump halorhodopsin from Natronomonas pharaonis." J Mol Biol **396**(3): 564-579.

Kurisu, G., et al. (2001). "Structure of the electron transfer complex between ferredoxin and ferredoxin-NADP+ reductase." Nature Structural & Molecular Biology **8**(2): 117-121.

Kurukulasuriya, P. and S. Rosenthal (2003). "Climate change and agriculture: A review of impacts and adaptations."

Kwak, J. M., et al. (2003). "NADPH oxidase AtrbohD and AtrbohF genes function in ROS-dependent ABA signaling in Arabidopsis." EMBO J **22**(11): 2623-2633.

Laemmli, U. K. (1970). "Cleavage of structural proteins during the assembly of the head of bacteriophage T4." Nature **227**(5259): 680-685.

Lawson, T. and M. R. Blatt (2014). "Stomatal size, speed, and responsiveness impact on photosynthesis and water use efficiency." Plant Physiol **164**(4): 1556-1570.

Lawson, T., et al. (2012). "Improving yield by exploiting mechanisms underlying natural variation of photosynthesis." Curr Opin Biotechnol **23**(2): 215-220.

Lee, M., et al. (2008). "The ABC transporter AtABCB14 is a malate importer and modulates stomatal response to CO2." Nat Cell Biol **10**(10): 1217-1223.

Lee, S., et al. (1999). "Oligogalacturonic acid and chitosan reduce stomatal aperture by inducing the evolution of reactive oxygen species from guard cells of tomato and Commelina communis." Plant Physiol **121**(1): 147-152.

Lefoulon, C., et al. (2014). "Voltage-sensor transitions of the inward-rectifying K+ channel KAT1 indicate a latching mechanism biased by hydration within the voltage sensor." Plant Physiol **166**(2): 960-975.

Leyman, B., et al. (2000). "Localization and control of expression of Nt-Syr1, a tobacco snare protein." The Plant Journal **24**(3): 369-382.

Leyman, B., et al. (1999). "A tobacco syntaxin with a role in hormonal control of guard cell ion channels." Science **283**(5401): 537-540.

Lipka, V., et al. (2007). "SNARE-ware: the role of SNARE-domain proteins in plant biology." Annu. Rev. Cell Dev. Biol. **23**: 147-174.

Liu, W. and C. N. Stewart, Jr. (2015). "Plant synthetic biology." Trends Plant Sci.

Lux, S. E., et al. (1989). "Cloning and characterization of band 3, the human erythrocyte anion-exchange protein (AE1)." Proceedings of the National Academy of Sciences **86**(23): 9089-9093.

MacRobbie, E. (1995). "ABA-induced ion efflux in stomatal guard cells: multiple actions of ABA inside and outside the cell." The Plant Journal **7**(4): 565-576.

MacRobbie, E. (1997). "Signalling in guard cells and regulation of ion channel activity." J Exp Bot **48**(Special Issue): 515-528.

Maeshima, M. (2000). "Vacuolar H+-pyrophosphatase." Biochimica et Biophysica Acta (BBA)-Biomembranes **1465**(1): 37-51.

Mahan, J. R. and D. R. Upchurch (1988). "Maintenance of constant leaf temperature by plants—I. Hypothesis-limited homeothermy." Environmental and experimental botany **28**(4): 351-357.

Mansfield, T., et al. (1990). "Some current aspects of stomatal physiology." Annu Rev Plant Biol **41**(1): 55-75.

Martinoia, E., et al. (2007). "Vacuolar transporters and their essential role in plant metabolism." J Exp Bot **58**(1): 83-102.

Masibay, A., et al. (1993). "Mutational analysis of the Golgi retention signal of bovine beta-1, 4-galactosyltransferase." Journal of Biological Chemistry **268**(13): 9908-9916.

Matsuno-Yagi, A. and Y. Mukohata (1977). "Two possible roles of bacteriorhodopsin; a comparative study of strains of Halobacterium halobium differing in pigmentation." Biochem Biophys Res Commun **78**(1): 237-243.

McAinsh, M. R., et al. (1992). "Visualizing changes in cytosolic-free Ca2+ during the response of stomatal guard cells to abscisic acid." Plant Cell **4**(9): 1113-1122.

McClure, P., et al. (1989). "Response of the membrane potential of maize roots to nitrate." Plant Physiol **89**: S31-S45.

McMurtrie, R. and Y. P. Wang (1993). "Mathematical models of the photosynthetic response of tree stands to rising CO2 concentrations and temperatures." Plant Cell Environ **16**(1): 1-13.

Meckel, T., et al. (2007). "Guard cells elongate: relationship of volume and surface area during stomatal movement." Biophys J **92**(3): 1072-1080.

Medlyn, B., et al. (2001). "Stomatal conductance of forest species after long-term exposure to elevated CO2 concentration: A synthesis." New phytologist **149**(2): 247-264.

Meidner, H. and C. Willmer (1993). "Circadian rhythm of stomatal movements in epidermal strips." J Exp Bot **44**(11): 1649-1652.

Minguet-Parramona, C., et al. (2015). "Emergent oscillatory properties in modelling ion transport of guard cells " Rythyms in Plants.

Mitchell, P. (1966). Chemiosmotic coupling in oxidative and photosynthetic phosphorylation, Glynn Research Bodmin.

Morsomme, P. and M. Boutry (2000). "The plant plasma membrane H+-ATPase: structure, function and regulation." Biochimica et Biophysica Acta (BBA)-Biomembranes **1465**(1): 1-16.

Munro, S. (1995). "An investigation of the role of transmembrane domains in Golgi protein retention." EMBO J **14**(19): 4695.

Murata, Y., et al. (2001). "Abscisic acid activation of plasma membrane Ca(2+) channels in guard cells requires cytosolic NAD(P)H and is differentially disrupted upstream and downstream of reactive oxygen species production in abi1-1 and abi2-1 protein phosphatase 2C mutants." Plant Cell **13**(11): 2513-2523.

Nagel, G., et al. (2002). "Channelrhodopsin-1: a light-gated proton channel in green algae." Science **296**(5577): 2395-2398.

Nogués, S. and N. R. Baker (2000). "Effects of drought on photosynthesis in Mediterranean plants grown under enhanced UV-B radiation." J Exp Bot **51**(348): 1309-1317.

Oesterhelt, D. and W. Stoeckenius (1971). "Rhodopsin-like protein from the purple membrane of Halobacterium halobium." Nature **233**(39): 149-152.

Ottmann, C., et al. (2007). "Structure of a 14-3-3 coordinated hexamer of the plant plasma membrane H+-ATPase by combining X-ray crystallography and electron cryomicroscopy." Mol Cell **25**(3): 427-440.

Outlaw, W. H. and J. Manchester (1979). "Guard cell starch concentration quantitatively related to stomatal aperture." Plant Physiol **64**(1): 79-82.

Palmgren, M. G. (2001). "Plant plasma membrane H+-ATPases: powerhouses for nutrient uptake." Annu Rev Plant Biol **52**(1): 817-845.

Pandey, S., et al. (2007). "Roles of ion channels and transporters in guard cell signal transduction." FEBS Lett **581**(12): 2325-2336.

Pastrana, E. (2011). "Optogenetics: controlling cell function with light." Nat Methods **8**(1): 24-25.

Paul, J. A. and K. Wahlberg (2008). A New Era of World Hunger.

Pearcy, R. W. (1990). "Sunflecks and photosynthesis in plant canopies." Annu Rev Plant Biol **41**(1): 421-453.

Pedersen, B. P., et al. (2007). "Crystal structure of the plasma membrane proton pump." Nature **450**(7172): 1111-1114.

Pei, Z.-M., et al. (2000). "Calcium channels activated by hydrogen peroxide mediate abscisic acid signalling in guard cells." Nature **406**(6797): 731-734.

Pei, Z.-M., et al. (1996). "A novel chloride channel in Vicia faba guard cell vacuoles activated by the serine/threonine kinase, CDPK." EMBO J **15**(23): 6564.

Pei, Z. M., et al. (2000). "Calcium channels activated by hydrogen peroxide mediate abscisic acid signalling in guard cells." Nature **406**(6797): 731-734.

Peiter, E., et al. (2005). "The vacuolar Ca2+-activated channel TPC1 regulates germination and stomatal movement." Nature **434**: 404-408.

Poffenroth, M., et al. (1992). "Sugar Concentrations in Guard Cells of Vicia faba Illuminated with Red or Blue Light Analysis by High Performance Liquid Chromatography." Plant Physiol **98**(4): 1460-1471.

Price, G. D., et al. (2011). "The prospect of using cyanobacterial bicarbonate transporters to improve leaf photosynthesis in C3 crop plants." Plant Physiol **155**(1): 20-26.

Pringle, C. (1999). "Virus Taxonomy 1999 The Universal System of Virus Taxonomy, updated to include the new proposals ratified by the International Committee on Taxonomy of Viruses during 1998." Archives of virology **2**(144).

Radin, J. W., et al. (1994). "Genetic variability for stomatal conductance in Pima cotton and its relation to improvements of heat adaptation." Proceedings of the National Academy of Sciences **91**(15): 7217-7221.

Raines, C. A. (2003). "The Calvin cycle revisited." Photosynth Res **75**(1): 1-10.

Raschke, K. and H. Schnabl (1978). "Availability of chloride affects the balance between potassium chloride and potassium malate in guard cells of Vicia faba L." Plant Physiol **62**(1): 84-87.

Rea, P. A. and R. J. Poole (1993). "Vacuolar H+-translocating pyrophosphatase." Annu Rev Plant Biol **44**(1): 157-180.

Reuff, M., et al. (2010). "Trafficking, lateral mobility and segregation of the plant K+ channel KAT1*." Plant Biol (Stuttg) **12**(s1): 99-104.

Ritte, G., et al. (1999). "Rates of sugar uptake by guard cell protoplasts of Pisum sativum L. related to the solute requirement for stomatal opening." Plant Physiol **121**(2): 647-656.

Ro, D.-K., et al. (2006). "Production of the antimalarial drug precursor artemisinic acid in engineered yeast." Nature **440**(7086): 940-943.

Roelfsema, M. R., et al. (2012). "Anion channels: master switches of stress responses." Trends Plant Sci **17**(4): 221-229.

Rosenzweig, C., et al. (2002). "Increased crop damage in the US from excess precipitation under climate change." Global Environmental Change **12**(3): 197-202.

Sage, R. F. (2004). "The evolution of C4 photosynthesis." New Phytol **161(2)**: 341-370.

Sahr, K. E., et al. (1994). "The structure and organization of the human erythroid anion exchanger (AE1) gene." Genomics **24**(3): 491-501.

Sasaki, J., et al. (1995). "Conversion of bacteriorhodopsin into a chloride ion pump." Science **269**(5220): 73-75.

Sasaki, T., et al. (2009b). "Effect of Chloride Binding on the Thermal Trimer–Monomer Conversion of Halorhodopsin in the Solubilized System." Biochemistry **48**(51): 12089-12095.

Sasaki, T., et al. (2009). "Halorhodopsin from Natronomonas pharaonis Forms a Trimer Even in the Presence of a Detergent, Dodecyl-β-d-maltoside." Photochem Photobiol **85**(1): 130-136.

Sauer, T., et al. (2010). "Agriculture and resource availability in a changing world: The role of irrigation." Water Resources Research **46**(6).

Schachtman, D. P., et al. (1992). "Expression of an inward-rectifying potassium channel by the Arabidopsis KAT1 cDNA." Science **258**(5088): 1654-1658.

Schiøtt, M. and M. G. Palmgren (2005). "Two plant Ca2+ pumps expressed in stomatal guard cells show opposite expression patterns during cold stress." Physiologia Plantarum **124**(2): 278-283.

Schobert, B. and J. K. Lanyi (1982). "Halorhodopsin is a light-driven chloride pump." J Biol Chem **257**(17): 10306-10313.

Schroeder, J. I. (1988). "K+ transport properties of K+ channels in the plasma membrane of Vicia faba guard cells." J Gen Physiol **92**(5): 667-683.

Schroeder, J. I., et al. (2001b). "Guard cell signal transduction." Annu Rev Plant Biol **52**(1): 627-658.

Schroeder, J. I., et al. (1987). "Voltage dependence of K+ channels in guard-cell protoplasts." Proceedings of the National Academy of Sciences **84**(12): 4108-4112.

Seki, A., et al. (2007). "Heterologous expression of Pharaonis halorhodopsin in Xenopus laevis oocytes and electrophysiological characterization of its light-driven Cl- pump activity." Biophys J **92**(7): 2559-2569.

Serrano, E. E., et al. (1988). "Red light stimulates an electrogenic proton pump in Vicia guard cell protoplasts." Proceedings of the National Academy of Sciences **85**(2): 436-440.

Serrano, R. (1989). "Structure and function of plasma membrane ATPase." Annu Rev Plant Biol **40**(1): 61-94.

Sharpe, R. M. and S. Offermann (2014). "One decade after the discovery of single-cell C4 species in terrestrial plants: what did we learn about the minimal requirements of C4 photosynthesis?" Photosynth Res **119**(1-2): 169-180.

Shimazaki, K., et al. (1986). "Blue light-dependent proton extrusion by guard-cell protoplasts of Vicia faba."

Spanswick, R. M. (1981). "Electrogenic ion pumps." Annual Review of Plant Physiology **32**(1): 267-289.

Sparkes, I. A., et al. (2006). "Rapid, transient expression of fluorescent fusion proteins in tobacco plants and generation of stably transformed plants." Nat Protoc **1**(4): 2019-2025.

Spreitzer, R. J. and M. E. Salvucci (2002). "Rubisco: structure, regulatory interactions, and possibilities for a better enzyme." Annu Rev Plant Biol **53**: 449-475.

Sze, H., et al. (1999). "Energization of plant cell membranes by H+-pumping ATPases: regulation and biosynthesis." The Plant Cell Online **11**(4): 677-689.

Sze, H., et al. (2002). "A simple nomenclature for a complex proton pump: VHA genes encode the vacuolar H+-ATPase." Trends Plant Sci **7**(4): 157-161.

Taiz, L. and E. Zeiger (2010). "Plant physiology." 782.

Talbott, L. D. and E. Zeiger (1993). "Sugar and organic acid accumulation in guard cells of Vicia faba in response to red and blue light." Plant Physiol **102**(4): 1163-1169.

Thiel, G., et al. (1992). "Membrane transport in stomatal guard cells: the importance of voltage control." J Membr Biol **126**(1): 1-18.

Thiel, G. and A. H. Wolf (1997). "Operation of K+-channels in stomatal movement." Trends Plant Sci **2**(9): 339-345.

Torsethaugen, G., et al. (1999). "Ozone inhibits guard cell K+ channels implicated in stomatal opening." Proceedings of the National Academy of Sciences **96**(23): 13577-13582.

Uemura, T., et al. (2005). "The longin domain regulates subcellular targeting of VAMP7 in Arabidopsis thaliana." FEBS Lett **579**(13): 2842-2846.

UN (2010). Socio-economic assessments of climate change impacts, The United Nations Development Programme - Bratislava Regional Centre.

UN (2013). World population prospects: The 2012 revision. New York, Population Division of the Department of Economic and Social Affairs of the United Nations Secretariat.

Van Kirk, C. A. and K. Raschke (1978). "Presence of chloride reduces malate production in epidermis during stomatal opening." Plant Physiol **61**(3): 361-364.

Váró, G., et al. (1996). "Proton transport by halorhodopsin." Biochemistry **35**(21): 6604-6611.

Vitale, A. and N. V. Raikhel (1999). "What do proteins need to reach different vacuoles?" Trends Plant Sci **4**(4): 149-155.

Von Caemmerer, S., et al. (2012). "The Development of C4 Rice: Current Progress and Future Challenges." Science **336**(6089): 1671-1672.

Von Caemmerer, S. v. and G. Farquhar (1981). "Some relationships between the biochemistry of photosynthesis and the gas exchange of leaves." Planta **153**(4): 376-387.

Voznesenskaya, E. V., et al. (2002). "Proof of C4 photosynthesis without Kranz anatomy in Bienertia cycloptera (Chenopodiaceae)." The Plant Journal **31**(5): 649-662.

Voznesenskaya, E. V., et al. (2001). "Kranz anatomy is not essential for terrestrial C4 plant photosynthesis." Nature **414**(6863): 543-546.

Wang, B., et al. (2012b). "Application of synthetic biology in cyanobacteria and algae." Front Microbiol **3**.

Wang, Y., et al. (2013). "PYR/PYL/RCAR abscisic acid receptors regulate K+ and Cl− channels through reactive oxygen species-mediated activation of Ca2+ channels at the plasma membrane of intact Arabidopsis guard cells." Plant Physiol **163**(2): 566-577.

Wang, Y., et al. (2014). "Systems analysis of guard cell membrane transport for enhanced stomatal dynamics and water use efficiency." Plant Physiol **164**(4): 1593-1599.

Wang, Y., et al. (2014b). "Overexpression of plasma membrane H+-ATPase in guard cells promotes light-induced stomatal opening and enhances plant growth." Proceedings of the National Academy of Sciences **111**(1): 533-538.

Wang, Y., et al. (2012). "Systems dynamic modeling of a guard cell Cl− channel mutant uncovers an emergent homeostatic network regulating stomatal transpiration." Plant Physiol **160**(4): 1956-1967.

Ward, J. M., et al. (2009). "Plant ion channels: gene families, physiology, and functional genomics analyses." Annu Rev Physiol **71**: 59-82.

Ward, J. M. and J. I. Schroeder (1994). "Calcium-activated K+ channels and calcium-induced calcium release by slow vacuolar ion channels in guard cell vacuoles implicated in the control of stomatal closure." Plant Cell **6**(5): 669-683.

Watson, R. T. and J. E. Pessin (2001). "Transmembrane domain length determines intracellular membrane compartment localization of syntaxins 3, 4, and 5." American Journal of Physiology-Cell Physiology **281**(1): C215-C223.

Wiggins, S. (2004). "Agriculture, hunger and food security."

Wille, A. C. and W. J. Lucas (1984). "Ultrastructural and histochemical studies on guard cells." Planta **160**(2): 129-142.

Williams, B. P., et al. (2012). "Molecular evolution of genes recruited into C 4 photosynthesis." Trends Plant Sci **17**(4): 213-220.

Willmer, C. and M. Fricker (1996). "Stomata." **Second Edition**.

Wingler, A., et al. (2000). "Photorespiration: metabolic pathways and their role in stress protection." Philosophical Transactions of the Royal Society B: Biological Sciences **355**(1402): 1517-1529.

Wong, J., et al. (2012). "Computational optogenetics: a novel continuum framework for the photoelectrochemistry of living systems." Journal of the Mechanics and Physics of Solids **60**(6): 1158-1178.

Wong, S., et al. (1979). "Stomatal conductance correlates with photosynthetic capacity."

Yizhar, O., et al. (2011). "Optogenetics in neural systems." Neuron **71**(1): 9-34.

Zeiger, E. and P. Hepler (1977). "Light and stomatal function: blue light stimulates swelling of guard cell protoplasts." Science **196**(4292): 887-889.

Zhang, B., et al. (2015). "The Arabidopsis R-SNARE VAMP721 Interacts with KAT1 and KC1 K+ Channels to Moderate K+ Current at the Plasma Membrane." Plant Cell: tpc. 15.00305.

Zhang, F., et al. (2006). "Channelrhodopsin-2 and optical control of excitable cells." Nat Methods **3**(10): 785-792.

Zhang, X., et al. (2006). "Agrobacterium-mediated transformation of Arabidopsis thaliana using the floral dip method." Nat Protoc **1**(2): 641-646.

Zhu, X. G., et al. (2010). "Improving photosynthetic efficiency for greater yield." Annu Rev Plant Biol **61**: 235-261.

10. Supplemental material

Supplemental table 10.1. List of primers designed for this research

1	CM-GWS-bCMO-attB1	attB1-taatggaaatcatcttcggacag
2	CM-GWA-bCMO 6His wo-attB2	attB2-cgtggtgatggtgatgatgagatccgagtgaagatccaccgtgtcc
3	CM-GWS-RbsL bCMO-attB1	attB1-taatggcttctagtatgctctcttctg
4	CM-GWS-TPT-attB1	attB1-taatggaatctagggtgctcactg
5	CM-GWA-GFP-attB5r	attB5r-ttacttgtacagctcgtccatgc
6	CM-GWS-TPT-attB5	attB5-taatggaatctagggtgctcactg
7	CM-GWA-AE1w/o-attB2	attB2-gtccacaggcatagcaacttc
8	CM-GWA-GFP-attB4	attB4-ttacttgtacagctcgtccatgc
9	CM-GWS-RbsL bCMO-attB4r	attB4r-atatggcttctagtatgctctcttctg
10	CM-GWA-bCMO 6His -attB3r	attB3-ttagtggtgatggtgatgatgagatccgagtgaagatccaccgtgtcc
11	CM-GWS-TPT-attB3	attB3-taatggaatctagggtgctcactg
12	CM-TPT-pHR-GFP FP 3592-3610(G020)	ctaaggctgctggaactgc
13	CM-TPT-pHR-GFP RP 3797-3816(G020)	atccagacaccacagactcg
14	CM-TPT-AE1 FP 3552-3572(G021)	gacctcttcctaacactgctc
15	CM-TPT-AE1 RP 3686-3706(G021)	gatgaggatagagataggcac
16	CM-SpeI-bCMO-FP	ggactagtatggaaatcatcttcggacag
17	CM-PmlI-bCMO 6His wo-RP	atacacgtggtgatggtgatgatgagatccgagtgaagatccaccgtgtcc
18	CM-SpeI-RbscL bCMO-FP	ggactagtatggcttctagtatgctctcttctg
19	CM-Ch-AE1 wo-attB4-RP	attB4-gtccacaggcatagcaacttc
20	CM-Rbcl-CMO-6His FP 4299-4320(G025)	catcttactaccactcattcgg
21	CM-Rbcl-CMO-6His RP 4444-4463(G025)	cgatgatgtggatgtaggtc
22	CM-PvuII-RbscL bCMO-FP	atacagctg atggcttctagtatgctctcttctg
23	CM-GW-B4-pHR wo-attB4	attB4-gtcatcatcagcaggggttc
24	CM-OePCR-A-Erexp	tcccaatggcatcgtaaagaac
25	CM-OePCR-B-Erexp	attagcattttacttgtacagctcgtc
26	CM-OePCR-C-Erexp	aatgctaatagcttctgttatgaaaatgaggttgctcttacttctaaa
27	CM-OePCR-D-Erexp	tttagaagtaagagcaacctcattttcataacagaagctattagcatt
28	CM-OePCR-E-Erexp	acttctaaacggccatgctagagt
29	CM-OePCR-F-Erexp	catgccggtcgatctagtaacatag

30	CM-OePCR-C2-Erexp	tacaagtaaaatgctaatagcttctgttatgaaaatgaggttgctcttacttctaaacggccatgc
31	CM-OePCR-G-Erexp	tacaagtaaaatgctaatagcttctgttatg
32	CM-OePCR-H-Erexp	gcatggccgtttagaagtaagagcaac
33	CM-BstZ17I-Erexp-GFPw/o-RP	atgtatacctcattttcataacagaacttgtacagctcgtccatgcc
34	CM-BstZ17I-Erexp-RFPw/o-RP	atgtatacctcattttcataacagaaggcgccggtggagtggcggc
35	CM-SP-AE1-FP	atgagaggtactccacttcttcttgttgtttctctttttttctcttcttcaggataagggactcgatctcaacgg
36	CM-AE1w/o-RP	gtccacaggcatagcaacttc
37	CM-GWS-SP-attB1	attB1-taatgagaggtactccacttcttc
38	CM-SP-pHR-FP	atgagaggtactccacttcttcttgttgtttctctttttttctcttcttcaggataccgagactctcccacctgt
39	CM-pHRw/o-RP	gtcatcatcagcaggggttc
40	CM-GWA-pHRw/o-attB2	attB2-cgtcatcatcagcaggggttc
41	CM-GWA-bCMO-6His-attB4	attB4-gagtgaagatccaccgtgtcc
42	CM-OePCR_B-linker-SYP121-RP	tccacctccacgcaatagacgccttgc
43	CM-OePCR_C-SYP121w/o-linker-2xHA-FP	ctattgcgtggaggtggatctggaggtggaagttacccatacgatgttcct
44	CM-OePCR_D-pHR-linker-2xHA-RP	agtctcggtacttccacctccagatccacctcctgcatagtccgggacgtc
45	CM-OePCR_E-linker-pHR-FP	ggtggaagtaccgagactctcccacct
46	CM-OePCR_A-attB1-2xHA-FP	ggggacaagtttgtacaaaaaagcaggcttaatgtacccatacgatgttcct
47	CM-OePCR_B-link-pHR-RP	tccacctccgtcatcatcagcaggggt
48	CM-OePCR_C-pHR-link-RFP-FP	gatgatgacggaggtggatctggaggtggaagtgcctcctccgaggacgtc
49	CM-OePCR_D-Syp121-link-RFP-RP	caaatcgttacttccacctccagatccacctccggcgccggtggagtggcg
50	CM-OePCR_E-link-Syp121-FP	ggtggaagtaacgatttgttttccagc
51	CM-GWS-AHA1-attB1	attB1-taatgtcaggtctcgaagat
52	CM-GWA-AHA1-ST-attB2	attB2-cctacacagtgtagtgatgtcc
53	CM-GWA-AHA1-st-attB2	attB2-cttactacacagtgtagtgatg
54	CM-GWS-AHA2-attB1	attB1-taatgtcgagtctcgaagatatc
55	CM-GWA-AHA2-ST-attB2	attB2-cctacacagtgtagtgactggg
56	CM-GWA-AHA2-st-attB2	attB2-cttactacacagtgtagtgactgg
57	CM-GWS-PiP2;1-attB1	attB1-taatggcaaaggatgtggaag
58	CM-GWA-PiP2;1-wo-attB2	attB2-cgacgttggcagcacttctg
59	CM-GWA-PiP2;1-st-attB2	attB2-cttagacgttggcagcacttct
60	CM-GWS-PiP2;7-attB1	attB1-taatgtcgaaagaagtgagcg
61	CM-GWA-PiP2;7-wo-attB2	attB2-cattggttgcgttgcttcg
62	CM-GWA-PiP2;7-st-attB2	attB2-cttaattggttgcgttgctt

63	CM-HindIII-MYB60-FP	cccaagcttcacaaggacac
64	CM-SpeI-MYB60-RP	ggactagttctagatctctctgagtc
65	CM-AHA-1361-1376-FP	gtcttaggtcgttggc
66	CM-AHA1-1546-1562-RP	gtttccttaccaatagc
67	CM-GWS-3xHA-attB1 (OePCR_A)	attB1-taatgtacccttatgatgttcctg
68	CM-OePCR_B-pHR-3xHA-RP	agtctcggtggcataatctggaacatc
69	CM-OePCR_C-3xHA-pHR-FP	gattatgccaccgagactctcccacct
70	CM-GWA-NpHR-wo-attB2 (OePCR_D)	attB2-catcatcagcaggggttcc
71	CM-GWA-NpHR-ST-attB2 (OePCR_D)	attB2-cttaatcatcagcaggggttcc
72	CM-OePCR_B-17pHR-3xHA-RP	tgtaacctcggcataatctggaacatc
73	CM-OePCR_C-3xHA-17pHR-FP	gattatgccgaggttacacagagagag
74	CM-OePCR_B-32pHR-3xHA-RP	agcgaggagggcataatctggaacatc
75	CM-OePCR_C-3xHA-32pHR-FP	gattatgccctcctcgcttcttctctc
76	CM-GWA-AHA1-wo-attB2	attB2-ccacagtgtagtgatgtcctgc
77	CM-GWA-AHA2-wo-attB2	attB2-ccacagtgtagtgactgggag
78	CM-OePCR_B-3xHA-1TMD_AHA1-RP	ataagggtatcgattatcaccattagc
79	CM-OePCR_C-1TMD_AHA1-3xHA-FP	gataatcgatacccttatgatgttcct
80	CM-GWA-3xHA-ST-attB2 (OePCR_D)	attB2-cttaggcataatctggaacatcg
81	CM-OePCR_B-3xHA-3TMD_AHA1-RP	ataagggtatctgtactttcggtgttg
82	CM-OePCR_C-3TMD_AHA1-3xHA-FP	aagtacagataccttatgatgttcct
83	CM-GWA-1TMD_AHA2-st-attB2	attB2-cttacctaccatcaccgttggc
84	CM-GWA-3TMD_AHA2-st-attB2	attB2-cttatctgtactttcggcgttg
85	CM-OePCR_C-1TMD_AHA1-2xHA	gataatcgatacccatacgatgttcct
86	CM-OePCR_C-3TMD_AHA1/2-2xHA	aagtacagatacccatacgatgttcct
87	CM-OePCR_C-1TMD_AHA2-2xHA	gatggtaggtacccatacgatgttcct
88	CM-OePCR_B-2xHA-1TMD_AHA1	gtatgggtatcgattatcaccattagc
89	CM-OePCR_B-2xHA-3TMD_AHA1	gtatgggtatctgtactttcggtgttg

90	CM-OePCR_B-2xHA-1TMD_AHA2	gtatgggtacctaccatcaccgttggc
91	CM-OePCR_B-2xHA-3TMD_AHA2	gtatgggtatctgtactttcggcgttg
92	CM-OePCR_B-lac-MYB60-RP	ttgactagatctagatctctctgagtc
93	CM-OePCR_C-MYB60-lac-FP	agatctagatctagtcaattggcaact
94	CM-OePCR_D-NruI-lac-RP	caatcgcgacgctgcagaac
95	CM-OePCR_B-2xHA-9TMDAHA2	gtatgggtacctaatctttgcaaattc
96	CM-OePCR_C-9TMDAHA2-2xHA	aagattaggtacccatacgatgttcct
97	CM-OePCR_B-AHA2-link	gagactcgaacttccacctccagatcc
98	CM-OePCR_C-link-AHA2	ggtggaagttcgagtctcgaagatatc
99	CM-GWA-5TMD-AHA2-ST-attB2	attB2-cttagtcaaattcccatatcaa
100	CM-GWA-7TMD-AHA2-ST-attB2	attB2-cttagttattgtccctaatgga
101	CM-GWA-9TMD-AHA2-ST-attB2	attB2-cttacctaatctttgcaaattc
102	CM-OePCR_B-2xHA-5TMDAHA2	gtatgggtagtcaaattcccatatcaa
103	CM-OePCR_C-5TMDAHA2-2xHA	gaatttgactacccatacgatgttcct
104	CM-GWA-6TMD-AHA2wo-attB2	attB2-cctttaagtttccagctatcag
105	CM-OEPCR_B-2xHA-7TMDAHA2	gtatgggtagttattgtccctaatgga
106	CM-OePCR_C-7TMDAHA2-2xHA	gacaataactacccatacgatgttcct
107	CM-GWA-8TMDAHA2wo-attB2	attB2-ccacgttcaacaaaagaccaac
108	CM-GWS-3-5TMDAHA2-attB1	attB1-taatgaaaaccaaggttcttaggg
109	CM-GWA-3-5TMDAHA2st-attB2	attB2-cttagtcaaattcccatatcaa
110	CM-OePCR_B-2xHA-3-5AHA2	gtatgggtagtcaaattcccatatcaa
111	CM-OePCR_B-3-6AHA2-link	cttggttttacttccacctccagatcc
112	CM-OePCR_C-link-3-6AHA2	ggtggaagtaaaaccaaggttcttagg
113	CM-GWA-3-6AHA2wo-attB2	attB2-ctttaagtttccagctatcag
11	CM-OePCR_B-LD721-link	ttgttgcgcacttccacctccagatcc

4		
115	CM-OePCR-C-link-LD721	ggtggaagtgcgcaacaatcgttgatc
116	CM-GWA-LD721-wo-attB2	attB2-caagcttgctaatctcatc
117	CM-GWS-2-10AHA2-attB1	attB1-taatgcctccggattggcaggat
118	CM-GWS-4-10AHA2-attB1	attB1-taatggatggaattgacaacctt
119	CM-beforeRB-FP	cgtaacttaggacttgtgcg
120	CM-GWS-6_10TMD-AHA2-attB1	attB1-taatgttctcagccttcatggttc
121	CM-GWS-8_10TMD-AHA2-attB1	attB1-taatgcacgagctaatgggtgcg
122	CM-GWA-4.5TMD-AHA2-attB2	attB2-cttaacggatggtgattgagac
123	CM-GWS-4.5_10TMD-AHA2-attB1	attB1-taatgattgtgtttggtttcatgc
124	CM-GWS-6_10TMD-AHA2-attB1(2)	attB1-taatgttctcagccttcatggttctgatc
125	CM-GWS-8_10TMD-AHA2-attB1(2)	attB1-taatgcacgagctaatgggtgcggtgtac
126	CM-GWA-AHA2wo-attB4	attB4-cacagtgtagtgactgggag
127	CM-GWS-bCMO-attB3	attB3-taatggaaatcatcttcggacag

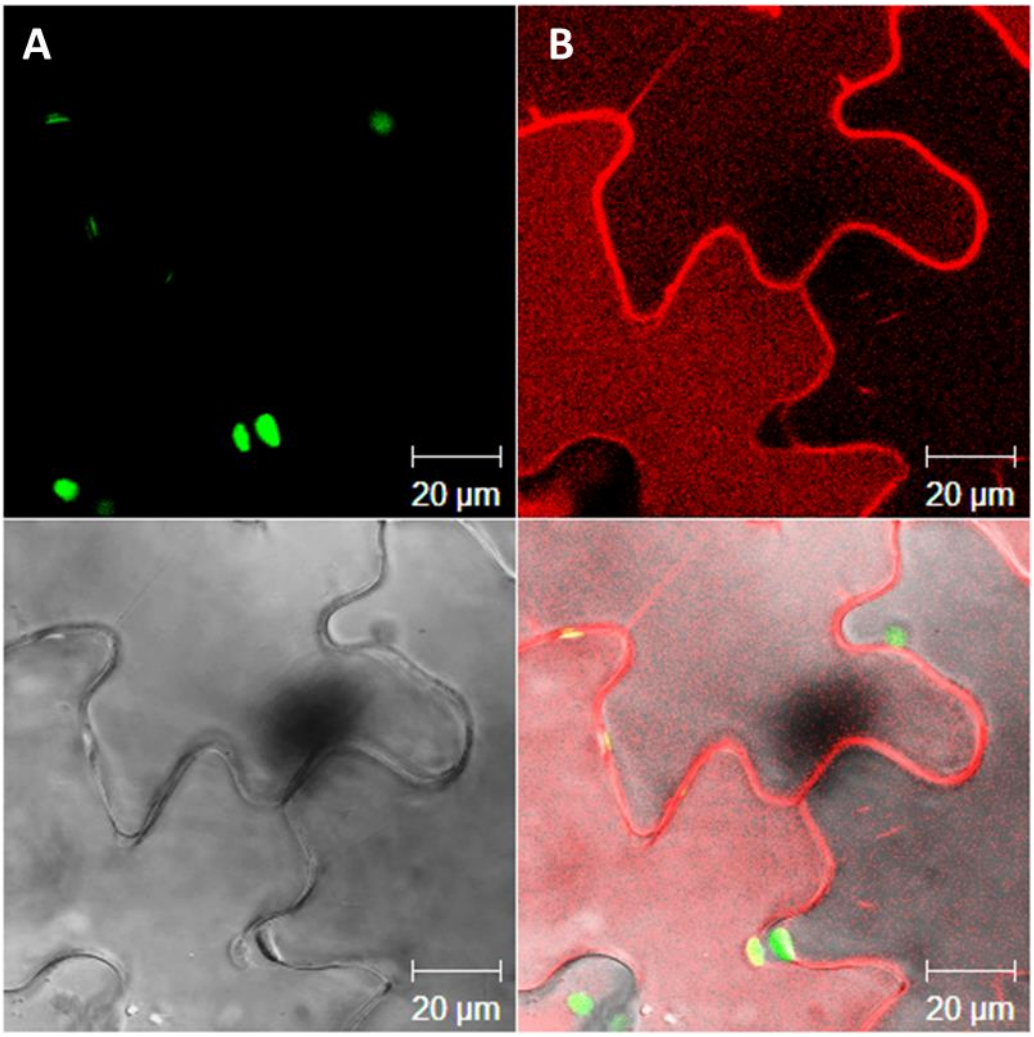

Supplemental figure 10.1. Expression of the construct 35S::^{1_17del}NpHR-RFP in transient transformed tobacco leaves after 3 days of transformation. RFP fluorescence indicates tonoplast localisation of NpHR in the epidermal cells (red B, D). The chlorophyll autofluorescence is shown in green (A, D). C is the bright field image, and D shows a merged image. The images are from 29-slice Z-stack through the epidermal cell with a 0.75 µm interval between slices. In all the images the scale bar is 20 µm

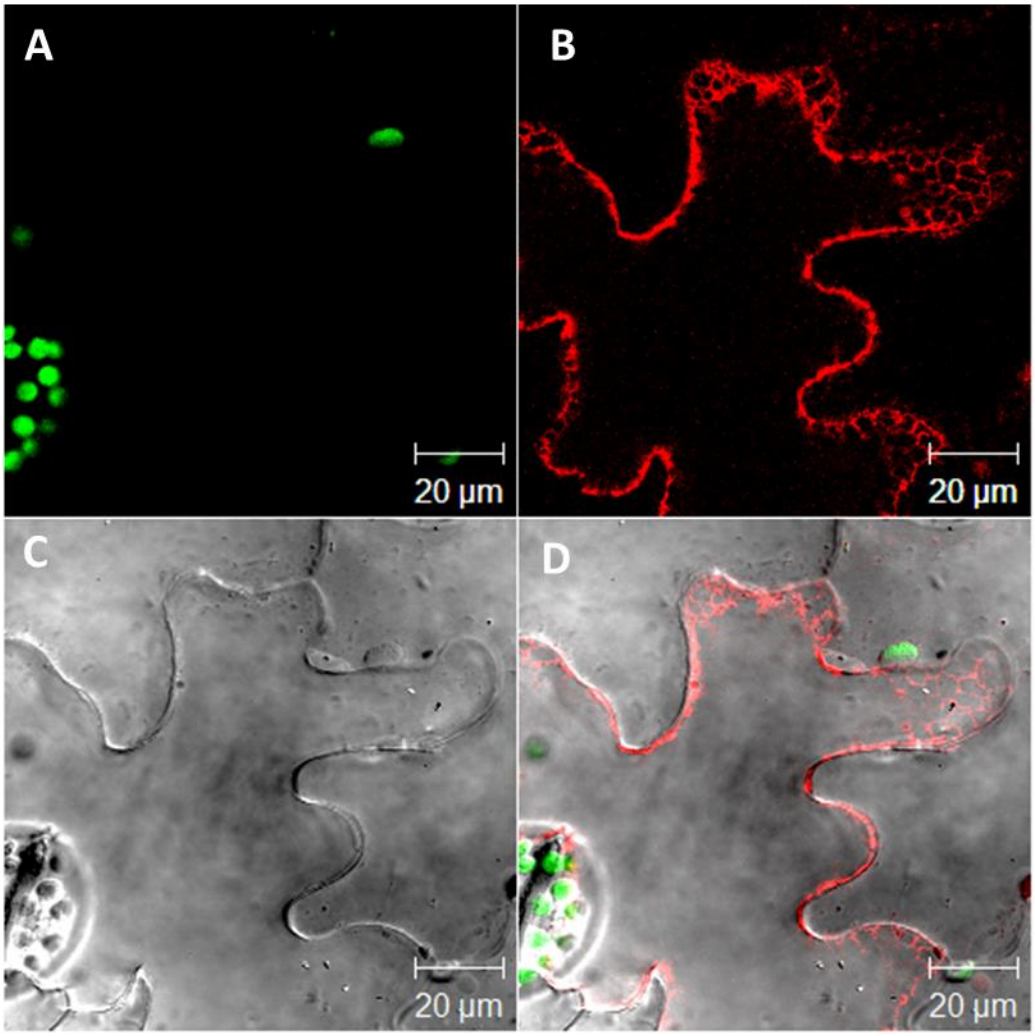

Supplemental figure 10.2. Expression of the construct 35S::RFP-^{1_17del}NpHR in transient transformed tobacco leaves after 3 days of transformation. RFP fluorescence indicates ER localisation of NpHR in the epidermal cells (red B, D). The chlorophyll autofluorescence is shown in green (A, D). C is the bright field image, and D shows a merged image. The images are from 15-slice Z-stack through the epidermal cell with a 0.75 µm interval between slices. In all the images the scale bar is 20 µm.

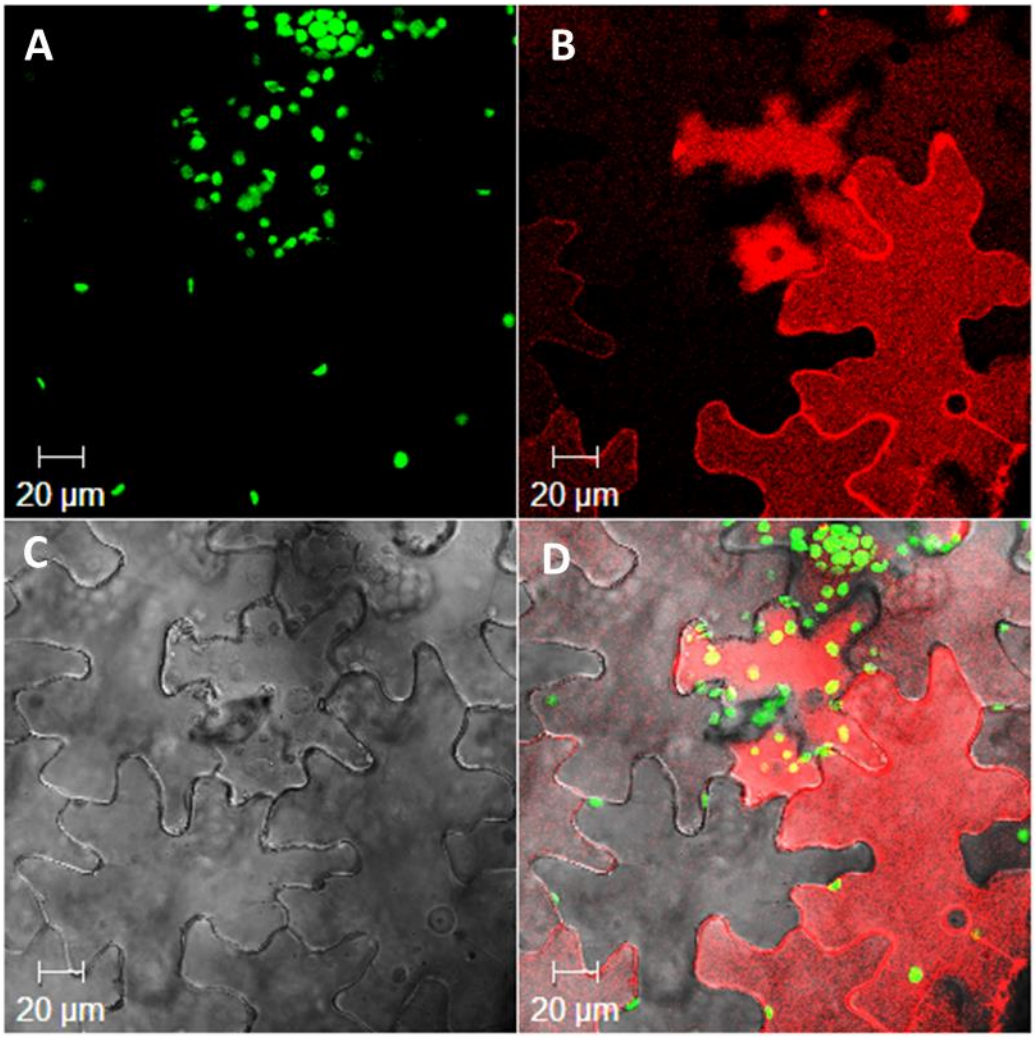

Supplemental figure 10.3. Expression of the construct 35S::$^{1-32del}$NpHR-RFP in transient transformed tobacco leaves after 3 days of transformation. RFP fluorescence indicates tonoplast localisation of NpHR in the epidermal cells (red B, D). The chlorophyll autofluorescence is shown in green (A, D). C is the bright field image, and D shows a merged image. The images are from 28-slice Z-stack through the epidermal cell with a 0.75 µm interval between slices. In all the images the scale bar is 20 µm

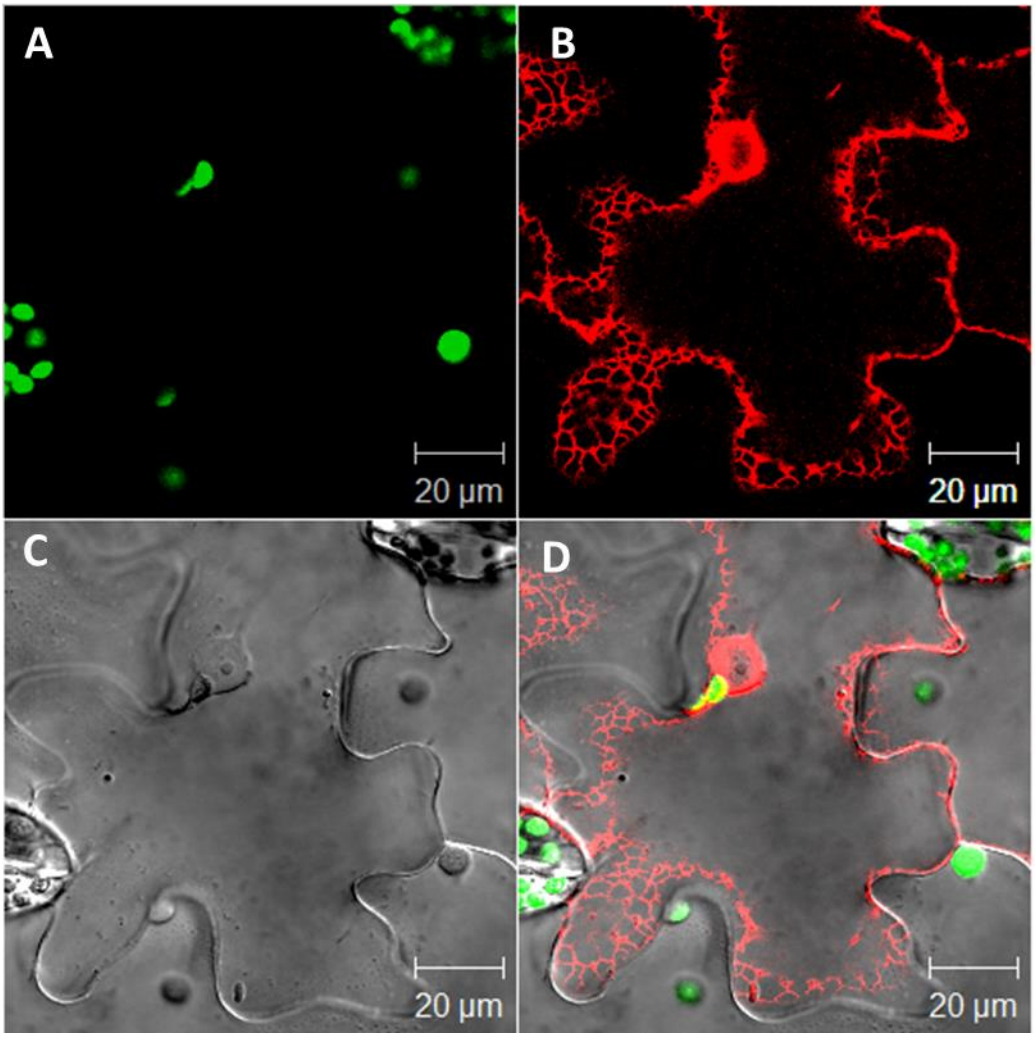

Supplemental figure 10.4. Expression of the construct 35S:: RFP-^{1_32del}NpHR in transient transformed tobacco leaves after 3 days of transformation. RFP fluorescence indicates ER localisation of NpHR in the epidermal cells (red B, D). The chlorophyll *autofluorescence* is shown in green (A, D). C is the bright field image, and D shows a merged image. The images are from 34-slice Z-stack through the epidermal cell with a 0.75 µm interval between slices. In all the images the scale bar is 20 µm.

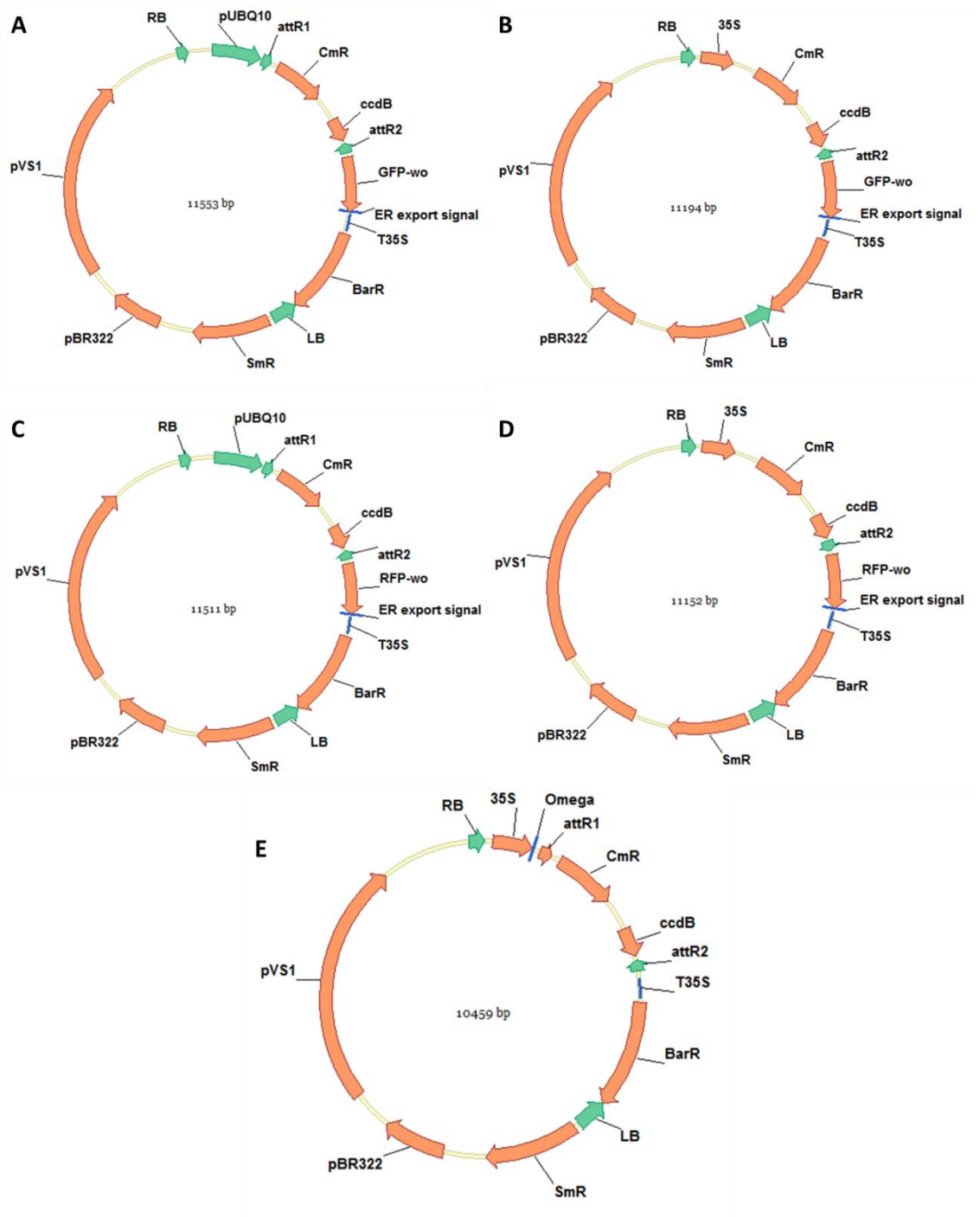

Supplemental figure 10.5. Vector maps representations. (A) the GFP marked was cut out from vector pUBC-GFP-DEST with the restriction enzymes SpeI and PsiIa and a PCR product containing GFP-ERexp was introduced instead into the vector with the restriction enzymes SpeI and BstZ17I. (B) the UBQ10 was cut out and discarded from vector A with the restriction enzymes PmeI and NcoI, and an insert containing 35S

promoter obtained from vector pBBb-R1R4-myc with the restriction enzymes PmeI and NcoI was introduced. (C) the RFP marker was cut out from vector pUBC-RFP-Dest with the restriction enzymes SpeI and PsiI and a PCR product containing RFP-ERexp was introduced instead into the vector with the restriction enzymes SpeI and BstZ17I. (D) the UBQ10 promoter was cut out from vector C with the restriction enzymes PmeI and SpeI, and instead it was introduced an insert containing the 35S promoter previously obtained from vector B which was cut with the restriction enzymes PmeI and SpeI. (E) the 35S promoter was cut out from pBBb-R1R4-myc with the restriction enzymes PmeI and NcoI, and it was introduced into the vector pUB-Dest, previously cut with the restriction enzymes PmeI and NcoI in order to remove the UBQ10 promoter. pBR322ori/pVS1ori: replication origins. RB/LF: right/left border. SmR: Spectinomycin resistance. CmR: Cloramphenicol resistance. nosP/nosT: nos promoter/nos terminator. BarR: BASTA resistance.T35S: 35S terminator. 35S: 35S strong promoter. pUBQ10: UBQ10 promoter. RFP/GFP: red/green fluorescent marker. *ccd*B: *ccd*B toxic gene. *att*B1/*att*B2: recombination sites. The vector sizes are 11553 bp (A), 11194 bp (B), 11511 bp (C), 11152 bp (D) and 10459 bp (E).

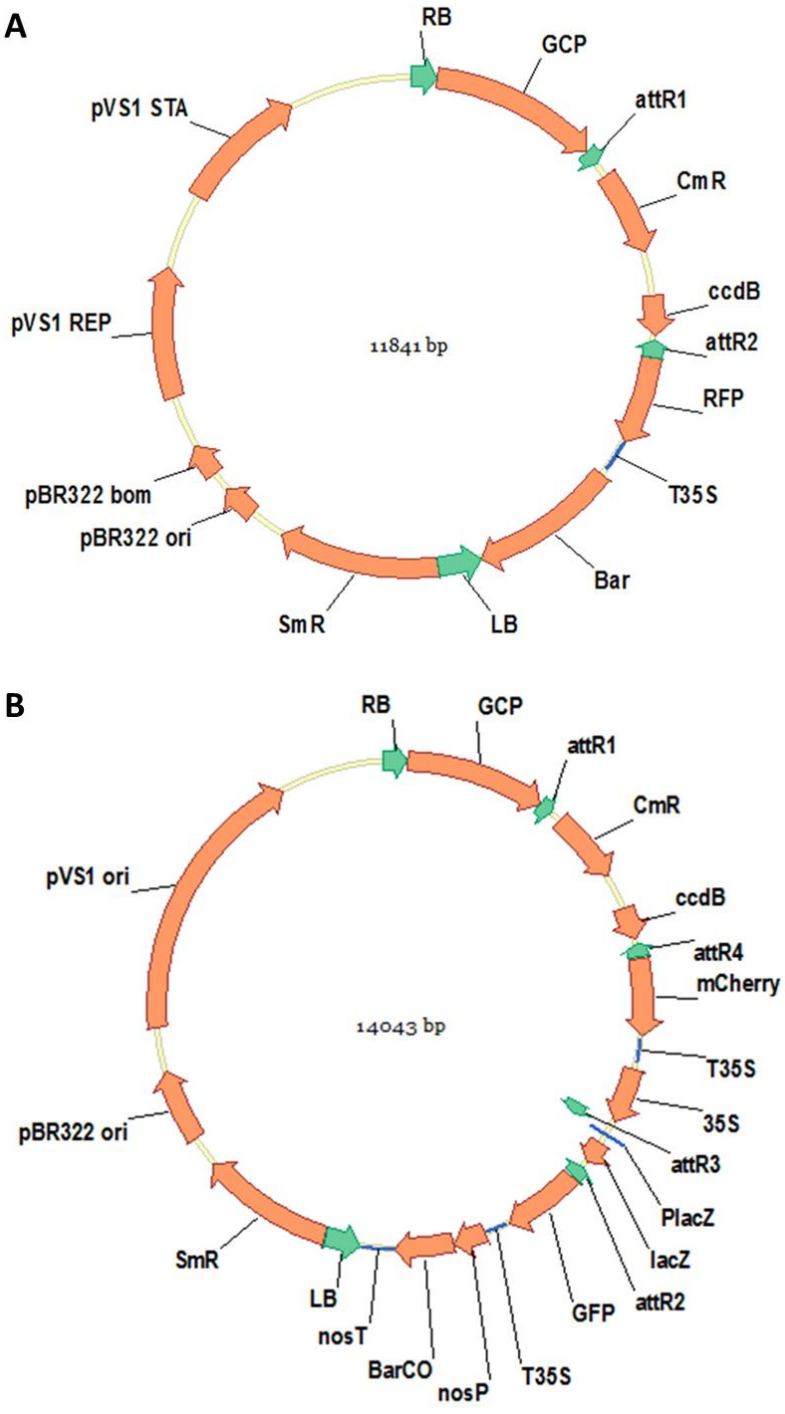

Supplemental figure 10.6. Vector maps representations. (A) the 35S promoter was cut out from vector pB7RWG2 with the restriction enzymes HindIII and SpeI and instead it was introduced an insert containing GCP previously obtained by PCR and ligated with the restriction enzymes HindIII and SpeI. (B) the 35S promoter was cut out from V319 with the restriction enzymes BspEI and PmeI, instead it was introduced an insert

containing the GCP previously obtained from the vector A cut with the restriction enzymes BspEI and PmeI. pBR322ori/pVS1ori: replication origins. RB/LF: right/left border. SmR: Spectinomycin resistance. CmR: Cloramphenicol resistance. nosP/nosT: nos promoter/nos terminator. BarR: BASTA resistance.T35S: 35S terminator. GCP: AtMYB60 promoter. 35S: 35S strong promoter. PlacZ: lacZ gene promoter. lacZ: lacZ gene for selection. RFP/mCherry/GFP: red/green fluorescent marker. *ccd*B: *ccd*B toxic gene. *att*B1/*att*B2/*att*B3/*att*B4: recombination sites. The vector sizes are 11841 bp (A) and 14044 bp (B).

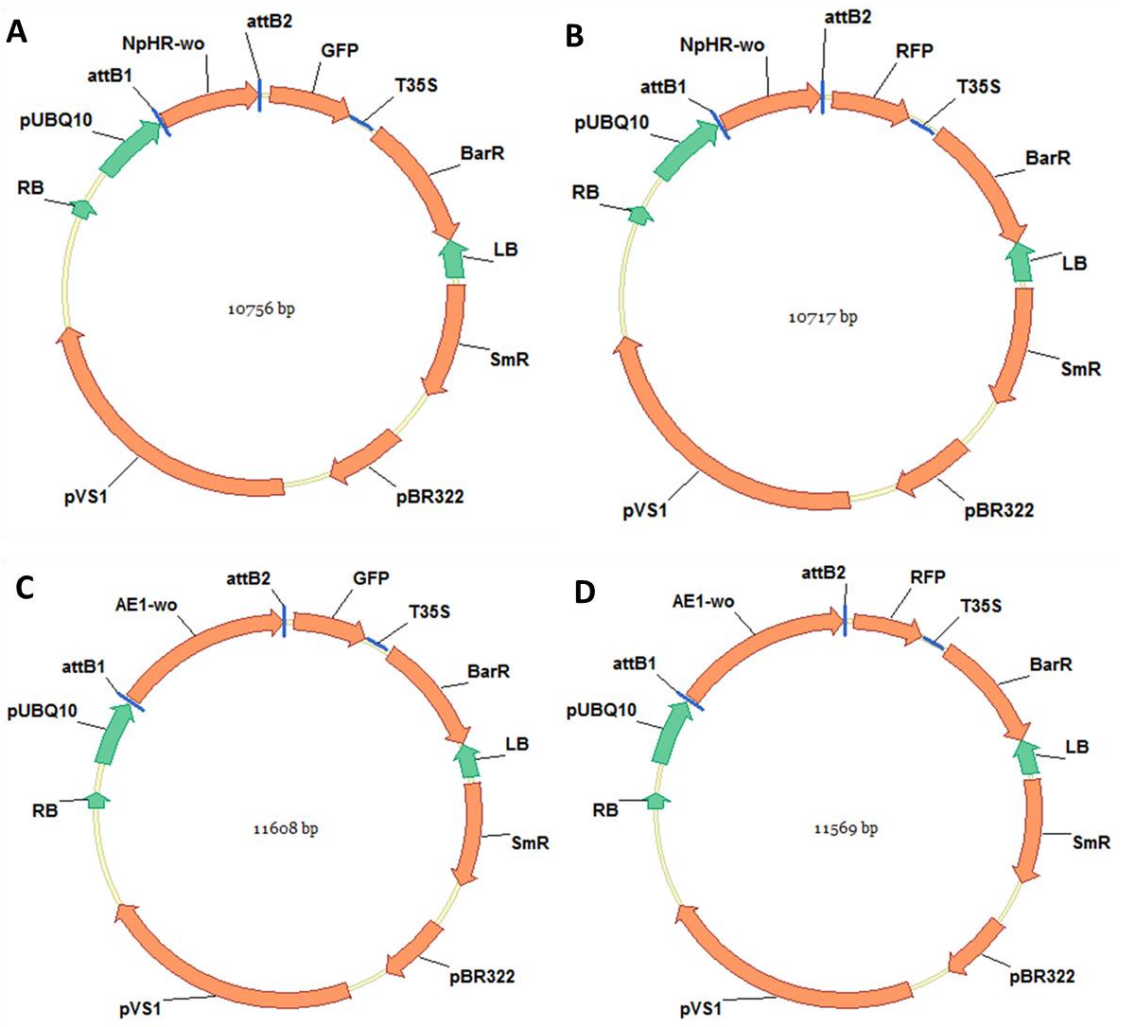

Supplemental figure 10.7. Map representation of the expression constructs UBQ10::NpHR-GFP (A), UBQ10::NpHR-RFP (B), UBQ10::AE1-GFP (C) and UBQ10::AE1-RFP (D). pBR322ori/pVS1ori: replication origins. RB/LF: right/left border. SmR: Spectinomycin resistance. BarR: BASTA resistance. T35S: 35S terminator. 35S: 35S strong promoter. pUBQ10: UBQ10 promoter. RFP/GFP: red/green fluorescent marker. *att*B1/*att*B2: recombination sites. The construct sizes are 10756 bp (A), 10717 bp (B), 11608 bp (C) and 11569 bp (D).

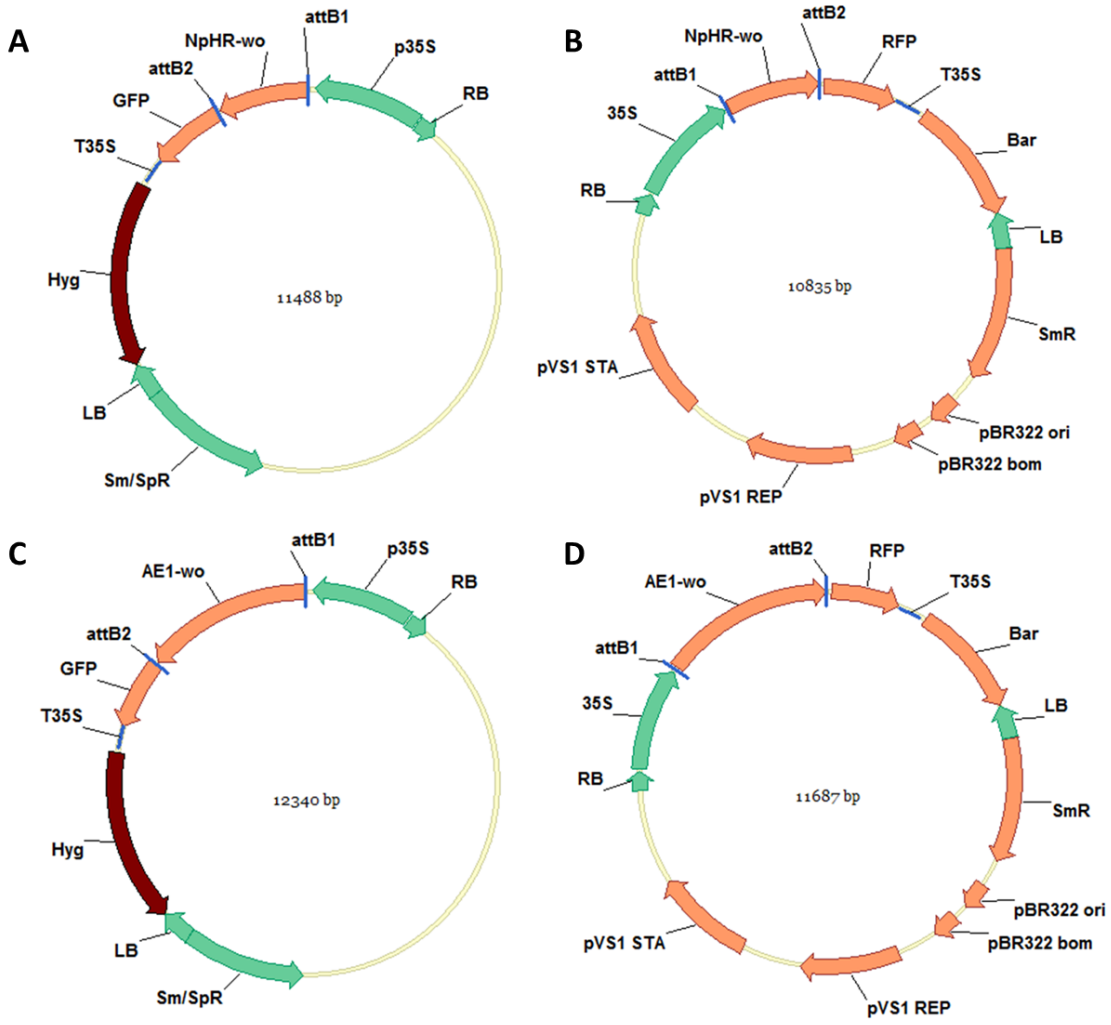

Supplemental figure 10.8. Map representation of the expression constructs 35S::NpHR-GFP (A), 35S::NpHR-RFP (B), 35S::AE1-GFP (C) and 35S::AE1-RFP (D). pBR322/pVS1 STA/REP: replication origins. RB/LF: right/left border. SmR: Spectinomycin resistance. CmR: Cloramphenicol resistance. Hyg: Hygromycin resistance. Bar: BASTA resistance.T35S: 35S terminator. 35S: 35S strong promoter. pUBQ10: UBQ10 promoter. RFP/GFP: red/green fluorescent marker. *att*B1/*att*B2: recombination sites. The construct sizes are 11488 bp (A), 10835 bp (B), 12340 bp (C) and 11687 bp (D).

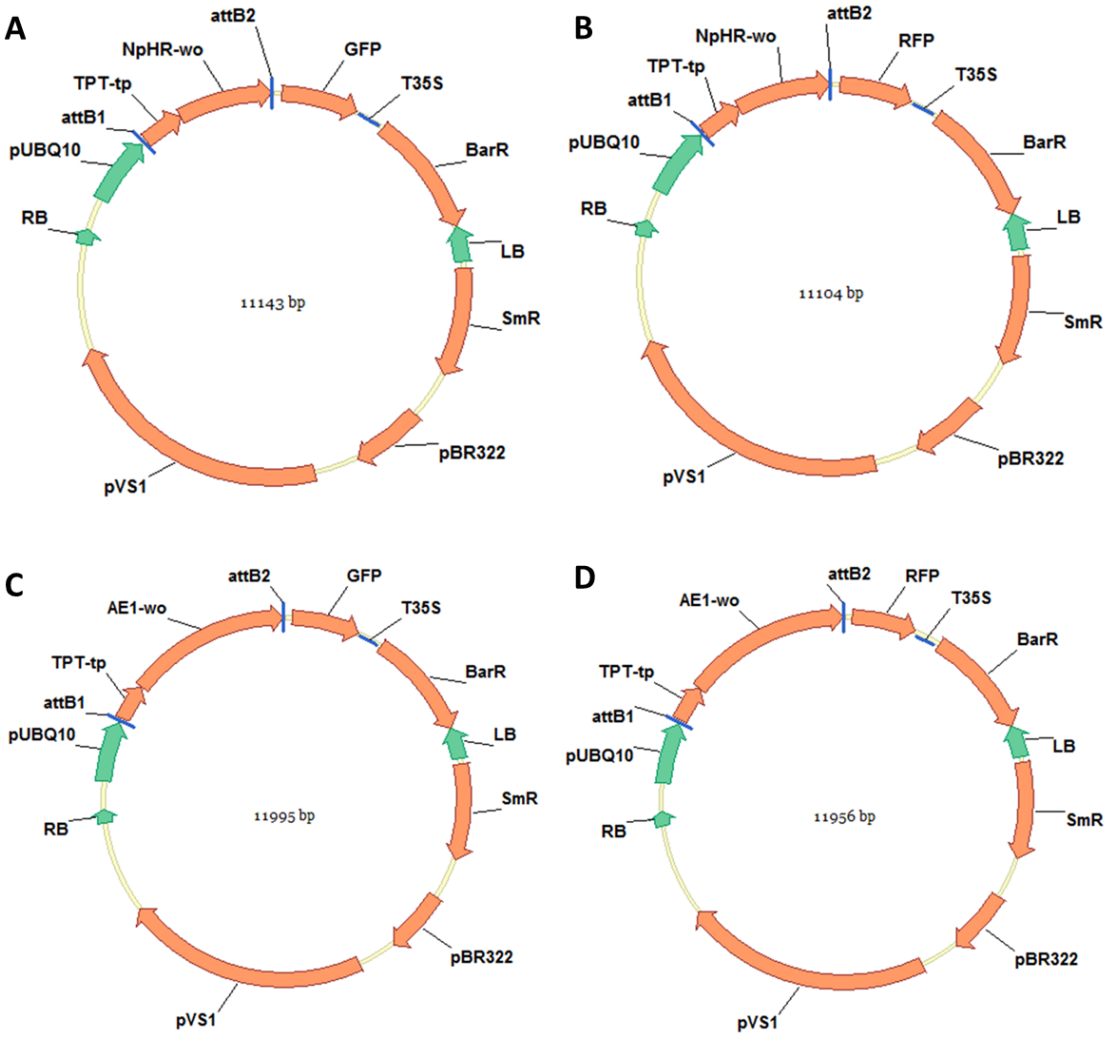

Supplemental figure 10.9. Map representation of the expression constructs UBQ10::TPT-NpHR-GFP (A), UBQ10::TPT-NpHT-RFP (B), UBQ10::TPT-AE1-GFP (C), UBQ10::TPT-AE1-RFP (D). TPT: triosephosphate translocator. pBR322/pVS1: replication origins. RB/LF: right/left border. SmR: Spectinomycin resistance. Bar: BASTA resistance.T35S: 35S terminator. 35S: 35S strong promoter. pUBQ10: UBQ10 promoter. RFP/GFP: red/green fluorescent marker. *att*B1/*att*B2: recombination sites. The construct sizes are 11143 bp (A), 11104 bp (B), 11995 bp (C) and 11956 bp (D).

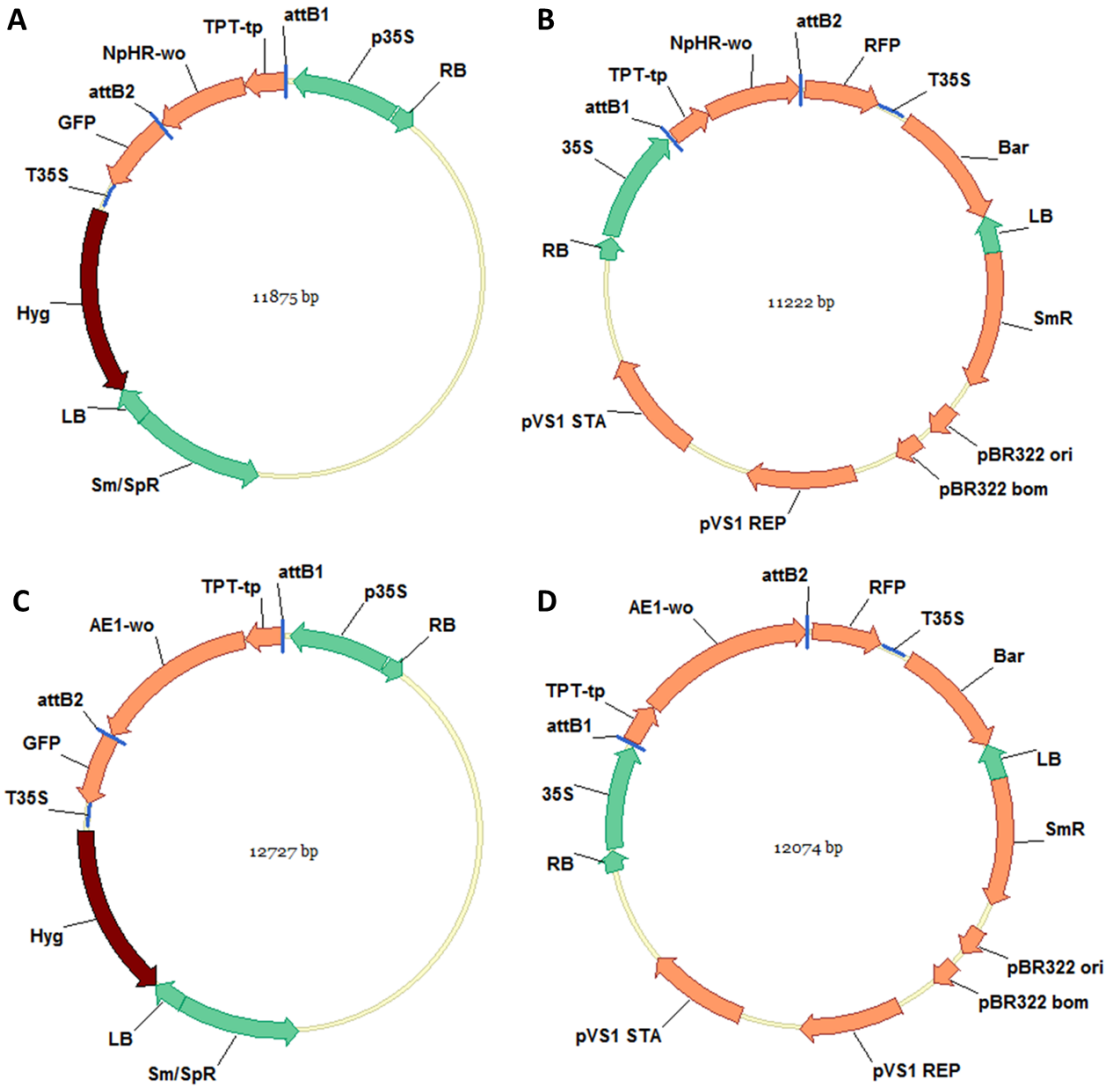

Supplemental figure 10.10. Map representation of the expression constructs 35S::-TPT-NpHR-GFP (A), 35S::TPT-NpHR-RFP (B), 35S::TPT-AE1-GFP (C), 35S::TPT-AE1-RFP (D). TPT: triosephosphate translocator. pBR322/pVS1: replication origins. RB/LF: right/left border. SmR: Spectinomycin resistance. Bar: BASTA resistance. T35S: 35S terminator. 35S: 35S strong promoter. pUBQ10: UBQ10 promoter. RFP/GFP: red/green fluorescent marker. *att*B1/*att*B2: recombination sites. The construct sizes are 11875 bp (A), 11222 bp (B), 12727 bp (C) and 12074 bp (D).

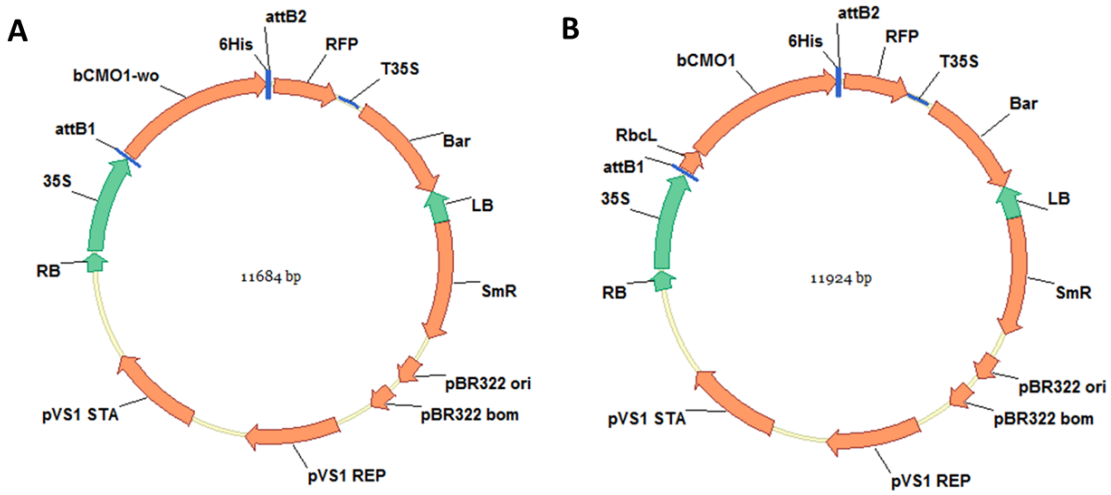

Supplemental figure 10.11 Map representation of the expression constructs 35S::bCMO1-RFP (A) and 35S::RbcL-bCMO1-RFP (B). RbcL: Rubisco large subunit. pBR322/pVS1: replication origins. RB/LF: right/left border. SmR: Spectinomycin resistance. Bar: BASTA resistance. T35S: 35S terminator. 35S: 35S strong promoter. pUBQ10: UBQ10 promoter. RFP: red fluorescent marker. *att*B1/*att*B2: recombination sites. The construct sizes are 11684 bp (A) and 11924 bp (B).

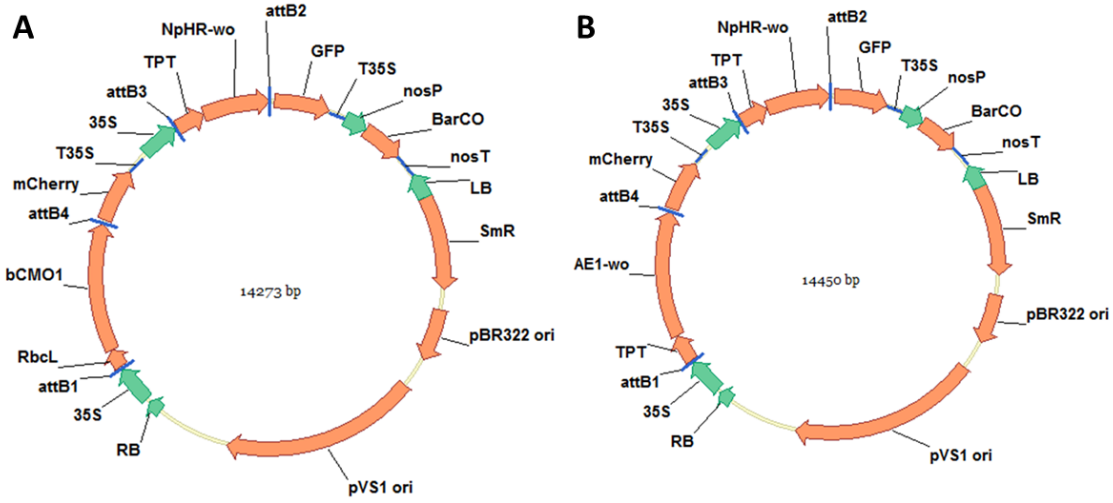

Supplemental figure 10.12. Map representation of the 2in1 expression constructs 35S::RbcL-bCMO1-mCherry and 35S::TPT-NpHT-GFP (A); and 35S:;TPT-AE1-mCherry and 35S::TPT-NpHR-GFP (B). pBR322ori/pVS1ori: replication origins. RB/LF: right/left border. SmR: Spectinomycin resistance. CmR: Cloramphenicol resistance. nosP/nosT: nos promoter/nos terminator. BarR: BASTA resistance.T35S: 35S terminator. GCP: AtMYB60

promoter. 35S: 35S strong promoter. pUBQ10: UBQ10 promoter. PlacZ: lacZ gene promoter. lacZ: lacZ gene for selection. mCherry/GFP: red/green fluorescent marker. *ccd*B: *ccd*B toxic gene. *att*B1/*att*B2/*att*B3/*att*B4: recombination sites. The construct sizes are 14273 bp (A) and 14450 bp (B).

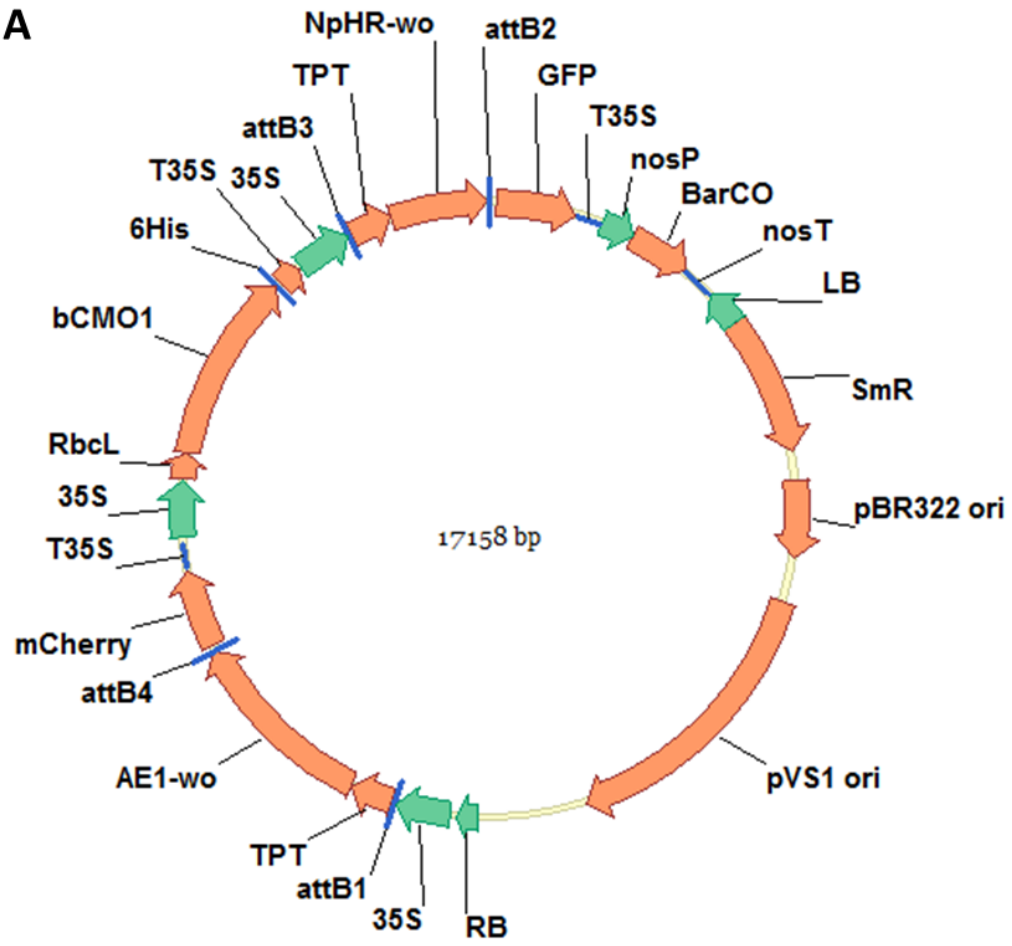

Supplemental figure 10.13. Map representation of the 3in1 expression construct 35S::TPT-AE1-mCherry, 35S::RbcL-bCMO1-6His and 35S::TPT-NpHR-GFP. To integrate the 35S::RbcL-bCMO1-6His between the two cassettes first vecto pUC35S-Ctags was cut with the restriction enzymes HpaI and PsiI, and a PvuII-RbcL-bCMO1-6His-PmlI insert obtained by PCR was inserted into the vector. The new construct was cut with the restriction enzyme StuI and the insert obtained was introduced to the 2in1 vector previously cut with the restriction enzymes PmL1 and EcoICRI. pBR322ori/pVS1ori: replication origins. RB/LF: right/left border. SmR: spectinomycin resistance. BarCO: BASTA resistance. nosP/nosT: nos promoter/nos terminator. T35S: 35S terminator. 35S: 35S strong promoter. mCherry/ GFP: red/green fluorescent marker. 6His: 6 histidine tag. TPT: triosephosphate translocator. *att*B1/*att*B2/*att*B3/*att*B4: recombination sites. The whole construct is 17158 bp.

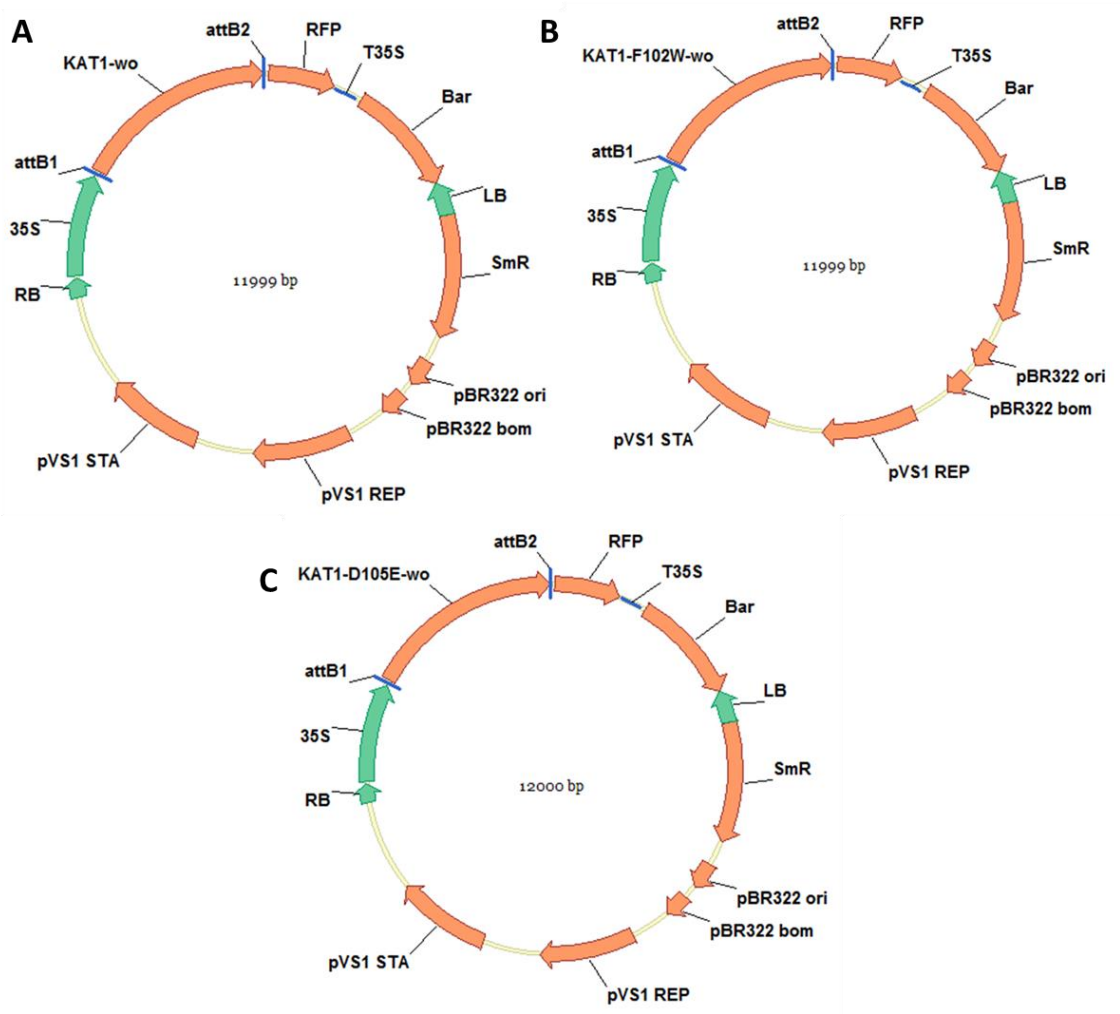

Supplemental figure 10.14. Map representation of the expression constructs 35S::KAT1-RFP (A), 35S::KAT1^{F102W}-RFP (B) and 35S::KAT1^{D105E}-RFP (C). pBR322/pVS1: replication origins. RB/LF: right/left border. SmR: Spectinomycin resistance. Bar: BASTA resistance. T35S: 35S terminator. 35S: 35S strong promoter. pUBQ10: UBQ10 promoter. RFP/GFP: red/green fluorescent marker. *att*B1/*att*B2: recombination sites. The construct sizes are 11999 bp (A), 11999 bp (B), and 12000 bp (C).

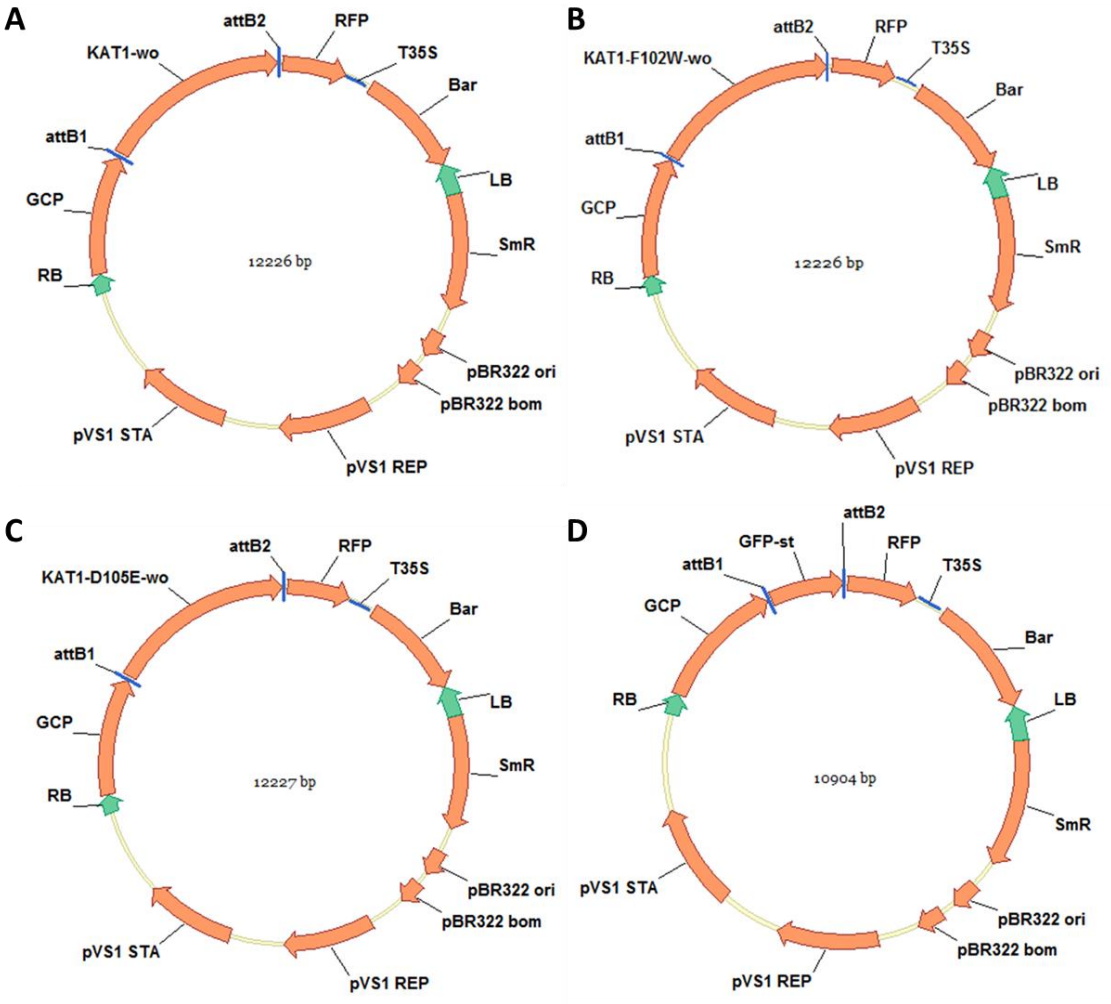

Supplemental figure 10.15. Map representation of the expression constructs GCP::KAT1-RFP (A), GCP::KAT1^{F102W}-RFP (B), GCP::KAT1^{D105E}-RFP (C) and GCP::GFP (D). pBR322/pVS1: replication origins. RB/LF: right/left border. SmR: Spectinomycin resistance. Bar: BASTA resistance. T35S: 35S terminator. GCP: guard cell promoter. pUBQ10: UBQ10 promoter. RFP/GFP: red/green fluorescent marker. *att*B1/*att*B2: recombination sites. The construct sizes are 12226 bp (A), 12226 bp (B), 12227 bp (C) and 10904 bp (D).

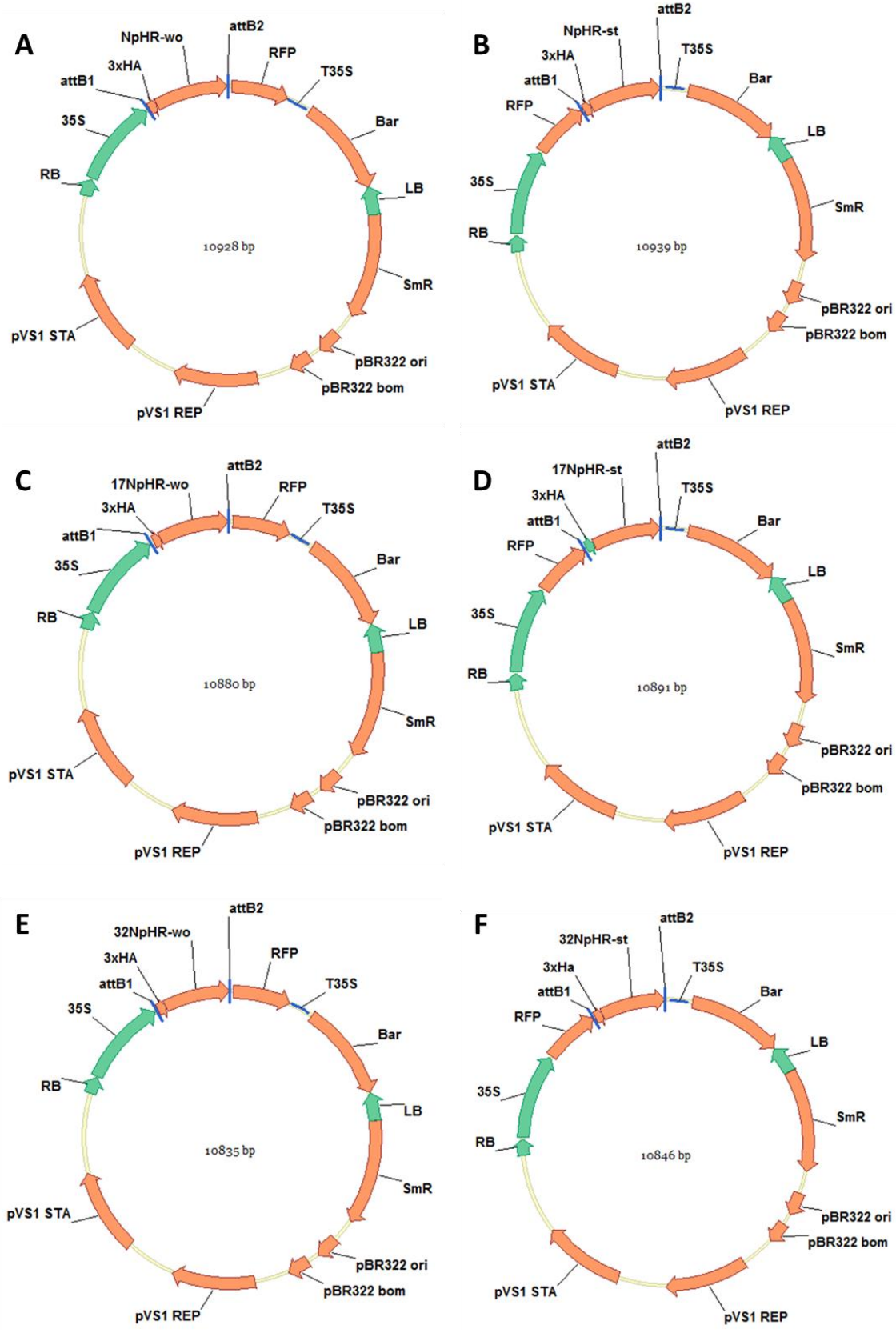
A
NpHR-wo
attB2
3xHA
RFP
attB1
T35S
35S
Bar
RB
LB
10928 bp
SmR
pVS1 STA
pBR322 ori
pBR322 bom
pVS1 REP
B
attB2
NpHR-st
3xHA
T35S
attB1
Bar
RFP
LB
35S
SmR
RB
10939 bp
pBR322 ori
pBR322 bom
pVS1 STA
pVS1 REP
C
attB2
17NpHR-wo
RFP
3xHA
T35S
attB1
35S
Bar
RB
LB
10880 bp
SmR
pVS1 STA
pBR322 ori
pBR322 bom
pVS1 REP
D
attB2
17NpHR-st
3xHA
T35S
attB1
Bar
RFP
LB
35S
SmR
RB
10891 bp
pBR322 ori
pBR322 bom
pVS1 STA
pVS1 REP
E
attB2
32NpHR-wo
3xHA
RFP
attB1
T35S
35S
Bar
RB
LB
10835 bp
SmR
pVS1 STA
pBR322 ori
pBR322 bom
pVS1 REP
F
attB2
32NpHR-st
3xHa
T35S
attB1
Bar
RFP
LB
35S
SmR
RB
10846 bp
pBR322 ori
pBR322 bom
pVS1 STA
pVS1 REP

Supplemental figure 10.16. Map representation of the expression constructs 35S::NpHR-RFP (A), 35S::RFP-NpHR (B), 35S::^{1_17del}NpHR-RFP (C), 35S::RFP-^{1_17del}NpHR (D), 35S::^{1_32del}NpHR-RFP (E) and 35S:: RFP-^{1_32del}NpHR (F). pBR322/pVS1: replication origins. RB/LF: right/left border. SmR: Spectinomycin resistance. Bar: BASTA resistance. T35S: 35S terminator. 35S: 35S strong promoter. pUBQ10: UBQ10 promoter. RFP/GFP: red/green fluorescent marker. *att*B1/*att*B2: recombination sites. The construct sizes are 10880 bp (A), 10891 bp (B), 10835 bp (C) 10846 and (D)

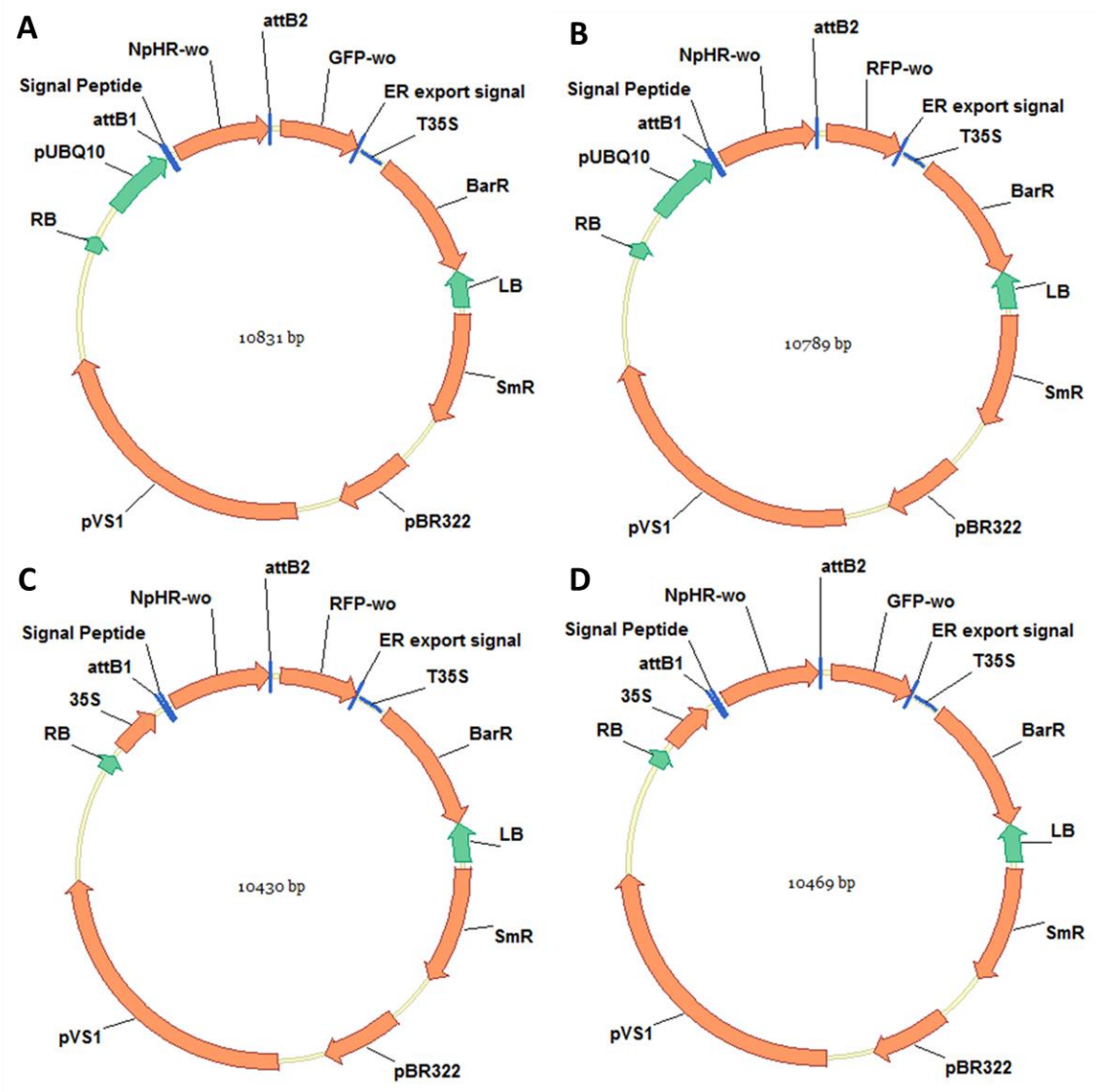

Supplemental figure 10.17. Map representation of the expression constructs UBQ10::SP-NpHR-GFP-ERexp (A), UBQ10::SP-NpHR-RFP-ERexp (B), 35S::SP-NpHR-GFP-ERexp (C) and 35S::SP-NpHR-RFP-ERexp. pBR322/pVS1: replication origins. RB/LF: right/left border. SmR: Spectinomycin resistance. Bar: BASTA resistance. T35S: 35S terminator. 35S: 35S strong promoter. pUBQ10: UBQ10 promoter. SP: signal peptide. RFP/GFP: red/green fluorescent marker. *att*B1/*att*B2: recombination sites. The construct sizes are 10831 bp (A), 10789 bp (B), 10430 bp (C) 10469 and (D)

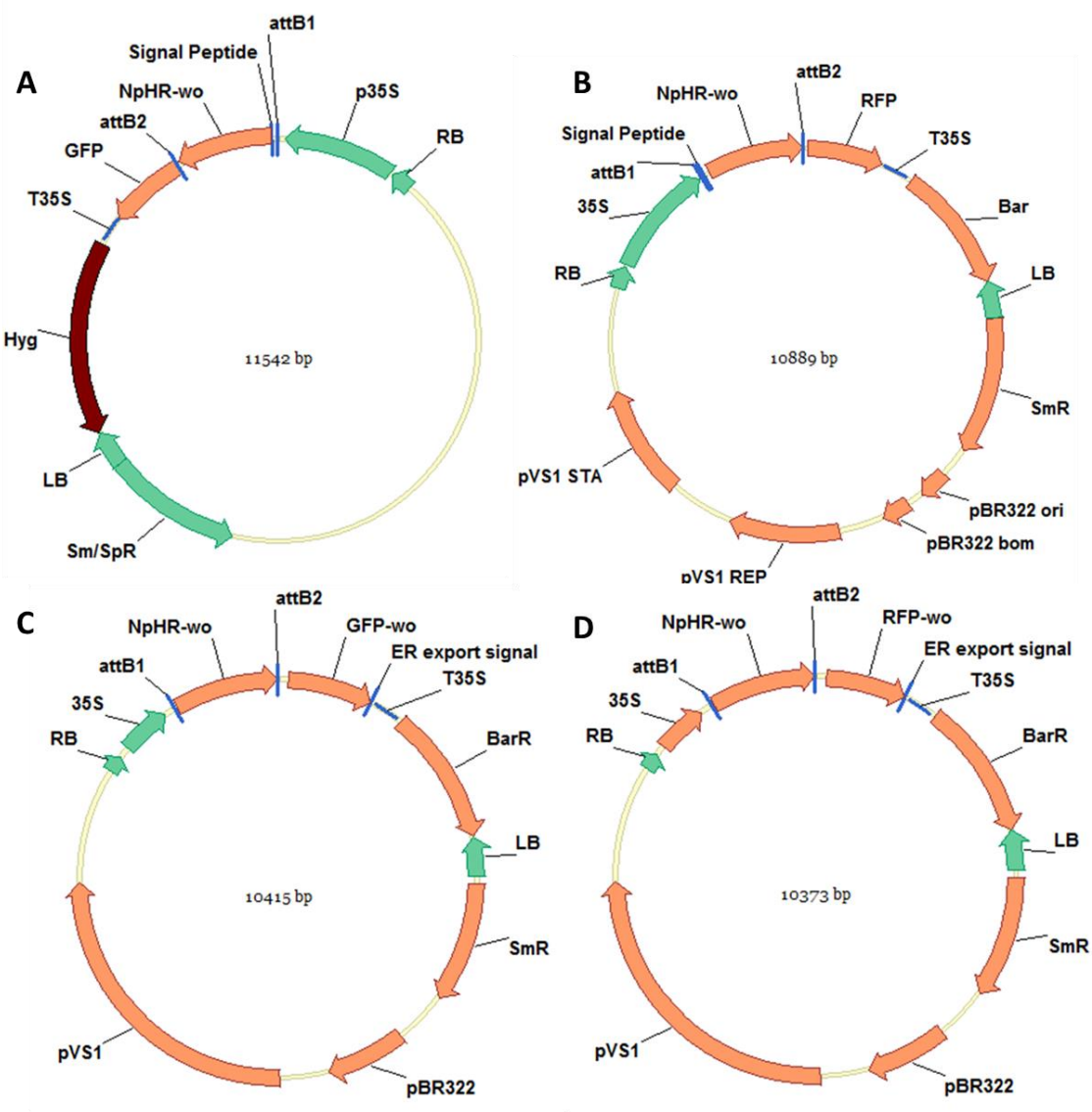

Supplemental figure 10.18 Map representation of the expression constructs 35S:: SP-NpHR-GFP (A), 35S::SP-NpHR-RFP (B), 35S::NpHR-GFP-ERexp (C), 35S::NpHR-RFP-ERexp (D). pBR322/pVS1: replication origins. RB/LF: right/left border. SmR: Spectinomycin resistance. Bar: BASTA resistance. SP: signal peptide. T35S: 35S terminator. 35S: 35S strong promoter. RFP/GFP: red/green fluorescent marker. *att*B1/*att*B2: recombination sites. The construct sizes are 11875 bp (A), 11222 bp (B), 12727 bp (C) and 12074 bp (D).

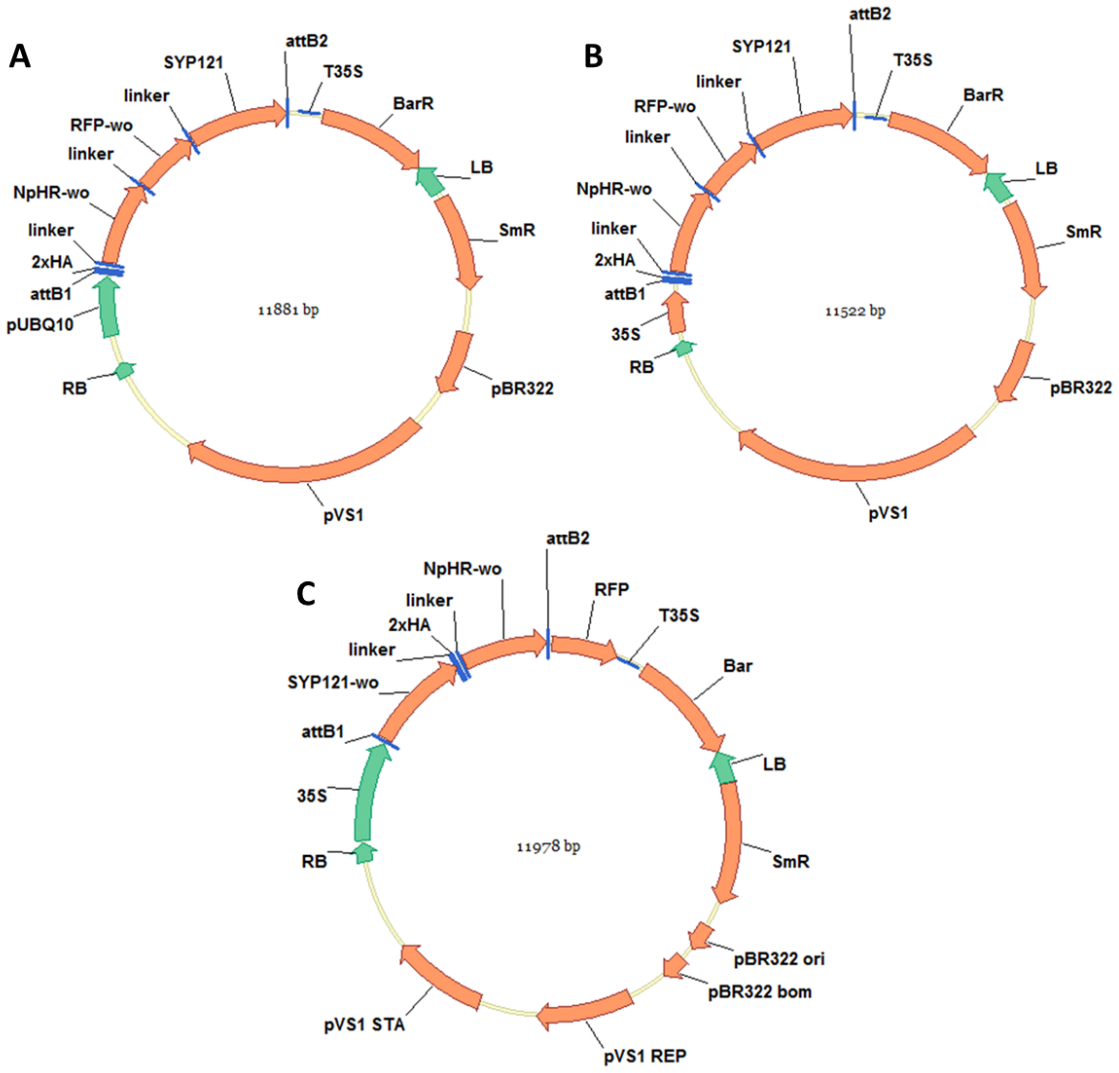

Supplemental figure 10.19. Map representation of the expression constructs UBQ10::NpHR-RFP-SYP (A), 35S::NpHR-RFP-SYP121 (B) and 35S::SYP121-NpHR-RFP (C). pBR322/pVS1: replication origins. RB/LF: right/left border. SmR: Spectinomycin resistance. Bar: BASTA resistance. 2xHA: 2 HA epitope tags. T35S: 35S terminator. 35S: 35S strong promoter. UBQ10: ubiquitine promoterRFP: red fluorescent marker. *att*B1/*att*B2: recombination sites. The construct sizes are 11881 bp (A), 11522 bp (B) and 11978 bp (C).

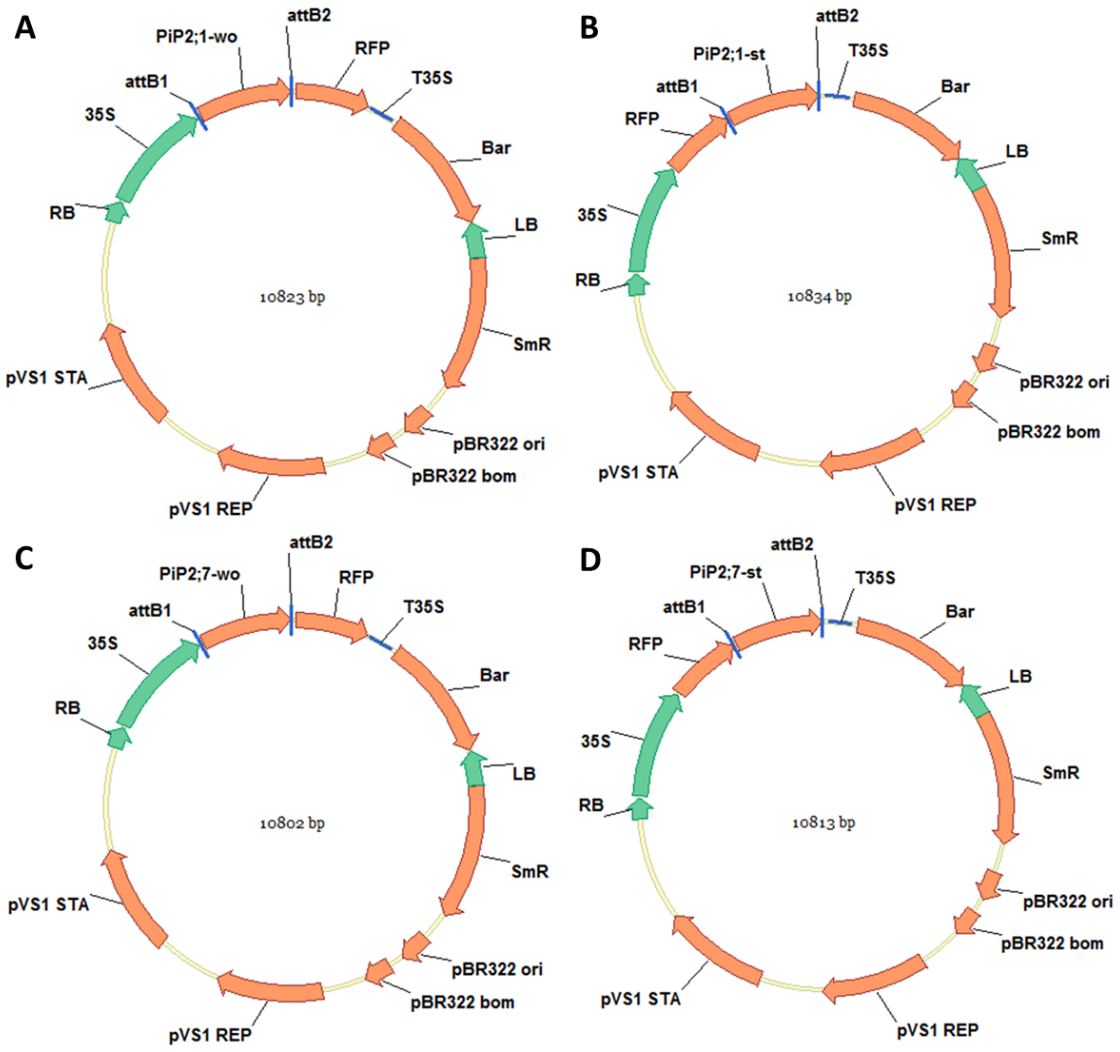

Supplemental figure 10.20. Map representation of the expression constructs 35S::PIP2;1-RFP (A), 35S::RFP-PIP2;1 (B), 35S::PIP2;7-RFP (C) and 35S::RFP-PIP2;7 (D). pBR322/pVS1: replication origins. RB/LF: right/left border. SmR: Spectinomycin resistance. Bar: BASTA resistance. T35S: 35S terminator. 35S: 35S strong promoter. pUBQ10: UBQ10 promoter. RFP: red fluorescent marker. *att*B1/*att*B2: recombination sites. The construct sizes are 10823 bp (A), 10834 bp (B), 10802 bp (C) and 10813 bp(D).

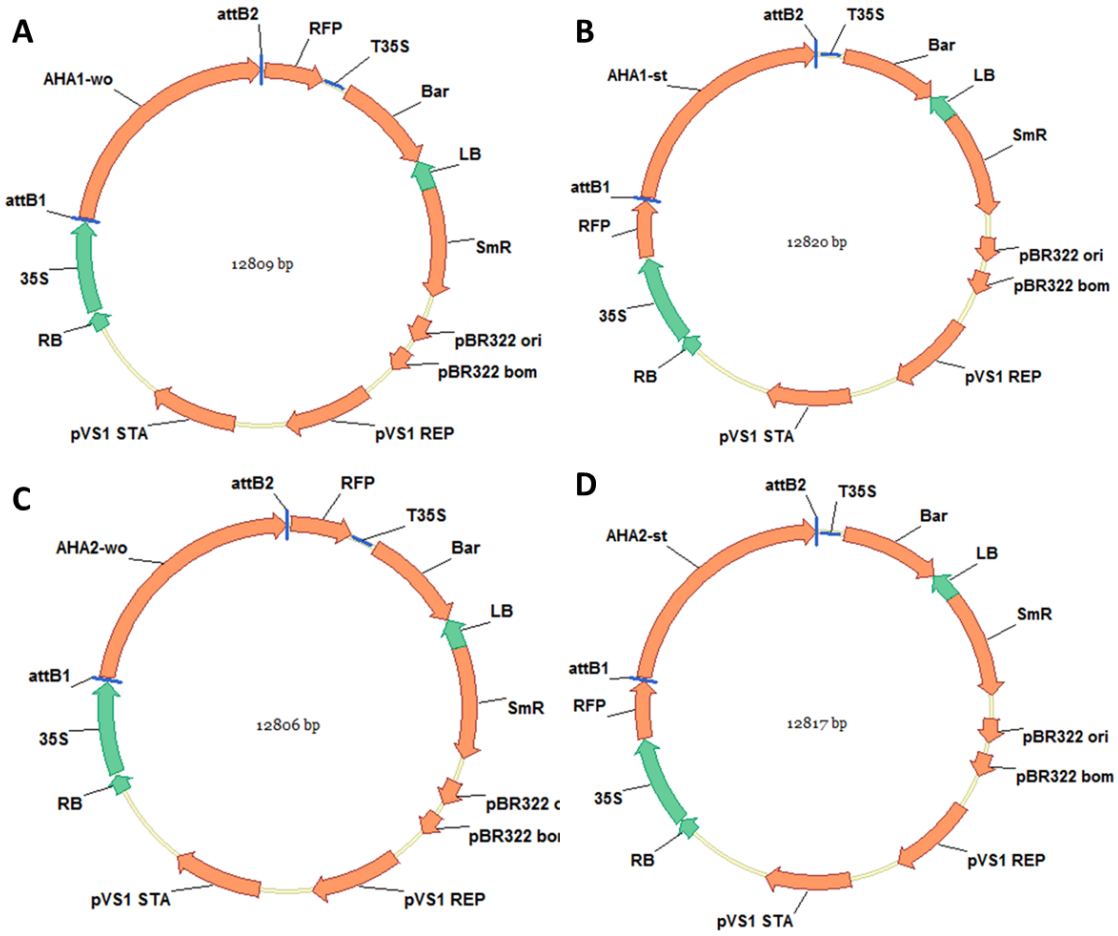

Supplemental figure 10.21. Map representation of the expression constructs 35S::AHA1-RFP (A), 35S::RFP-AHA1 (B), 35S::AHA2-RFP (C) and 35S::RFP-AHA2 (D). pBR322/pVS1: replication origins. RB/LF: right/left border. SmR: Spectinomycin resistance. Bar: BASTA resistance. T35S: 35S terminator. 35S: 35S strong promoter. RFP: red fluorescent marker. *att*B1/*att*B2: recombination sites. The construct sizes are 10823 bp (A), 10834 bp (B), 10802 bp (C) and 10813 bp(D).

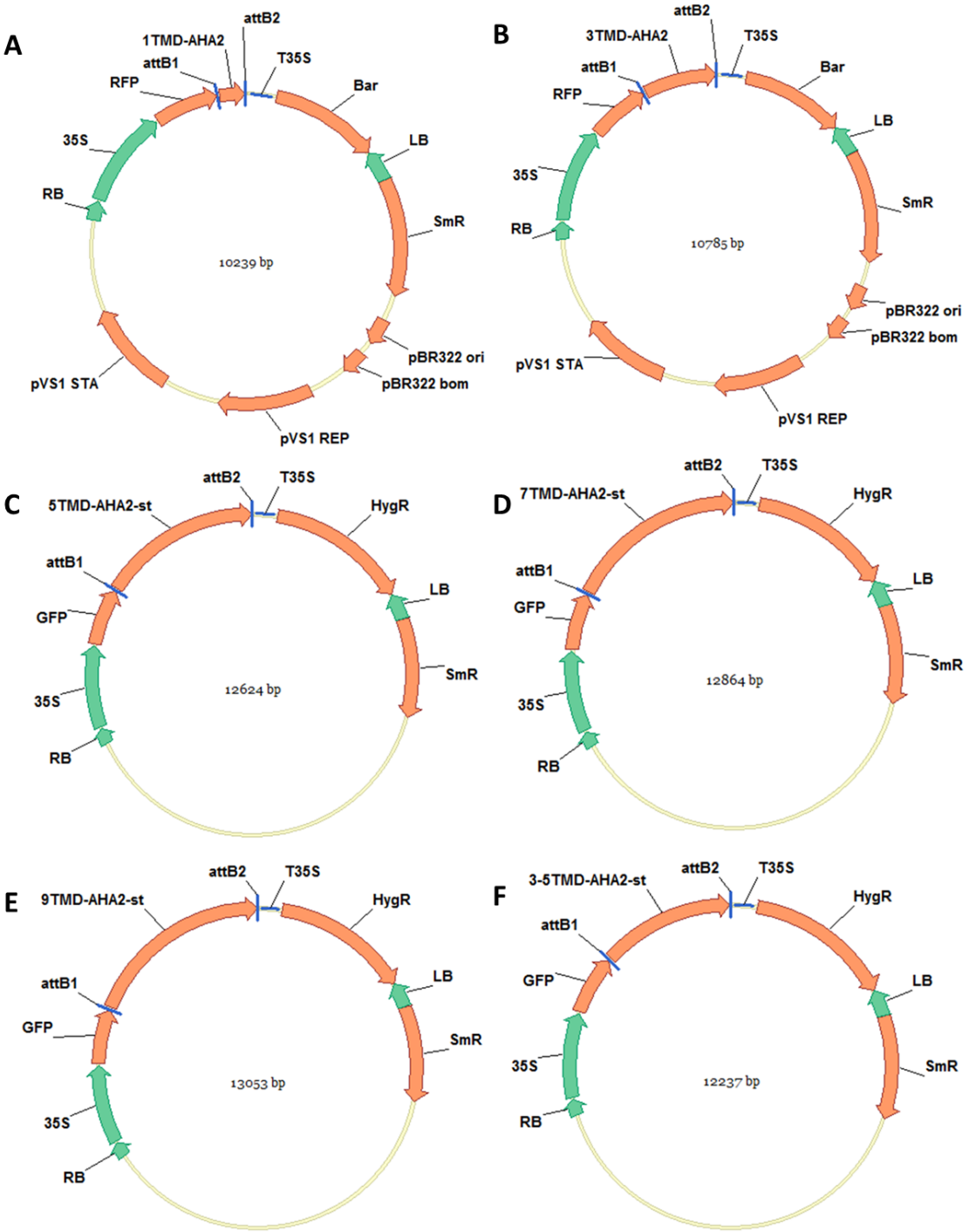

Supplemental figure 10.22. Map representation of the expression constructs 35S::RFP-1TMD_AHA2 (A), 35S::RFP-3TMD_AHA2 (B), 35S::GFP-5TMD_AHA2 (C), 35S::GFP-7TMD_AHA2 (D), 35S::GFP-9TMD_AHA2 (E) and 35S::GFP-3'5TMD_AHA2 (F). pBR322/pVS1: replication origins. RB/LF: right/left border. SmR: Spectinomycin resistance. Bar: BASTA resistance. T35S: 35S terminator. 35S: 35S strong promoter. RFP:

red fluorescent marker. *att*B1/*att*B2: recombination sites. The construct sizes are 12624 bp (A), 12864 bp (B), 13053 bp (C) and 12237 bp (D).

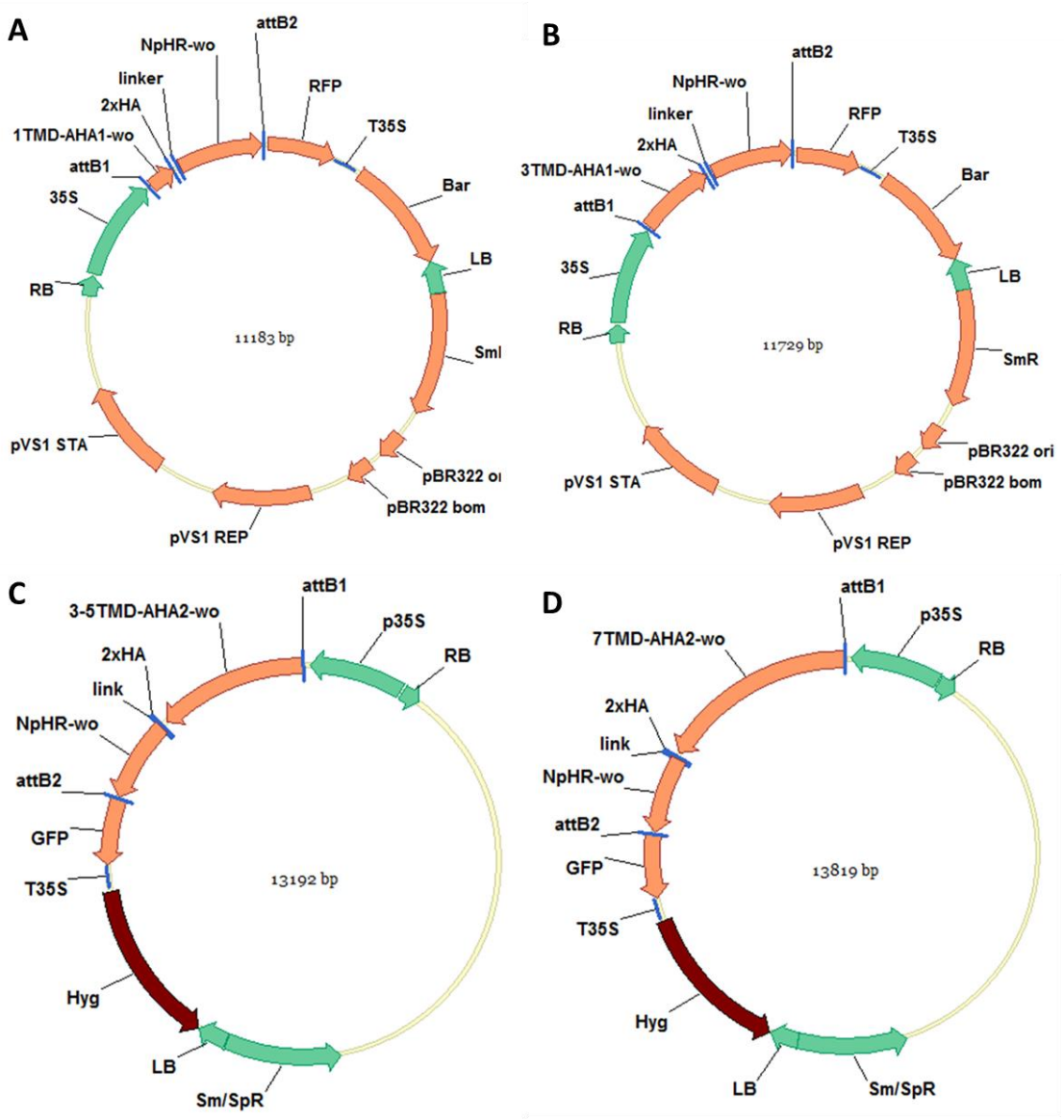

Supplemental figure 10.23. Map representation of the expression constructs 35S::1TMD_AHA2-NpHR-RFP (A), 35S::3TMD_AHA2-NpHR-RFP (B), 35S::3'5TMD_AHA2-NpHR-GFP (C), 35S::7TMD_AHA2-NpHR-GFP (D). pBR322/pVS1: replication origins. RB/LF: right/left border. SmR: Spectinomycin resistance. Bar: BASTA resistance. T35S: 35S terminator. 35S: 35S strong promoter. RFP/GFP: red/green fluorescent marker. *att*B1/*att*B2: recombination sites. The construct sizes are 12624 bp (A), 12864 bp (B), 13053 bp (C) and 12237 bp (D).

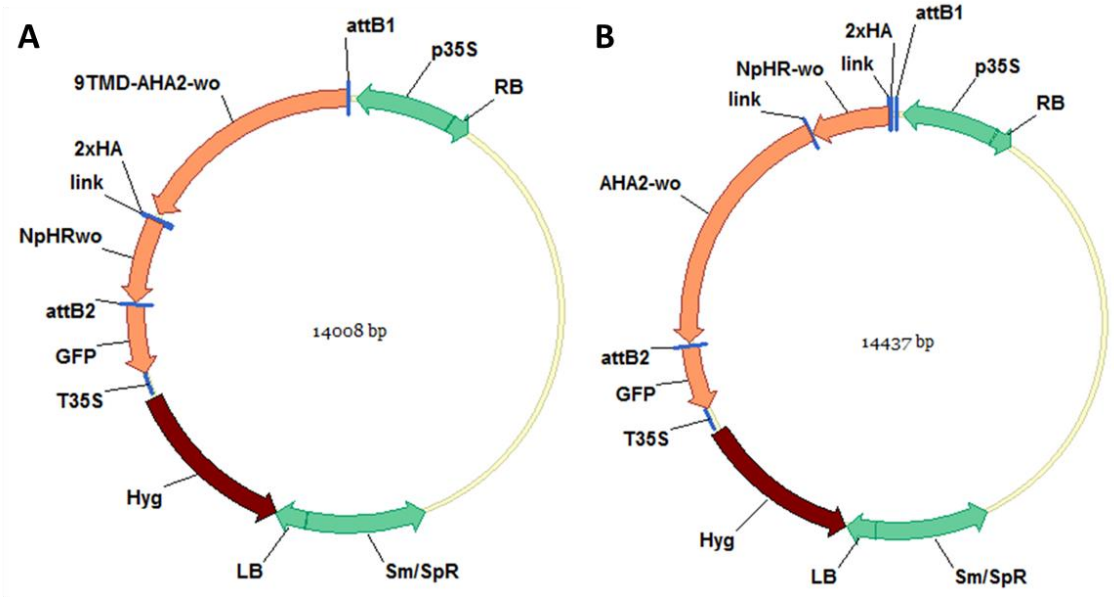

Supplemental figure 10.24. Map representation of the expression constructs 35S::9TMD_AHA2-NpHR-GFP (A) and 35S:: NpHR-AHA2-GFP (B). pBR322/pVS1: replication origins. RB/LF: right/left border. SmR: Spectinomycin resistance. Hyg: Hygromycin resistance. Bar: BASTA resistance. 2xHA: 2 HA epitope tags. T35S: 35S terminator. 35S: 35S strong promoter. GFP: green fluorescent marker. *att*B1/*att*B2: recombination sites. The construct sizes are 14008 bp (A) and 14437 bp (B).

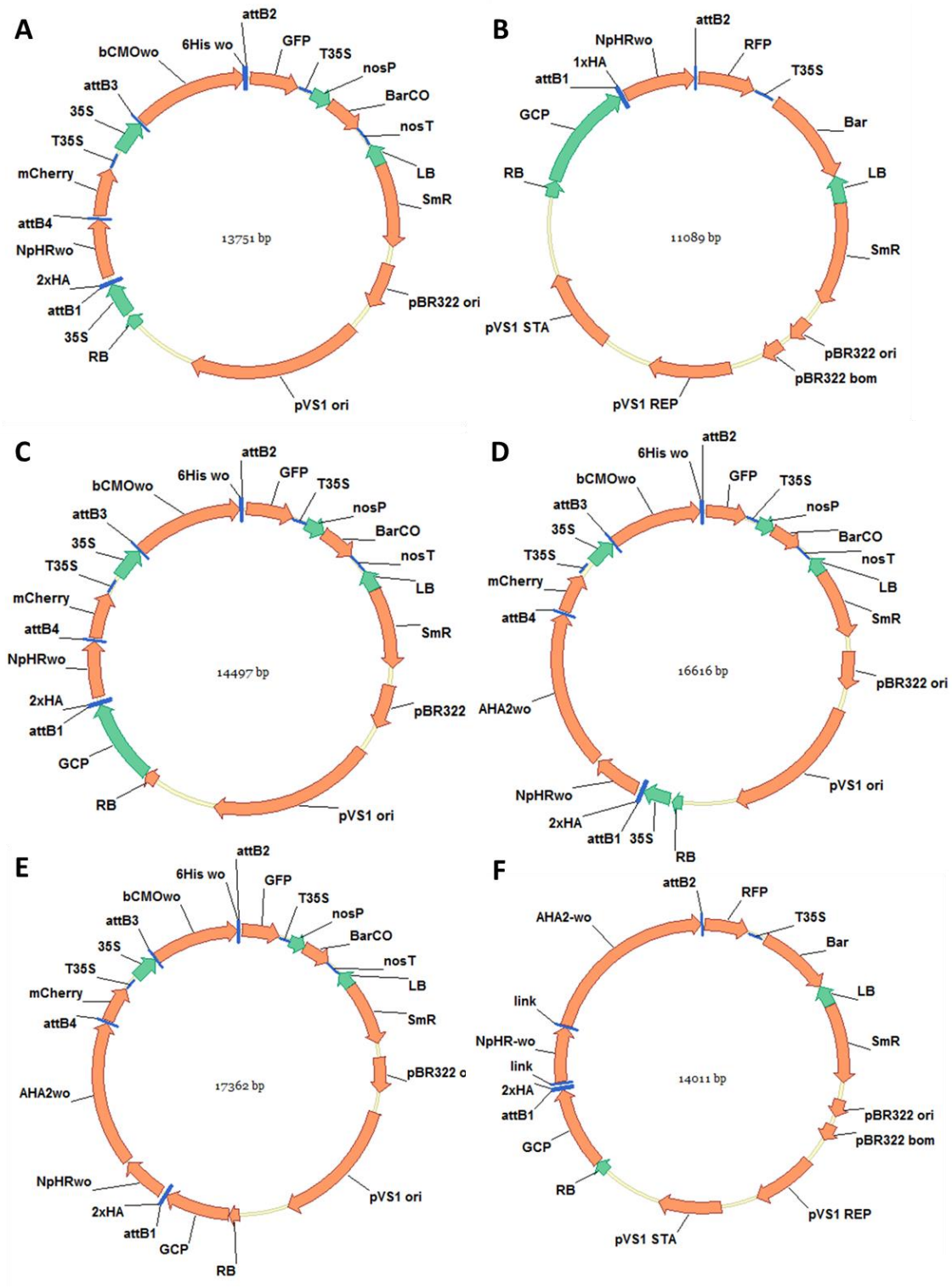

Supplemental figure 10.25. Map representation of the expression constructs 2in1 35S::NpHR-mCherry and 35S::bCMO1-GFP (A); GCP-NpHR-RFP (B); 2in1 GCP-NpHR-mCherry and 35S::bCMO-GFP (C); 2in1 35S::NpHR-AHA2-RFP and 35S::bCMO-GFP (D); 2in1 GCP-NpHR-AHA2-RFP and 35S::bCMO1-GFP (E); and GCP-NpHR-AHA2-RFP (F).

pBR322/pVS1: replication origins. RB/LF: right/left border. SmR: Spectinomycin resistance. Bar: BASTA resistance. T35S: 35S terminator. 35S: 35S strong promoter. GCP: guard cell promoter. nosP/nosT: nos promoter/nos terminator. RFP/mCherry/GFP: red/green fluorescent marker. *att*B1/*att*B2/*att*B3/*att*B4: recombination sites. The construct sizes are 13751 bp (A), 11089 bp (B), 14497 bp (C), 16616 bp (D), 17362 bp (E) and 14011 (F).